Analysis of SUMO-protein modification and its effect on cellular processes

Inaugural-Dissertation

zur

Erlangung des Doktorgrades

der Mathematisch-Naturwissenschaftlichen-Fakultät

der Universität zu Köln

vorgelegt von

Stefan Pabst

aus Köln

Köln, 2021

Berichterstatter: (Gutachter) Prof. Dr. R. Jürgen Dohmen

Prof. Dr. Kay Hofmann

Tag der mündlichen Prüfung: 03.11.2021

Table of contents

Abstract

Conjugation of SUMO (small ubiquitin-related modifier) to a substrate protein is a posttranslational modification, which can have various consequences on the substrate's activity, localization and stability. Structurally very similar to ubiquitin, SUMO is attached to a substrate in a similar enzymatic cascade, but in contrast, SUMO is not an immediate degradation signal for the substrate. However, ULS (ubiquitin ligases for sumoylated proteins) negatively regulate the abundance of SUMO conjugates by ubiquitylation which in turn leads to proteasomal degradation. Additionally, the desumoylating enzymes, in *S. cerevisiae* primarily Ulp2, negatively control the length of SUMO chains. Preliminary experiments from our laboratory have demonstrated that a failure in the control of sumoylation causes mitochondrial fragmentation. Dnm1 is the key enzyme for mitochondrial fission and it is known that sumoylation regulates the activity of its human ortholog Drp1. Motivated by these reports, a starting question was whether Dnm1 is sumoylated as well. In order to answer this question, various methods for the analysis of SUMO conjugates were established and applied. One of these methods was the application of cleavage-resistant SUMO variants, carrying the mutation Q95P, for the stabilization of these conjugates. Furthermore an optimized protocol for denaturing purification of SUMO and ubiquitin conjugates was established. In the following, this purification method was the basis for an approach to identify sumoylation sites by the application of the mass spectrometry optimized variant 8H-Smt3-KallR-I96R. In addition to identifying new SUMO substrates (for example the $(Na^+, K^+)/H^+$ antiporter Vnx1), this analysis revealed N-terminal modification of SUMO, presumably by ubiquitin. From a more physiological point of view, the effect of the SUMO system on Dnm1 localization was investigated. Generation of a Ulp2 variant with a low-temperature degron and application of an improved mtGFP construct revealed that fragmentation of mitochondria occurs in the course of one day at restrictive temperature and is therefore probably a consequence of the accumulation of sumoylated proteins. Furthermore, it was discovered that specifically in the strain *dnm1*Δ *fzo1*Δ, defective in mitochondrial dynamics, the absence of ULS leads to an increase in the formation of *petite* colonies. This in turn suggests that in particular in the absence of the mitochondrial quality control systems of fission and fusion, ULS are important to ensure respiratory competence. Regarding Dnm1 itself, a ubiquitylation of this protein could be demonstrated. However, at the same time under the applied conditions, a sumoylation of Dnm1 seems to be unlikely. Cdc11 could be successfully employed as a known SUMO substrate which confirmed the general capability of the applied methods. In agreement with the detection of ubiquitylated forms, it was found that Dnm1 is degraded via the ubiquitin-proteasome system. Furthermore, ethanol was discovered as a treatment that leads to degradation of Dnm1. Summarized, the methods established in the course of this study will be useful tools for the analysis of SUMO conjugates, and the finding of ubiquitylated Dnm1 could be a starting point for further analysis of this modification in respect to mitochondrial dynamics.

Zusammenfassung

Die Konjugation von SUMO (*small ubiquitin-related modifier*) an ein Substratprotein ist eine posttranslationale Modifikation, die verschiedene Auswirkungen auf die Aktivität, Lokalisierung und Stabilität des Substrats haben kann. Strukturell sehr ähnlich zu Ubiquitin, wird SUMO in einer vergleichbaren enzymatischen Kaskade an ein Substrat gebunden, aber im Gegensatz dazu ist SUMO kein unmittelbares Abbausignal für das Substrat. Allerdings regulieren ULS (*ubiquitin ligases for sumoylated proteins*) die Menge der SUMO-Konjugate durch Ubiquitylierung, was wiederum zum proteasomalen Abbau führt. Zusätzlich regulieren die desumoylierenden Enzyme, in *S. cerevisiae* vor allem Ulp2, die Länge der SUMO-Ketten. Vorläufige Experimente in unserem Labor haben gezeigt, dass ein Versagen der Kontrolle von Sumoylierung zur mitochondrialen Fragmentierung führt. Dnm1 ist das Schlüsselenzym für die mitochondriale Teilung und es ist bekannt, dass die Sumoylierung die Aktivität seines menschlichen Orthologs Drp1 reguliert. Ausgehend von diesen Arbeiten stellte sich die Frage, ob auch Dnm1 sumoyliert ist. Um diese Frage zu beantworten, wurden verschiedene Methoden zur Analyse von SUMO-Konjugaten entwickelt und angewendet. Eine dieser Methoden war der Einsatz von nicht-spaltbaren SUMO-Varianten, die die Mutation Q95P tragen, zur Stabilisierung dieser Konjugate. Außerdem wurde ein optimiertes Protokoll für die denaturierende Aufreinigung von SUMO- und Ubiquitin-Konjugaten entwickelt. Diese Aufreinigungsmethode bildete im Folgenden die Grundlage für einen Ansatz zur Identifizierung von Sumoylierungsstellen durch Anwendung der massenspektrometrisch optimierten Variante 8H-Smt3-KallR-I96R. Neben der Identifizierung neuer SUMO-Substrate (z. B. des (Na^+, K^+)/H^+-Antiporters Vnx1) ergab diese Analyse eine N-terminale Modifikation von SUMO, vermutlich durch Ubiquitin. Aus physiologischer Sicht wurde die Wirkung des SUMO-Systems auf die Lokalisierung von Dnm1 untersucht. Die Erzeugung einer Ulp2-Variante mit einem Niedrigtemperatur-Degron und die Anwendung eines verbesserten mtGFP-Konstrukts zeigten, dass die Fragmentierung der Mitochondrien im Laufe eines Tages bei restriktiver Temperatur auftritt und daher wahrscheinlich eine Folge der Anhäufung sumoylierter Proteine ist. Darüber hinaus wurde festgestellt, dass speziell im Stamm *dnm1*Δ *fzo1*Δ, der in der mitochondrialen Dynamik defekt ist, das Fehlen von ULS zu einer verstärkten Bildung von *petite*-Kolonien führt. Dies wiederum deutet darauf hin, dass ULS insbesondere bei Fehlen der mitochondrialen Qualitätskontrollsysteme der Teilung und Fusion wichtig sind, um die Atmungsfähigkeit zu erhalten. Für Dnm1 selbst konnte eine Ubiquitylierung dieses Proteins nachgewiesen werden. Gleichzeitig scheint eine Sumoylierung von Dnm1 unter den gegebenen Bedingungen jedoch unwahrscheinlich zu sein. Cdc11 konnte erfolgreich als bekanntes SUMO-Substrat eingesetzt werden, was die generelle Eignung der angewandten Methoden bestätigt. In Übereinstimmung mit dem Nachweis von ubiquitylierten Formen wurde festgestellt, dass Dnm1 über das Ubiquitin-Proteasom-System abgebaut wird. Außerdem wurde Ethanol als eine Behandlung entdeckt, die zum Abbau von Dnm1 führt. Zusammenfassend lässt sich sagen, dass die im Rahmen

dieser Arbeit etablierten Methoden nützliche Werkzeuge für die Analyse von SUMO-Konjugaten darstellen, und dass die Entdeckung von ubiquityliertem Dnm1 ein Ausgangspunkt für die weitere Analyse dieser Modifikation in Bezug auf die mitochondriale Dynamik sein könnte.

1 Introduction

1.1 Protein homeostasis and degradation systems

Protein homeostasis, also termed proteostasis, is of critical importance for the maintenance of cellular functions. In order to maintain the functionality of the proteome, major processes that determine protein functions and abundance, such as protein synthesis, folding, post-translational modifications and protein degradation are regulated on multiple layers (Powers et al., 2009). Many neurodegenerative diseases, such as AD (Alzheimer's disease) (Morawe et al., 2012), HD (Huntington's disease) (Labbadia and Morimoto, 2013), ALS (amyotrophic lateral sclerosis) (Robberecht and Philips, 2013) and PD (Parkinson's disease) (Lehtonen et al., 2019), are linked to malfunctioning proteostasis. This circumstance has led to an increased interest in understanding the molecular basis of proteostasis networks. On one side of the spectrum of proteostasis, securing protein function, are protein translation and assistance in folding by chaperones. By this activity, chaperones reduce the risk of protein misfolding and aggregation (Powers et al., 2009). On the other side of the spectrum, numerous pathways negatively control the abundance of proteins (***Figure 1.1***).

The most prominent degradation pathways are the UPS (ubiquitin-proteasome system), which is of great interest for our laboratory and this study, and autophagy. Both systems play different roles in the cell. The UPS is mainly responsible for the degradation of soluble, short-lived proteins which have been marked for degradation by attachment of the small protein ubiquitin (Kocaturk and Gozuacik, 2018). The substrates can be functional proteins that have to be negatively controlled, for example cyclins, or misfolded proteins which have to be eliminated in order to avoid potentially harmful effects (Wang and Maldonado, 2006). These substrates are then recognized and degraded by and within the barrel-shaped multi-subunit protein complex proteasome (Reggiori and Klionsky, 2013), as described in more detail in the following chapter.

In contrast, autophagy is mainly responsible for the degradation of macromolecular complexes and organelles (Reggiori and Klionsky, 2013). This process can be divided into two major types, namely microautophagy and macroautophagy. During microautophagy, the vacuole directly engulfs the target and degrades it, as it was described for mitochondria, peroxisomes and parts of the nuclear membrane (Reggiori and Klionsky, 2013). By contrast, macroautophagy is characterized by the formation of double-membrane vesicles around the cargo, followed by fusion with the vacuolar membrane and release of the cargo into the vacuole.

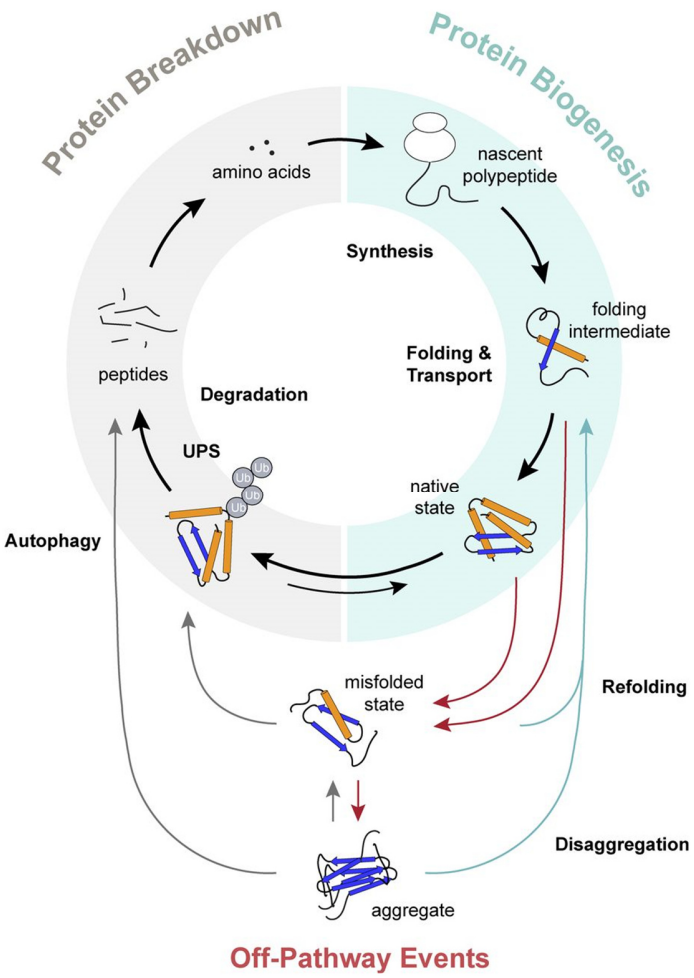

Figure 1.1: The two sides of proteostasis: Protein biogenesis and protein degradation
Out of free amino acids polypeptides are synthesized and, via folding intermediates and in some cases transport, a protein is present in its native state. Either directly or upon misfolding, the protein can become ubiquitylated. Furthermore, intermediate states where misfolded proteins form aggregates can occur. In general, with the exception of synthesis, these processes are reversible, meaning that via disaggregation and refolding, proteins can return to a native state. When a protein has become ubiquitylated and the ubiquitin moieties are not removed by ubiquitin specific proteases, this substrate (or target) is degraded by the proteasome. By another pathway, protein aggregates can be degraded via autophagy. Both, the UPS (ubiquitin-proteasome system) and autophagy lead to irreversible destruction of the substrate, yielding free peptides that replenish the pool of free amino acids. Figure taken from Sala et al., 2017.

Specialized pathways mediate macroautophagy of specific targets, for example mitophagy for mitochondria, pexophagy for peroxisomes or ribophagy for ribosomes. Expectedly, a physiological role for autophagy is the degradation of dysfunctional organelles, however, it is also important for recycling of nutrients, especially under starvation conditions (Reggiori and Klionsky, 2013). For example, it has been shown that during starvation, autophagy is required for providing dNTP (deoxyribonucleotide triphosphate) pools for maintaining mtDNA (mitochondrial DNA) synthesis. Consequently, autophagy-deficient yeast cells became respiratory dysfunctional upon starvation (Medeiros et al., 2018).

1.2 The ubiquitin-proteasome system

The UPS has a dual role in the context of protein degradation since it performs the degradation of specific proteins, where a limited half-life is part of their regulation, but it also performs the degradation of misfolded or otherwise abnormal proteins and is therefore a part of the protein quality control systems (Lecker et al., 2006). A well-characterized example for the role in regulation of a protein function is the degradation of cyclins in a cell cycle-dependent manner. It was already known that degradation of cyclins is required for the exit of mitosis (Murray et al., 1989). Shortly after, by analysis of cell extracts from *Xenopus* eggs, it was found that the degradation of cyclin, which together with $p34^{cdc2}$ forms the MPF (M-phase promoting factor), requires a specific region in its N-terminus. Fusion of this region to other proteins was sufficient to cause their degradation. Furthermore, it could be demonstrated that degradation of the cyclin occurred via the UPS (Glotzer et al., 1991). This report was probably one of the first that precisely characterized the role of the UPS in a physiological process, and at the same a specific region in the target protein could be identified.

The quality control function of the UPS plays a crucial role in counteracting protein aggregates, which can arise as a consequence of the presence of misfolded proteins. It was found that misfolded proteins appear increasingly in the course of aging, for example in *C. elegans* (Ben-Zvi et al., 2009), and aggregation of specific proteins leads to a number of diseases, such as AD, ALS, HD or PD (Amm et al., 2014; Ross and Poirier, 2004). Recently, in *C. elegans* it was discovered that during ageing, by increased activity of deubiquitylating enzymes, global ubiquitylation is reduced. Specific targets that accumulate during ageing could be identified and it was demonstrated that their abundance determines life-span. For example, one of these proteasome substrates is the IFB-2 intermediate filament (Koyuncu et al., 2021).

However, it was also suggested that, in some cases, protein aggregation serves as a protective mechanism that sequesters toxic protein species, and it has to be noted that protein misfolding can be both, a cause or a result of stress (Basaiawmoit and Rattan, 2010). The UPS exerts quality control not only on cytosolic proteins, but also on ER (endoplasmic reticulum) localized proteins via ERAD (Endoplasmic reticulum-associated degradation), or on proteins in the nucleus (Amm et al., 2014), as explained in more detail in chapter 1.2.4.

The UPS relies on the attachment of ubiquitin to substrate proteins, a process which is performed by an enzymatic cascade of a ubiquitin-activating enzyme (E1), one of several ubiquitin-conjugating enzymes (E2) and one of many ubiquitin-protein ligases (E3) which mediate substrate specificity for the last step of the conjugation of ubiquitin to a target protein. In many but not all cases, ubiquitin conjugation, also

termed ubiquitylation, leads to degradation of the target protein by the proteasome. The individual steps in ubiquitylation and their molecular basis are explained in more detail in the following sections and schematically illustrated in ***Figure 1.2***.

1.2.1 Ubiquitin

Ubiquitin is a small protein of 76 amino acids with a molecular weight of ~ 8.5 kDa (Xu and Jaffrey, 2013). Its name originates from the fact that ubiquitin is present in all eukaryotes and its essential role for eukaryotic cell physiology is underlined by its conservation across diverse species. This becomes clear, for example, by the fact that ubiquitin from *Saccharomyces cerevisiae* and humans only differ in three amino acids (Zuin et al., 2014).

Ubiquitylation belongs to the group of PTMs (post-translational modifications) and ubiquitin is the founding member of the group of UBLs (ubiquitin-like proteins), which for example also contains SUMO (small ubiquitin-like modifier). Via its C-terminus, ending with a glycine-residue, ubiquitin is conjugated to an ε-amino group of a lysine residue of a substrate protein, forming an isopeptide bond (Pickart, 2001). However, it has been demonstrated that by the activity of the E2 enzyme Ube2w, ubiquitin can also be conjugated to the N-terminus of a substrate (Scaglione et al., 2013). Furthermore, for a couple of proteins non-canonical ubiquitylation of cysteine, serine or threonine was found (McDowell and Philpott, 2013). Most likely, N-terminal and non-canonical ubiquitylation are relatively uncommon but it is certainly an interesting observation that these are in principle possible.

If multiple lysine residues of the same substrate are ubiquitylated with one ubiquitin moiety each, this substrate is termed multi-monoubiquitylated (Komander and Rape, 2012). An example for such a substrate in humans is EGFR (epidermal growth factor receptor) (Haglund et al., 2003). Furthermore, a ubiquitin moiety can be conjugated to an already substrate-bound ubiquitin. Such a sequential conjugation of ubiquitin moieties to one another is termed polyubiquitylation which leads to the formation of a ubiquitin chain on a substrate that can have a length of two to many moieties (Komander and Rape, 2012). Polyubiquitylation can occur on one of the seven lysine residues of ubiquitin or on its N-terminus, the latter of which generates linear ubiquitin chains. In a ubiquitin chain, the linkage type can be homogenous, if always the same residues are targeted by the following moiety, or mixed if different residues are chosen in the process of chain formation. Moreover, also branched ubiquitin chains with the attachment of multiple moieties to the same preceding ubiquitin have been found, for example on cyclin A (Meyer and Rape, 2014). The physical properties of specific ubiquitin chains are different and determine their effect

on the substrate protein. A well-known chain type is the K48 ubiquitin chain, wherein ubiquitin moieties are linked to each other via Lys48. In this chain type, ubiquitin moieties interact with each other via their hydrophobic Ile44 patches. This leads to a characteristic compact structure of K48-tetraubiquitin (Eddins et al., 2007; Komander and Rape, 2012). K48-linked ubiquitin chains lead to degradation of the substrate protein by the proteasome and tetraubiquitin is the minimal chain length for efficient targeting to the proteasome (Thrower et al., 2000). In contrast, K63-linked ubiquitin chains have a more elongated and flexible conformation and have been described as modification with a function in various cellular processes (Tenno et al., 2004) like for example inheritance of mitochondrial DNA in *S. cerevisiae* (Fisk and Yaffe, 1999). Altogether, many different non-proteolytic roles of ubiquitylation have been described, such as regulation of a substrate's activity, its interactions with other proteins, or its localization (Komander and Rape, 2012).

1.2.2 The ubiquitylation process

In *S. cerevisiae*, there are four genes that encode ubiquitin, namely *UBI1*, *UBI2*, *UBI3* and *UBI4*. In *UBI1*, *UBI2* and *UBI3*, ubiquitin is fused to ribosomal proteins (Finley et al., 1989) whereas *UBI4* encodes an ORF (open reading frame) of five ubiquitin repeats (Ozkaynak et al., 1987). Under normal conditions, the cellular ubiquitin pool is primarily generated by expression of *UBI1*, *UBI2* and *UBI3* but under stress conditions, expression of *UBI4* is induced (Finley et al., 1987). Matching this role as a stress-induced gene, transcription of *UBI4* is activated by the transcription factor Rpn4 which is also responsible for transcriptional activation of proteasome subunit expression when the proteasome is overloaded (London et al., 2004). In all cases, ubiquitin is released from the fusion partner through cleavage by a DUB (deubiquitylating enzyme) (Grou et al., 2015).

As mentioned before, the process of ubiquitylation is performed by three different enzymes, a ubiquitin-activating enzyme (E1), a ubiquitin-conjugating enzyme (E2) and a ubiquitin-protein ligase (often termed only ubiquitin-ligase or E3 ligase) (E3). In *S. cerevisiae*, only one ubiquitin-activating enzyme is known, namely Uba1, which is essential for viability. During its activation, the C-terminal glycine of ubiquitin forms a thioester bond to a cysteine residue of Uba1. This reaction is ATP (adenosine triphosphate)-dependent and leads to an intermediate state, thus the ubiquitin is activated (McGrath et al., 1991). Such an activated ubiquitin molecule is then transferred to one of budding yeast's eleven ubiquitin-conjugating enzymes, also forming a thioester bond with a cysteine of the E2 enzyme (Finley et al., 2012). Subsequently, a ubiquitin-ligase interacts with the E2 enzyme and the substrate protein, and thereby indirectly mediates interaction of E2 and substrate so that ubiquitin can be transferred from the E2 enzyme to usually a lysine

residue of the substrate. Therefore, the E3 enzymes provide the substrate specificity within the UPS, and consequently there are 60 – 100 ubiquitin-ligases in *S. cerevisiae* (Finley et al., 2012). Summarized, the number of family members and the substrate specificity increase from E1 to E3. Usually, the E2 enzyme can interact with a number of different E3 ligases, and also the E3 ligase can interact with different E2 enzymes. For some E2 enzymes, a chain type specificity was found. For example, UBE2S, which cooperates with the E3 ligase APC/C (anaphase promoting complex/cyclosome), is specific for K11-linkages. Furthermore, the E3 ligase Parkin preferentially assembles K6- and K11-chains on depolarized mitochondria for subsequent mitophagy (Swatek and Komander, 2016).

Ubiquitin-ligases are generally classified into three groups, the most prevalent RING (Really Interesting New Gene) type, the HECT (Homologous to the E6-AP Carboxyl Terminus) type (Huibregtse et al., 1995) and the most recently described RBR (RING-between-RING) type (Gundogdu and Walden, 2019; Walden and Rittinger, 2018). The RING-type domain of the respective E3 class coordinates two zinc ions and is responsible for interaction with the ubiquitin-conjugating enzyme, and ubiquitin-transfer occurs directly from the E2 enzyme to the substrate (Metzger et al., 2014). The RING-domain often mediates dimerization of these ubiquitin ligases like for example in mammalian RNF4 (Liew et al., 2010). Furthermore, SCF (Skp1–Cdc53–F-box) E3 ubiquitin ligase complexes belong to the group of RING-type E3 ligases. In budding yeast, Skp1 was found to interact with F-box proteins via their F-box motifs, thus Skp1 is a central component of this E3 ligase complex (Bai et al., 1996). Furthermore, Skp1 binds to Cdc53 so that it indirectly connects Cdc53 to the F-box protein (Patton et al., 1998). These complexes are modular E3 ligases with Rbx1 (or Hrt1) providing the RING-domain, and the F-box protein mediating substrate specificity (Joazeiro and Weissman, 2000; Seol et al., 1999). One example of an F-box protein is Mdm30, which mediates ubiquitylation of Fzo1 and thereby facilitates mitochondrial fusion (Cohen et al., 2011; Escobar-Henriques et al., 2006; Fritz et al., 2003).

In contrast, HECT-type E3 ligases mediate ubiquitin transfer with an intermediate step in which ubiquitin is bound to the active site cysteine of the E3 ligase by a transthiolation reaction (Huibregtse et al., 1995). RBR-type ligases recognize the E2-enzyme in a way similar to the canonical RING-type ligases but ubiquitylation occurs via a ubiquitin-thioester intermediate involving a cysteine residue in the second RING-domain of the same ligase, so that RBR-type ligases feature characteristics of both previously mentioned types (Gundogdu and Walden, 2019).

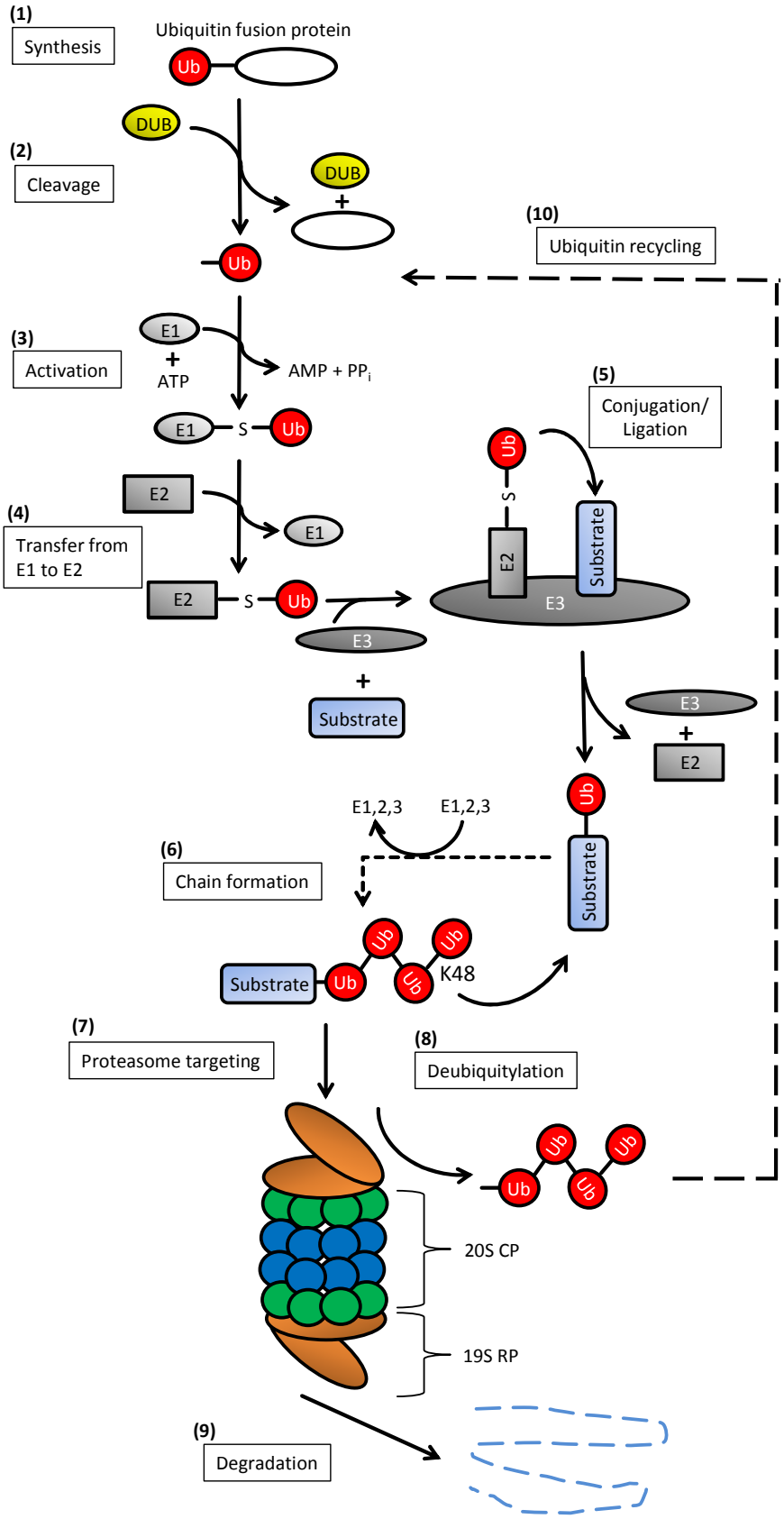

Figure 1.2: The ubiquitin-proteasome system

Schematically, the individual processes within the ubiquitin-proteasome system are illustrated. Ubiquitin is syntesized as a

translation fusion (1) that becomes cleaved by a DUB (deubiquitylating enzyme) (2). Ubiquitin is activated by the E1 enzyme (3), transferred to an E2 enzyme (4) and conjugated to a substrate via an E3 ligase mediated interaction (5). By repitition of this process, a ubiquitin chain is formed on the substrate (6) and in the case of K48-linked ubiquitin the substrate is targeted to the proteasome (7). Deubiquitylation can remove ubiquitin from a substrate to prevent proteasomal targeting or ubiquitin is cleaved by proteasomal DUBs (8) before degradation (9). Free ubiquitin can engage in following rounds of ubiquitylation (10). Figure taken and modified from Stefan Pabst, Master Thesis, 2015.

1.2.3 Deubiquitylation

DUBs (deubiquitylating enzymes) are ubiquitin-specific proteases with 22 putative members in *S. cerevisiae* (Suresh et al., 2020). DUBs serve three principle physiological purposes. The first one is, as mentioned previously, the cleavage of ubiquitin from ribosomal proteins or from the polyubiquitin chain generated by translation of the ubiquitin encoding genes. This function can be carried out by several different DUBs, so that, with the exception of the proteasomal subunit Rpn11, none of the DUBs is essential for viability in *S. cerevisiae* (Amerik and Hochstrasser, 2004). The fact that DUBs cleave N-terminal translational fusions of ubiquitin can be used in order to generate engineered proteins with different N-termini (see results chapter 2.6.3).

The second function of DUBs is essentially counteracting ubiquitylation. This may be regarded as a quality control mechanism for mistakenly ubiquitylated proteins. Shortening of the ubiquitin chain length can reduce the chain length to less than four moieties which in turn is not sufficient for efficient proteasomal targeting (Amerik and Hochstrasser, 2004). Furthermore, by their deubiquitylation functions, DUBs can regulate ubiquitylation of specific substrates. For example, two DUBs act on the mitofusin Fzo1 in order to regulate mitochondrial fusion. The first one, Ubp2, removes ubiquitin from Fzo1 and thereby prevents its degradation, which in turn allows Fzo1 to perform mitochondrial fusion. The second DUB acting on Fzo1, Ubp12, removes another, fusion-promoting, type of ubiquitylation from Fzo1. Therefore, Ubp12 inhibits mitochondrial fusion. Another layer of complexity is added by the finding that Ubp12 inhibits the pro-fusion function of Ubp2 (Simões et al., 2018). This intriguing example illustrates that DUBs function in the fine-tuning of ubiquitylation and thereby of the function of specific proteins, thereby DUBs can play key roles in the regulation of a biological process.

The third function of DUBs is the removal of ubiquitin from substrates that have been targeted to the proteasome. Due to this activity, ubiquitin is not degraded with the substrate but instead, it is recycled and replenishes the cellular ubiquitin pool so that it can be used in following rounds of ubiquitylation. In *S. cerevisiae* the DUB Rpn11 is a subunit of the 19S regulatory particle of the proteasome and performs the above noted function (Guterman and Glickman, 2004). Furthermore, the DUB Ubp6 is typically found

in the proteasome in substoichiometric quantity, meaning that it is not an integral component of proteasomes (Aufderheide et al., 2015).

1.2.4 The 26S Proteasome

The 26S proteasome consists of the 20S CP (core particle) and one or two 19S RPs (regulatory particles) which are located at the top and bottom of the 20S CP (Schweitzer et al., 2016). The 20S CP is a multi-subunit complex of ~ 700 kDa with an essentially barrel-like shape, inside of which the proteolysis of substrates is performed (Murata et al., 2009). In proliferating yeast, proteasomes are mainly localized in the nucleus, whereas in quiescent cells, proteasomes are found primarily in the cytosol in PSGs (proteasome storage granules) (Laporte et al., 2008; Wendler and Enenkel, 2019).

The 20S CP is composed of four heptameric rings stacked on each other. The two inner rings are identical and formed by seven different β-subunits each. The two outer rings are identical, as well, and are formed by seven different alpha subunits. Therefore, the structure of the 20S CP can be described as $\alpha_7\beta_7\beta_7\alpha_7$. Within this 20S CP, the subunits β1, β2 and β5 of the two inner rings perform the proteolytic activity. β1 has caspase-like, β2 has trypsin-like and β5 has chymotrypsin-like activity (Britton et al., 2009; Heinemeyer et al., 1997; Marques et al., 2009).

The 19S RP can be subdivided into the base and the lid. In *S. cerevisiae*, within the base, there are six Rtp (regulatory particle ATPase) subunits and two Rpn (regulatory particle non-ATPase) subunits and the lid consists of eight Rpn subunits. Rpn10 connects base and lid of the 19S RP (Pickart and Cohen, 2004). The 19S RPs are involved in recognition, deubiquitylation and unfolding of the substrate prior to its degradation (Pickart and Cohen, 2004). In addition to these stoichiometric proteasomal subunits, there are shuttling factors, which mediate substrate targeting and are only transiently associated with the proteasome (Saeki, 2017). Alternative to the 19S RP, a protein termed Blm10 can bind to the 20S CP and stimulate proteolytic activity. In yeast cells, Blm10 is predominantly found in Blm10-CP-RP complexes (Schmidt et al., 2005). It was reported that Blm10 in a ubiquitin-independent manner is required for efficient degradation of Dnm1 and that this turnover is necessary for maintaining mitochondrial function, presumably by counteracting too high Dnm1-levels (Tar et al., 2014). Another example of a substrate which is degraded in a ubiquitin-independent mechanism, is ODC (ornithine decarboxylase) (Murakami et al., 1992). Furthermore, Rpn4, a transcription activator for proteasomal genes, is degraded by the proteasome in a ubiquitin-independent manner so that a negative feedback loop controls transcription of proteasomal genes (Xie and Varshavsky, 2001).

The proteasome is a target for the drug bortezomib/Velcade™ in the treatment of multiple myeloma due to the susceptibility of the respective cells to proteasome inhibition (Kisselev et al., 2012). Another proteasome inhibitor is MG132 which inhibits the chymotryptic activity of β5, which is rate-limiting for proteolysis (Lee and Goldberg, 1998). For use in experiments with yeast, usually a strain with deleted *PDR5* is used for proteasome inhibition since the absence of this drug efflux pump makes application of MG132 more effective (Fleming et al., 2002).

1.3 The SUMO System

SUMO (small ubiquitin-like modifier), like ubiquitin, is a small protein that serves as a post-translational modification. Although human SUMO-1 und ubiquitin have only 18% sequence identity on amino acid level, structurally both modifiers are very similar (Bayer et al., 1998). While ubiquitin in many cases serves as a degradation signal (see chapter 1.2), SUMO conjugation (termed sumoylation) does not directly target the substrate for degradation (Johnson, 2004). Instead, SUMO can be regarded as a modification that generally changes the physical properties of a substrate, which can have various consequences. Only to mention some examples, sumoylation can influence protein-protein interactions (Cox et al., 2017), it can positively or negatively affect ubiquitylation of a substrate (Desterro et al., 1998; Uzunova et al., 2007) and it can regulate the localization of a substrate (Wen et al., 2017).

Sumoylation occurs mostly but not exclusively in the nucleus (Johnson, 2004). For example, in budding yeast, septins at the bud neck are strongly sumoylated in a cell cycle-dependent manner (Johnson and Blobel, 1999; Takahashi and Kikuchi, 2008). An example of non-nuclear sumoylation in humans is the SUMO modification of Drp1 at the mitochondria/ER (endoplasmic reticulum) interface (Prudent et al., 2015). Typically, only less than 1% of a substrate is sumoylated at a given time, and due to this small fraction of sumoylated substrate, the analysis of sumoylated proteins is relatively difficult (Johnson, 2004). However, especially by the application of MS (mass spectrometry), many SUMO-substrates have been identified (Denison et al., 2005; Hannich et al., 2005; Paasch et al., 2018; Panse et al., 2004; Wohlschlegel et al., 2004; Zhou et al., 2004). Furthermore, elaborate methods have been established for the simultaneous determination of a substrate's sumoylated lysine residue in yeast (Albuquerque et al., 2015; Esteras et al., 2017) and in human cells (Lamoliatte et al., 2017). A comparison of different methods for the identification of SUMO-substrates by mass spectrometry is made in chapter 2.4.1.

The first identified SUMO substrate was human RanGAP1 (Ran GTPase-activating protein 1) (Mahajan et al., 1997; Matunis et al., 1996). This is an example for modulation of protein-protein interactions by this

modification, since sumoylation of RanGAP1 promotes its interaction with the nuclear pore complex protein RanBP2 (Mahajan et al., 1997). As noted above, another well-studied example is the sumoylation of septins in *S. cerevisiae*. Septin rings form at the bud neck and are thought to serve as a scaffold for other factors and to form a diffusion barrier in cytokinesis (Mostowy and Cossart, 2012). It was found that the septins Cdc3, Cdc11 and Shs1 become sumoylated at the mother side of the bud neck during mitosis and that these modifications disappear again at cytokinesis. In G_2/M phase, these septins probably account for the majority of the yeast's SUMO conjugates (Johnson and Blobel, 1999). Sumoylation of septins is therefore an example of cell cycle-regulated sumoylation.

In addition to these examples, sumoylation was found to play a role in many other biological processes. A well-known example is the sumoylation of PCNA (proliferating cell nuclear antigen) where SUMO or ubiquitin can, alternatively, modify the same lysine residue (Hoege et al., 2002). However, PCNA is a trimer so that simultaneous ubiquitylation and sumoylation cannot be ruled out. Still, both modifications have different outcomes. While monoubiquitylation promotes error-prone translesion synthesis in response to DNA damage, sumoylated PCNA recruits Srs2 which in turn prevents recombination (Gareau and Lima, 2010). Furthermore, sumoylation stimulates subsequent ubiquitylation by the ubiquitin ligase Rad18 (Parker and Ulrich, 2012). Other processes which involve sumoylation are, exemplarily, regulation of transcription (Garcia-Dominguez and Reyes, 2009), regulation of DNA repair (Sarangi and Zhao, 2015), nuclear import (Rothenbusch et al., 2012), prevention of protein aggregation (Krumova et al., 2011) and, in human cells, mitochondrial fission (Braschi et al., 2009).

1.3.1 SUMO

As noted earlier, ubiquitin and SUMO are structurally very similar. SUMO is a protein of ~ 11 kDa and possesses the ββαββαβ fold, typical for members of the ubiquitin family. However, ubiquitin and SUMO have different charge topologies (Bayer et al., 1998), which is probably the main reason for the difference in interaction partners. Like ubiquitin, SUMO has a double-glycine C-terminus for the formation of an isopeptide bond with a substrate protein's lysine residue. A difference between both modifiers is the presence of the approximately 20 amino acid long flexible N-terminal extension in SUMO. This extension plays a crucial role for the formation of SUMO chains since, both in *S. cerevisiae* SUMO (Smt3) and in mammalian SUMO2/3, it contains lysine residues in a sumoylation consensus motif ΨKXE/D (Ψ is a hydrophobic residue and X is any amino acid) (Ulrich, 2008; Zhao et al., 2014). Consequently, SUMO chain formation in budding yeast occurs on K11, K15, or K19, which are located in the N-terminal extension (Bylebyl et al., 2003) with K15 as the preferred acceptor for chain formation (Bencsath et al., 2002).

Although most sumoylation on substrates occurs via the above-mentioned consensus motif, it was found that approximately 40% of known sumoylation sites are not placed in such a motif (Zhao et al., 2014). It has been shown that, in general, sumoylation and particularly HMW (high molecular weight) SUMO conjugates, presumable chains, are strongly increased upon stress treatments such as 10% ethanol, oxidative stress, osmotic stress, or heat (Pabst et al., 2019; Srikumar et al., 2013). However, in comparison to the functions of mono-sumoylation, the physiological roles of SUMO chains are less well understood (Keiten-Schmitz et al., 2020). Non-covalent interaction of SUMO often occurs via a SIM (SUMO interaction motif) of the interaction partner. SIMs are usually classified into three types, depending on the exact amino acid sequence. These are ΨΨXΨAcAcAcAcAc (SIMa), ΨΨDLT (SIMb) and AcAcAcAcAcΨXΨΨ (SIMr) with Ψ = V, I or L and Ac = D, E or S. Consistently, proteins with several SIMs show a preference for SUMO chains (Praefcke et al., 2012; Vogt and Hofmann, 2012).

Sumoylation is essential for viability in the vast majority of eukaryotic organisms, as it is the case in *S. cerevisiae* (Johnson et al., 1997). In contrast, in *Schizosaccharomyces pombe*, the SUMO gene *pmt3* is not essential for viability but *pmt3*Δ cells have a growth defect (Tanaka et al., 1999). Although *SMT3* is an essential gene in *S. cerevisiae*, the ability to forms chains is apparently not essential, as seen by the fact that a yeast strain exclusively expressing a SUMO variant where all lysine residues have been replaced by arginine (Smt3-KallR), is viable even though its doubling time is increased (Bylebyl et al., 2003; Srikumar et al., 2013).

Whereas in budding yeast only one SUMO isoform was found, encoded by *SMT3*, for humans five SUMO isoforms were described. Due to the absence of a lysine residue within a sumoylation consensus motif in the N-terminal extension, human SUMO1 does not form chains. In contrast, SUMO2 and SUMO3, which are very similar and therefore often summarized as SUMO2/3, possess K11 in a sumoylation consensus motif and form polymeric chains (Tatham et al., 2001). Therefore, modification of an already existing SUMO2/3 chain by SUMO1 limits chain length (Matic et al., 2008). SUMO4 has an amino acid sequence similar to SUMO2/3 and was found to be expressed mainly in the kidney (Bohren et al., 2004) but also in the placenta (Baczyk et al., 2017). The most recently identified member of the SUMO family is SUMO5. This isoform is conserved in primates and has the strongest expression in testes (Liang et al., 2016).

At this point, it should be noted that ubiquitin and SUMO are not the only Ubls (ubiquitin-like proteins) in *S. cerevisiae*. Other Ubls in budding yeast are Rub1 (homologous to mammalian NEDD8) (Hochstrasser, 1996; Lammer et al., 1998), Atg8, which becomes conjugated to the lipid phosphatidylethanolamine (Ichimura et al., 2000), Atg12 (Mizushima et al., 1998), and Urm1 (Furukawa et al., 2000). Atg8 and Atg12 are required for autophagy (Reggiori and Klionsky, 2013).

1.3.2 The sumoylation process

The process of sumoylation is very similar to the one of ubiquitylation (see chapter 1.2.2). In *S. cerevisiae*, SUMO is expressed from the gene *SMT3* with a C-terminal –ATY (alanine-threonine-tyrosine) extension. These three amino acids are cleaved by Ulp1 during Smt3 maturation, leaving mature Smt3 with 98 amino acids and the C-terminal glycine accessible for conjugation (Li and Hochstrasser, 1999). The sumoylation machinery described in the following is specific for Smt3 and due to their function in sumoylation a number of these enzymes is required for viability (Dohmen, 2004). In principle, sumoylation involves activity of the SUMO-activating enzyme (E1), the SUMO-conjugating enzyme (E2) and a SUMO-ligase (E3).

After the maturation of Smt3, the C-terminal glycine of Smt3 forms a thioester bond with the SUMO-activating enzyme in an ATP-dependent mechanism. The E1 for Smt3 is a heterodimer of Uba2 and Aos1, both of which are essential for viability and together resemble the structure of the ubiquitin-activating enzyme Uba1. The Uba2 subunit bears the active site cysteine that performs Smt3 activation (Dohmen et al., 1995; Johnson et al., 1997).

After its activation, SUMO is transferred from the E1 to the SUMO-conjugating enzyme Ubc9 and another thioester is formed. Since Ubc9 is the only SUMO-conjugating enzyme, it is essential for viability (Johnson and Blobel, 1997). An interesting ability of Ubc9 is the direct transfer of Smt3 to the lysine residue of a substrate protein so that the C-terminal glycine of Smt3 forms an isopeptide bond to a substrate's lysine residue. Direct interaction of Ubc9 with a substrate involves binding of Ubc9 to a sumoylation consensus motif (Bernier-Villamor et al., 2002). Still, sumoylation of a substrate occurs much more efficiently with cooperation of a SUMO-ligase (Lin et al., 2002). It was shown that Ubc9 can undergo auto-sumoylation at lysine residues K153 and K157, two non-consensus sumoylation sites, which are close to the C-terminus. This auto-sumoylation was described as a negative regulator for the sumoylation of septins and probably also other substrates (Ho et al., 2011). It was hypothesized that auto-sumoylation of Ubc9 interferes with non-covalent interaction of Ubc9 and SUMO, which usually promotes chain formation (Ho et al., 2011; Knipscheer et al., 2007). Moreover, it was proposed that the binding of E1, which normally binds to Ubc9 close to the SUMO-binding motif, is obstructed by auto-sumoylation of Ubc9 (Bencsath et al., 2002; Ho et al., 2011). Consistent with the fact, that most of the sumoylation occurs in the nucleus, E1 and E2 are mostly nuclear localized (Dohmen, 2004).

Although not essential for sumoylation *in vitro*, SUMO E3 ligases mediate the interaction between the E2 enzyme and the substrate and thereby facilitate transfer of SUMO to a substrate's lysine residue. By this activity, SUMO ligases also provide substrate specificity for sumoylation. In *S. cerevisiae*, Siz1, Siz2/Nfi1, Mms21 and Zip3/Cst9 have been described as SUMO ligases (Jalal et al., 2017). Siz1 was found to be the

main enzyme mediating sumoylation of septins and it is localized mainly to the mother side of the bud neck in M-phase (Johnson and Gupta, 2001). This coincides with the sumoylation of septins, which occurs primarily on the mother side of the bud neck during mitosis, as well (Johnson and Blobel, 1999). Furthermore, it was demonstrated that Siz1 physically interacts with Ubc9 and Cdc11 (Takahashi et al., 2001). Interestingly, it was additionally shown that overexpression of Siz1 had a negative effect on septin sumoylation (Takahashi et al., 2001), which is an example for paradoxical behavior of substrate sumoylation as a consequence of changes in the SUMO conjugation system. This paradoxical outcome might explain the finding of Siz1 as a multi-copy suppressor of a *ulp2* mutant, which is devoid of this chain-processing SUMO specific protease (Strunnikov et al., 2001; Takahashi et al., 2001). This is particularly interesting since in this thesis, the septin Cdc11 showed paradoxical behavior as a result of the expression of specific SUMO variants (chapter 2.2.2). Siz1 and Siz2 are very similar, including their RING-like domain (also termed SP-RING (Siz/PIAS RING) (Dohmen, 2004)) and their SUMO interacting sequence. However, Western Blots revealed that the majority of septin sumoylation is performed by Siz1 and not Siz2 (Takahashi et al., 2001). In contrast, for example Top2 is sumoylated even if either Siz1 or Siz2 is absent but not in the double deletion mutant *siz1*Δ *siz2*Δ, suggesting that both E3 ligases are able to perform Top2 sumoylation (Reindle et al., 2006). Single deletions of the individual genes do not cause a strong phenotype but the simultaneous deletion of *SIZ1* and *SIZ2* causes a growth defect (Takahashi et al., 2001).

Mms21 was identified as subunit of an eight-protein complex, which is involved in DNA repair. In principle, Mms21 is essential for viability, however, this is not due to its activity as SUMO ligase since point mutations inactivating the ligase function are not lethal but cause sensitivity to DNA damage (Zhao and Blobel, 2005). Nevertheless, such an SP-RING domain mutant of *MMS21*, which allows growth in either *siz1*Δ or *siz2*Δ, is synthetically lethal with *siz1*Δ *siz2*Δ, indicating that the three SUMO ligases share a common essential function. An example of a substrate that can be sumoylated by Siz ligases and Mms21 is Net1 (Reindle et al., 2006). This fits well with the finding that mass spectrometry has revealed a large number of different sumoylation sites in Net1, as detailed in the results section. The fourth SUMO ligase identified in *S. cerevisiae* is Zip3/Cst9 which is involved in sumoylation at chromosomes during meiosis (Cheng et al., 2006).

1.3.3 Negative regulation of sumoylation

Two principle mechanisms have been described for the negative control of sumoylation. The first one is the cleavage of SUMO moieties from substrate proteins. This of course means that the substrate itself and also the removed SUMO are still present in the cell. The second general mechanism counteracting

sumoylation is the ubiquitylation and proteasomal degradation of SUMO-substrates. This process is intrinsically irreversible so that the substrate is not only desumoylated but removed from the pool of proteins (Miteva et al., 2010). Both mechanisms are described in the following.

1.3.3.1 Desumoylating enzymes

Three desumoylating enzymes have been described for *S. cerevisiae*, namely Ulp1 (UbL-specific protease 1), Ulp2 and Wss1 (weak suppressor of Smt3 1) (Hickey et al., 2012). However, after its first classification as SUMO-dependent isopeptidase (Mullen et al., 2010), such an activity of Wss1 was contradicted and instead, it was characterized as DNA-dependent protease (Stingele et al., 2014).

For humans, in total nine enzymes with desumoylating activity have been found (Jia et al., 2019). The initially described six desumoylating enzymes in mammals belong to the group of SENPs (sentrin-specific proteases), which have homology to Ulp1 from yeast. In 2012, a second group of mammalian desumoylating enzymes was described, consisting of DeSI-1 (DeSumoylating Isopeptidase 1) and DeSI-2 (Shin et al., 2012). In the same year, another desumoylating enzyme for mammals, belonging to a different group than the previously found ones, was described as USPL-1 (ubiquitin-specific protease-like 1) (Schulz et al., 2012).

1.3.3.1.1 Ulp1

The very first discovery of a SUMO-specific protease was made in *S. cerevisiae* with Ulp1 (Li and Hochstrasser, 1999). Ulp1 is required for the cleavage of the C-terminal –ATY of Smt3, a process termed maturation. Due to this essential function in the process of sumoylation, it is not surprising that Ulp1 is essential for viability. Consistently, a strain lacking *ULP1* was viable when the cells expressed *SMT3* without C-terminal –ATY. Nevertheless, the respective strain had a very pronounced growth defect and grew only after 1-3 weeks of incubation, indicating that Ulp1 has functions in addition to Smt3 maturation (Li and Hochstrasser, 1999). Ulp1 is localized at nuclear pores by interaction with karyopherins. The expression of only the catalytic C-domain of Ulp1 is lethal since it is no longer restrained by interaction with the nuclear pore, which requires the N-terminal part of Ulp1. This lethal effect is caused by presence of Ulp1 in the nucleus, while its presence in the cytosol is not toxic but even rescues knockout of *ULP1*. These results might indicate that uncontrolled desumoylation of nuclear proteins by Ulp1 is lethal and that the function of Ulp1 does not strictly depend on its localization to the nuclear pore (Panse et al., 2003). Furthermore, during mitosis, Ulp1 is targeted to the septin ring and at the end of M-phase desumoylates septins (Elmore

et al., 2011; Makhnevych et al., 2007). Mechanistically speaking, Ulp1 cleaves SUMO moieties at any position in the chain, not necessarily beginning with the most distal one. Therefore, Ulp1 cleaves SUMO chains stochastically in an *endo* mode (Eckhoff and Dohmen, 2015).

1.3.3.1.2 Ulp2

In contrast to Ulp1, for Ulp2 a sequential (or *exo*) mode of action was shown, meaning that SUMO chains are depolymerized from the distal end (Eckhoff and Dohmen, 2015). Moreover, it was shown that at least three SUMO moieties are required for recruitment of Ulp2 to a SUMO chain and that the chain is cleaved down to two moieties which remain on the substrate. Therefore, it was proposed that Ulp2 plays a role in limiting the length of SUMO chains (Eckhoff and Dohmen, 2015). *In vivo*, Ulp2 seems to mediate desumoylation of specific substrates whereas Ulp1 is responsible for broad desumoylation of cellular SUMO substrates (Albuquerque et al., 2016, 2018). Another difference between both proteases is that in contrast to Ulp1's tethering to the nuclear pore, Ulp2 is present mainly in the nucleoplasm (Schwienhorst, et al. 2000; Kroetz et al., 2009; Panse et al., 2003).

Quantitative mass spectrometry has revealed that Ulp2 is especially involved in regulation of the sumoylation of proteins at the rDNA, the centromere and origins of DNA replication (Albuquerque et al., 2016). A well-studied role of Ulp2 is counteracting the sumoylation of proteins involved in rDNA (ribosomal DNA) silencing like the RENT (Regulator of nucleolar silencing and telophase exit) complex (Gillies et al., 2016). In this case, at least part of the specificity is provided by the shuttling factor Csm1 which mediates recruitment of Ulp2 to these loci (Liang et al., 2017). Desumoylation of factors present at rDNA prevents their ubiquitylation which otherwise would reduce binding of these proteins to rDNA and inhibit proper rDNA silencing (Dhingra and Zhao, 2017; Gillies et al., 2016). Consistently, deletion of the subunit *SLX5* of Uls2 (ubiquitin ligase for sumoylated proteins 2) could rescue some of the phenotypes of *ulp2*Δ. Among these sumoylated proteins at the rDNA are Net1, Tof2 and Fob1 (Gillies et al., 2016). Since the sumoylation of Net1 is discussed in the course of the mass spectrometry analysis in this thesis, more details of sumoylation and its regulation at the rDNA are described in the respective section (see chapter 2.4.2).

Another process involving the function of Ulp2 is the control of sumoylation at kinetochores. Ulp2 is targeted to the CMM (Ctf3-Mcm16-Mcm22) complex via Ulp2's CCR (C-terminal conserved region). There, it targets sumoylated subunits of the kinetochore via its SIM. Single mutations affecting either kinetochore-targeting or binding to SUMO caused an increased rate of chromosome loss and this effect was much stronger in a mutant that is impaired in both interactions, namely *ulp2-SIM^{3A}CCR^{3A}* (Suhandynata et al., 2019). This example, like the previously mentioned function of Csm1, highlights

substrate-specific recruitment of Ulp2. Similar to the *ulp2-SIM^{3A}CCR^{3A}* mutant, the strain *smt3-KallR* had an elevated chromosome loss rate, however, a *ulp2-SIM^{3A}CCR^{3A} smt3-KallR* double mutant prevented most of the chromosome loss observed in the single mutants. This suggests that the exact levels of sumoylation at the kinetochore are crucial for prevention of chromosome loss (Suhandynata et al., 2019).

An interesting phenotype of *ulp2*Δ is the development of a specific aneuploidy, the doubling of chromosome numbers of chromosomes I and XII (Ryu et al., 2016). This aneuploidy could be reversed by re-introduction of *ULP2* (Ryu et al., 2016) or extended passaging, the latter of which led to acquired mutations in genes promoting sumoylation, such as *UBA2*, *AOS1* or *UBC9* as a long-term adaptation (Ryu et al., 2018). The aneuploidy itself is a short-term adaptation allowing increased dosage of specific proteins, among them the Ccr4 deadenylase on chromosome I (Ryu et al., 2018).

1.3.3.2 Ubiquitin ligases for sumoylated proteins

The second principle mechanism for negative control of sumoylation is the targeting of SUMO substrates by ULS (ubiquitin ligases for sumoylated proteins), also termed STUbLs (SUMO-targeted ubiquitin ligases). Since their first characterization in 2007 (Cheng et al., 2007; Prudden et al., 2007; Sun et al., 2007; Uzunova et al., 2007; Xie et al., 2007), a number of ULS in various organisms have been described. Among the first described ULS are Uls1 and the heterodimeric Uls2 (Slx5-Slx8) from budding yeast (Mullen and Brill, 2008; Uzunova et al., 2007; Xie et al., 2007). Another ULS from *S. cerevisiae* is Rad18, which is known for ubiquitylation of sumoylated PCNA (Parker and Ulrich, 2012). In the same year as Uls1 and Uls2, a ULS in *S. pombe* was described, which is composed of Slx8 (orthologue of budding yeast Slx8) and either Rfp1 or Rfp2. Rfp1 and Rfp2 in turn are orthologues of human RNF4, and it was shown that RNF4 is able to complement for Slx8-Rfp1/2 mutants in *S. pombe* (Prudden et al., 2007; Sun et al., 2007) and for either Slx5 or Slx8 in *S. cerevisiae* (Uzunova et al., 2007). In the following year, several studies demonstrated that arsenic trioxide stimulates SUMO2/3 modification of PML (promyelocytic leukemia) and that this leads to targeting and ubiquitylation of PML by RNF4, which in turn causes proteolysis of PML (Lallemand-Breitenbach et al., 2008; Tatham et al., 2008; Weisshaar et al., 2008). An early discovery of a ULS in human cells was the VHL (von Hippel-Lindau) protein. HIF1α (hypoxia-inducible factor 1α) becomes sumoylated upon hypoxia and this sumoylation leads to recognition and ubiquitylation by VHL, ultimately resulting in proteasomal degradation. Interestingly, SENP1 counteracts sumoylation of HIF1α and thereby prevents it from being degraded (Cheng et al., 2007). Moreover, it was found that VHL is a substrate recognition subunit of a Cullin RING ubiquitin ligase complex (Girardini et al., 2019). This example illustrates how both, a SUMO-specific protease and a ULS, function together in regulation of the abundance of a sumoylated

substrate. Recently, a novel specificity of a human ULS was described. The ULS Arkadia/RNF111 specifically recognizes SUMO2/3 chains that have been capped by SUMO1, the latter of which does generally not promote further chain elongation. This finding demonstrates a chain-type specificity of a human ULS (Sriramachandran et al., 2019). Overall, common features of ULS are the presence of a RING-domain and at least one SIM for the recognition of sumoylated proteins (Sriramachandran and Dohmen, 2014). After mentioning various examples of ULS in yeast and mammals, in the following, the budding yeast enzymes Uls1 and Uls2 are introduced in more detail. In ***Figure 1.3***, the process of targeting of a sumoylated protein by ULS is illustrated.

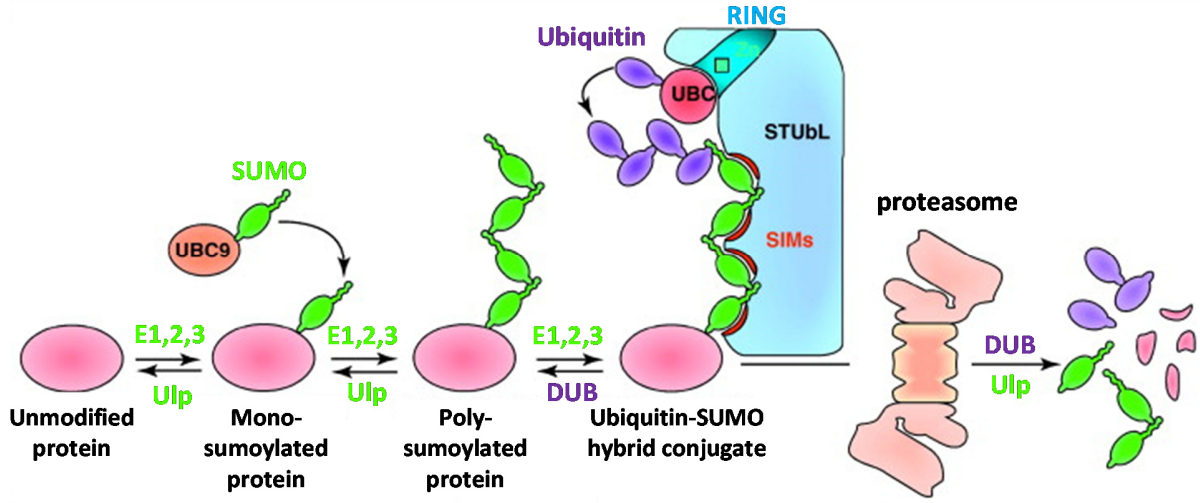

Figure 1.3: Targeting of a sumoylated protein by a STUbL/ULS
A SUMO substrate is sumoylated by the activity of E1 (Uba2/Aos1), E2 (Ubc9) and a SUMO E3 ligase. By repetition of sumoylation, a SUMO chain is formed which causes the targeting by a STUbL/ULS (SUMO-targeted ubiquitin ligase/ubiquitin ligase for sumoylated proteins) via multiple SIMs (SUMO-interaction motifs). The ULS recruits a UBC (ubiquitin-conjugating enzyme) via the RING (really interesting new gene) domain and ubiquitin is transferred usually to the distal SUMO moiety. The ubiquitylated substrate is targeted to the proteasome and after deubiquitylation (and presumably desumoylation) degraded. Sumoylation and deubiquitylation are reversible by the activity of Ulp (UbL-specific protease) enzymes and DUBs (deubiquitylating enzymes), respectively. Figure taken and modified from Praefcke et al., 2012.

1.3.3.2.1 Uls1

Uls1 was first described as ULS when it was discovered that a deletion of *ULS1* caused the accumulation of HMW SUMO conjugates. The same was true for a deletion of *SLX5* and the effect was enhanced in a strain lacking both enzymes, Uls1 and Slx5, so that it was suggested that Uls1 and Uls2 have overlapping function. In the same study, it was proposed that Uls1 and Uls2 interact with either of the ubiquitin E2 enzymes Ubc4 or Ubc5 for ubiquitylation of sumoylated proteins (Uzunova et al., 2007). As typical for ULS enzymes, Uls1 has a RING-domain in its C-terminal region and four SIMs in its N-terminal half. In between,

it possesses a Swi2/Snf2-like translocase motif (Sriramachandran and Dohmen, 2014). Uls1 is primarily localized in the nucleoplasm and the nucleolus (Shirai and Mizuta, 2008).

One function of Uls1, involving its function as Swi2/Snf2-like translocase, is the removal of toxic Rad51-DNA complexes. Rad51 is a recombinase that functions in meiotic and mitotic recombination which plays a role in high-fidelity repair. However, Rad51 also spontaneously binds to undamaged chromatin, which causes genomic instability. Rdh54 removes these spontaneous Rad51-DNA complexes, while Rad54 primarily removes Rad51 from damage-associated foci. Like Uls1, Rdh54 and Rad54 are Swi2/Snf2-like translocases and it was shown that Rad54 and Uls1 are able to substitute for Rdh54 in removal of toxic non-damage associated Rad51-DNA complexes (Shah et al., 2010). However, it was not clarified if the Swi2/Snf2 related functions of Uls1 require its SIMs (Sriramachandran and Dohmen, 2014).

In contrast to Uls1's role as a ubiquitin ligase for the degradation of sumoylated proteins (Uzunova et al., 2007), the *S. pombe* homolog of Uls1, Rrp2, was shown to stabilize sumoylated Top2 and to protect it from ULS-dependent degradation by Rfp1/2-Slx8 (Wei et al., 2017). In principle, this goes in line with the observation that the overexpression of SIM-containing proteins, like Uls1 and Slx5, stabilized HMW SUMO conjugates *in vivo*. Here, it has to be mentioned that, in this case, due to their application in a yeast two-hybrid assay, Uls1 and Slx5 were fused to GAD (Gal4 activation domain) and that both proteins lacked their RING-domain (Uzunova et al., 2007). Still, it seems plausible that under certain circumstances SIM-containing proteins protect polysumoylated substrates from degradation and, as seen for Rrp2, this can even be contrary to the proposed role as ULS. Furthermore, a recent study demonstrated that Uls1 interacts with the sumoylated form of the nuclease Yen1, but does not regulate its steady state levels (Bauer et al., 2019).

1.3.3.2.2 Uls2

Uls2 is a heterodimer composed of Slx5 and Slx8. Both subunits contain RING domains and Slx5 bears several SIMs, while Slx8 has only one SIM (Sriramachandran and Dohmen, 2014; Uzunova et al., 2007). The function of Uls2 as ULS was described in two publications in 2007 (Uzunova et al., 2007; Xie et al., 2007). It appears that within the complex, Slx8 provides the main function as ubiquitin ligase, while Slx5 with its several SIMs mediates interaction with sumoylated substrates (Xie et al., 2007). As demonstrated with the substrate Siz2, multi-sumoylation was not sufficient for efficient targeting by Uls2 whereas poly-sumoylated Siz2 was ubiquitylated by Uls2, primarily at the most distal SUMO moiety (Mullen and Brill, 2008). In our laboratory, by application of translational fusion proteins containing SUMO chains of

different lengths and GFP, it was demonstrated that a chain of two Smt3 moieties is the minimal signal for targeting by Uls2 leading to its degradation (Lennard-Maximilian Döring, Master Thesis, 2017). As noted above, Ulp2 cleaves SUMO chains down to two SUMO moieties (Eckhoff and Dohmen, 2015). Taken together, these results suggest that even after cleavage by Ulp2, SUMO substrates can be targeted by Uls2. Interestingly, the same substrates were not efficiently degraded via Uls1 (Lennard-Maximilian Döring, Master Thesis, 2017).

On a macroscopic scale, a typical phenotype of *slx5*Δ and *slx8*Δ is that streak outs give rise to very heterogeneous colony sizes (Mullen et al., 2001) and that these colonies have jagged edges, a phenotype termed "nibbled". This phenotype is often associated with a misregulation of 2µ-plasmid copy number in mutants of the SUMO system (Chen et al., 2005; Ii et al., 2007). The "nibbled" phenotype is a consequence of the presence of slow growing cells with clonal lethality (Ii et al., 2007). On a microscopic scale, these mutants suffer from mitotic defects, such as aneuploidies, reflecting the centromere-specific functions of Uls2 (van de Pasch et al., 2013), and GCRs (gross chromosomal rearrangements) (Zhang et al., 2006). These observations fit well with the fact that *SLX5* and *SLX8* were initially discovered as essential genes in the absence of the DNA helicase Sgs1, which itself is required for genome stability (Mullen et al., 2001). Recently, it was found that Uls2 is present at specific genomic loci and that the ULS-dependent ubiquitylation at these sites serves as stress adaptation (Höpfler et al., 2019). Other processes involving the function of Uls2 are the translocation of double strand breaks to nuclear pores, which regulates DNA repair (Horigome et al., 2016), ubiquitylation of proteins in proximity to the rDNA (as discussed in chapter 2.4.2) (Gillies et al., 2016), and quality control of nuclear proteins like a mutant version of the transcription factor Mot1 (Wang and Prelich, 2009). Interestingly, Uls1 and Slx5 directly interact with each other and this interaction negatively regulates the function of Slx5 (Tan et al., 2013). Overall, it can be summarized that Uls2 has a wide variety of functions and most of these appear to be related to genome stability.

1.4 Mitochondrial dynamics

Mitochondria are most commonly known for their major role in supplying eukaryotic cells with energy in the form of ATP (adenosine triphosphate) by action of the TCA (tricarboxylic acid) cycle and OXPHOS (oxidative phosphorylation). Hence, mitochondria are often referred to as the powerhouses of the cell. However, in the course of time, it became clear that mitochondria are involved in a large number of additional physiological processes, such as apoptosis, autophagy, redox signaling and calcium homeostasis (Tilokani et al., 2018). Mitochondria have evolved from a bacterial ancestor and became endosymbionts

(Gray et al., 1999) so that these organelles have two membranes, the IMM (inner mitochondrial membrane) and the OMM (outer mitochondrial membrane). Between these two, the IMS (intermembrane space) is located and the space surrounded by the IMM is termed mitochondrial matrix (Malina et al., 2018). The matrix and the IMM harbor most of the mitochondrial proteins (Vögtle et al., 2011). For example, the TCA cycle takes place in the matrix (Scagliola et al., 2020) and the respiratory chain, which generates ATP by OXPHOS is located at the IMM, more specifically in cristae which are folds of the IMM (Cogliati et al., 2013). Mitochondria are found in almost all eukaryotic cells and are in general essential for viability, as it is the case in *S. cerevisiae*. Budding yeast does not depend on OXPHOS for viability as the metabolism can be sustained by alcoholic fermentation. Nonetheless, yeast cells are not viable without mitochondria because the function of mitochondria in Fe/S (iron-sulfur) cluster synthesis is essential (Kispal et al., 2005). Additionally, mitochondria play important roles in many more processes. These are for example amino acid and lipid metabolism, as well as heme synthesis (Malina et al., 2018). After giving a short overview of mitochondria, in the following the introduction focuses on two specific aspects of mitochondrial biology, namely mtDNA (mitochondrial DNA) and mitochondrial dynamics.

1.4.1 Mitochondrial DNA

The mitochondrial genome is encoded on mostly linear but in some copies circular mtDNA located in the matrix. The circular molecules of mtDNA are thought to serve as templates for replication via a rolling circle mechanism (Maleszka et al., 1991; Westermann, 2014). In *S. cerevisiae*, mtDNA is organized in 10 – 40 nucleoids per cell with several mtDNA copies per nucleoid (Westermann, 2014). A circular mtDNA copy has a length of 85.6 kb (kilobases), while linear mtDNA is present in concatemers with variable lengths (Westermann, 2014). Together, the mtDNA molecules represent approximately 15% of the cellular DNA content (Malina et al., 2018). In budding yeast, mtDNA encodes only eight proteins, 24 tRNAs (transfer RNAs), and two rRNAs (ribosomal RNAs). Seven of these eight proteins are components of OXPHOS complexes and one is a ribosomal subunit (Malina et al., 2018). In *S. cerevisiae*, mtDNA is replicated by the mitochondrial DNA polymerase Mip1, an ortholog of human POLG (polymerase gamma), and transcription is performed by the mitochondrial RNA polymerase Rpo41 in cooperation with the transcription factor Mtf1 (Tang et al., 2011). Translation is carried out by the specialized mito-ribosome (Desai et al., 2017). However, except for the abovementioned eight proteins, all other genes, encoding the ~ 1000 mitochondrial proteins (Vögtle et al., 2017), have been transferred to the nucleus in the course of evolution and the gene products are synthesized in the cytosol (Malina et al., 2018). For these proteins, mitochondria have import systems in their membranes. For the OMM, this is the TOM (translocase of the

outer membrane) complex, and for the IMM these are two different TIM (translocase of the outer membrane) complexes. TIM22 binds to substrates destined for the IMM while TIM23 transports substrates into the matrix. Additionally, the SAM (sorting and assembly machinery) complex mediates translocation of previously imported proteins from the IMS into the OMM (Dolezal et al., 2006). In budding yeast, mtDNA is not essential for viability, consistent with the fact that cells do not completely depend on OXPHOS for growth. Therefore, cells can lose mtDNA and the resulting strain, devoid of mtDNA is denoted as ρ^0 (rho^0). Strains with mutant, dysfunctional mtDNA are labeled as ρ^- (rho$^-$) (Dunn et al., 2006). In either case, mitochondria as such are still inherited and essential for viability. Yeast that is either ρ^0 or ρ^- is termed *petite* due to the fact that the respective colonies are smaller than those of wild type (Contamine and Picard, 2000; Malina et al., 2018). Moreover, *petite* yeast requires a fermentable carbon source for growth (Dunn et al., 2006).

1.4.2 Mitochondrial fusion and fission

Mitochondria are highly dynamic organelles forming a network with constant fusion and fission. A central role of these processes is the organellar quality control. While the fusion of mitochondria allows content mixing and repair of damaged mitochondria, fission separates damaged mitochondria from the network so that these can be eliminated by mitophagy (Braun and Westermann, 2011). However, it was proposed that fission is not absolutely required for mitophagy (Mendl et al., 2011). By fusion, in contrast, differently damaged mtDNAs can complement each other. This is particularly important since, among other reasons, due to exposure to ROS (reactive oxygen species) mtDNA has a ten times higher mutation rate than nuclear DNA (Sato et al., 2006). Furthermore, the mitochondrial network is dynamically shaped in response to the metabolic needs of the cell. Metabolically highly active cells generally have an extended network, while in non-dividing cells, mitochondria are fragmented. Moreover, fission allows inheritance of mitochondria and plays a role in apoptosis, even in yeast, which points to conservation of this process (Braun and Westermann, 2011; Fannjiang et al., 2004). Fusion of the OMM is performed by the mitofusin Fzo1 while the IMM fusion is carried out by Mgm1 and both processes are coordinated by Ugo1 (Westermann, 2008). The function and abundance of Fzo1 are governed by a complex regulation involving ubiquitylation and its deconjugation. The E3 ligase SCF^{MDM30} ubiquitylates Fzo1 in a way that promotes its function in fusion of the OMM whereas another, unknown, ligase ubiquitylates Fzo1 for degradation. The DUB Ubp12 counteracts fusion-promoting ubiquitylation and Ubp2 removes degradation-promoting ubiquitylation. The ubiquitin-selective chaperone Cdc48 in turn regulates the activities of these two DUBs (Anton et al., 2013; Simões et al., 2018). This example demonstrates the fine-tuning of mitochondrial dynamics by a PTM

of the ubiquitin family in *S. cerevisiae*. The key enzyme for mitochondrial fission in yeast is Dnm1, which will be discussed in more detail below. As one can expect, *fzo1*Δ cells have very fragmented mitochondria whereas *dnm1*Δ cells have a very condensed highly interconnected mitochondrial network (Sesaki and Jensen, 1999). Moreover, the lack of fusion in *fzo1*Δ causes a *petite* phenotype in this strain (Rapaport et al., 1998). In contrast, the *dnm1*Δ *fzo1*Δ double mutant is not generally *petite* but still exhibits phenotypes, which can be attributed to the deficiency in mitochondrial dynamics. For example, *dnm1*Δ *fzo1*Δ has a high rate of *petite* formation due to an increase in the number of dysfunctional, structurally impaired mtDNA (Osman et al., 2015). Furthermore, the strain *dnm1*Δ *mgm1*Δ shows impaired respiration, higher stress sensitivity, decreased mitophagy and reduced lifespan (Bernhardt et al., 2015).

1.4.3 The mitochondrial fission enzymes Dnm1 in yeast and Drp1 in humans

In 1998, it was first described that the dynamin-related GTPase Dnm1 is required for normal mitochondrial morphology (Otsuga et al., 1998). Shortly after, its role in antagonizing Fzo1 was discovered, and Dnm1 was described as a mediator for mitochondrial fission (Bleazard et al., 1999; Sesaki and Jensen, 1999). Other three key enzymes for mitochondrial fission are Fis1, Mdv1 and Caf4. Fis1 is evenly located in the OMM with the N-terminus exposed into the cytoplasm (Mozdy et al., 2000) and via a TPR (tetratricopeptide repeat) domain interacts with either of the two cytosolic proteins Mdv1 or Caf4 (Zhang and Chan, 2007). One of the adaptors Mdv1 or Caf4, which are mostly redundant, binds to Fis1 with its N-terminal helices and recruits Dnm1 with the adaptor's WD40 domain so that Dnm1 is targeted to the OMM (Zhang and Chan, 2007). Dnm1 itself contains four major domains, namely the GTPase domain, the middle domain, which promotes oligomerization, the insert B domain, and the GED (GTPase effector domain). Mdm33 is an integral protein of the inner membrane and supports mitochondrial fission but is not absolutely essential for this process (Klecker et al., 2015). The main enzymes involved in mitochondrial fission and fusion are illustrated in ***Figure 1.4***.

By cryo-EM (cryo electron microscopy), Mears and colleagues could show that Dnm1 assembles into helical tubes around lipid bilayers and that, by conformational changes of Dnm1, these helices undergo constriction when GTP is added. The helix that is formed by Dnm1 is in fact a 2-start helix, meaning that two strands (or filaments) of the helix are wound around each other so that Dnm1 molecules laterally interact with molecules of another strand. In a ratchet movement, both strands perform a sliding motion and constrict the membrane below.

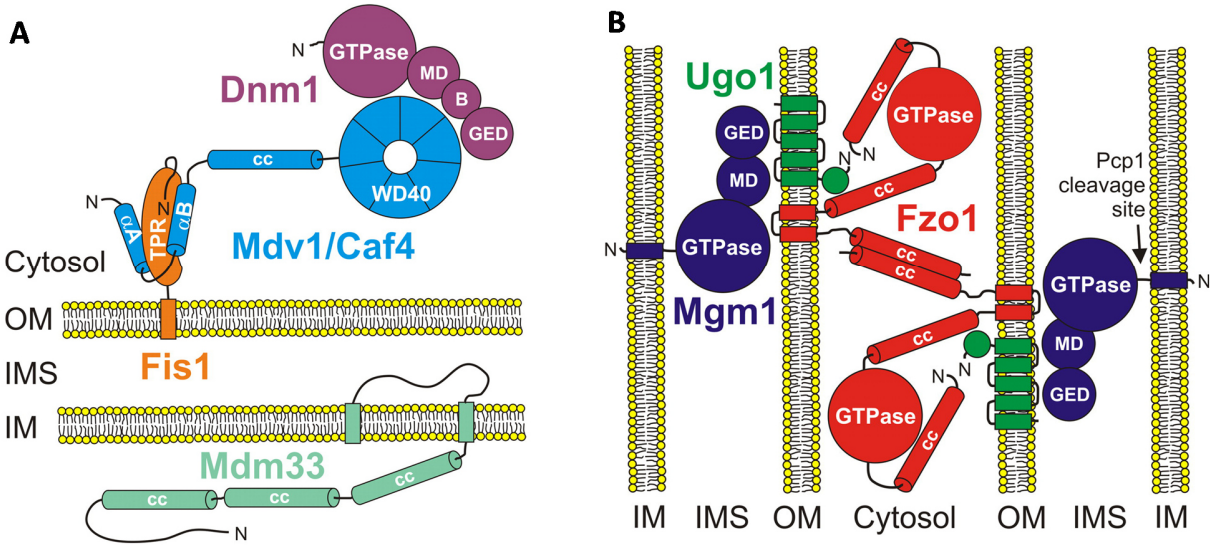

Figure 1.4: The key enzymes in mitochondrial fission und fusion in budding yeast
A) The key enzymes for mitochondrial fission at the OM are the mitochondrial anchor Fis1, the adaptor Mdv1/Caf4 and the GTPase Dnm1. A supporting enzyme located in the IM is Mdm33. **B)** The key enzyme for outer membrane fusion is Fzo1, while Mgm1 mediates inner membrane fusion. The protease Pcp1 is able to remove the transmembrane domain from Mgm1. Ugo1 coordinates both processes. MD: middle domain, B: insert B, GED: GTPase effector domain, CC: coiled coil, TPR: tetratricopeptide repeat, OM: outer membrane, IMS: intermembrane space, IM: inner membrane. Figures A) and B) were taken from Westermann, 2008.

In vitro, the authors observed release of Dnm1 from the lipids after GTP hydrolysis and constriction, however, it was suggested that, *in vivo*, Mdv1 may tether Dnm1 to the OMM and allow several consecutive rounds of constriction (Mears et al., 2011). *In silico* analysis confirmed that the Dnm1 molecule is optimized to induce membrane curvature (Lee et al., 2017).

In addition to the previously mentioned enzymes for fission, it was shown that a protein complex consisting of Dnm1, Mdm36 and Num1 is located at the cell cortex and required for efficient mitochondrial division (Hammermeister et al., 2010). As previously mentioned, it was suggested that Blm10-associated proteasomes are required for the negative control of Dnm1 levels which otherwise cause excessive fragmentation of mitochondria (Tar et al., 2014). This directly links Dnm1 to the UPS.

Furthermore, initial results from our laboratory have demonstrated a possible link between mitochondrial dynamics and the SUMO system. It was observed that yeast strains with a defect in the negative control of sumoylation, such as *uls1*Δ *slx5*Δ and *ulp2*Δ, frequently have fragmented mitochondria. Conversely, strains with a defect in sumoylation had a more extended mitochondrial network than the wild type. *uls1*Δ *slx5*Δ *dnm1*Δ had highly interconnected mitochondria, as typical for *dnm1*Δ (Christian Pichlo, Bachelor Thesis, 2011). Together, these findings led to the preliminary hypothesis that sumoylation of Dnm1 might stimulate fission, and that ULS and Ulp2 are required for a negative control of sumoylated Dnm1.

For humans, the sumoylation of the Dnm1 ortholog Drp1 has been described in 2004 (Harder et al., 2004) and since then, its role in fission has been extensively studied. One of these studies demonstrated that SENP5 is required for the negative regulation of sumoylated Drp1, as seen by the fact that silencing of SENP5 caused mitochondrial fragmentation (Zunino et al., 2007). Sumoylation of Drp1 is performed by the mitochondrial SUMO ligase MAPL (mitochondrial anchored protein ligase) (Braschi et al., 2009), however in yeast, a mitochondria-anchored SUMO ligase has not been found so far. The MAPL-mediated sumoylation of Drp1 stabilizes mitochondria/ER (endoplasmic reticulum) contacts. This platform is required for mitochondrial constriction, calcium influx into mitochondria, cristae remodeling and cytochrome C release, processes that are involved in apoptosis (Prudent et al., 2015). Not directly related to Drp1, but still interesting, is the fact that even in mitochondria, sumoylated Sirt3 was found and that this substrate is regulated by SENP1 (Wang et al., 2019). This finding demonstrates that at least in human cells, in principle sumoylated proteins can be present inside of mitochondria.

Altogether, the findings of mitochondrial fragmentation in *uls1*Δ *slx5*Δ and the well-documented role of sumoylated Drp1 in mitochondrial fission in humans was the motivation to ask if in yeast Dnm1 is sumoylated and if so, whether this plays a role in mitochondrial dynamics. The putative control of mitochondrial dynamics by ULS would be an aspect that has so far not been described for human cells and would constitute a novel type of regulation for mitochondrial dynamics.

1.5 Aims

Previous experiments from our laboratory led to the working hypothesis that Dnm1 might be a SUMO substrate and that this sumoylation promotes mitochondrial fission. The observation of mitochondrial fragmentation in *uls1*Δ *slx5*Δ and *ulp2*Δ was consequently explained as a lack of control of sumoylated Dnm1. However, this hypothesis was mainly based on these microscopical observations and only preliminary experiments pointed towards a post-translational modification of Dnm1. Furthermore, also mitochondrial proteins other than Dnm1 might provide a link to the SUMO system. Motivated by the starting question if Dnm1 is sumoylated and ubiquitylated, in this study methods for the investigation of a possible connection between sumoylation and mitochondrial dynamics were established and refined. Therefore, this possible link was examined from different perspectives, like the specific detection of PTMs, as exemplified for Dnm1, or physiological interactions between the SUMO system and mitochondria. For this reason, the following results section is subdivided according to the experimental approaches that were

developed and employed to analyze these issues as noted in the following with the respective chapter indicated in brackets.

- determination of the influence of the UPS and sumoylation on steady state protein levels (2.1)
- application of engineered SUMO variants for facilitating detection of sumoylated proteins (2.2)
- establishment of a protocol for denaturing purification of SUMO and ubiquitin conjugates (2.3)
- mass spectrometry for the identification of SUMO substrates and sumoylation sites (2.4)
- respiratory competence of yeast impaired in mitochondrial dynamics and control of sumoylation (2.5)
- microscopy of protein localization and mitochondrial morphology in SUMO system mutants (2.6)

2 Results

2.1 Degradation of Dnm1 via the ubiquitin-proteasome system

2.1.1 Degradation of Dnm1 is compromised in ubiquitylation-deficient strain

In earlier studies, it was already shown that the human ortholog of Dnm1, termed Drp1, is sumoylated (Harder et al., 2004; Wasiak et al., 2007; Zunino et al., 2007) and that this modification controls mitochondrial fission (Braschi et al., 2009; Guo et al., 2013; Prudent et al., 2015). These reports prompted our group to investigate mitochondrial morphology in mutants with defects in SUMO conjugation or the control of SUMO conjugation in the model organism *Saccharomyces cerevisiae*. It could be shown that in yeast strains defective in the control of sumoylation, the mitochondria displayed a fragmentation phenotype (Christian Pichlo, Bachelor Thesis, 2011). At the same time, indications for a more interconnected mitochondrial network in strains with defects in SUMO conjugation were found (Christian Pichlo, Bachelor Thesis, 2011). This led to the hypothesis that, in yeast, sumoylation is generally a driver for mitochondrial fission, presumably by modification of enzymes which are part of the fission machinery. Regarding the previously mentioned reports, Dnm1 was a possible candidate for a SUMO target driving mitochondrial fission in yeast. Consequently, lack of control of sumoylated Dnm1 might explain mitochondrial fragmentation in *uls1*Δ *slx5*Δ and *ulp2*Δ mutants.

One step in order to test this hypothesis was to evaluate if Dnm1 levels change upon inhibition of sumoylation or ubiquitylation, since control by a ULS (ubiquitin ligase for sumoylated proteins) would require consecutive attachment of both modifiers to Dnm1. For this purpose, C-terminally 2HA-tagged Dnm1 was expressed in a *uba1-ts* mutant strain, which is impaired in ubiquitylation and *uba2-ts* mutants, impaired in sumoylation. In a previous study, it could already be shown that Dnm1 levels are increased in *uba1-ts* at 25°C (2-fold) and even more upon a 3.5 hours heat shock at 37°C (2.6-fold) (Stefan Pabst, Master Thesis, 2015). This already suggested that Dnm1 is likely a substrate for ubiquitin-dependent degradation. However, the increase of Dnm1 levels in *uba2-ts* mutants was less pronounced at 25°C (1.5-fold) and absent upon the heat shock (Stefan Pabst, Master Thesis, 2015). Since these results were obtained by application of plasmid-encoded Dnm1, which was overexpressed, in order to further analyze the degradation of Dnm1, yeast strains with a chromosomally encoded C-terminal 2HA-6His-tag on Dnm1 were constructed. This allowed analysis of Dnm1 at physiological steady state levels, which are ~8-fold below Dnm1 steady state levels when it is expressed from a plasmid under control of P_{CUP1} without copper induction (data not shown).

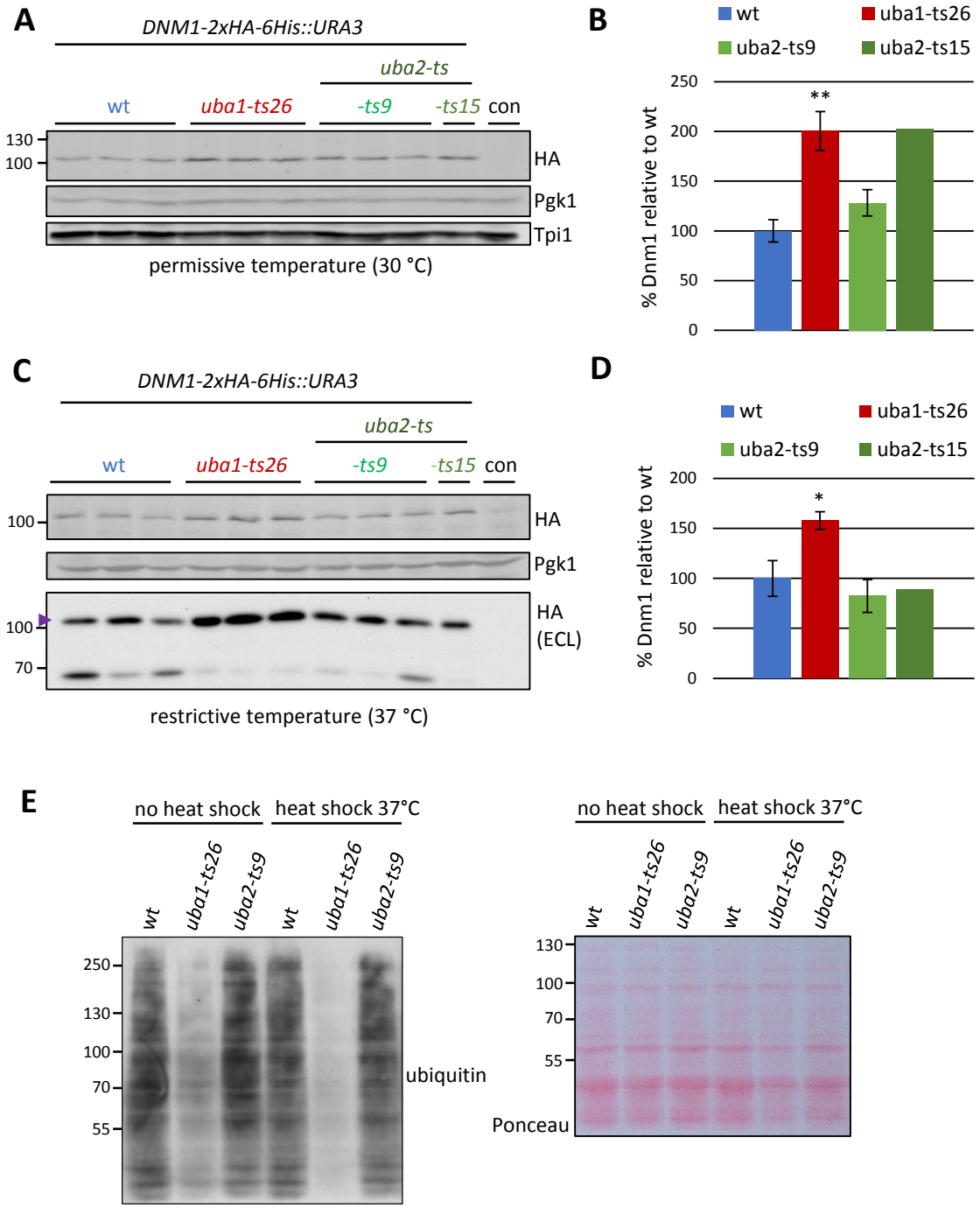

Figure 2.1: Increased Dnm1 levels upon proteasome inhibition

A) Western Blot analysis using 8% SDS-PAGE and semi-dry transfer onto a nitrocellulose membrane with 1.6 mA/cm² for 1.5 hours. The membrane was probed with anti-HA (3F10) (1:1000, rat), anti-Pgk1 (1:10000, mouse) and anti-Tpi1 (1:40000, rabbit) antibodies. Applied secondary antibodies were anti-rat 680, anti-mouse 800 and anti-rabbit 800. Bound fluorescent secondary antibodies were detected with an Odyssey scanner. Strains with *DNM1-2HA-6His* were YSP28 1-3 (wt), YSP29 1-3 (*uba1-ts26*), YSP30 1-3 (*uba2-ts9*) and YSP38 (*uba2-ts15*). Strain YSP31 served as a control without HA-tag. The cells were grown in SD -Ura at 30 °C. **B)** Statistical evaluation of the results in A) with relative Dnm1 levels in relation to Pgk1 and Tpi1 as loading controls (average of both loading controls). n=3 except for YSP38, where only one transformant was obtained. Statistical analysis was made with two-tailed, heteroscedastic t-test, *p<0.05; **p<0.01 **C)** Same as in A) with following changes: The primary antibodies used were anti-HA (3F10) (1:2000, rat) and anti-Pgk1 (1:5000, mouse) but no anti-Tpi1. As secondary antibodies, anti-rat 800 and anti-mouse 680 were used. Strain JD47-13C served as a control without HA-tag. All other strains were the same as used for A). Cells were grown in SD -Ura to exponential growth phase, then shifted to 37 °C for 3.5 hours. Lower panel: Western Blot analysis of the same samples, using 6% SDS-PAGE and semi-dry transfer onto a PVDF (polyvinylidene difluoride) membrane with 1.3 mA/cm² for 2 hours. As antibodies, anti-HA (3F10) (1:2000, rat) and anti-rat-POD were used. Bound secondary antibody was detected with Bio-Rad ECL (enhanced chemiluminescence) and X-ray film. The purple arrow indicates full length Dnm1. **D)** Statistical evaluation of the results obtained by Odyssey scan in C) with

relative Dnm1 levels in relation to Pgk1 as loading control. n=3 except for YSP38, where only one transformant was obtained. Statistical analysis was made with two-tailed, heteroscedastic t-test, *p<0.05; **p<0.01 **E)** Western Blot analysis using 8% SDS-PAGE and semi-dry transfer onto a PVDF membrane with 1.3 mA/cm² for 2 hours. The membrane was probed with anti-ubiquitin antibody (P4D1) (1:5000, mouse). As secondary antibody, anti-mouse-POD was used. Bound secondary antibody was detected with self-made ECL and X-ray film. Tested strains were YSP28-1 (wt), YSP29-1 (*uba1-ts26*) and YSP30-1 (*uba2-ts9*). The cells were grown in SD -Ura either at 30 °C or shifted to 37 °C for 3.5 hours before harvesting, as indicated. On the right, Ponceau-staining of the same membrane is shown.

This in turn avoids putative aggregate formation due to overexpression, a problem that might be particularly present when working with Dnm1, as specified below.

Analysis of Dnm1 levels in the ubiquitylation-deficient strain *uba1-ts26* and the sumoylation-deficient *uba2-ts* strains generally confirmed previous results from experiments with plasmid-encoded DNM1-2HA under control of P_{CUP1}. Here, it could be demonstrated that Dnm1 levels in *uba1-ts26* were indeed significantly increased at permissive temperature 25°C (2-fold) (***Figure 2.1*** A, B) and after heat shock at 37°C (1.6-fold) (***Figure 2.1*** C, D), which confirms previous results and suggests that ubiquitylation is involved in the degradation of Dnm1. The ubiquitylation deficiency in *uba1-ts* was confirmed by Western Blot and, as expected, this effect was even stronger at 37°C. In contrast, overall ubiquitylation in *uba2-ts* mutants was unchanged (***Figure 2.1*** E).

Dnm1 levels in *uba2-ts9* were slightly elevated at permissive temperature (1.3-fold) (***Figure 2.1*** A, B) and, although this effect is not statistically significant, taking into account previous results, it is still conceivable that a lack of sumoylation causes an increase in Dnm1 steady state levels. The analysis using the *uba2-ts15* mutant confirms these results (2-fold increase) (***Figure 2.1*** A, B). However, only one transformant of this genotype was tested. Similarly to results obtained with plasmid-encoded *DNM1-2HA*, at higher temperatures, the Dnm1 levels in *uba2-ts* were not elevated. Still, it is noticeable, that the amount of a putative Dnm1 degradation products at ~70 kDa is decreased in *uba1-ts* and *uba2-ts*, which might be a hint for altered degradation of Dnm1 in these mutants (***Figure 2.1*** C). Taken together, the results obtained with either plasmid-encoded or genomically tagged Dnm1-2HA suggest that ubiquitylation promotes degradation of Dnm1. Additionally, sumoylation might contribute to degradation of Dnm1, which is abrogated at higher temperatures. A possible explanation for the latter observation could be that at higher temperatures degradation of Dnm1 shifts to stress-related pathways. Pathways, which are important for the degradation of misfolded proteins after heat shock have been described already, for example a Ubr1- and Ubr2-mediated pathway (Nillegoda et al., 2010) or a Hul5-mediated pathway (Fang et al., 2011). Furthermore, a network of ubiquitin-ligases for protection against protein aggregates was described (Theodoraki et al., 2012). In a report by Wallace and colleagues, Dnm1 was described as one of ~170 proteins that aggregate upon heat shock (Wallace et al., 2015). Taken together, the current results from our group and reports from other groups suggest that Dnm1 is degraded via a ubiquitin-dependent pathway and it is subject to aggregation at high temperatures.

2.1.2 Stabilization of Dnm1 upon proteasome-inhibition

Prompted by the observation of elevated Dnm1 levels in *uba1-ts*, the steady state levels in additional strains were checked. Regarding the initial hypothesis that Dnm1 levels might be controlled by ULS enzymes, which mediate degradation of sumoylated proteins, it was obvious to analyze Dnm1 levels in the respective mutants. However, in none of these mutants, *uls1*Δ, *slx5*Δ or *uls1*Δ *slx5*Δ, increased Dnm1 levels were detected (data not shown). It has to be noted, that this observation does not necessarily exclude involvement of ULS enzymes in the degradation of Dnm1 because for other substrates it was demonstrated that overexpression of ULS enzymes is required for the detection of changes in substrate steady state levels (Lennard-Maximilian Döring, Master Thesis, 2017). However, also the simultaneous overexpression of *SLX5* and *SLX8* did not cause reduction of Dnm1-levels (data not shown).

Furthermore, ULS enzymes are expected to specifically control the levels of the sumoylated fraction of a substrate and due to the fact that usually this fraction amounts to less than 1% of the respective substrate (Johnson, 2004), the impact of ULS enzymes on the steady state levels of the unmodified substrate is likely limited.

The previously applied C-terminal 2HA-6His-tag on Dnm1 has been useful for the analysis of steady state levels in various strains, however, the signal intensity was not sufficient to properly detect putative modified forms of Dnm1. Therefore, by application of a PCR product and homologous recombination (Janke et al., 2004), new yeast strains were generated, in which Dnm1 bears a C-terminal 6HA-tag, which allows a more sensitive detection. Indeed, the new epitope allowed the detection of Dnm1-species running above the main band in SDS-PAGE (***Figure 2.2*** A). *DNM1-6HA* was introduced into mutants of interest and effects of the mutations on steady state levels and modified forms of Dnm1 were analyzed (***Figure 2.2***). The analysis confirmed that both mutants impaired in sumoylation, *siz1*Δ *siz2*Δ and *uba2-ts*, did not significantly alter steady state levels of Dnm1. Additionally, the mutant *ulp2*Δ, impaired in the control of SUMO chains, did not significantly alter Dnm1 levels either (***Figure 2.2*** B).

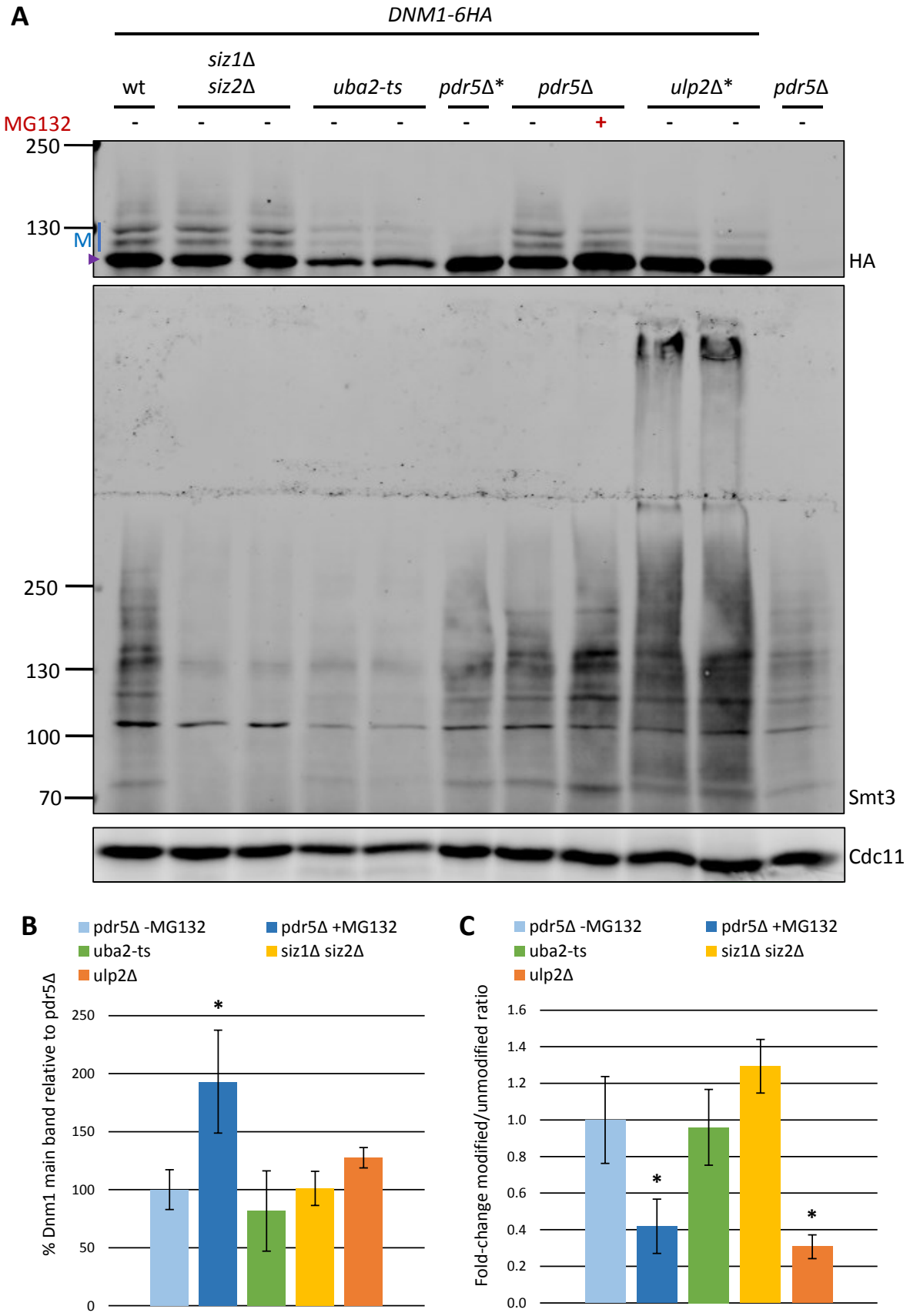

Figure 2.2: Increased Dnm1 levels upon proteasome inhibition

A) Representative Western Blot analysis using 8% SDS-PAGE and wet transfer onto a nitrocellulose membrane with two mini gels in the same chamber at 100 V, 400 mA for 1 hour at 4 °C. The membranes were probed with anti-HA (3F10) (1:1000, rat), anti-Smt3 (1:10000, rabbit) and anti-Cdc11 (1:5000, rabbit) antibodies. Applied secondary antibodies were anti-rat 680

(1:5000) and anti-rabbit 800 (1:5000). Bound secondary antibodies were detected with an Odyssey scanner. Cdc11 signal is much stronger than Smt3 and Cdc11 runs below the depicted range for Smt3, so these detections do not interfere with each other. Strains transformed with *DNM1-6HA* were MB2 (wildtype), YGA34 (*pdr5*Δ), YKU25-2a (*uba2-ts*), EJY326 (*siz1*Δ *siz2*Δ) and YLD38-1 (*ulp2*Δ). Strain YGA34 served as a control without HA-tag. The cells were grown at 30 °C in YPD. For the MG132 treatment, *pdr5*Δ-cultures were split and one half was incubated for 2 more hours without treatment and the other half was treated with 20 µM MG132 and grew for 2 more hours, as well. The purple arrow indicates full length, unmodified Dnm1. Blue M indicates the most prominent modified forms of Dnm1. An asterisk (*) at the respective sample indicates that the strain had an additional untagged *DNM1*-allele. **B)** Statistical evaluation of the results in A) with relative Dnm1 levels in relation to Cdc11 as loading control. Analysis relied on two Western Blots with different sets of transformants. The same sample of wildtype with *DNM1-6HA* was loaded on both gels to allow comparison of samples from both Western Blots to each other. *pdr5*Δ with and without MG132: n=3 each, *siz1*Δ *siz2*Δ: n=4, *uba2-ts*: n=4, *ulp2*Δ: n=3. *pdr5*Δ* is excluded from the statistical analysis. Statistical analysis was made with two-tailed, heteroscedastic t-test for the mutants and with two-tailed, paired t-test for MG132-treatment, *p<0.05. For this analysis, *pdr5*Δ untreated served as wildtype. **C)** Statistical evaluation of the results in A) with a calculated ratio of modified forms marked with "M" to unmodified Dnm1 marked with a purple arrow. The ratio, as it was measured in untreated *pdr5*Δ cells, was defined as 1.0 and the ratios in other strains were calculated accordingly. Statistical analysis was made as explained for B).

After it was found that a defect in ubiquitylation leads to increased Dnm1 levels, an open question was, if degradation of Dnm1 occurs via the proteasome. In order to test this, proteasomal activity was inhibited by MG132, a proteasome inhibitor that inhibits degradation of short-lived proteins (Lee and Goldberg, 1996). This compound is a substrate analogue blocking the chymotrypsin-like activity of the proteasome, which is rate-limiting in protein degradation (Lee and Goldberg, 1998). Since in previous reports, it was demonstrated that proteasome inhibitors work more effectively in strains with a deletion of the *PDR5* gene encoding a drug efflux pump (Fleming et al., 2002), a *pdr5*Δ mutant was used for these experiments.

Inhibition of the proteasome by MG132 caused a 1.9-fold increase in the amount of Dnm1 within 2 hours (***Figure 2.2*** B). This observation, together with the previously described effect of *uba1-ts,* suggests that Dnm1 is degraded by the UPS (ubiquitin-proteasome system). Therefore, it was interesting to see how the detected modified forms, specifically the two bands running above the main band, behave in the tested mutants. In the quantification, the ratio between these modified forms of Dnm1 and the main band was assessed (***Figure 2.2*** C). This analysis showed that the modifications do not significantly change in *siz1*Δ *siz2*Δ and *uba2-ts* mutants (***Figure 2.2*** C) although the Western Blot confirmed reduced sumoylation in these strains (***Figure 2.2*** A). Hence, it is very unlikely that the two prominent bands running above Dnm1 are sumoylated forms. Interestingly, however, the two bands stayed at similar intensity upon MG132-treatment. This means that the amount of modified Dnm1 remained mostly unchanged upon proteasome inhibition although levels of unmodified Dnm1 increased. Thus, the ratio of modified to unmodified Dnm1 was decreased upon proteasome inhibition (***Figure 2.2*** C). The conclusion from this is that the pool of modified, as later confirmed (***Figure 2.11***) most likely ubiquitylated Dnm1 remains stable, independent from an increase in overall Dnm1 levels. It is conceivable that ubiquitylation of a certain Dnm1 population depends on other rate-limiting processes like a specific localization or the availability of certain ubiquitin-ligases and it is possible that these modifications do not necessarily lead to degradation but are primarily regulatory. Furthermore, it should be noted that inhibition of the proteasome by MG132 is generally incomplete and an increase

in overall ubiquitin-conjugates is limited due to remaining activity of tryptic and caspase-like catalytic subunits of the proteasome (Collins et al., 2010).

In *ulp2*Δ cells, the ratio was shifted to unmodified Dnm1 (***Figure 2.2*** C). To understand this, it should be noted that a previous report described that loss of Ulp2 causes a duplication of chromosomes I and XII (Ryu et al., 2016). Consistently, PCR analysis of the *ulp2*Δ strains used in this study revealed that the here applied transformants possess a *DNM1-6HA* allele and a *DNM1* allele which is untagged. Therefore, the total amount of Dnm1 is probably doubled compared to *pdr5*Δ, which is used as reference, and only the HA-tagged fraction is detected on the Western Blot. The constant amount of modified forms of Dnm1 is distributed along the whole, doubled, pool of Dnm1 and therefore the ratio of modified to unmodified forms is reduced. This conclusion would also explain the reduced detection of modified Dnm1 in transformant *pdr5*Δ*, for which it was found that it has a *DNM1-6HA* allele and an untagged *DNM1* allele, as well. Summarized, the results from ***Figures 2.1*** and ***2.2*** suggest that Dnm1 is degraded via the ubiquitin-proteasome system. In contrast, an influence of SUMO system components on Dnm1 stability could not be found. Furthermore, the pool of modified, likely ubiquitylated forms of Dnm1 remains constant, even at increased Dnm1 levels.

2.1.3 Ethanol-treatment reduces Dnm1 levels

Now that indications for degradation of Dnm1 via the UPS were obtained, it was interesting to find conditions at which Dnm1 degradation is accelerated. In preliminary experiments wherein different stress conditions were tested, it was noticed that ethanol might reduce Dnm1 levels. In order to test this systematically, three independent transformants of *pdr5*Δ *DNM1-6HA* were treated with different ethanol concentrations, ranging from 2% to 10%, for 30 minutes and Dnm1 levels were analyzed by Western Blot (***Figure 2.3*** A).

The experiment indicated that the amount of unmodified full-length Dnm1 (U) decreases with increasing ethanol-concentrations. In this experiment, the Dnm1 levels were minimal at 8% and 10% ethanol with approximately 0.3-fold change compared to Dnm1 in an untreated culture (**Figure 2.*3*** A, B). Furthermore, the two modified forms of Dnm1 (M) running immediately above unmodified Dnm1, decreased with increasing ethanol-concentration, as well (**Figure 2.*3*** A, B). Strikingly, while full-length Dnm1 decreased, the degradation products of Dnm1 (D) were increased upon ethanol treatment. Ethanol caused approximately 1.5-fold to 2-fold elevated amount of Dnm1 degradation products and this was quite similar across the different ethanol concentrations (***Figure 2.3*** A, B). This observation was not so clearly visible on the Western Blot but became apparent when the loading differences indicated by TCE (trichloroacetic acid) staining were considered in a quantification.

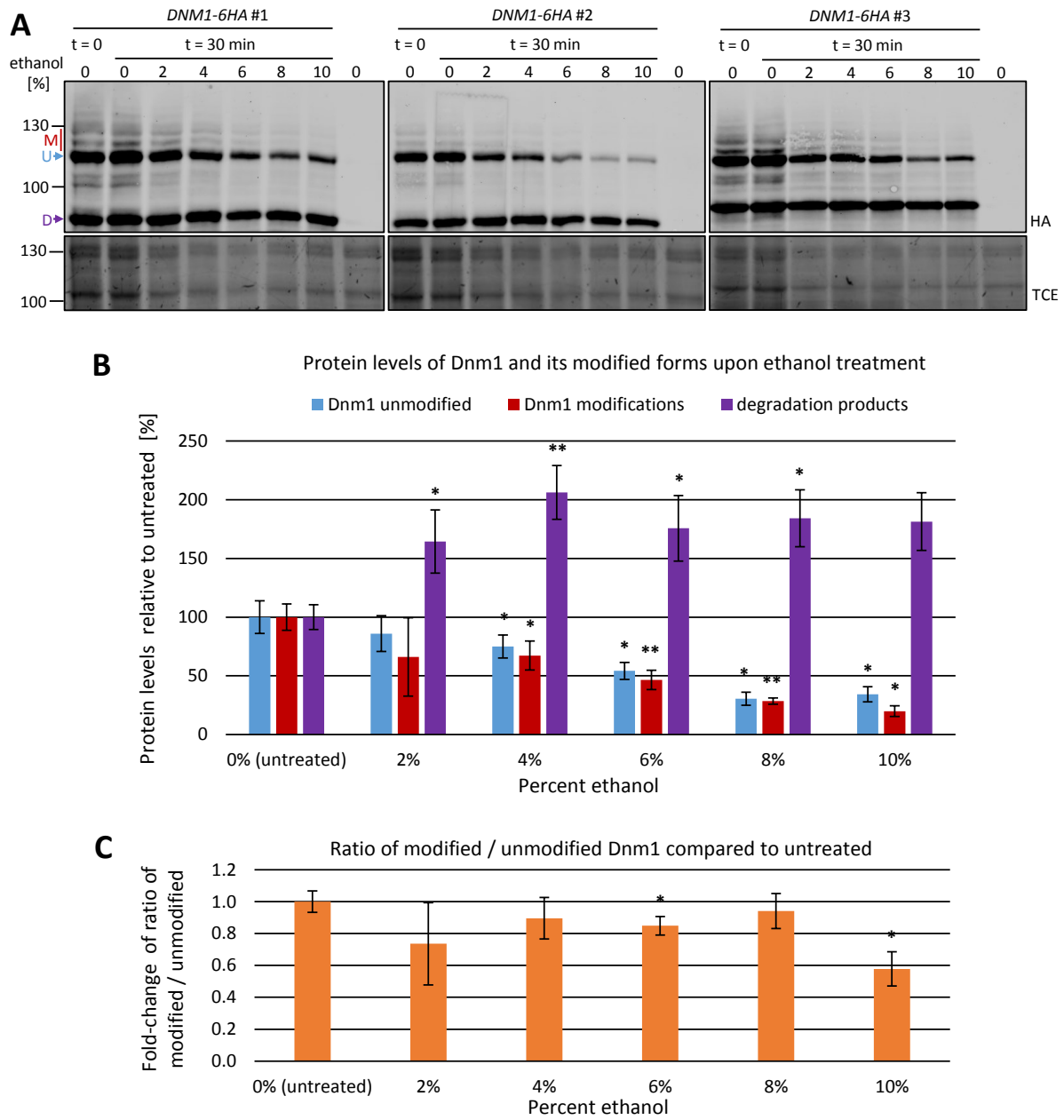

Figure 2.3: Ethanol-treatment causes reduction in Dnm1 levels

A) Western Blot analyses of three independent transformants using 8% SDS-PAGE and wet transfer onto nitrocellulose membranes with three mini gels on the same power supply set to 100 V, 400 mA for 2 hours at 4°C. The polyacrylamide-gels contained TCE, which allowed detection of loaded proteins from lysates prior to Western Blotting. The membranes were probed with anti-HA (3F10) antibody (1:1000, rat). Applied secondary antibody was anti-rat 680. Bound secondary antibody was detected with an Odyssey scanner. Three independent transformants for *pdr5*Δ DNM1-6HA were tested. Strain JD47-13C served as a control without HA-tag. The cells were grown at 30 °C in YPD to exponential growth before treatment. For the ethanol treatment, exponentially growing *pdr5*Δ cultures were split and ethanol was added to reach the indicated percentage. In order to keep the culture volumes equal among the cultures, water was added instead of ethanol where required. After start of the treatment, cultures were incubated for additional 30 minutes before harvesting. For comparison, for each Western Blot, one sample of the culture before start of the treatment was loaded, as well. "U" indicates full length, unmodified Dnm1. "M" indicates the most prominent modified forms of Dnm1. "D" indicates a prominent degradation product of Dnm1. **B)** Statistical evaluation of the results in A) with relative levels of unmodified Dnm1, modified Dnm1 and degradation products in relation to TCE as loading control. First, for each form of Dnm1 individually, all values were calculated relative to the sample from t = 0. Then, the respective levels in the untreated sample, 30 min, were defined as 100% and the values of the treated samples were calculated relative to this. Statistical analysis was made with a two-tailed, paired t-test in order to compare the values of treated samples with the respective ones of the untreated sample, n=3 (for each condition), *p<0.05, **p<0.01. **C)** Statistical evaluation of the results in A) with a calculated ratio of modified forms (M) to unmodified Dnm1 (U). The ratio, as it was measured for untreated (at time point 30 min), was defined as 1.0 and the ratios under the

indicated conditions were calculated accordingly. Statistical analysis was made with a two-tailed, paired t-test in order to compare the values of treated samples with the respective ones of the untreated samples, *p<0.05.

Like in previous experiments, also here the ratio of modified Dnm1 to unmodified Dnm1 was potentially interesting and was therefore assessed. This analysis revealed that upon treatment with 10% ethanol, the amount of modified Dnm1 in relation to the unmodified protein was the lowest with approximately 0.6 compared to untreated (***Figure 2.3*** C). A possible explanation for this is that the modified forms, which probably already bear one or two ubiquitin-moieties, are degraded faster than a previously unmodified Dnm1.

Taken together, the results of the treatment suggest that ethanol causes degradation of Dnm1, which is indicated by reduction of unmodified full-length Dnm1 and an increase in degradation products. Previous experiments already suggested that Dnm1 is degraded via the UPS. Therefore, it is likely that the UPS also mediates the ethanol-induced degradation of Dnm1. However, whether both, constitutive and ethanol-induced degradation of Dnm1 occur via the same or distinct pathways remains an open question.

2.2 Application of non-cleavable Smt3-Q95P and other SUMO variants for improved detection of SUMO conjugates

2.2.1 Expression of *smt3*-Q95P causes a strong global increase in SUMO conjugates

Western Blots of crude extracts with HA-tagged Dnm1 have shown bands running above unmodified Dnm1, which are probably modified forms. Furthermore, it was shown that these forms do not necessarily increase when cellular Dnm1 levels are elevated (***Figure 2.2***), thus the amount of these putative conjugates is limited by other factors than solely Dnm1 levels. Additionally, it was found that, apparently, these modified forms of Dnm1 disappear faster than unmodified Dnm1 upon ethanol treatment (***Figure 2.3***). Initial results also suggested that the UPS is involved in degradation of Dnm1 (***Figure 2.1*** and ***Figure 2.2***), thus ubiquitylation is a very likely candidate for this modification. However, also sumoylation could not be entirely excluded as a relevant Dnm1 modification, taking into account that multiple modified forms of Dnm1 exist at the same time. In order to characterize these modified forms of Dnm1, various approaches were applied.

The rationale behind these approaches was generally purification of Dnm1 and detection of ubiquitin or SUMO by respective antibodies or the other way round, purification of cellular ubiquitin or SUMO conjugates and detection of HA-tagged Dnm1. One of the early approaches was an HA-tag co-immunoprecipitation (co-IP) of HA-tagged Dnm1 (***Figure 2.9***). As usually required for co-IPs, the lysis and purification were performed under native conditions. This, in principle, might be an obstacle since

under native lysis conditions, without inhibition of desumoylating enzymes, SUMO is cleaved from its substrate during handling, as shown for human SUMO2 (Békés et al., 2011). In the same study, the authors demonstrated that the mutation Q90P in SUMO2 prevents desumoylation of SUMO substrates (Békés et al., 2011). In order to be able to perform co-IPs for detection of sumoylated forms of a protein, a corresponding *smt3* mutant was established in our laboratory, as described below.

The mutation Q90P in SUMO2 corresponds to Q95P in Smt3 of *S. cerevisiae* (***Figure 2.4***). Therefore, in order to prevent desumoylation, the yeast SUMO variant *smt3-Q95P* was constructed (Natasha Petreska, Bachelor Thesis, 2013). This mutant was encoded on a low-copy centromeric (*CEN*) plasmid (Gietz and Sugino, 1988) and expressed from the P_{GAL1} promoter, which is repressed in the presence of glucose and induced in the presence of galactose when glucose is absent (Johnston et al., 1994). This allows temporally controlled expression of the SUMO mutant. Compared to other promoters, P_{GAL1} is very strong when active (Peng et al., 2015), which allows high expression levels of the SUMO variant. Furthermore, the SUMO variant was expressed in the mature form without the C-terminal ATY extension in order to bypass the necessity of Ulp1-mediated maturation of Smt3. Additionally, the SUMO variants bore an N-terminal 2HA-tag for sensitive and specific detection with commercially available antibodies. Moreover, this tag induces a band shift of the modified protein, which might be helpful in the identification of sumoylated forms of a substrate.

Previous studies have shown that SUMO chain formation predominantly occurs via the three lysine-residues K11, K15 and K19 located in the flexible N-terminal region of Smt3 (Bylebyl et al., 2003). For the analysis of a specific sumoylated substrate, it might be beneficial to reduce the complexity of the SUMO pattern caused by chains of different lengths. Therefore, a SUMO variant with the additional mutations K11R, K15R and K19R (K11,15,19R) was applied (***Figure 2.4***). Due to the lack of these lysine residues in the N-terminal region, this mutant does not efficiently form chains (Bylebyl et al., 2003). Since this mutant, as well as the others, is expressed from a CEN plasmid in addition to the endogenous Smt3, chain formation is not completely inhibited but due to overexpression and the resistance towards cleavage, a general shift towards monosumoylation or multi-monosumoylation (and shorter chains) is expected, especially of the conjugates detected by anti-HA immunoblotting.

```
                                                SUMO2 MAD-E-----KPKEGVKTENN[...]QQTGG-VY
                                                 Smt3 MSDSEVNQEAKP-E-VKPEVK[...]EQIGG-ATY
                                 2xHA-Smt3 MSLINIFYPYDVPDYAGYPYDVPDYAGSMSDSEVNQEAKP-E-VKPEVK[...]EQIGG
                               2xHA-Smt3-Q95P MSLINIFYPYDVPDYAGYPYDVPDYAGSMSDSEVNQEAKP-E-VKPEVK[...]EPIGG
2xHA-Smt3-K11,15,19R,Q95P MSLINIFYPYDVPDYAGYPYDVPDYAGSMSDSEVNQEARP-E-VRPEVR[...]EPIGG
```

Figure 2.4: Amino acid sequences of SUMO2, Smt3 and Smt3-variants
The alignment shows the amino acid sequences of human SUMO2 and *S. cerevisiae* Smt3. The N-terminal part is aligned as common in the literature (Newman et al., 2017). Brackets […] indicate 74 residues which are not displayed. Endogenous SUMO2 and Smt3 are generated with C-terminal extensions -VY and -ATY, respectively. For the Smt3-variants, the 2xHA-tag is displayed in blue, the Q95P-mutation in green and the lysine to arginine exchanges in orange.

Previous studies had already shown that expression of the 2HA-tagged mutant *smt3-Q95P* from the P_{GAL1} promoter caused a drastic increase in detected SUMO conjugates, compared to P_{GAL1}-*2HA-SMT3*, even when the lysis was carried out under denaturing conditions (Natasha Petreska, Bachelor Thesis, 2013). In the study presented here, the effect of *smt3-Q95P* on cellular SUMO conjugates was further analyzed. For this purpose, three different 2HA-tagged SUMO gene variants, namely SMT3, *smt3-Q95P* and *smt3-K11,15,19R,Q95P* were expressed from the P_{GAL1} promoter. The effects were analyzed in wild-type and the ULS mutant *uls1*Δ *slx5*Δ, which is known to accumulate HMW (high molecular weight) SUMO conjugates due to a lack of their proteolytic control (Uzunova et al., 2007) (***Figure 2.5***).

First of all, the results from ***Figure 2.5*** indicate that an N-terminally tagged Smt3 is conjugated to substrate proteins, which in turn proves that it is accepted by the sumoylation machinery and can be used for the specific detection of SUMO conjugates. Consistent with earlier studies (Uzunova et al., 2007), due to a lack of proteasomal degradation of SUMO conjugates, *uls1*Δ *slx5*Δ cells accumulated HMW SUMO conjugates, especially noticeable in the stacking gel, where in wild-type yeast no SUMO conjugates could be detected (compare lanes 3 and 4, as well as 5 and 6) (***Figure 2.5*** B).

The main goal of the described experiment was to investigate if the Q95P mutation indeed stabilizes SUMO conjugates. The Western Blot analysis clearly shows that this is the case (***Figure 2.5*** A). Here, it can be observed that, particularly in the molecular weight range up to approximately 150 kDa, there was a drastic increase in HA-signal if the expressed 2HA-Smt3 bears the Q95P-mutation (compare lanes 3 and 5) (***Figure 2.5*** A). Likewise, in the *uls1*Δ *slx5*Δ mutant, 2HA-smt3-Q95P expression further increased overall levels of SUMO conjugates (compare lanes 4 and 6). Consistently, the amount of free SUMO was reduced due to the Q95P-mutation.

Expression of the variant *s*mt3-K11,15,19R,Q95P led to increased sumoylation levels, as well, when compared to expression of SMT3 (compare lanes 3 and 7). The overall levels of SUMO conjugates were similar between smt3-Q95P and smt3-K11,15,19R,Q95P, which suggests that both variants are conjugated with the same efficiency and the conjugates have similar stabilities (compare lanes 5 and 7). Here, it should be noted, that the amount of SUMO conjugates might overwhelm cellular mechanisms for the control of these conjugates, especially ULS-mediated degradation. The most striking effect of the lysine to arginine exchanges was the absence of HMW SUMO conjugates in *uls1*Δ *slx5*Δ cells (lane 8). This clearly indicates that the HMW conjugates forming in *uls1*Δ *slx5*Δ require lysine residues in the N-terminal extension, thus these HMW conjugates consist of SUMO chains. This in turn confirms results from earlier studies showing that ULS enzymes are necessary for the control of SUMO chains (Uzunova et al., 2007). Furthermore, it is noticeable that Smt3-K11,15,19R,Q95P migrates faster than Smt3-Q95P, an effect that has been observed before (Bylebyl et al., 2003).

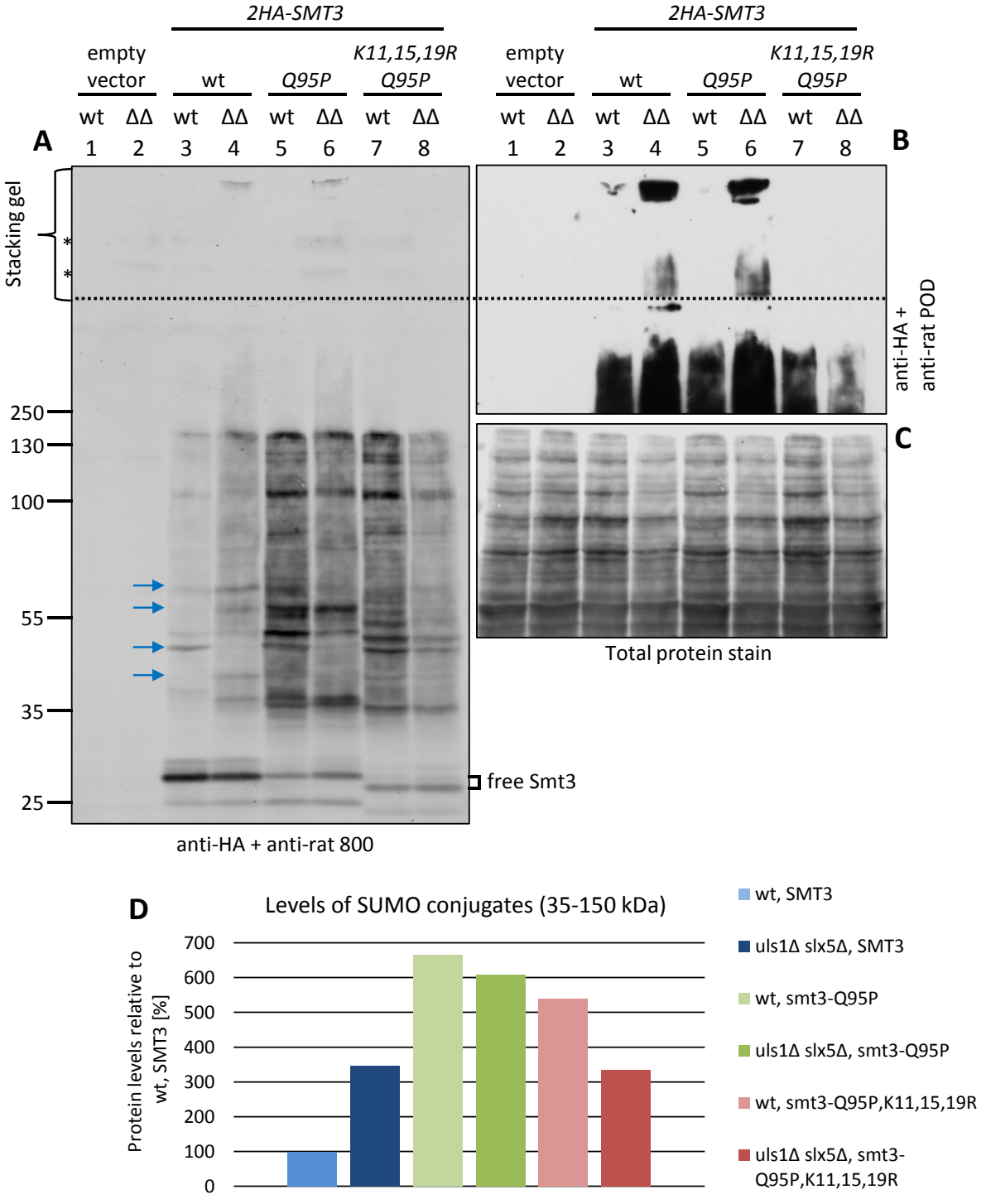

Figure 2.5: Alterations in sumoylation patterns in the ULS mutant *uls1Δ slx5Δ* and upon expression of smt3 variants

A) Western Blot analysis using a large gel for 8% SDS-PAGE and semi-dry transfer onto a nitrocellulose membrane with 1.2 mA/cm² for 2 hours. The stacking gel was blotted together with the resolving gel, as indicated. The membrane was probed with anti-HA (3F10) (1:1000, rat) and anti-rat Alexa Fluor 800 (1:5000) antibodies. Bound secondary antibody was detected with an Odyssey scanner. Asterisks (*) indicate unspecific signals. Blue arrows indicate distinct bands, which are discussed in the main text. ΔΔ is *uls1Δ slx5Δ* (YKU121) and wt is the congenic wild-type JD47-13C. Applied plasmids were pMM43 (*2HA-SMT3*), pNP3 (*2HA-smt3-Q95P*), pNP4 (*2HA-smt3-K11,15,19R,Q95P*), and YCplac111 as empty vector. Cells grew in SRaff -Leu at 30°C and after one doubling, galactose was added to a final concentration of 2% to induce expression of the smt3-variant.

In the presence of galactose, the cultures grew for additional three hours before they were harvested. **B)** For a more sensitive detection of HMW-conjugates, the same membrane as shown in A) was probed with anti-rat POD (1:5000). Bound secondary antibody was detected with Thermo Fisher Femto ECL and X-ray film. Depicted is the upper part of the membrane. **C)** Before antibody incubations, Total Protein Stain was applied as a loading control and detected with an Odyssey scanner. **D)** Quantification of the results in A) using Total Protein Stain as a loading control. The signals obtained with wild-type yeast expressing *2HA-SMT3* was defined as 100%. The content of A), B) and C) was part of the publication (Pabst et al., 2019). For this thesis, modifications to the respective figure were made.

At first glance, it seems that the sample *uls1*Δ *slx5*Δ smt3-Q95P displayed less SUMO conjugates in the molecular weight range from 35 kDa to 150 kDa (lane 6). However, taking into account the loading (***Figure 2.5*** C), the three lanes 5-7 had similar levels of SUMO conjugates. Compared to wild-type yeast expressing normal S*MT*3 (lane 3), wild-type yeast expressing *smt3-Q95P* (lane 5) had 6.7-fold increased levels of SUMO conjugates, *uls1*Δ *slx5*Δ expressing *smt3-Q95P* (lane 6) had 6.1-fold increased levels and wild-type yeast expressing *s*mt3-K11,15,19R,Q95P (lane 7) had 5.4-fold increased levels of SUMO conjugates (***Figure 2.5*** D). Therefore, this experiment suggests that in a situation where 2HA-smt3-Q95P is overexpressed, the ULS enzymes, presumably due to their relatively low expression levels, do not efficiently counteract the bulk of the SUMO conjugates in the medium molecular weight range. Probably, this effect is enhanced by sequestering of ULS enzymes by heavily sumoylated substrates, as they are visible in extracts from *uls1*Δ *slx5*Δ cells in the stacking gel. Furthermore, it is noticeable that, apparently, Smt3-K11,15,19R,Q95P is conjugated with similar efficiency compared to Smt3-Q95P (compare lanes 5 and 7). An advantage of the HA-tag is that mutations in Smt3 do not alter antibody recognition, which allows this comparison. A rather surprising result is that upon expression of *smt3-K11,15,19R,Q95P*, the levels of SUMO conjugates in *uls1*Δ *slx5*Δ are lower than in wild-type yeast (lane 8). A possible, yet speculative explanation refers to previous work in *S. pombe* (Wei et al., 2017). There, it was shown that Rrp2, the *S. pombe* homolog of Uls1, protects sumoylated Top2 from degradation by another ULS enzyme since Rrp2 and the other ULS compete for binding of the SUMO chain, but binding of Rrp2 to sumoylated Top2 does not lead to its degradation. Therefore, it can be speculated that binding of Uls1 to (multi-)monosumoylated substrates modified by Smt3-K11,15,19R,Q95P might also cause protection rather than degradation of the substrate. Furthermore, it was already shown that overexpression of Uls1 and other SIM containing proteins causes stabilization of SUMO conjugates in *S. cerevisiae* (Uzunova et al., 2007). This explanation would assume that another factor, distinct from Uls1 and Uls2, mediates degradation of (multi-)monosumoylated substrates in *uls1*Δ *slx5*Δ. Here, it should be noted that Slx8, a RING- and SIM-bearing subunit of heterodimeric Uls2 (Uzunova et al., 2007), and Rad18 are still present in these cells. Rad18 was described as a ULS with preference for sumoylated PCNA (proliferating cell nuclear antigen) (Parker and Ulrich, 2012). So, a speculative explanation for the results obtained here would be that Uls1 protects monosumoylated substrates from degradation via other (SUMO-targeted) ubiquitin ligases which is of course not possible in *uls1*Δ *slx5*Δ.

Interesting observations can be made by following distinct bands of specific SUMO conjugates. Some examples are marked by blue arrows. Here it becomes apparent, that an increase in overall SUMO conjugates does not necessarily increase the amount of a specific SUMO conjugate. For example, some bands, which are well visible in the wild-type, disappear in *uls1*Δ *slx5*Δ cells. Consistently, not all detectable bands are enhanced upon expression of smt3-Q95P. These indications demonstrate the dynamic nature of SUMO conjugation and its regulation. In addition to the stability of SUMO conjugates, there are other factors, which might contribute to the abundance of certain conjugates and could explain this, sometimes counterintuitive behavior. For example, especially due to the Q95P-mutation, specific monosumoylated species or shorter chains are likely extended to form longer chains. Additionally, the sumoylation of distinct substrates is regulated differently, thus it is conceivable that substrates are susceptible to excess sumoylation to different degrees. Factors here could be the localization, accessibility, availability or even previous other posttranslational modifications. Furthermore, it was shown that sumoylation is required for cell cycle progression (Dieckhoff et al., 2004; Eifler and Vertegaal, 2015; Seufert et al., 1995). On the other hand, ULS enzymes play a role in mitosis (van de Pasch et al., 2013), and desumoylation of kinetochore components by Ulp2 ensures correct chromosome segregation (Suhandynata et al., 2019). Given the fact that sumoylation and its negative regulation play a role in cell division, and taking into account that sumoylation itself was found to be cell cycle-regulated (Johnson and Blobel, 1999), it is conceivable that the here applied mutant strain *uls1*Δ *slx5*Δ and SUMO variants cause secondary effects which could explain the paradoxical behavior of specific sumoylated species.

2.2.2 Application of SUMO variants for the detection of modified Cdc11

Now that the impact of the SUMO variants on overall cellular sumoylation has been analyzed, exemplarily their effects on a specific substrate were examined. For this purpose, Western Blot membranes were reprobed with an antibody against Cdc11, a protein, which was already reported as a SUMO substrate (Johnson and Blobel, 1999) (***Figure 2.6***). Here it should be noted that the experiment was made with two independent sets of transformants with the same outcome. ***Figure 2.6*** shows one of these sets. First of all, already in strains expressing only endogenous Smt3, bands migrating slower than the main Cdc11-band can be detected (lanes 1 and 2). Obviously, these bands are likely candidates for posttranslationally modified Cdc11. Unexpectedly, detection of modified Cdc11 was decreased upon overexpression of *2HA-SMT3* (lanes 3 and 4). Reasons for paradoxical behavior of certain SUMO conjugates have been discussed in the previous chapter. The fact that the Q95P mutation apparently stabilizes the modified form(s) (lane 5) allows the speculation that, upon overexpression of *2HA-SMT3*, desumoylation of Cdc11 is enhanced, so that the amount of modified Cdc11 is even reduced.

Even if this is hypothetical, a possible explanation would be that enhanced overall sumoylation, presumably of septins in close proximity of Cdc11, causes recruitment of Ulp2, similar to what was described for its recruitment to kinetochores (Suhandynata et al., 2019), and Ulp2 initiates desumoylation of Cdc11. However, since overexpression of *2HA-SMT3* alone does not drastically increase the amounts of cellular SUMO conjugates (***Figure 2.8***), this remains speculative. Another explanatory approach refers to a study in which it was demonstrated that autosumoylation of Ubc9 at C-terminal lysine residues negatively regulates septin sumoylation (Ho et al., 2011). Changes in expression levels of *SMT3* or expression of the here applied variants might alter the sumoylation state of Ubc9, which in turn could have an effect on the sumoylation rate of certain substrates, like in this case Cdc11.

Nevertheless, in the cases in which SUMO is non-cleavable due to Q95P, a modified form of Cdc11 is well detectable in wild-type yeast (lanes 5 and 7) and, although weaker, also in *uls1*Δ *slx5*Δ (lanes 6 and 8). The most relevant observation here is that, presumably due to fusion of the 2HA-tag to Smt3-Q95P, the modified form of Cdc11 is shifted towards a higher molecular weight (green arrow) (lanes 5 – 8). This induced band-shift indicates that Cdc11 is sumoylated and that this modification can be detected in an exponentially growing cell culture. Previously, it has been shown that the majority of sumoylated Cdc11 occurs during mitosis (Johnson and Blobel, 1999).

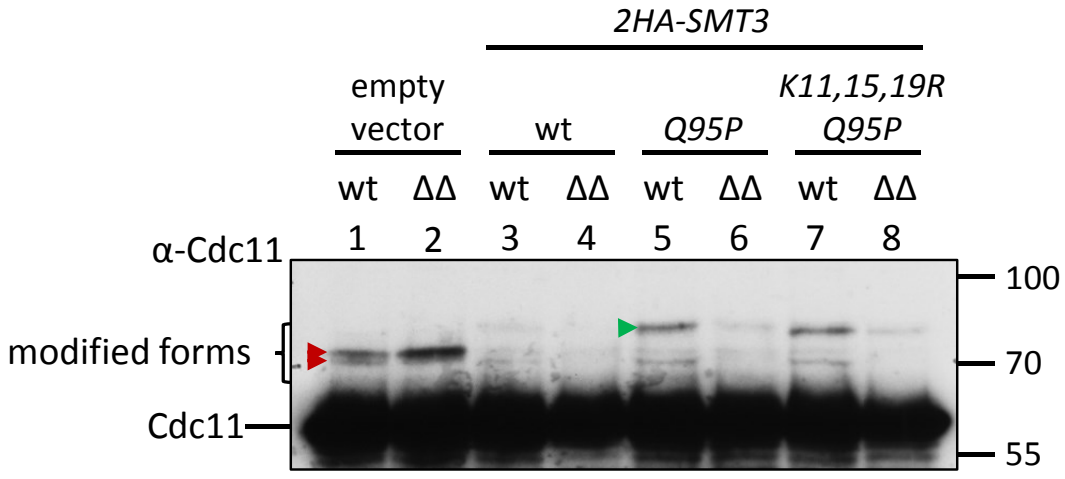

Figure 2.6: HA-tagged SUMO causes a detectable shift in sumoylated Cdc11
Reprobing of the membrane displayed in ***Figure 2.5***. The membrane was probed with anti-Cdc11 (1:1000, rabbit) and anti-rabbit POD (1:5000) antibodies. Bound secondary antibody was detected with Thermo Fisher Femto ECL and X-ray film. Red arrows indicate non-shifted bands. The green arrow indicates an induced band shift. For growth and blotting conditions, as well as loading control, see ***Figure 2.5***. ΔΔ is *uls1*Δ *slx5*Δ (YKU121) and wt is the congenic wild-type JD47-13C.

Apparently, the fraction of cells, which were in the respective phase when they were harvested, was sufficient to make these sumoylated forms detectable under the conditions applied here. The two modified forms running at approximately 70 kDa (red arrows) are still detected in the presence of 2HA-Smt3-Q95P. It should be noted, however, that these yeast strains still express endogenous *SMT3*. Therefore, a remaining non-shifted band is expected. Nevertheless, the fact that the signal of at least

one of the 70-kDa bands is reduced, supports the notion that a band shift has occurred. The mass difference between the two forms running at approximately 70 kDa is very small, so it can be almost certainly excluded that this difference is caused by an additional SUMO modification. An explanation for this double-band could be that the sumoylated form of Cdc11 is phosphorylated in the upper one of these two bands. This is plausible considering that Cdc11 is known to be phosphorylated (Ficarro et al., 2002; MacGilvray et al., 2020; Swaney et al., 2013). Furthermore, on closer examination, it can be noticed that the shifted form of modified Cdc11 migrates a little bit faster with the variant 2HA-Smt3-K11,15,19R,Q95P, like it was observed for the free form (***Figure 2.5***). This can be regarded as additional evidence indicating that this detected form of Cdc11 is sumoylated.

Surprisingly, the discussed shifted bands are less abundant in *uls1*Δ *slx5*Δ. As mentioned before, different reasons could be underlying. An easy explanation would be that, at a given time point, relatively more *uls1*Δ *slx5*Δ cells are present in cell cycle stages where Cdc11 is not sumoylated. However, it was reported that *slx5*Δ undergoes a temporary mitotic arrest and therefore requires more time for completion of mitosis (van de Pasch et al., 2013) where relatively large amounts of Cdc11 are expected to be sumoylated. Thus, the explanation for the observed results is probably not that simple. Ultimately, general changes in proteostasis and SUMO homeostasis in *uls1*Δ *slx5*Δ might be responsible for the observed reduction of Cdc11 sumoylation.

2.2.3 *smt3-Q95P* expression is well tolerated in the wild-type but toxic in strains lacking *SLX5*

An important question for the application of the introduced SUMO variants is, if and how they affect cell physiology. The most obvious assay is to test whether the expression of the respective constructs impairs the growth of yeast. Additionally, it was asked if the SUMO variants are particularly harmful for strains with a defect in the proteolytic control of SUMO conjugates. Therefore, the respective variants were expressed in wild-type and mutants and growth on an agar plate was assessed. On SD (synthetic glucose medium) plates, plasmids encoding *2HA-smt3-Q95P* did not influence growth since the expression was not induced (data not shown). However, growth on SGal (synthetic galactose medium), where expression is induced, revealed effects of 2HA-Smt3-Q95P on yeast growth (***Figure 2.7***).

First of all, in wild-type yeast, none of the overexpressed SUMO variants caused a general growth defect (***Figure 2.7*** A). This means that, although the relatively strong growth defect of *ulp2*Δ cells indicated that desumoylation is of critical importance (***Figure 2.18***), overexpression of non-cleavable SUMO variants alone, surprisingly, does not seem to be a major problem for cell physiology. However, it should be noted that endogenous *SMT3* is still expressed, although Western Blot analyses suggested that it constitutes a minority compared to the Q95P variants (***Figure 2.8***). Therefore, an open question

remains, if and how yeast cells would grow, which solely express *smt3-Q95P*. Like it was shown for wild-type yeast, also in the *uls1*Δ mutant, the tested SUMO variants did not cause a growth defect under normal growth conditions (***Figure 2.7*** A).

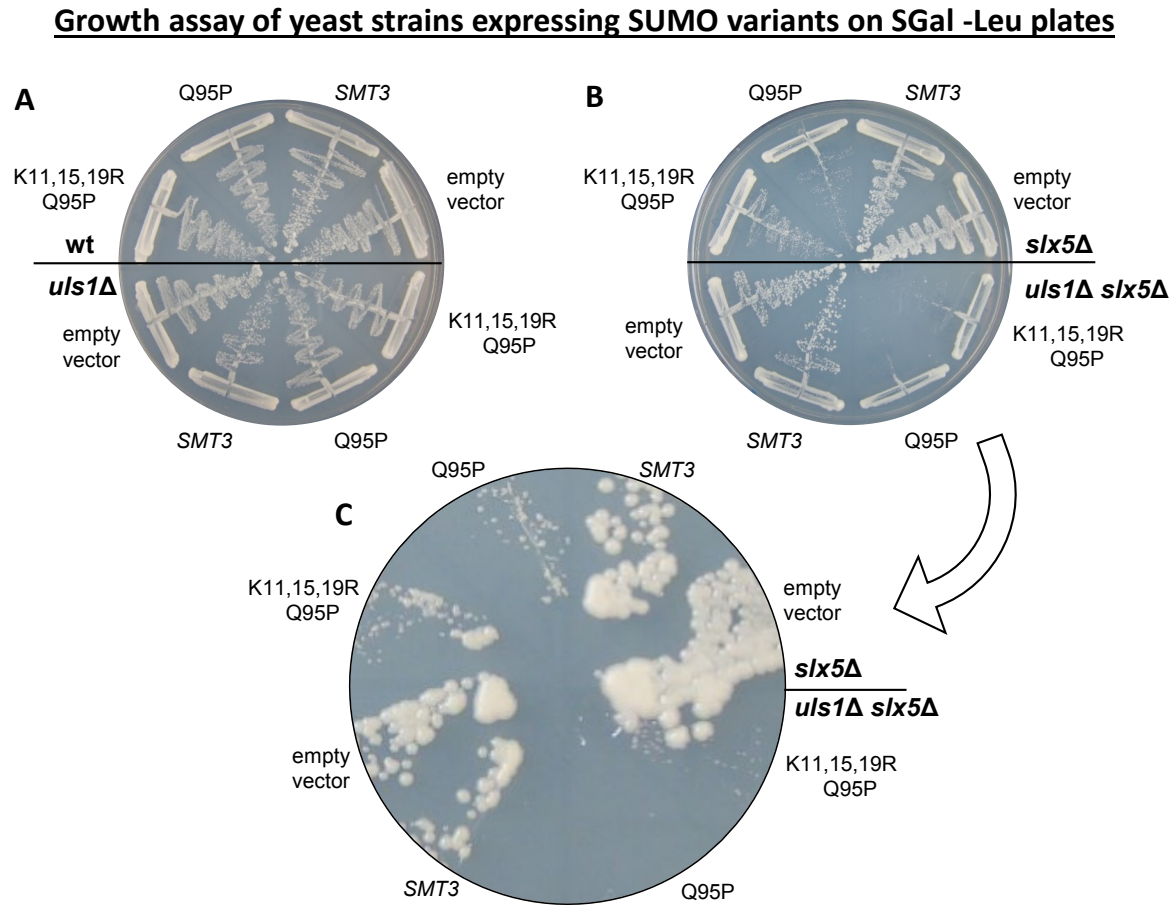

Figure 2.7: Effect of expression of SUMO variants on growth of strains with defects in proteolysis of sumoylated proteins
The indicated yeast strains harboring a plasmid with one of the P_{GAL1}-SUMO variants (*2HA-SMT3*, *2HA-smt3-Q95P* or *2HA-smt3-K11,15,19R,Q95P*) were pregrown on SRaff (synthetic raffinose medium) and streaked out on SD -Leu and SGal -Leu. On SD -Leu, the plasmids had no effect on yeast growth since expression of the SUMO variants is not induced (not shown). **A)** The plate on the left with wt and *uls1*Δ was incubated for three days at 30°C. **B)** The plate on the right with *slx5*Δ and *uls1*Δ *slx5*Δ was incubated for six days at 30°C. **C)** Shows a magnified photo of the plate from B) after eight days incubation so that sizes of individual colonies can be compared. On SGal -Leu, shown here, expression of *2HA-smt3-Q95P* or *2HA-smt3-K11,15,19R,Q95P* caused a severe growth defect in *slx5*Δ and *uls1*Δ *slx5*Δ. The strains are *uls1*Δ (YKU149), *slx5*Δ (YKU87), *uls1*Δ *slx5*Δ (YKU121) and the congenic wild-type JD47-13C. The content of A and B) was part of the publication (Pabst et al., 2019). For this thesis, modifications to the respective figure were made.

In striking contrast, overexpression of *2HA-smt3-Q95P* caused a severe growth defect in the *slx5*Δ and *uls1*Δ *slx5*Δ mutants (***Figure 2.7*** B, C). This is best visible when the sizes of individual colonies are compared (***Figure 2.7*** C). This suggests that proteolysis of non-cleavable SUMO by Slx5, probably via the dimer Slx5-Slx8, is required for proper growth of yeast colonies. Overexpression of wild-type *2HA-SMT3* did not cause a major growth defect in *slx5*Δ or *uls1*Δ *slx5*Δ, which indicates that overexpression of N-terminally tagged and otherwise wild-type SUMO per se is not a major problem. Thus, the non-cleavable property of 2HA-Smt3-Q95P is the cause of a growth defect in *slx5*Δ and *uls1*Δ *slx5*Δ.

Overexpression of *2HA-smt3-K11,15,19R,Q95P* caused a growth defect in these mutants as well. This effect is milder, however, than with chain-forming SUMO. The fact that the K11,15,19R mutations, which prevent formation of the typical HMW-conjugates in *uls1*Δ *slx5*Δ (***Figure 2.5***), slightly reduced the toxicity of Q95P in *slx5*Δ and *uls1*Δ *slx5*Δ showed that the toxicity of 2HA-smt3-Q95P is caused, at least in part, by uncontrolled HMW conjugates. However, 2HA-Smt3-K11,15,19R,Q95P still causes a growth defect in *slx5*Δ and *uls1*Δ *slx5*Δ although it does not efficiently form chains (Bylebyl et al., 2003). At this point, it should be noted that endogenous, chain-forming SUMO is still present in these cells. Therefore, it is likely that, to some extent, chains are formed and at one point terminated by 2HA-Smt3-K11,15,19R,Q95P. These chains would then be non-cleavable by Ulp2, which normally removes single SUMO moieties from the distal end of chains (Eckhoff and Dohmen, 2015), and would also not be degraded via Slx5. Additionally, at this point, it cannot be excluded that Slx5 has some activity towards multi-monosumoylated substrates, which might explain toxicity of 2HA-Smt3-K11,15,19R,Q95P in strains lacking *SLX5*.

The strain *uls1*Δ *slx5*Δ, devoid of both ULS enzymes, Uls1 and Uls2 (Slx5-Slx8), responds to overexpression of the SUMO variants similar to *slx5*Δ (***Figure 2.7*** B, C). Nevertheless, in line with other experiments, although *uls1*Δ alone does not have a very strong phenotype, additional deletion of *ULS1* in *slx5*Δ strengthens the phenotype (compare to general growth phenotype, ***Figure 2.18***). This suggests that most of SUMO-targeted ubiquitylation occurs via Slx5-Slx8, but Uls1 might have partly overlapping function, which explains why expression of *2HA-smt3-Q95P* and *2HA-smt3-K11,15,19R,Q95P* is more harmful in *uls1*Δ *slx5*Δ compared to *slx5*Δ.

In summary, these results confirm the hypothesis that SUMO conjugates need to be negatively regulated and that this occurs by desumoylation or proteolytic control by ULS. If both of these control mechanisms fail, the respective strain does not grow, so it can be concluded that these two mechanisms are responsible for controlling the vast majority of SUMO conjugates. Furthermore, the toxicity of 2HA-Smt3-Q95P in certain mutant yeast strains shows that the possibility of time-restricted expression of these SUMO variants is beneficial for their application in experiments.

2.2.4 Expression of different SUMO variants does not change Dnm1 levels

Different SUMO variants have been introduced and analyzed in the previous chapter. One of these is 2HA-Smt3-K11,15,19R,Q95P. This variant still has six lysine residues that are not in the N-terminal extension. As mentioned before, it was reported that Smt3 chain formation occurs mostly via the three residues K11, K15 and K19 in this extension (Bylebyl et al., 2003), and results presented here show the lack of HMW conjugates in the respective mutant (***Figure 2.5***). Still, it might be beneficial to entirely exclude further sumoylation of a previously attached SUMO moiety. For this purpose, previously in our

group an *smt3* variant was generated that has all lysine-residues exchanged to arginine. This would only allow hypothetical linear SUMO chains via the N terminus, however, so far this type of Smt3 linkage has not been detected so far, in contrast to ubiquitin, where such a linkage was found (Kirisako et al., 2006). Thus, it can be assumed that attachment of Smt3-KallR to a substrate does not result in a SUMO chain. Furthermore, it should be noted that this lysine-less mutant can also not be ubiquitylated directly. Ubiquitylation of the substrate itself is of course still possible. For the following application, the variant *smt3-KallR* was combined with the Q95P mutation in a plasmid for expression under control of the P_{GALS}-promoter, which is a truncated and therefore weaker variant of P_{GAL1} (Mumberg et al., 1994). In contrast to previous constructs, this variant did not bear an N-terminal HA-tag, so that it can be combined with an HA-tagged substrate for detection.

Moreover, as demonstrated in the previous chapter, a tagged Smt3 variant can be applied in order to induce a band shift of a putative sumoylated form of the substrate. Since Dnm1 runs at approximately ~105 kDa (***Figure 2.1***), the 2HA-tag is probably not sufficient for an easy detection of a band shift. Therefore, instead of a 2HA-tag, mCherry (Shaner et al., 2004) with a molecular weight of 26.7 kDa was N-terminally fused to Smt3-Q95P to allow a detectable band-shift. Furthermore, mCherry enables analyses with fluorescence microscopy in other types of experiments. The mCherry-Smt3-Q95P variant applied here has no lysine to arginine exchange, thus it should be able to form chains.

Additionally, Smt3-Q95P without HA-tag was employed, as well as wild-type Smt3. Overexpression of wild-type *SMT3* from P_{GAL1} should clarify if high expression levels alone already lead to increased levels of SUMO conjugates. In order to compare the overall sumoylation patterns of the SUMO variants described in this chapter, Western Blot analyses with an anti-Smt3 antibody were performed (***Figure 2.8***). The Western Blot revealed that overexpression of *SMT3* alone only has a minor effect on overall sumoylation levels. This means that the increase of SUMO conjugates displayed in ***Figure 2.5*** (lane 5) is predominantly caused by the non-cleavable property of 2HA-smt3-Q95P rather than the fact that it was expressed from the P_{GAL1} promoter.

In contrast, expression of *smt3-Q95P*, *smt3-K11,15,19R-Q95P* or *mCherry-smt3-Q95P* led to a strong increase in the levels of SUMO conjugates (***Figure 2.8***). Here, it also becomes apparent that the levels of SUMO conjugates of P_{GAL1}-*smt3-Q95P* and P_{GALS}-*smt3-KallR,Q95P* are very similar, thus neither the reduced expression level from P_{GALS} nor the lysine-to-arginine exchanges in KallR caused significant reduction of SUMO conjugates when compared to P_{GAL1}-*smt3-Q95P*. This in turn confirms the previously mentioned idea that the expression levels of *SMT3* are not decisive for the amount of SUMO conjugates.

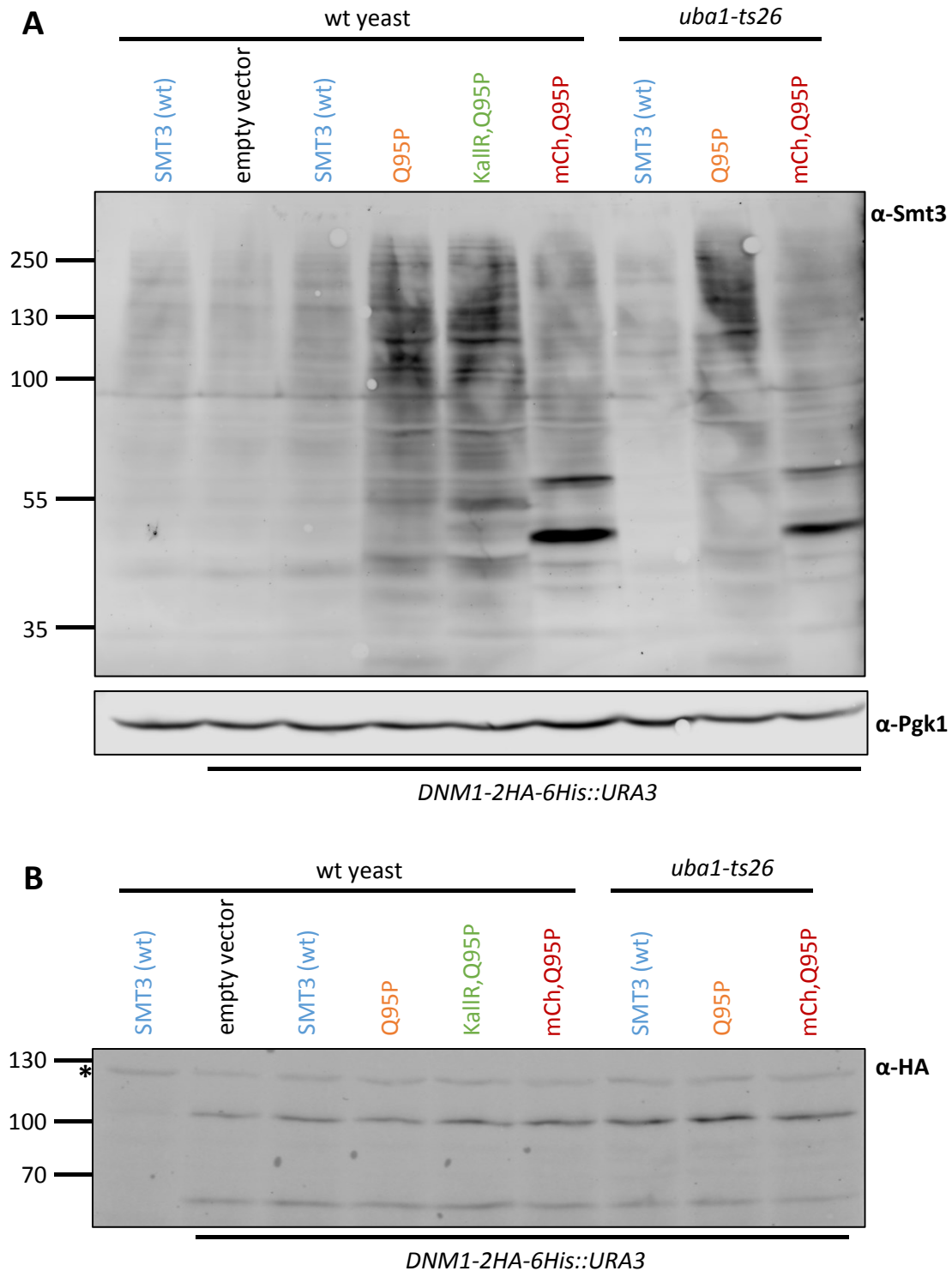

Figure 2.8: Sumoylation pattern and Dnm1 levels upon SUMO variant expression in wild-type and *uba1-ts*

A) Western Blot analysis using 6% SDS-PAGE and semi-dry transfer on a nitrocellulose membrane with 1.3 mA/cm² for 2 hours. The membrane was probed with primary antibodies anti-Smt3 (1:10000) and anti-Pgk1 (1:5000), and afterwards the secondary antibodies anti-rabbit Alexa Fluor Plus 800 (1:5000) and anti-mouse Alexa Fluor Plus 680 (1:5000). Bound secondary antibodies were detected with an Odyssey scanner. The transformed strains were *uba1-ts26 DNM1-2HA-6His* (YSP29) and the congenic wild-type *DNM1-2HA-6His* (YSP28). Wild-type JD47-13C YCplac33 served as an untagged control. Applied plasmids were pSP45 (P_{GAL1}- *SMT3*), pSP46 (P_{GAL1}-*smt3-Q95P*), pJD658 (P_{GALS}-*smt3-KallR,Q95P*), pSP41 (P_{GAL1}-*mCherry-smt3-Q95P*). As empty vector instead of the plasmids, YCplac111 was used. Cells grew in SRaff –Leu -Ura (SRaff –Trp -Ura for pJD658) at 30°C and, after one doubling, galactose was added to a final concentration of 2% to induce expression of the Smt3 variant. In the presence of galactose, the cultures grew for additional three hours before they were harvested. **B)** Probing of the same membrane as shown in A) with primary antibody anti-HA 3F10 (1:2000) and secondary antibody anti-rat 800 (1:5000). Bound secondary antibody was detected with an Odyssey scanner.

Furthermore it can be concluded that Smt3-KallR,Q95P is apparently efficiently conjugated. As seen in previous experiments (***Figure 2.5***), the global sumoylation pattern is not drastically changed compared to a chain-forming variant of Smt3-Q95P.

Another variant applied here was mCherry-Smt3-Q95P. Here, it is noticeable that the amount of overall SUMO conjugates is decreased compared to Smt3-Q95P. This suggests that N-terminal mCherry causes an impairment in conjugation. Nevertheless, mCherry-Smt3-Q95P still causes an accumulation of more SUMO conjugates than wild-type Smt3. Noticeably, two strong bands at ~ 50 kDa and ~ 65 kDa, respectively, occur upon expression of *mCherry-smt3-Q95P*. Possibly, the band at ~ 50 kDa indicates Ubc9 bearing mCherry-Smt3-Q95P via a thioester bond. Accumulation of this species is conceivable since apparently mCherry causes a conjugation defect. The band running above, at ~65 kDa, could be Ubc9 bearing mCherry-Smt3-Q95P with additional autosumoylation at a lysine residue. Autosumoylation of Ubc9 at its C-terminus has been described previously as negative regulator of sumoylation activity (Ho et al., 2011). In the ubiquitylation-defective strain *uba1-ts*, the overall impression is the same as in wild-type yeast, meaning that a ubiquitylation defect apparently does not have a strong effect on the behavior of the SUMO variants.

For Dnm1, the expression of the SUMO variants does not seem to have a large effect on steady state levels of the unmodified form (***Figure 2.8*** B). However, as known from previous experiments (***Figure 2.1***), Dnm1 steady state levels seem to be increased in *uba1-ts* considering that these samples are probably underloaded as indicated by the Pgk1 signals. At the same time, like previously noticed, it seems like the relative amount of the putative degradation product at ~70 kDa is decreased in *uba1-ts*. These observations were confirmed by chemiluminescent detection of Dnm1-2HA-6His, which allows detection with a better signal-to-noise ratio (data not shown). The latter detection also was used in order to detect putative modified forms of Dnm1, however, even upon expression of the SUMO variants, no modified forms of Dnm1 could be detected (data not shown). In this context, it should be noted that this experiment was conducted with Dnm1-2HA-6His, since Dnm1-6HA, as shown in other experiments, was established later in the course of the study.

Taken together, in this and the previous chapters, different SUMO variants, with different features like epitope tag, fluorescent tag, resistance towards cleavage, and disability to form chains, were established. These, as demonstrated with the SUMO substrate Cdc11, can be useful tools for the analysis of distinct sumoylated forms of a substrate, or for the analysis of global sumoylation levels under certain conditions.

2.2.5 Application of Smt3-Q95P in immunoprecipitations of Dnm1

As mentioned in chapter 2.2.1, initially one reason for the establishment of Smt3-Q95P was the possibility of stabilizing SUMO conjugates in a native immunoprecipitation. Now, that the effects of Smt3-Q95P and other SUMO variants were examined, Smt3-Q95P was applied in such a pulldown experiment (***Figure 2.9***). In this experiment, the genomic version *DNM1-2HA-6His* was used, as already in previous experiments. The 2HA-tag should allow specific immunoprecipitation of Dnm1 along with its modified forms. Ideally, these modified forms would then be detectable with an antibody against Smt3. In order to enrich a putative mono-sumoylated form of Dnm1, also Smt3-KallR,Q95P was applied in the pulldown. Furthermore, since, according to previous results, ubiquitin-mediated degradation of Dnm1 is likely, a pulldown in *uba1-ts* was performed. This, at least hypothetically, should stabilize Dnm1 and possibly its modified forms as well.

In ***Figure 2.9*** A, a representative immunoprecipitation of Dnm1-2HA-6His is shown. Detection with an anti-HA antibody shows that large amounts of Dnm1 could be purified in the respective samples as indicated by a blue arrow. Signals detected at around 130 kDa can be found in all samples including the ones without *DNM1-2HA-6His.* Therefore, these signals are not specific for Dnm1. Possibly, they are produced by reactivity of the anti-rat POD antibody towards anti-HA antibodies that were removed from the beads and of which disulfide bridges were not entirely dismantled. Nevertheless, specific Dnm1-2HA-6His signals can be detected at high molecular weight around 250 kDa, which are probably high molecular weight modified forms of Dnm1. The enrichment of Dnm1 in the immunoprecipitation apparently allows detection of these high molecular weight species, while in previous experiments with crude extracts of Dnm1-2HA-6His, this was not possible. The overall pattern of these HMW-forms of Dnm1 is very similar in the four respective lanes. Although in such a pulldown experiment, quantitative comparisons have to be considered with caution, here it looks like the HMW-forms of Dnm1 were more abundant with co-expression of Smt3-Q95P. Furthermore, in *uba1-ts26*, these bands seemed to be more intense. However, as known from previous experiments, Dnm1 is stabilized in *uba1-ts26*, therefore this sample probably contained more Dnm1 already in the beginning of the pulldown, which might be the underlying reason for this observation. Co-expression of *smt3-KallR,Q95P* did not lead to obvious changes in the band pattern of HMW-Dnm1 species, however, it should be noted that here, like in previous experiments, endogenous Smt3 is still present. Following these initial observations, it was conceivable that the detected, apparently modified, forms of Dnm1 are sumoylated.

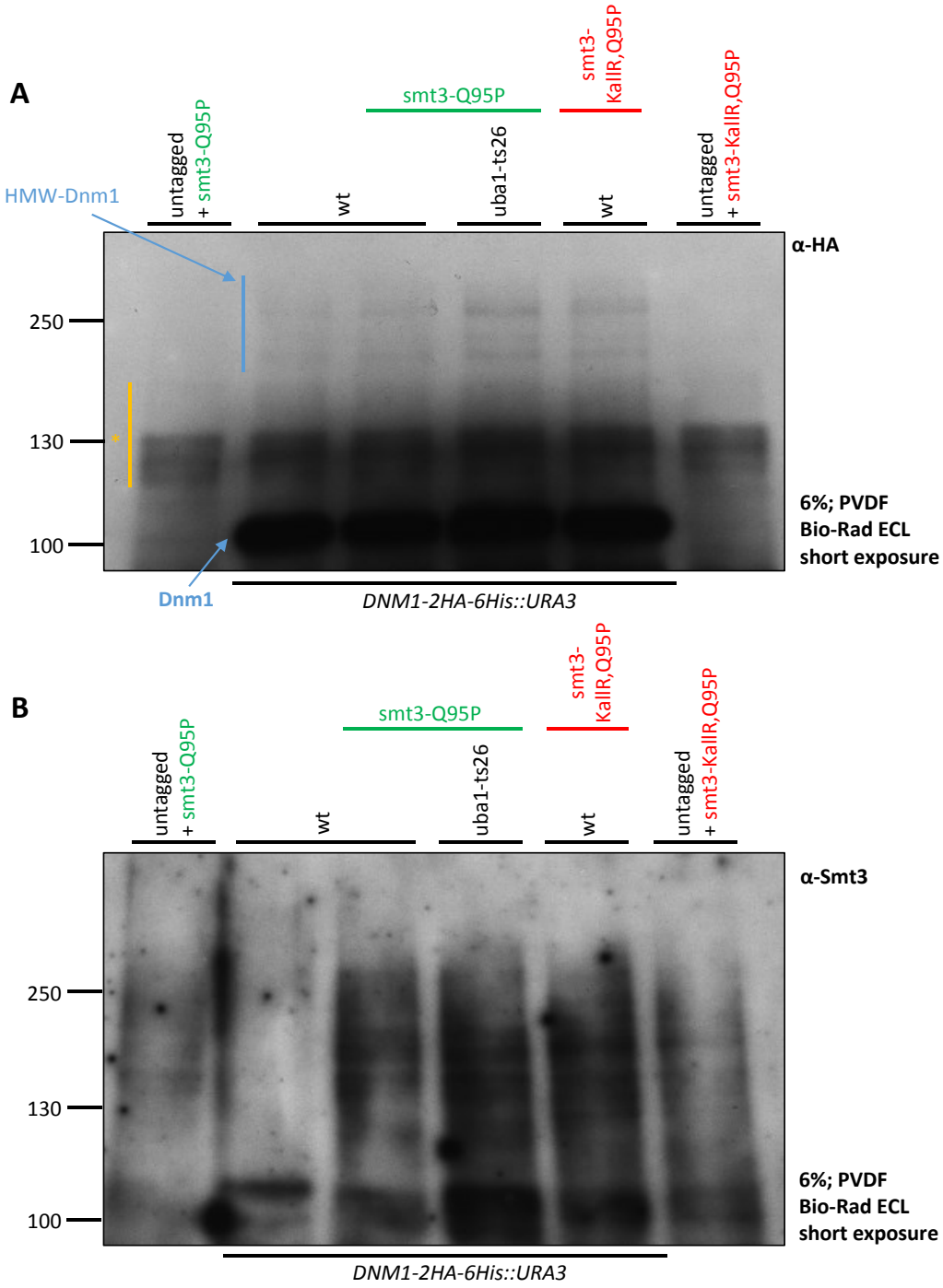

Figure 2.9: HA-immunoprecipitation of Dnm1 and probing for sumoylated forms

A) Western Blot analysis using 6% SDS-PAGE and semi-dry transfer on a PVDF membrane with 1.2 mA/cm² for 2 hours. The membrane was probed with the primary antibody anti-HA 3F10 (1:2000) and secondary antibody anti-rat POD (1:5000). Bound secondary antibody was detected with ECL substrate (Bio-Rad) and X-ray film. The transformed strains were wild-type *DNM1-2HA-6His* (YSP28) and *uba1-ts26 DNM1-2HA-6His* (YSP29). Wild-type JD47-13C YCplac33 served as an untagged control. Applied plasmids were pSP46 (P_{GAL1}-*smt3-Q95P*) and pJD658 (P_{GALS}-*smt3-KallR,Q95P*). As empty vector instead of the plasmids, YCplac111 was used. Cells grew in SRaff –Leu -Ura (SRaff –Trp -Ura for pJD658) at 30°C and after one doubling, galactose was added to a final concentration of 2% to induce expression of the *smt3* variant. In the presence of galactose, the cultures grew for additional three hours before they were harvested. Presented here are 50% (corresponding to 9 OD*ml) of HA-beads boiled in loading buffer after native glass bead lysis and HA-immunoprecipitation. Yellow line and asterisk indicate non-specific bands. **B)** The same samples as described in A) were analyzed by SDS-PAGE and Western Blot with the settings described in A). The membrane was probed with the primary antibody anti-Smt3 (1:10000) and secondary antibody anti-rabbit POD (1:5000).

In order to further investigate this hypothesis, the same samples were analyzed by SDS-PAGE and Western Blot with subsequent detection of Smt3 (***Figure 2.9*** B). First of all, as expected, in the sample without co-expression of *smt3-Q95P*, the least amount of SUMO conjugates were detected, presumably due to cleavage *in vivo* or during the native immunoprecipitation. In all of the three samples where Dnm1-2HA-6His was purified and an *smt3-Q95P* variant was co-expressed, strong signals for SUMO conjugates could be detected. However, it can be noticed that also in the controls without Dnm1-2HA-6His (left-most and right-most lanes), SUMO conjugates are detected.

Therefore, a question is, if the SUMO signals detected after purification of Dnm1-2HA-6His are specific for Dnm1. On one hand, no distinct bands can be observed which are clearly solely visible in samples with Dnm1-2HA-6His, on the other hand, immunoprecipitation of Dnm1-2HA-6His apparently leads to an increase in detected SUMO conjugates. At this point, it is very important to take into account that the immunoprecipitation of Dnm1 was performed under native conditions. Therefore, it is conceivable that, along with Dnm1, its interaction partners were co-purified. Consequently, an increase in SUMO conjugates after Dnm1 immunoprecipitation, as seen in ***Figure 2.9*** B, does not necessarily mean that Dnm1 itself is sumoylated but it could also indicate that other sumoylated proteins are co-purified with Dnm1 due to presence in the same protein complex.

Taken together, the immunoprecipitation presented here yielded preliminary results which made sumoylation of Dnm1 plausible. At the same time, involvement of the UPS in the degradation of Dnm1 is very likely (see ***Figure 2.1*** and ***Figure 2.2***). For these reasons, the possibilities of Dnm1 sumoylation and/or ubiquitylation were further investigated by another variation of a pulldown, as described in the following chapter.

2.3 Application of His-tagged Smt3 and ubiquitin for purification of modified proteins

2.3.1 Establishment of a method for specific purification of 8His-Smt3 and its conjugates

As described in the previous chapter, Smt3-Q95P can be applied for preserving SUMO conjugates during a native immunoprecipitation. This kind of experiment has given initial indications for a putative sumoylation of Dnm1. At the same time, experiments in different yeast strains have shown that Dnm1 is probably degraded via the UPS.

In order to analyze these putative modifications of Dnm1 and other substrates, an additional experimental approach was established. In this setup, a yeast strain with *8His-SMT3*, expressed from its authentic genomic locus, was applied. This strain solely expresses the 8His-tagged version of *SMT3*, so that in contrast to the plasmid-based variants only this tagged SUMO species is present in the cell, which in turn is an advantage for the interpretation of results. Previous studies already showed that 8His-Smt3 exhibits a sumoylation pattern very similar to wild-type Smt3 (Wohlschlegel et al., 2004). This 8His-tag can be used for IMAC (immobilized metal affinity chromatography) with Nickel (Ni^{2+}) or Cobalt (Co^{2+}) beads. One key advantage of this method is that the purification can be conducted under denaturing conditions in 8 M urea. Therefore, the risk of proteolytic cleavage of SUMO conjugates is greatly reduced. Furthermore, it can be assumed that all detected modifiers are covalently bound to their substrates. Another advantage is that, under these conditions, all proteins should be soluble, so the potential risk of precipitation can be avoided. Additionally, if *8His-SMT3* is combined with an epitope-tagged substrate, the modified forms can be detected with an antibody that is specific for the respective substrate, so that the problematic detection of unspecifically binding proteins should be reduced, due to the much lower number of potentially detected bands (compare to ***Figure 2.9*** B).

While the approach from ***Figure 2.9*** allows the testing of a single substrate for different modifications on the same membrane, the approach presented here, with *8His-SMT3,* in principle allows the testing of different substrates for sumoylation within the same purification. This is particularly helpful if antibodies against several endogenous proteins are available. Furthermore, a purification of global SUMO substrates can be used for mass spectrometric analysis of the SUMO proteome (Denison et al., 2005; Hannich et al., 2005; Panse et al., 2004; Wohlschlegel et al., 2004; Zhou et al., 2004).

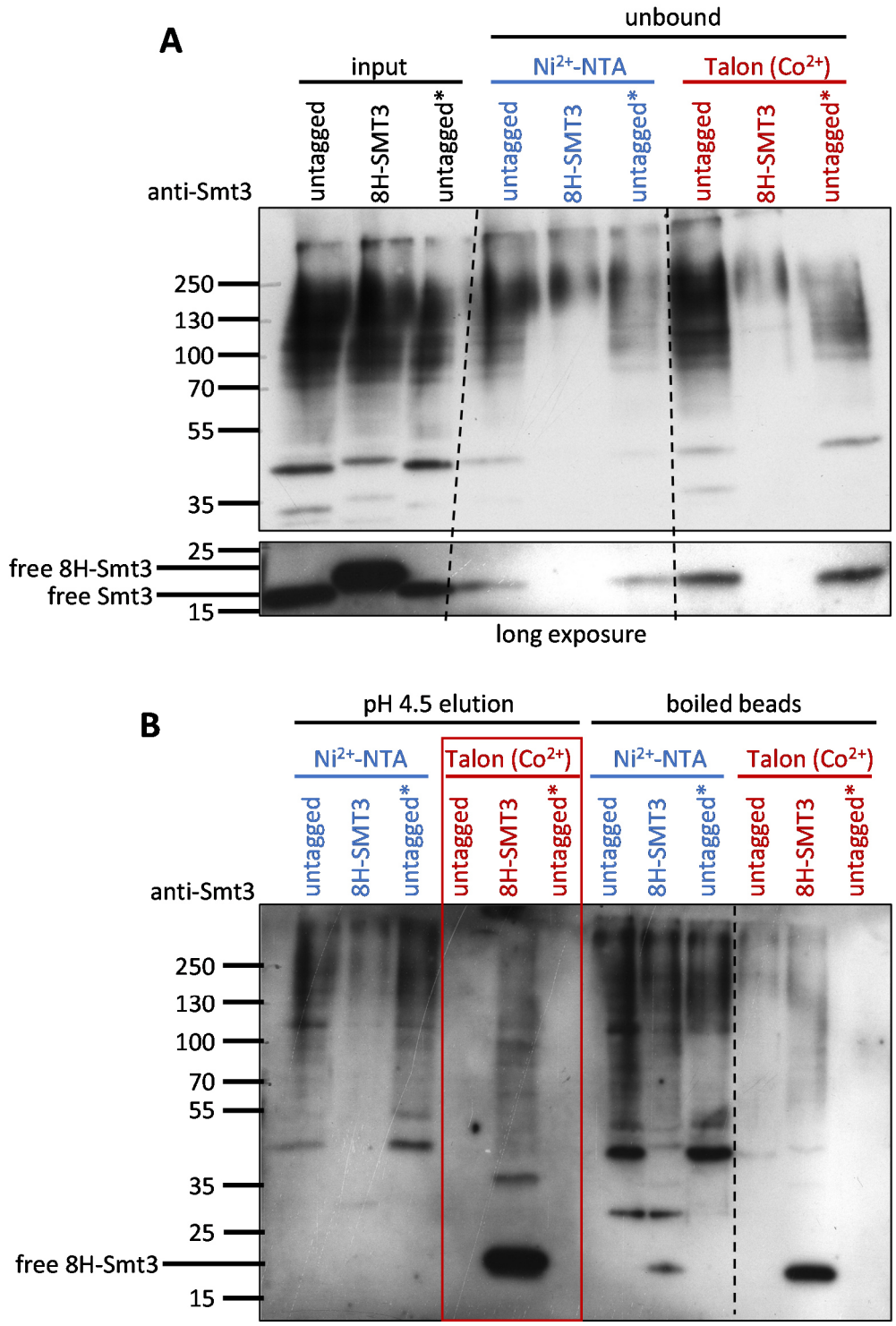

Figure 2.10: Purification of 8His-Smt3 and its conjugates by Co^{2+}-beads

A) Western Blot analysis using 10% SDS-PAGE and semi-dry transfer on a PVDF membrane with 0.7 mA/cm² for 2 hours with subsequent boiling for 20 minutes. The membrane was probed with anti-Smt3 (1:10000) and anti-rabbit POD (1:5000) antibodies. Bound secondary antibody was detected with ECL and X-ray film. The applied strains were untagged wild-type (JD47-13C), *8His-SMT3* (Sc. 1879) and untagged* (*DNM1-2HA-6His,* YSP28, however for this experiment this strain can be considered as untagged control). Cells grew in YPD at 30°C for two doublings before harvesting. Loaded were 1.6% (100% = 15 OD*ml) of input and unbound fractions before and after binding to the indicated beads, respectively. The lower panel shows the same membrane with longer exposure time. **B)** Western Blot analysis with the same settings as described for A). Loaded were 8% of an elution with pH 4.5 and 8% of subsequently boiled beads. The red rectangle highlights successful and specific elution of 8H-Smt3 in the respective sample, as seen for SUMO conjugates, as well as free 8H-Smt3. A part of the content of A) and B) was part of the publication (Pabst et al., 2019). For this thesis, additional samples were included and the figure was edited.

A representative Western Blot analysis of a glass bead lysis in 8 M urea with subsequent purification of 8His-Smt3 with Ni^{2+} or Co^{2+} beads is presented in ***Figure 2.10***. In the input fraction, it is visible that *8His-SMT3* and the untagged control have a similar amount of SUMO conjugates after glass bead lysis. Noticeably, free 8His-Smt3 runs slower than the untagged variant. As expected, after binding to Ni^{2+} or Co^{2+}, the amounts of 8His-Smt3 conjugates are significantly reduced while the amount of untagged Smt3 is not reduced to the same degree. This effect is particularly well visible for free 8His-Smt3 and the untagged variant (***Figure 2.10*** A).

Interestingly, during the elution with low pH, the Ni^{2+} and Co^{2+} beads behaved very differently. When pH 4.5 was applied to Ni^{2+}-NTA, apparently, unspecifically bound proteins were released from the beads in the untagged control while this pH was not sufficient for elution of most of the 8His-Smt3 conjugates (***Figure 2.10*** B). In contrast, application of pH 4.5 to Co^{2+} beads led to a release of the previously bound 8His-Smt3 conjugates. At the same time, here no detectable amounts of untagged Smt3 conjugates were released from the control purifications. Thus, a specific purification and elution could be performed for 8His-Smt3 by using Co^{2+} beads, as indicated by the red rectangle (***Figure 2.10*** B). It can be concluded that, with the conditions applied here, a successful purification of 8His-Smt3 conjugates with Ni^{2+} could not be achieved. In contrast, purification with Co^{2+} beads allowed a specific elution of 8His-Smt3 conjugates. The main reason for this difference is probably that, according to manufacturers, Co^{2+} has a higher specificity for His-tagged proteins than Ni^{2+}. Furthermore, elution from Co^{2+} can be achieved with milder conditions compared to Ni^{2+}, therefore pH 4.5 was apparently not sufficient for elution of 8His-Smt3 conjugates from Ni^{2+}, while for Co^{2+} it was. Here, it might be important to consider that a SUMO chain bears several 8His-tags, so that possibly elution requires harsher conditions than that of other His-tagged proteins.

In order to determine how many conjugates remained on the beads after elution, the beads were boiled in loading buffer. Since the elution of 8His-Smt3 from Ni^{2+} was very inefficient, many conjugates were detectable after boiling of the beads, as well as unspecifically bound Smt3 conjugates in the controls. Also for Co^{2+}, some 8His-Smt3 conjugates could be detected after boiling, however, apparently, most of the conjugates were released already during the elution with pH 4.5. Since the purification of 8His-Smt3 with Co^{2+} yielded promising results, this method was chosen for following experiments.

2.3.2 Dnm1 is ubiquitylated *in vivo*

After conditions for specific purification of 8H-Smt3 conjugates were established (***Figure 2.10***), this method was applied for investigation of the putative sumoylation of a specific protein, in this case Dnm1. Since, according to previous results, both sumoylation and ubiquitylation of Dnm1 were

conceivable, an analogous approach was conducted for 8H-Smt3 and 6H-Ub in order to clarify the nature of previously detected HMW-conjugates of Dnm1. Here, it should be noted, that, in contrast to *8H-SMT3*, *6H-Ub* is encoded on a plasmid and expressed from the P_{GAL1} promoter, therefore, the respective cultures grew in YPGal for *6H-Ub* expression. Apart from this, the following purification was carried out simultaneously and equally for both modifiers. As for the experiment presented in ***Figure 2.10***, here a denaturing cell lysis and purification was performed with the aforementioned advantages. One change, however, was that here magnetic Co^{2+} beads were applied, which have several advantages. Most importantly, these magnetic beads allow removing the whole volume of a wash solution, which allows to reduce the elution volume compared to the conventional agarose beads. This was important since a very high concentration of the eluate was desired for the detection of conjugates of low abundance. Furthermore, previously conducted experiments had suggested that elution with low pH can be inefficient when the elution volume is small (data not shown). Therefore, here the elution was performed by adding 500 mM imidazole to the Co^{2+} beads.

Western Blot analysis with anti-HA detection for Dnm1-6HA shows the appearance of two distinct bands and a smear, which is specific for samples with 6H-Ub (***Figure 2.11*** A, B). In samples without 6H-Ub these signals are not detectable with a comparable intensity. Therefore, these signals specifically indicate the presence of ubiquitylated forms of Dnm1. Unmodified Dnm1 could be detected in all samples except for the untagged control, indicating that to some degree unmodified Dnm1 itself binds to Co^{2+} beads. However, for the analysis of conjugates, this band can be ignored. Apparently, treatment with H_2O_2 did not have a large effect on the ubiquitylation pattern of Dnm1 as such. The signal intensity of ubiquitylated Dnm1-6HA is reduced upon H_2O_2 treatment but it should be noted that also the amount of unmodified Dnm1 is apparently reduced in this sample. This observation was confirmed by analysis of input fractions (data not shown). However, this effect was not seen for the other eluates with previous H_2O_2 treatment (data not shown), so it is not clear, if this is a general effect of H_2O_2.

For the purification of 8H-Smt3, the situation is different. Signals for Dnm1-6HA can be detected after purification of 8H-Smt3 in the sample where cells were treated with H_2O_2. However, the same bands, although with lower intensity, can be detected in the respective control without 8H-Smt3.

These bands might be identical to the ones detected for ubiquitylated Dnm1, therefore, probably, the respective bands in the 8H-Smt3 purification occur due to minor unspecific binding of ubiquitylated Dnm1 to Co^{2+} beads (***Figure 2.11*** B). In order to get an impression of the purity of the obtained eluates and to compare the total protein amounts, prior to the Western Blot, a TCE staining of the gel was performed (***Figure 2.11*** C). First of all, it is noticeable that the total protein content of the 8H-Smt3 purification is very similar to the one in the negative control without 8H-tag. That means that although

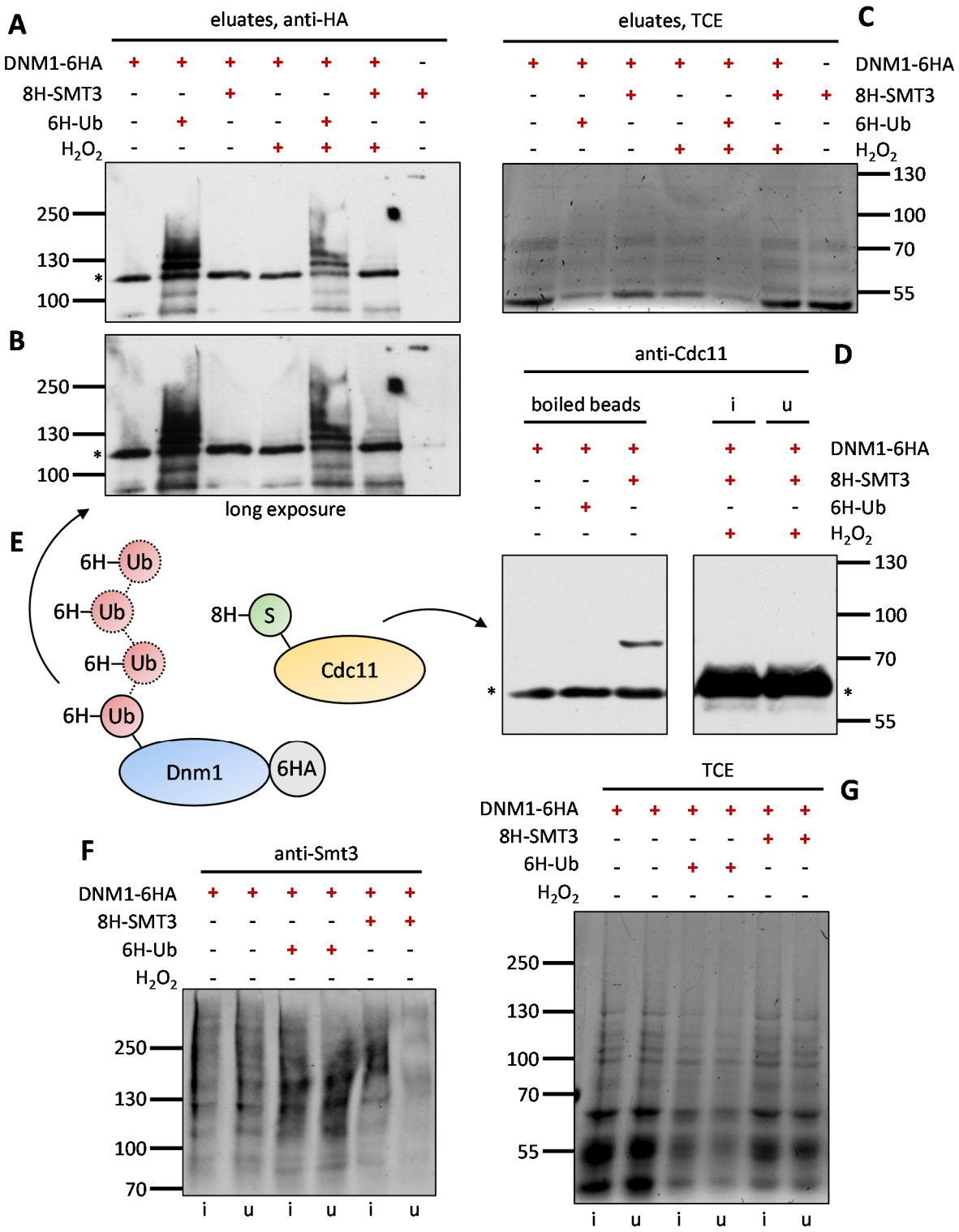

Figure 2.11: Detection of ubiquitylated Dnm1 and sumoylated Cdc11 after denaturing purification of 6H-Ub and 8H-Smt3

A) Western Blot analysis using 8% SDS-PAGE and wet transfer on a nitrocellulose membrane (9 cm x 7 cm) with 100 V and 400 mA for one hour in the cold room. The membrane was probed with anti-HA 3F10 (1:1000) and anti-rat POD (1:5000) antibodies. Bound secondary antibody was detected with Femto ECL and X-ray film. An asterisk indicates unmodified Dnm1. The applied strains were *pdr5Δ::hph DNM1-6HA::HIS3*, *pdr5Δ::hph DNM1-6HA::HIS3* pKU103, *8H-SMT3::TRP1 DNM1-6HA::HIS3* and *8H-SMT3::TRP1*. Cells grew in YPD (with the exception described below) at 30°C for 2-3 doublings, then cells were incubated for 10 more minutes, either with or without 1 mM H_2O_2 before harvesting. *pdr5Δ::hph DNM1-6HA::HIS3* pKU103 grew in YPGal at 30°C in order to induce *6H-Ub* expression from the plasmid pKU103. Loaded were 47% (100% = 200 OD*ml) of an imidazole elution of a denaturing purification of 8H-Smt3 and 6H-Ub with magnetic Co^{2+} beads. **B)** Same membrane as in A) with longer exposure time. **C)** TCE staining of the gel used for Western Blot from A) and B). **D)** Western Blot analysis with the same procedure as in A). The membrane was probed with anti-Cdc11 (1:1000) and anti-rabbit POD (1:5000) antibodies. An asterisk indicates unmodified Cdc11. Loaded were samples of the same pulldowns as in A) but beads

which were taken up in loading buffer and boiled (33% of the material was loaded here) (left part) and exemplary input and unbound (1.1% each) were loaded. This experiment serves as control which shows that sumoylated proteins could be purified. **E)** Schematic representation of the identified modified species, (poly-) ubiquitylated Dnm1 and sumoylated Cdc11. **F)** Western Blot with the same settings as described for A). The membrane was probed with anti-Smt3 (1:10000) and anti-rabbit Alexa Fluor Plus 800 (1:5000) antibodies. Bound secondary antibody was detected with an Odyssey scanner. Loaded were 0.6% of input (i) and unbound (u) before and after binding to Co^{2+} beads, respectively. **G)** TCE staining of the gel used for Western Blot from F).

in respect to Smt3 such a purification with Co^{2+} beads is pure (***Figure 2.10*** B), the majority of proteins in the eluate is coming from non-specific binding of cellular proteins. This observation was already made in previous studies (Wohlschlegel et al., 2004), in this case with Ni^{2+}-NTA, and it was concluded that even if an enrichment of sumoylated proteins occurred, their amount was still low compared to the general background. The result of such a purification can still be exploited, of course, however, it underlines the importance of a proper untagged control. Furthermore, apparently the protein content was reduced in 6H-Ub purifications, possibly due to the fact that the cells grew in YPGal and 6H-tagged ubiquitin was overexpressed, which might have an effect on the OD/protein ratio. However, since these samples showed the most intense HA-signals for conjugates (***Figure 2.11*** A, B), this should not be problematic.

In order to confirm that sumoylated proteins were enriched in the performed purification, fractions of the boiled beads were analyzed by Western blotting with an anti-Cdc11 antibody (***Figure 2.11*** D). In the boiled beads fraction, a modified form of Cdc11 was detected, which is specific for *8H-SMT3*. This indicates that, in contrast to what was seen for Dnm1, sumoylated Cdc11, but no ubiquitylated forms, could be detected. The same was true for H_2O_2-treated samples with very similar amounts of sumoylated Cdc11 compared to untreated cultures (data not shown). Furthermore, input and unbound material of one of the purifications were analyzed on the same Western blot, but 30-fold less sample was loaded compared to the boiled beads samples. In both, input and unbound material, no modified forms of Cdc11 were detected although the signals for unmodified Cdc11 were very intense, which in turn demonstrates that the sumoylated form of Cdc11 was strongly enriched after the purification. Altogether, the results for Cdc11 confirm that sumoylated substrates (***Figure 2.11*** E) could be identified with the here conducted approach, and that the identification of ubiquitylated forms, like for Dnm1, is not a generally occurring circumstance.

In order to further evaluate the method as such, input and unbound fractions were analyzed by an anti-Smt3 Western Blot (***Figure 2.11*** F). As expected, application of Co^{2+} beads caused a noticeable reduction of SUMO conjugates in the unbound fraction. At the same time, such a reduction of SUMO conjugates was not observed in other samples, indicating that the binding of 8H-Smt3 conjugates to Co^{2+} beads had worked. Therefore, it is unlikely that a technical problem can explain the difference between 6H-Ub and 8H-Smt3 for the detection of modified Dnm1.

Additionally, by TCE staining of the respective gel, it was confirmed, that the input fractions of *8H-SMT3* and the untagged control contained similar amounts of proteins (***Figure 2.11*** G). As explained before, 6H-Ub had lower protein levels from the beginning, which should not play a role for the final result. Furthermore, the comparison between input and unbound material indicates similar overall protein amounts in both fractions of a respective sample, which in turn means that the vast majority of cellular proteins did not unspecifically bind to Co^{2+} beads. This underlines general specificity of the approach. The effect of ubiquitin and SUMO depletion in the unbound fraction of the TCE staining cannot be seen, however, this can be explained with the low abundance of the respective conjugates compared to the overall protein content.

In short, the results presented in this and the previous chapters suggest that Dnm1 is ubiquitylated (***Figure 2.11***) and degraded via the ubiquitin-proteasome system (***Figure 2.1*** and ***Figure 2.2***). Furthermore, it could be shown that Dnm1 turnover is apparently enhanced upon ethanol treatment (***Figure 2.3***). An open interesting question is whether specifically the ubiquitylated forms of Dnm1 shown in ***Figure 2.11*** lead to its degradation or if they have a regulatory function. Several approaches (***Figure 2.1***, ***Figure 2.2***, ***Figure 2.8***, ***Figure 2.9*** and ***Figure 2.11***) have been performed in order to investigate the putative sumoylation of Dnm1. In these experiments, however, sumoylation of Dnm1 could not be clearly demonstrated. Therefore, at this point, it is unlikely that a major fraction of Dnm1 is sumoylated. Still, as it is known that usually only a very small subset of a substrate is sumoylated (Johnson, 2004), it cannot be excluded that a minor fraction of Dnm1 is sumoylated under certain conditions.

2.4 Analyses of SUMO conjugates by mass spectrometry

2.4.1 Mass spectrometry after denaturing purification of 8H-Smt3 conjugates

Previously, it was demonstrated that 8H-Smt3 can be used in order to purify the SUMO conjugates of yeast cells under denaturing conditions by the application of Co^{2+}-beads (***Figure 2.10***). Furthermore, it was shown that exemplarily sumoylated Cdc11 could be purified and detected within the bulk of sumoylated proteins with the same method (***Figure 2.11***). Preceding studies have exploited the same or similar methods in order to identify SUMO conjugates by mass spectrometry. An approach very similar to the one described below was applied by Wohlschlegel and colleagues (Wohlschlegel et al., 2004). Like in this study, the authors made use of a yeast strain which expresses *SMT3* fused to a sequence encoding an N-terminal 8His-tag from the endogenous locus. In the cited publication and in the study presented here, sumoylated proteins were purified by Ni^{2+}- or Co^{2+}-coated beads under denaturing conditions. Other studies, which were published around the same time, made use of similar but still varying techniques. Notably, different types of tags and techniques have been applied for the purification of sumoylated proteins. For example, sequential affinity purification techniques with Ni-NTA- and FLAG-beads have been applied (Denison et al., 2005; Zhou et al., 2004). An even more sophisticated technique was used in a study where after Talon- and FLAG-bead purification, TEV-protease was utilized in order to elute sumoylated proteins from agarose-beads (Hannich et al., 2005). A rather different approach was chosen by Panse and colleagues (Panse et al., 2004). Here, the authors made use of an N-terminal ProtA (Protein A) tag which allows purification of ProtA-Smt3 by IgG-coated beads. However, this procedure required binding under native conditions, which makes the respective study unique. Although it was tried to circumvent potential co-purification of binding partners of SUMO-targets by washings with high concentrations of $MgCl_2$, it could not entirely be excluded that some of the substrates detected by mass spec were non-covalently binding to sumoylated proteins. This was also mentioned as a major difference by authors of comparable studies (Hannich et al., 2005). More recently, efforts were made in order to determine the SUMO-modified lysine residues of substrate proteins in *Saccharomyces cerevisiae* (Albuquerque et al., 2015; Esteras et al., 2017), as explained further below, and in human cells (Lamoliatte et al., 2017).

For the first attempt of identification of sumoylated proteins in this study, an approach similar to the one from Wohlschlegel and colleagues (Wohlschlegel et al., 2004) was conducted. One advantage of this approach is the use of the small 8His-tag, which is assumed to have less potential impact on the function of SUMO, compared to double- or larger tags. In the respective strain, *8H-SMT3* is expressed from the endogenous locus, so the strain has physiological levels of SUMO conjugates, as demonstrated earlier

(***Figure 2.10, Figure 2.11***). Furthermore, a purification under strictly denaturing conditions was conducted, so that only directly sumoylated substrates should be detected by mass spectrometry. As described above, in some of the previous studies, a two-step purification by Ni-NTA and FLAG M2 was performed, however, this requires changing from a denaturing buffer to a native one, which poses a potential risk of material loss, for example due to low solubility of certain proteins. Additionally, FLAG M2 beads have a greatly reduced binding capacity compared to Ni^{2+} or Co^{2+}-beads. Therefore, a higher purity may come at the cost of reduced yield. This in turn is a potential problem since low abundant SUMO-substrates might be below the detection level in mass spectrometry, as was also argued in aforementioned studies (Denison et al., 2005; Panse et al., 2004; Wohlschlegel et al., 2004).

For the results presented in ***Figure 2.12***, cell pellets with 1000 OD*ml were lysed by glass beads in denaturing buffer with 8 M urea at pH 8.0. 8His-Smt3 conjugates were then bound to Co^{2+}-coated Talon beads over night at room temperature. After washings with pH 6.5, two consecutive elutions with pH 4.3 were performed. These two eluates per strain were then analyzed by mass spectrometry. Since the aim was not only to identify SUMO substrates but also to determine changes in *uls* mutants, the analysis was in parallel performed in *8His-SMT3*-expressing wildtype, *slx8*Δ, and *ULS1*-shutoff (P_{GAL1}-*ULS1* in YPD) strains. A wildtype strain with untagged *SMT3* was treated accordingly and served as a negative control.

In ***Figure 2.12*** A-C, for the three tested strains, the 20 candidates with the largest difference compared to the negative control are presented. For *8His-SMT3* in wildtype, only 18 candidates were considered as relevant, meaning that the $\log_2$ difference was ≥ 0.58, which in turn indicates an enrichment of at least 1.5 compared to the negative control. The results were obtained by independent measurements of the two consecutive elutions. The p-values were calculated but not considered for the assessment of the relevance for the respective candidate since both measurements originate from the same purification. Instead, for this first mass spectrometric approach, the candidates were rated according to their difference value, as indicated in ***Figure 2.12*** A-C.

Notably, six of the candidates, marked in purple, were enriched in all of the six measurements (***Figure 2.12*** A-C). Among these are trivial candidates like Smt3 itself and the SUMO-conjugating enzyme Ubc9. Furthermore, the well-characterized SUMO substrate Cdc3 (Johnson and Blobel, 1999) was enriched in all samples. Additionally, Cdc3 was apparently more abundant in *slx8*Δ compared to the other two strains, as highlighted in ***Figure 2.12*** C. Therefore, it is a conceivable substrate for Uls2-mediated degradation and especially due to the limited knowledge about Uls2 substrates, further investigation might be beneficial.

A

8H-SMT3 in wild-type strain, candidates with highest difference			
Protein name	**Gene name**	**log_2 difference**	**Found in literature**
Proteasome subunit beta type-6	***PRE7***	**12.66**	**(L)**
Ubiquitin-like protein SMT3	***SMT3***	**4.96**	**target for pulldown**
Proteasome subunit beta type-7	*PRE4*	2.39	(L)
SUMO-conjugating enzyme UBC9	***UBC9***	**2.19**	**D, W, Z, H, E, A**
Aminomethyltransferase, mitochondrial	***GCV1***	**1.32**	
Cell division control protein 3	***CDC3***	**1.31**	**D, W, P, Z, H, E, A**
Phosphatidate cytidylyltransferase	***CDS1***	**1.14**	
40S ribosomal protein S29-B	*RPS29B*	0.94	
Suppressor protein MPT5	***MPT5***	**0.90**	
ATP-dependent RNA helicase HAS1	*HAS1*	0.85	W
37S ribosomal protein MRP21, mitochondrial	*MRP21*	0.80	Paasch (mito)
Mitochondrial metal transporter 1	*MMT1*	0.79	
DNA-directed RNA polymerases I, II, and III subunit RPABC1	*RPB5*	0.78	
40S ribosomal protein S29-A	*RPS29A*	0.76	
Heat shock protein SSB1	***SSB1***	**0.67**	**P**
Protein PBP4	*PBP4*	0.66	
ATPase GET3	***GET3***	**0.59**	
V-type proton ATPase subunit H	*VMA13*	0.59	

Candidate in all three strains
Additionally candidate in *slx8Δ*

B

8H-SMT3 in P_{GAL1}-*ULS1* (*ULS1* shutoff), candidates with highest difference			
Protein name	**Gene name**	**log_2 difference**	**Found in literature**
Ubiquitin-like protein SMT3	***SMT3***	**4.84**	**target for pulldown**
SUMO-conjugating enzyme UBC9	***UBC9***	**1.93**	**D, W, Z, H, E, A**
Proteasome subunit beta type-6	***PRE7***	**1.76**	**(L)**
60S acidic ribosomal protein P1-alpha	*RPP1A*	1.60	
Cell division control protein 3	***CDC3***	**1.30**	**D, W, P, Z, H, E, A**
Phosphatidate cytidylyltransferase	***CDS1***	**1.09**	
Family of serine hydrolases 1	***FSH1***	**1.04**	
Putative uncharacterized protein YMR082C	*YMR082C*	0.95	
Maintenance of telomere capping protein 1	***MTC1***	**0.89**	
Nicotinamide/nicotinic acid mononucleotide adenylyltransferase 2	***NMA2***	**0.88**	
Probable 1,3-beta-glucanosyltransferase GAS3	*GAS3*	0.86	W
DNA-directed RNA polymerases I, II, and III subunit RPABC5	***RPB10***	**0.80**	
Suppressor protein MPT5	***MPT5***	**0.79**	
Ubiquitin-activating enzyme E1 1	***UBA1***	**0.77**	
Histidine--tRNA ligase, mitochondrial	***HTS1***	**0.76**	
Uncharacterized membrane protein YGR149W	***GPC1***	**0.74**	
C-5 sterol desaturase	*ERG3*	0.69	
NADH-cytochrome b5 reductase 1	***CBR1***	**0.68**	
ATPase-stabilizing factor 15 kDa protein	*STF2*	0.67	
Nascent polypeptide-associated complex subunit beta-1	*EGD1*	0.67	

Candidate in all three strains
Additionally candidate in *slx8Δ*

C

***8H-SMT3* in *slx8Δ*, candidates with highest difference**			
Protein name	**Gene name**	**log_2 difference**	**Found in literature**
Ubiquitin-like protein SMT3	***SMT3***	**4.01**	**target for pulldown**
Proteasome subunit beta type-6	***PRE7***	**3.78**	**(L)**
Glyceraldehyde-3-phosphate dehydrogenase 1	*TDH1*	3.34	D, E
Reticulon-like protein 2	*RTN2*	3.26	
Cell division control protein 3	***CDC3***	**3.24**	**D, W, P, Z, H, E, A**
NADPH-dependent alpha-keto amide reductase	*YDL124W*	3.07	
SUMO-conjugating enzyme UBC9	***UBC9***	**2.75**	**D, W, Z, H, E, A**
Carbamoyl-phosphate synthase arginine-specific large chain	*CPA2*	2.64	P
Glucokinase-1	*GLK1*	2.34	
Ribonucleoside-diphosphate reductase small chain 2	*RNR4*	2.30	
Hexokinase-1	*HXK1*	2.14	
Ubiquitin-activating enzyme E1 1	***UBA1***	**2.04**	
Proliferating cell nuclear antigen	*POL30*	1.99	D, W, P, Z, H, E, A
Glycerol-1-phosphate phosphohydrolase 2	*GPP2*	1.93	
Glycogen phosphorylase	*GPH1*	1.86	
Glycerol 2-dehydrogenase (NADP(+))	*GCY1*	1.79	D
Ribonucleoside-diphosphate reductase small chain 1	*RNR2*	1.78	D, E
Cell division control protein 10	*CDC10*	1.71	P
Sphingosine-1-phosphate lyase	***DPL1***	**1.68**	
Endoplasmic reticulum vesicle protein 25	***ERV25***	**1.68**	

Candidate in all three strains, enriched in *slx8Δ*
Additionally candidate in *ULS1* shutoff

D

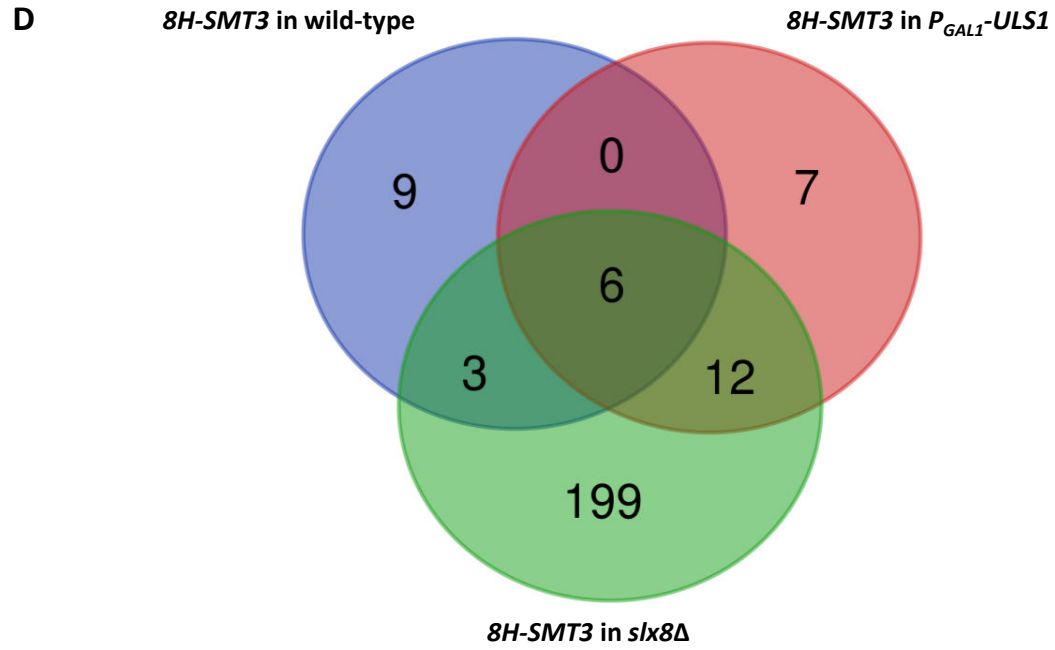

Figure 2.12: Results of mass spectrometric analysis after denaturing 8H-Smt3 purification in different strains
A) – C) 8H-Smt3 conjugates were purified with Co^{2+}-beads under denaturing conditions in wild-type yeast (*8H-SMT3*, Sc.1879), P_{GAL1}-*ULS1* (*8H-SMT3* P_{GAL1}-*ULS1*, yAS18) after transcriptional shutoff and *slx8*Δ (*8H-SMT3 slx8*Δ, MM4-1). As untagged congenic control, JD47-13C was treated accordingly. For each purification, 1000 OD*ml yeast pellets were applied. Of each purification,

two consecutive elutions with pH 4.3 were performed and analyzed by mass spectrometry in collaboration with Clara Türk and Markus Krüger. Therefore, two independent mass spectrometric measurements were performed for the same purification. A protein is regarded as candidate if the difference compared to untagged is ≥ 1.5 (meaning $\log_2$ difference is ≥ 0.58) and it was found in both measurements in the *8H-SMT3* expressing strain. The p-value was not considered for this analysis. The tables show the 20 (or 18 in A)) candidates with the highest difference scores in the respective strain. Candidates which are also candidates in other strains are marked in bold in the indicated color. *CDC3* is marked in yellow as a candidate which was found in all measurements with enrichment in *slx8*Δ compared to the other strains. The right-most column shows if the protein was found in previous studies, indicated by the respective letter. P: Panse et al., 2004, W: Wohlschlegel et al., 2004, Z: Zhou et al., 2004, D: Denison et al., 2005, H: Hannich et al., 2005, A: Albuquerque et al., 2015, , E: Esteras et al., 2017, L: Lamoliatte et al., 2017. The latter one is a study from mammalian cells, therefore, the (L) is in brackets. Paasch (mito) indicates that this is a mitochondrial protein, which was found as substrate in Paasch et al., 2018. **D)** Venn diagram which indicates the overlap of candidates in the three strains.

The aforementioned examples confirm that known SUMO substrates could be identified by the method applied here. Interestingly, Pre7/β6, a subunit of the proteasome core particle (Groll et al., 1999), was in addition found as a candidate in all six measurements. Furthermore, at least in wild-type, Pre4/β7, another component of the proteasome core was found as candidate for sumoylation. So far, in *S. cerevisiae* these proteins are not known as SUMO targets. However, in human cells, for all of the 14 different subunits of the normal proteasome CP (core particle), sumoylation sites could be detected (Lamoliatte et al., 2017). Some of the proteasomal subunits were heavily modified and in total, 128 modified lysine-residues present on the proteasome could be detected in the study (Lamoliatte et al., 2017). The majority of sumoylation of the CP occurred at the outer surface of the structure and, upon MG132-treatment, sumoylation was increased, which in turn promoted translocation of the proteasome into the nucleus, where it co-localized with PML NBs (promyelocytic leukemia protein nuclear bodies) (Lamoliatte et al., 2017). Therefore, it might be interesting to ask if sumoylation of Pre7 can be confirmed, which would establish that sumoylation of the proteasome CP occurs in yeast as well.

Other candidates which were enriched in both of the two measurements of the three tested strains are Cds1 and Mpt5. Both of these proteins were previously not reported as SUMO substrates. Cds1 catalyzes the conversion of CTP (cytidine triphosphate) and PA (phosphatidic acid) to CDP-DAG (cytidine-diphosphate diacylglycerol) and diphosphate (Liu et al., 2014; Shen et al., 1996; Tamura et al., 2013). CDP-DAG, synthesized by Cds1 in the ER, is a central intermediate for phospholipid biosynthesis. It could be shown that in mitochondria, another enzyme, Tam41, synthesizes CDP-DAG (Tamura et al., 2013). Still, *CDS1* is required for cell growth (Shen et al., 1996), and due to its key biological function in phospholipid biosynthesis, a possible sumoylation might be of interest.

Mpt5, also named Puf5 or Uth4, is an RNA-binding protein which binds to ~ 1000 RNA targets and thereby exerts post-transcriptional control on mRNA targets involved in various processes (Wilinski et al., 2015). One of these functions is ensuring cell wall integrity, which in turn promotes longevity (Kaeberlein and Guarente, 2002). Furthermore, Mpt5 is required for relocalization of gene silencing Sir proteins to the

nucleolus in old yeast cells (Kennedy et al., 1997). Additionally, by binding to the 3'-UTR (3'-untranslated region) of the *HO* mRNA, the expression of this endonuclease, which stimulates mating type switch, is repressed. Thereby, Mpt5 prevents synthesis of the HO protein in daughter cells (Tadauchi et al., 2001). As indicated in ***Figure 2.12***, Mpt5 is a putative SUMO substrate and further examination might be of interest.

Within the top candidates, a number of already published SUMO substrates were found. One well-studied SUMO-substrate is Pol30 (also termed PCNA (proliferating cell nuclear antigen)) with involvement in DNA replication and bypassing of DNA-lesions (Arbel et al., 2020; Parker et al., 2008). Other previously published substrates are Tdh1 and Rnr2 (Denison et al., 2005; Esteras et al., 2017). Notably, out of the screened literature, only these two publications found these two SUMO-substrates. However, since Esteras and colleagues identified the modified lysine-residues of both, these are still high-confidence candidates. The fluctuations in detected SUMO substrates across the different studies suggest that the detection of respective peptides is to some degree stochastic, as also stated by the authors of one study (Lamoliatte et al., 2017). Furthermore, all studies have variations in the applied methods, which can also explain differences in the candidates found.

As presented in ***Figure 2.12*** D, by far the most SUMO targets were identified in *slx8*Δ. On the one hand, this is to some degree expected, due to a defect in degradation of SUMO substrates, on the other hand, it should be noted here that in general the abundance of proteins may differ in *slx8*Δ compared to wildtype. This means that the overall protein background could be different in *slx8*Δ, which is probably responsible for changes in the measured intensities of some proteins. This circumstance has to be kept in mind and for future approaches as it highlights the importance of using an untagged control of the isogenic background for the respective purification and mass spectrometry. Nevertheless, most of the highest-ranked candidates in *slx8*Δ were found in other strains as well and/or these are known SUMO targets. This leads to the conclusion that, despite the mentioned obstacles, genuine substrates were identified in *slx8*Δ, with Cdc3 as putative candidate for Uls2-mediated degradation, as described above.

In order to obtain more robust results, with an approach very similar to the one described before, the purification of 8H-Smt3 conjugates and subsequent mass spectrometry were performed with a larger set of replicates. Furthermore, in order to improve the method, some changes were made in the protocol. This time, as congenic control, the strain MB2 was used instead of JD47-13C since MB2 has a functional *TRP1* gene, like *8H-SMT3::TRP1*. This should circumvent potential differences in protein composition of

A

8H-SMT3 **in wild-type strain, Top 40 candidates sorted by difference**

Gene name	-log$_{10}$ p-value *8H-SMT3* vs control	log$_2$ Difference *8H-SMT3* vs control	Present in number of purifications (n=4)		Found in previous experiment (also see *Figure 2.12*)	Found in literature
			8H-SMT3	control		
OCT1	8.57	7.65	4	0		
SMT3	2.53	7.60	4	2	wt, *ULS1* shutoff, slx8Δ	target
RPN5	2.94	4.04	4	0		
YCK2	5.75	3.73	4	0		D
MDM20	6.05	3.07	4	4		
NOP7	2.87	2.99	4	0		E, W
CAB2	4.11	2.98	4	0		
UBA1	3.41	2.97	4	0	*ULS1* shutoff, *slx8Δ*	
CPR6	2.24	2.97	3	0	*slx8Δ*	
UBC4	3.67	2.79	4	4		
PAT1	5.95	2.78	4	4		
RPA135	1.69	2.78	4	0		D, W
TSA1	5.07	2.74	4	0	*slx8Δ*	D, Z
YNL011C	3.83	2.71	4	0		
TES1	2.76	2.63	4	0		
TMA108	2.19	2.57	4	1		
PGM1	3.34	2.47	4	0		
ADE2	4.13	2.45	4	0		
SKY1	4.34	2.38	4	0		
ARP3	2.96	2.35	4	0		
NCP1	2.90	2.28	4	0	*slx8Δ*	D, W
RTT107	2.14	2.27	4	4		
HAS1	5.10	2.27	4	4	wt	W
APL4	2.35	2.27	4	0		
RPE1	3.07	2.23	4	0	*slx8Δ*	
SCP160	4.04	2.20	4	4		
NOG1	2.16	2.19	4	4		W
PET18	2.86	2.15	4	0		
MSC3	3.91	2.11	4	0		
RIB7	2.33	2.09	4	0		
PDE2	4.78	2.09	4	4		
ARC19	2.21	2.06	4	0		
UFO1	2.68	2.06	4	0		
URA1	3.36	2.04	4	4		W
SPE3	1.64	2.03	4	3	*slx8Δ*	
ARG1	3.11	2.03	4	0	*slx8Δ*	W
TRP4	1.94	2.02	4	0		
TRS31	2.72	2.00	4	0		
DBP7	2.04	1.98	4	0		
SEC24	2.14	1.98	4	0		

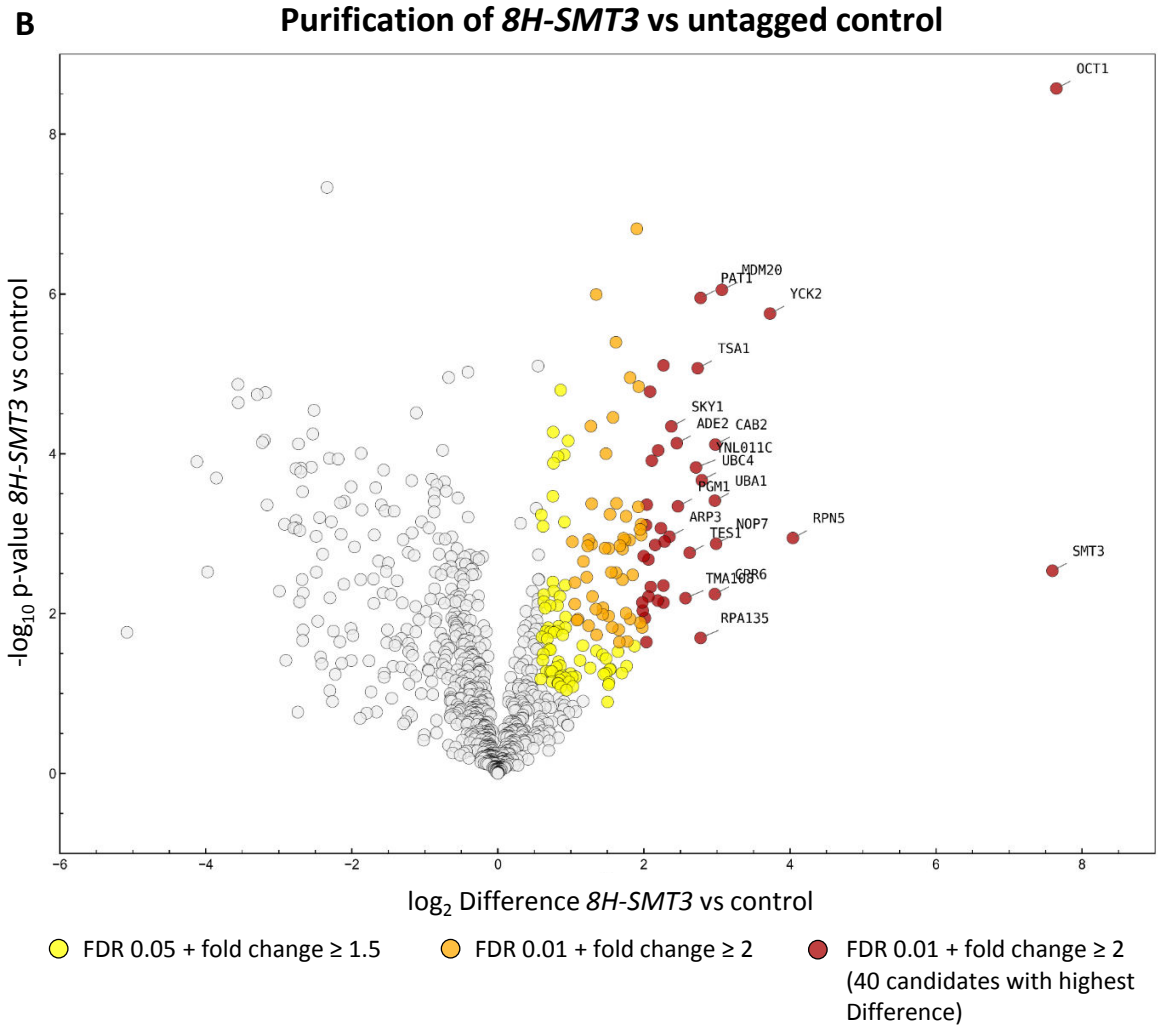

Figure 2.13 Results of mass spectrometric analysis in four replicates of wildtype and untagged control
A) 8H-Smt3 conjugates were purified with magnetic Co^{2+}-beads under denaturing conditions in wild-type yeast (*8H-SMT3*, Sc.1879). As untagged congenic control, strain MB2 was treated accordingly. For each purification, 1250 OD*ml yeast pellets were applied. Four independent purifications and mass spectrometric analyses were carried out for each of the two strains. Instead of a conventional elution, the beads were directly subjected to LysC and tryptic digestion. Analysis by mass spectrometry was performed in collaboration with Theresa Bock and Markus Krüger. A protein is considered as a candidate if the difference compared to untagged is ≥ 2 (meaning $\log_2$ difference is ≥ 1) with an FDR (false discovery rate) of 0.01. If a protein was detected at least three times in at least one of the strains but not in all measurements, missing values (NaN) were replaced by values generated by a normal distribution which is shifted 1.8-fold downward. In the table, it is indicated in how many of the four runs for each strain, the respective protein was found originally. With the criteria mentioned above, 92 candidates were identified and out of these, the 40 candidates with the highest differences are displayed in the table. The $-\log_{10}$ p-values, determined by two-tailed homoscedastic t-test, are indicated, as well. Proteins, which were found in the previous mass spectrometry analysis (***Figure 2.12***), are written in red. Proteins, which were described as candidates in the literature are highlighted in yellow and the respective study is indicated by an abbreviation (W: Wohlschlegel et al., 2004, Z: Zhou et al., 2004, D: Denison et al., 2005, E: Esteras et al., 2017). **B)** Volcano plot of the results from the same mass spectrometric analysis as in A) with all identified proteins displayed. All proteins with fold-change ≥ 1.5 at an FDR 0.05 but not matching the stricter criteria are shown in yellow and all proteins matching the stricter criteria fold-change ≥ 2 at an FDR 0.01 are shown in orange. Out of the 92 candidates matching strict criteria, the 40 highest scores in difference are shown in red, with the top 20 candidates annotated by name.

both strains due to presence or absence of *TRP1*. Furthermore, this time the lysis buffer was not supplemented with NH_4HCO_3. In the first run (***Figure 2.12***), this chemical was used in order to prevent protein carbamylation, which can be problematic for mass spectrometric analysis of proteins after application of urea-based buffers (Sun et al., 2014). However, it was noticed that NH_4HCO_3 causes foam formation during glass bead lysis, which is not desired, so NH_4HCO_3 was omitted in this run during glass bead lysis. Another change was that, this time, instead of usual agarose beads, magnetic Co^{2+}-coated beads were used. Accordingly, instead of centrifugation steps, a magnetic rack was applied to collect the beads. Moreover, this time the digest with LysC was performed directly on the beads. Later, to the same sample trypsin was added. Use of magnetic beads in combination with an on-bead digest allowed to keep the sample volume small and thus to obtain highly concentrated samples, which in turn facilitated downstream processing for mass spectrometric analysis. For the results presented above (***Figure 2.13***), for each of the two strains, four purifications and mass spectrometric analyses were performed with 1250 OD*ml pellets each.

The candidate with the highest difference to the untagged control measured in this mass spectrometry approach was Oct1 which is a peptidase located in the mitochondrial matrix. The majority of mitochondrial proteins possess a presequence for mitochondrial import via TOM (translocase of the outer membrane) and TIM23, the presequence translocase of the inner membrane (Endo and Yamano, 2009; Vögtle et al., 2011). In the mitochondrial matrix, this presequence is cleaved by MPP (mitochondrial processing peptidase). In some cases, the resulting intermediate protein is cleaved a second time, and one peptidase responsible for this activity is Oct1. Oct1 cleaves an octapeptide from the N-terminus and it was proposed that Oct1 thereby functions to convert destabilizing N-termini (according to the N-end rule) into stabilizing ones. Thus, Oct1 controls the stability of its substrates (Vögtle et al., 2011). In a recent study, a SILAC (stable isotope labelling by amino acids in cell culture) experiment was conducted with 6H-Smt3 and the authors could identify a number of mitochondrial proteins with SUMO modification, which did not rely on mitochondrial targeting of the substrate. The authors concluded that SUMO marks mitochondrial proteins in the cytosol upon import failure and thereby serves as quality control for nonfunctional and nonimported proteins (Paasch et al., 2018). Therefore, it is plausible that also in the experiments described above, mitochondrial proteins are detected as substrates, for example Mrp21 (***Figure 2.12***), which was also detected in the aforementioned study (Paasch et al., 2018), and Oct1 (***Figure 2.13***).

Another interesting potentially sumoylated protein is the ubiquitin-activating enzyme Uba1 (***Figure 2.12-13***). So far, this enzyme was not reported as SUMO substrate. However, it appeared as a candidate in the first mass spectrometry run in *ULS1* shutoff and *slx8*Δ (***Figure 2.12*** B - C) and in the second mass

spectrometry experiment (***Figure 2.13***). For this reason and due to our general interest in the crosstalk of ubiquitylation and sumoylation, this putative sumoylation might be of interest for further analysis.

In the volcano plot (***Figure 2.13*** B), the candidates matching the defined criteria (fold-change ≥ 2 and FDR 0.01) are highlighted in orange and red, the latter for the 40 candidates with the highest difference that are also displayed in the table (***Figure 2.13*** A). Noticeably, a relatively large number of proteins have reduced intensities compared to the control. One possible explanation for this observation would be that in the untagged control, proteins which contribute to the general background do not compete with genuinely binding 8H-Smt3 conjugates. Therefore, some of the background might be even enhanced in the untagged control. A second possible explanation, although seeming less likely, is that the 8H-tagged Smt3 causes some secondary effects that change the abundance of certain proteins.

2.4.2 Identification of sumoylation sites in wild-type and *ulp2*Δ

With the mass spectrometry experiments presented so far, a number of already published SUMO substrates were identified. In general, this can be considered as proof of concept for the conducted approach. Some of the found targets are very well described, like Cdc3, while others have been mentioned in only one of the aforementioned publications. Furthermore, an overlap between the mass spectrometry runs presented here could be found, however, within the screened literature and in the results described here, there were fluctuations in the identified candidates. Some of the differences can be explained with variations in the procedures, but it was also already described that results tend to differ between mass spectrometry runs (Lamoliatte et al., 2017). At this point, it is unclear whether some of the identified SUMO substrates are false positives. Therefore, in order to generate more reliable data on SUMO substrates, an aim in this study was to identify modification sites of sumoylated proteins. The identified peptides in this case are specific for SUMO-modified lysine residues, thus the likelihood of false positive candidates should be greatly reduced. Furthermore, the analysis was additionally carried out in *ulp2*Δ in order to find out if particular sumoylation sites can be specifically detected in wildtype or *ulp2*Δ. Moreover, this experiment should serve to establish the method and additional yeast strains with *8H-smt3-KallR-I96R* were generated so that the method detailed below can be used for the examination of sumoylation sites in different mutant backgrounds.

Previous studies made use of different techniques for the identification of sumoylation sites. In Albuquerque et al., 2015, the authors compared two approaches. In one approach 6His-3FLAG-smt3-I96R was purified by Ni-NTA- and anti-FLAG-beads. The mutation I96R leads to a GG-remnant on the

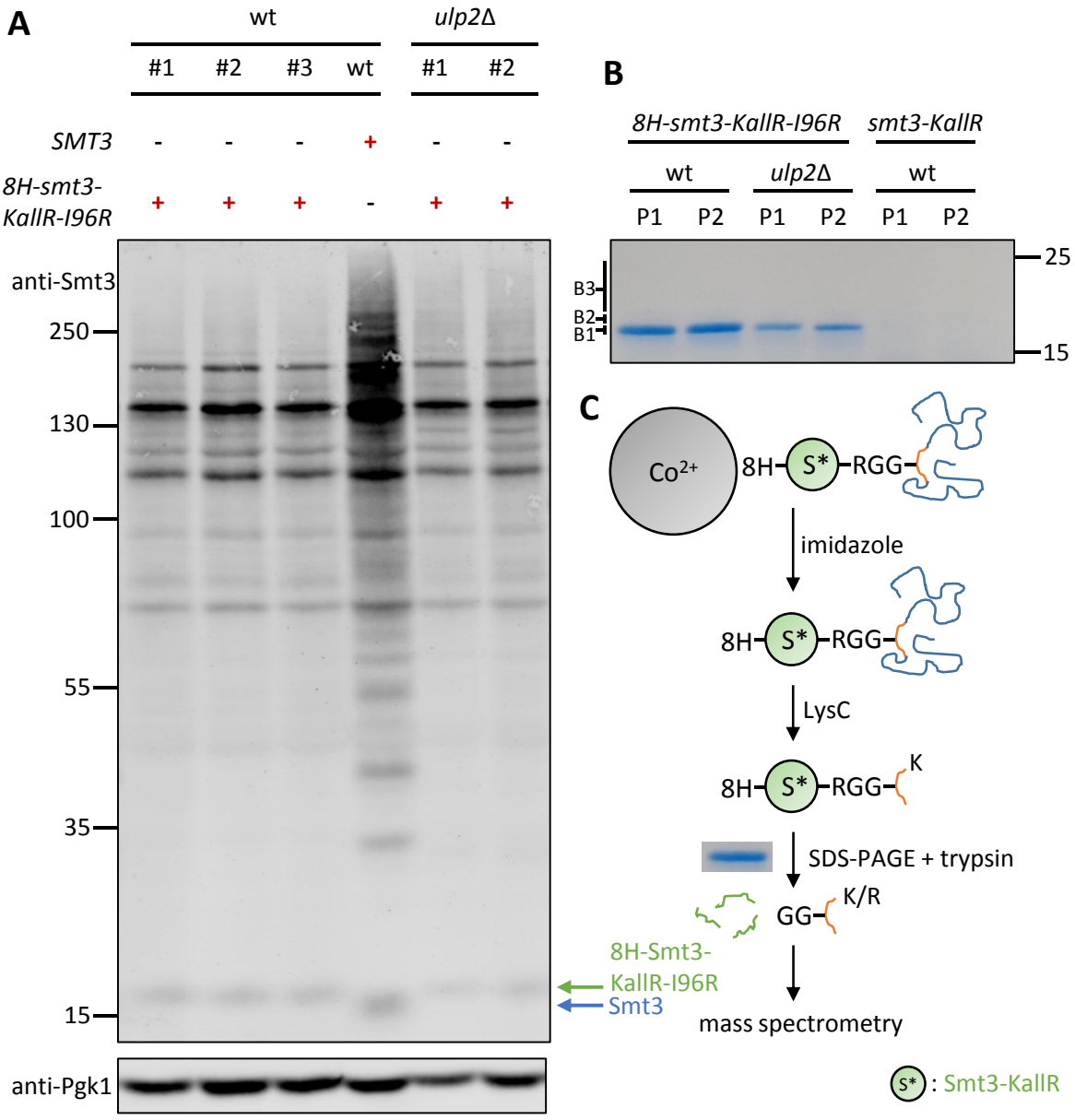

Figure 2.14 Application of 8H-Smt3-KallR-I96R for mass spectrometry

A) Western Blot analysis using a large 8% polyacrylamide gel for SDS-PAGE and wet transfer on a nitrocellulose membrane (14 cm x 14 cm) with 100 V and 400 mA for three hours in the cold room. The membrane was probed with anti-Smt3 (1:10000) and anti-Pgk1 (1:5000) antibodies. As secondary antibodies, anti-rabbit 800 (1:5000) and anti-mouse 680 (1:5000) were used. Bound secondary antibodies were detected with an Odyssey scanner. Bands that show free Smt3 and 8H-Smt3-KallR-I96R, respectively, are indicated by arrows. The applied wild-type strains are derived from MB2. *8H-smt3-KallR-I96R* #1-3: YSP105-1-3, independently generated transformants. *ulp2*Δ strains are derived from YLD38-1. *ulp2*Δ *8H-smt3-KallR-I96R* #1-2: YSP106-1-2, independently generated transformants. Untransformed MB2 served as congenic control for wild-type *SMT3*. Cells grew in YPD at 30°C for 2 doublings before harvesting. Loaded were 1 OD*ml of cells boiled in loading buffer. **B)** Coomassie staining using a large 12% polyacrylamide gel for SDS-PAGE. The staining was carried out following Dyballa and Metzger, 2012, a procedure described under Candiano's recipe in the respective publication. The three slices which were cut out of each lane and analyzed by mass spectrometry are marked with B1, B2 and B3. These are fractions after the LysC-digest. wt *8H-smt3-KallR-I96R*: derived from JD47-13C, YSP104-1; *ulp2*Δ *8H-smt3-KallR-I96R*: YSP106-1; wt *smt3-KallR*: derived from JD47-13C, YSP103-1. P1 and P2 represent purifications from separate pellets with 2000 OD*ml each. Cells grew in YPD at 30°C and were collected at an OD_{600} of 2. **C)** Schematic representation of the procedure for purification and mass spectrometry for targets of 8H-Smt3-KallR-I96R. The orange

part of the denatured polypeptide (blue) highlights a SUMO-modified peptide as it is later detected by mass spectrometry. S*: Smt3-KallR. See main text for further explanation.

sumoylation site after tryptic digest instead of a longer remnant as it would be the case for wild-type Smt3. The GG-modified peptides are easier to identify by mass spectrometry and indicate the sumoylated lysine-residue. In a second approach described by these authors, the same SUMO variant and purification protocol were applied, but additionally, after the FLAG-purification, all lysine residues were acetylated by acetic anhydride. The proteins were bound to Ni-NTA again and substrate peptides were released by Ulp1 cleavage. The lysine residue with previous SUMO modification had been protected from acetylation in contrast to all other lysine-residues. Since trypsin does not cleave behind acetylated lysine, the authors could identify sumoylation sites by the presence of the C-terminal lysine in the peptide generated by trypsin digestion. Altogether, with both methods, 53 sumoylation sites were identified with eight sites found in both approaches (Albuquerque et al., 2015). In a following study, the GG-remnant method was developed further. The authors made use of 8H-smt3-KallR-I96R, where all lysine-residues were replaced by arginine and which has the aforementioned I96R-mutation (Esteras et al., 2017).

A very similar approach with the same SUMO variant, expressed from the endogenous locus, was conducted in the study presented here. First of all, the sumoylation pattern of strains expressing *8H-smt3-KallR-I96R* was compared with a strain expressing endogenous *SMT3*. The Western Blot clearly indicates that the signal intensity of SUMO conjugates is reduced in *8H-smt3-KallR-I96R* (***Figure 2.14*** A). One obvious explanation for this would be that the mutant Smt3 is not conjugated with the same efficiency as wild-type Smt3, particularly due to the mutation I96R, close to the C-terminus. Another possible explanation for the observed effect would be that the anti-Smt3 antibody does not recognize the SUMO mutant with the same affinity as wild-type Smt3. Here it can be argued that, in a previous experiment, no differences between Smt3-Q95P and Smt3-KallR-Q95P could be seen in respect to overall signal intensity (***Figure 2.8***). Therefore, it seems more likely that conjugation of 8H-Smt3-KallR-I96R is impaired. Deletion of *ULP2* does not seem to have a major effect on the sumoylation pattern with 8H-Smt3-KallR-I96R. However, since this variant does not form chains and Ulp2 is known to act mainly on SUMO chains, this seems plausible. An interesting observation is that wild-type SUMO apparently forms a ladder-like pattern in the low molecular weight range on the Western Blot, while these signals are absent in *8H-smt3-KallR-I96R*. Possibly, these are unanchored SUMO chains, however, at this point it is unclear how these would arise. Altogether, the SUMO mutant seems to be less efficiently conjugated but since it still allows viability of the respective strains, it can be applied in the following experiment.

SUMO-acceptor sites identified by the application of 8H-Smt3-KallR-I96R					
Gene name	SUMO acceptor lysine (K) site found in Esteras et al. site found in Esteras et al. and Albuquerque et al. site found in Liang et al. (specific for Net1) site found in Esteras et al., Albuquerque et al. and Liang et al.	Present in number of analyses of *8H-smt3-KallR-I96R* (n=2 per strain)		Found in previous experiment (also see ***Figure 2.12***)	Found in literature
		wildtype	*ulp2Δ*		
AFT2	KFKENLR	0	1		
APC2	NIKFKNNLR	1	0		
BEM3	FNKMNLR	1	0		
CBF2	IDDADKFIR	1	0		W, E
CSN9	VTKEYLVQNLR	1	0		
CTF18	PKKFLDLVGNEK	1	0		
GPM1	NLFTGWVDVKLSAK	2	0		D, Z, H, E
HIS5	IINEEKMR	1	0		
HMO1	TTDPSVKLK	1	1		D, Z, H, E
JHD2	KNNYDSIR	1	0		
MRP8	EFKDIPDLK	1	1	MS 1 *slx8Δ*	D, W, Z, E, A
NET1	ELKEGPSSPASILPAK	0	1		D, W, E, A, Li
NET1	IKSSIVEEDIVSR	0	1		D, W, E, A, Li
NET1	ITSGMLKIPEPR	0	1		D, W, E, A
NET1	IVPQDSDSSSFPKSDLFK	0	1		D, W, E, A
NET1	SQAEPSGIVEPKR	0	1		D, W, E, A
NET1	SAVSESSVTNSKISEQMAK	0	1		D, W, E, A
NET1	VADLKSANIGGEDLNK	0	1		D, W, E, A
PRX1	TVRSVFVIDPKK	1	0	MS 1 *slx8Δ*	
PSO2	MSRKSIVQIR	1	0		
REP2	MDDIETAKNLTVK	0	1		D, E
RPC53	GFIKSEGSGSSLVQK	2	1		D, W, Z, H, E, A
RPL34A;RPL34B	AFLIEEQKIVK	2	0		E
RPL4B;RPL4A	LNPYAKVFAAEK	1	0		D, H, E
RPL8B;RPL8A	NFGIGQAVQPKR	2	0		D, E
RPS17B;RPS17A	YYPKLTLDFQTNK	2	0		Z, E
SHS1	EIKQENENLIR	0	1	MS 1 *slx8Δ*	D, W, P, Z, H, E, A
SUM1	IKNEIPINSLLPSSK	1	1		D, W, E, A
SWI1	ELELERKER	1	0		
UBC9	VLLQAKQYSK	1	0	MS 1 wt, *ULS1* shutoff, *slx8Δ*	D, W, Z, H, E, A
VNX1	KSMINIR	2	2		

Figure 2.15 SUMO acceptor sites identified by the application of 8H-Smt3-KallR-I96R

List of identified SUMO acceptor sites after completion of the procedure described in ***Figure 2.14*** and in the main text. On the initial list of putative candidates, certain criteria were applied. One is that the modified lysine residue was not allowed to be the one that constitutes a new C-terminus of a peptide after cleavage with LysC and trypsin. Additionally, the respective peptide was not allowed to be present in the control analysis. The here presented sites are displayed in alphabetical order according to the gene name. The expected SUMO modification site is highlighted in red font. Noteworthy, in the peptide from Ctf18, the two lysine residues were found as simultaneously sumoylated. Furthermore, sites which were described in Esteras et al., 2017 are marked in yellow and sites, which were additionally found by Albuquerque et al., 2015 are marked in green. Sumoylation sites of Net1,

which were found in Liang et al., 2017 are marked in blue. Sumoylation sites in Net1, which were found in all three aforementioned studies are marked in pink. It is indicated in how many independent mass spectrometry analyses the respective peptide was identified in the study presented here. Moreover, it is noted if the protein, but not necessarily the same site, was identified as SUMO target in the first mass spectrometry analysis presented before (***Figure 2.12***) and/or in the literature. P: Panse et al., 2004, W: Wohlschlegel et al., 2004, Z: Zhou et al., 2004, D: Denison et al., 2005, H: Hannich et al., 2005, A: Albuquerque et al., 2015, E: Esteras et al., 2017, Li: Liang et al., 2017 (the last publication only for Net1).

Yeast cells were lysed with glass beads in denaturing buffer containing 8 M urea. SUMO-modified proteins were bound to magnetic Co^{2+}-beads and after washing steps eluted with imidazole. The eluate was digested with LysC. Since the applied SUMO variant does no longer contain lysine, it is resistant to this digestion, so that after this treatment intact 8H-Smt3-KallR-I96R is bound to the modified peptide from the substrate. Subsequently, the digested eluate was loaded on a polyacrylamide-gel for SDS-PAGE. A Coomassie staining showed a single intense band which most likely is intact 8H-Smt3-KallR-I96R (***Figure 2.14*** B). For analysis, this band and two additional slices directly above were excised. As expected, the later identified candidates were present in either slice B1 or B2. After excision of the bands, an in-gel tryptic digest was performed and the peptides were extracted and analyzed by mass spectrometry. SUMO-modified peptides bear a GG-remnant on the modified lysine-residue (***Figure 2.14*** C).

In ***Figure 2.15***, the 31 identified SUMO-acceptor sites are presented. For the interpretation, generally, the results can be grouped into three categories. The first category consists of 15 sumoylation sites that were previously described in the aforementioned studies. These acceptor sites can be regarded as confirmation for the conducted approach and thereby serve as positive controls. Out of these 15 sites, 6 sites were identified in at least three studies, including this one, which suggests that these sites, present in Mrp8, Net1, Rpc53, Shs1, Sum1 and Ubc9, are relatively abundant and/or easily detectable. Consistently, Ubc9 (Ho et al., 2011; Klug et al., 2013), Rpc53 (Wang et al., 2018) and Shs1 (Johnson and Blobel, 1999) are well-characterized SUMO substrates. The second category is formed by six newly identified sites belonging to previously found SUMO targets. Cbf2 and Gpm1, which were published as SUMO-substrates (***Figure 2.15***), belong to this group (Denison et al., 2005; Esteras et al., 2017; Hannich et al., 2005; Wohlschlegel et al., 2004; Zhou et al., 2004). Remarkably, for Net1 seven sumoylation sites were identified, including three new ones, as elaborated below. Furthermore, a sumoylation site in the mitochondrial peroxiredoxin Prx1 (Pedrajas et al., 2000) was identified. This enzyme was found as a candidate already in a previous mass spectrometry analysis in this study, specifically in *slx8*Δ but not among the top 20 candidates and therefore not listed in ***Figure 2.12***. However, here it should be noted that it is well possible that Prx1 was sumoylated in the cytosol due to a failure in its mitochondrial import, like it was described for other mitochondrial proteins (Paasch et al., 2018). The third category of identified lysine residues consists of ten sumoylation sites of ten different proteins, which have not been described as SUMO substrates in any of the

aforementioned studies. One peculiarity here is that, according to the conducted analysis, in Ctf18 two consecutive lysine residues are sumoylated at the same time. Another interesting observation is that the depicted modification site in Vnx1 was identified in all of the four analyses, twice in a wildtype background and twice in *ulp2*Δ. Vnx1 is a vacuolar (Na^+,K^+)/H^+ antiporter (Cagnac et al., 2007, 2020) which is involved in the regulation of vacuolar pH (Cagnac et al., 2020). The fact that K843 was identified as sumoylated in all of the four replicates makes this finding trustworthy and it might be worthwhile to confirm sumoylation of Vnx1 and investigate a putative physiological role of this modification.

As mentioned above, for Net1, seven sumoylation sites were found (***Figure 2.15***). This is particularly interesting since, combined with the sites found in Albuquerque et al., 2015, in Esteras et al., 2017 and in the study focusing on Net1 from Liang et al., 2017, in total 17 unique sumoylation sites were identified in Net1. Four sites were identified in Albuquerque et al., 2015, twelve sites in Esteras et al., 2017, two sites in Liang et al., 2017, and seven sites in the current study with a fraction of these overlapping (***Figure 2.16***). For example, K268 was found as sumoylated in all mentioned studies. Taken together, Net1 is probably the protein with the largest number of known sumoylation sites in *S. cerevisiae*, so far.

Net1 is a component of the RENT (Regulator of nucleolar silencing and telophase exit) complex, together with Sir2 and Cdc14 (Shou et al., 1999). By interaction with Fob1, this complex localizes to the RFB (replication fork barrier) which is present at rDNA repeats within the nucleolus. In addition to proteins of the RENT-complex, Tof2 binds to Fob1 (Huang et al., 2006). One function of these proteins, located at the rDNA, is the suppression of transcription by RNA polymerase II, also termed rDNA silencing (Huang et al., 2006). It was already reported that the proteins implicated in rDNA silencing, including the RENT-complex, are strongly sumoylated, and that Ulp2 counteracts this sumoylation (Gillies et al., 2016). The recruitment of Ulp2 to this location is mediated by Csm1 (Liang et al., 2017). It was suggested that uncontrolled sumoylation of Net1, Tof2 and Fob1 at the rDNA causes their ubiquitylation by Slx5-Slx8, which in turn leads to reduced binding of these proteins to the rDNA locus. This may occur directly due to the ubiquitylation itself or due to following proteasomal degradation of these SUMO targets (Gillies et al., 2016). Specifically for Tof2 it was shown that polysumoylation causes its degradation via Slx5-Slx8 (Liang et al., 2017). Overall, excessive sumoylation of associated proteins followed by ubiquitylation is detrimental to proper rDNA silencing (Dhingra and Zhao, 2017). Therefore, loss of *SLX5* could rescue some of the defects arising in *ulp2*Δ (Gillies et al., 2016). In addition to its role in rDNA silencing, Net1 regulates cell cycle progression by nucleolar sequestration and release of Cdc14 (Waples et al., 2008) and stimulates rRNA synthesis by RNA polymerase I (Shou et al., 2001). Previously, it was already reported that sumoylation of Net1 is performed by two types of SUMO ligases, the Siz ligases and Mms21 (Reindle et al.,

2006). Altogether, Net1 is a SUMO-substrate in a process that is a prime example for the interplay of sumoylation, desumoylation and SUMO-targeted ubiquitylation followed by degradation.

The involvement of specific sumoylation sites of Net1 in these processes was not analyzed in detail so far and the large number of sumoylation sites on Net1 leaves open various questions. An obvious question is, how many SUMO moieties are conjugated to Net1 at the same time. Multi-sumoylation on various lysine-residues seems plausible here. Furthermore, it is interesting to ask if modifications of the lysine residues have individually different roles and outcomes, or if they are mostly redundant and sumoylation on Net1 is versatile. In order to further investigate Net1 sumoylation, for a preliminary experiment, the *NET1* gene was C-terminally tagged with *6HA.* In a Western Blot analysis of a crude extract, an apparently modified form of Net1 could be detected (data not shown), so this could be a starting point for further investigation of Net1 sumoylation. With K268, an apparently strongly sumoylated lysine-residue was identified which would be a suitable target for mutational analysis.

Identification of Net1 sumoylation sites in different studies

A

Albuquerque et. al., 2015 (4) Esteras et al., 2017 (12) **Liang et al., 2017 (2)** This study (7)	
K155	PVSLYKSVKRS
K266	IDAGKKIKSSI
K268	AGKKIKSSIVE
K366	TSGMLKIPEPR
K377	ISEIEKELKEG
K380	IEKELKEGPSS
K505	TIVEKKSQAEP
K517	GIVEPKRMTNF
K537	EDTNDKLLEKE
K541	DKLLEKEILPT
K618	SSSFPKSDLFK
K623	KSDLFKMIEGD
K665	DIDNSKPDPRN
K790	SVTNSKISEQM
K866	IDRQQKETTSR
K876	RVADLKSANIG
K1078	HDLPRKVRPSL

B

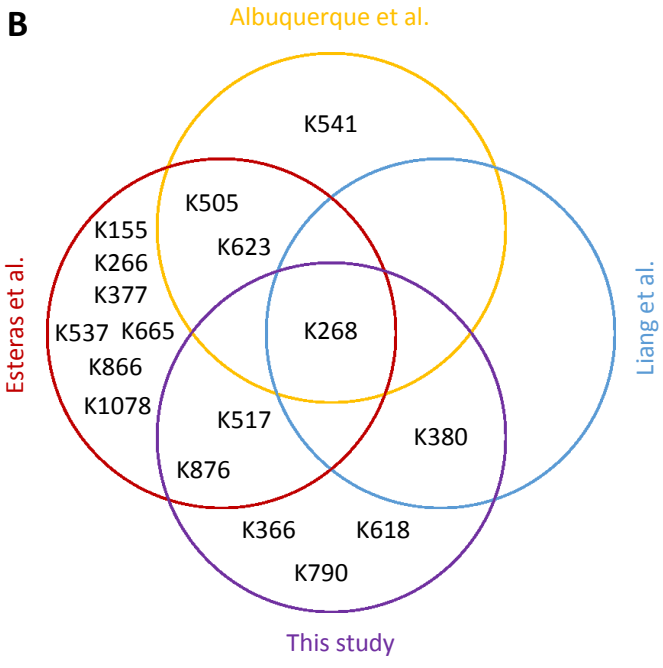

Figure 2.16 Identification of Net1 sumoylation sites in different studies
A) Shown are the altogether 17 distinct sumoylation sites of Net1 within the sequence context of five residues to the left and to the right. The depiction of the modified K indicates in which of the four studies it was found as sumoylated. In Albuquerque et al., 2015, four sites were identified in Net1, in Esteras et al., 2017 twelve sites, in Liang et al., 2017 two sites, and in this study seven

sites. Accordingly, the K is highlighted by yellow background, red font, bold fold or underlining, with possible overlap. **B)** Graphical representation of the table in A) in a Venn diagram.

Summarizing, the lists of SUMO-substrates identified in the three mass spectrometry experiments in this chapter serve as resource for future studies and specific sumoylation sites, as listed in ***Figure 2.15***, might be interesting for mutational analysis. The comparison of results between different studies should facilitate the evaluation of the reliability and relevance of the identification of a specific SUMO substrate. Furthermore, the established method for the identification of sumoylation sites can be applied in additional strains and under distinct conditions for insights into biological processes.

2.4.3 The N-terminus of Smt3 is processed and modified by another protein modifier

In our studies, so far an open question was if the N-terminus of Smt3 can be modified by protein modifiers such as Smt3 itself or ubiquitin. This might have implications for experiments performed with Smt3-KallR where otherwise the formation of SUMO chains or ubiquitylation of this SUMO moiety would not be possible. In order to answer this question, the dataset generated by the experiment from chapter 2.4.2 was searched for peptides from 8H-Smt3-KallR-I96R, including putative modifications of the N-terminus. The results are summarized in ***Figure 2.17***.

The first interesting observation is that the N-terminal peptides of 8H-Smt3-KallR-I96R did not start with methionine but instead with the second encoded residue, serine. This suggests that the leading methionine is cleaved by an aminopeptidase. This is in line with a previously formulated rule stating that the residue following the N-terminal methionine determines if the methionine is cleaved by the enzyme MAP (methionine aminopeptidase). Serine is one of the amino acids that lead to cleavage of the preceding methionine (Wingfield, 2017). Therefore, as detected in this study's dataset, the serine S2 is the N-terminus of Smt3 *in vivo* (***Figure 2.17*** A). Expectedly, these peptides are not detected in *smt3-KallR* since the 8H-tag is missing. This underlines specificity of the detection of peptides from 8H-Smt3-KallR-I96R. Furthermore, the N-terminal peptide of 8H-Smt3-KallR-I96R was found in the fractions B1, B2 and B3 in both, wild-type and *ulp2*Δ. This makes sense since 8H-Smt3-KallR-I96R is not cleaved by LysC and it is conjugated to substrate peptides of different lengths, which are resolved by SDS-PAGE. For the same reason many internal peptides of 8H-Smt3-KallR-I96R can be found in all of the fractions (***Figure 2.17*** A).

Intriguingly, in three samples, the N-terminal peptide of 8H-Smt3-KallR-I96R was found to be modified by GG at its N-terminus. This GG is expected to originate from a previous N-terminal modification by another protein modifier. 8H-Smt3-KallR-I96R can be excluded in this case since the tryptic digest would leave more

A

Detection of processed and modified N-terminus of 8H-Smt3-KallR-I96R

	Present in number of samples (B1 - B3 are fractions with increasing M.W., derived from SDS-PAGE, see ***Figure 2.14*** B) (n = 2 for each fraction)								
	smt3-KallR (control)			wt *8H-smt3-KallR-I96R*			*ulp2Δ 8H-smt3-KallR-I96R*		
Sequence	B1	B2	B3	B1	B2	B3	B1	B2	B3
SDHHHHHHHHSEVNQEAR	0	0	0	**2**	**2**	**1**	**1**	**1**	**1**
SDHHHHHHHHSEVNQEARPEVR	0	0	0	**2**	**2**	**1**	**1**	0	0
SDHHHHHHHHSEVNQEARPEVRPEVR	0	0	0	**2**	**2**	0	0	0	0
PEVRPEVR	1	1	1	2	2	1	2	2	2
PEVRPEVRPETHINLR	1	1	2	2	2	1	2	2	2
PEVRPETHINLR	1	1	2	2	2	1	2	2	1
PETHINLR	1	1	2	2	1	1	2	2	2
VSDGSSEIFFR	1	1	2	2	2	1	2	2	2
VSDGSSEIFFRIR	0	0	0	1	1	0	0	0	0
RTTPLRR	0	0	0	1	0	0	0	0	0
RLMEAFAR	0	0	0	2	1	0	0	0	0
LMEAFAR	0	0	0	2	2	0	0	1	1
QGREMDSLR	0	0	0	1	0	0	0	0	0
FLYDGIR	1	1	2	2	2	1	1	2	2
IQADQTPEDLDMEDNDIIEAHR	0	0	0	2	2	1	2	1	2
GGSDHHHHHHHHSEVNQEAR	0	0	0	**1**	0	0	0	0	0
GGSDHHHHHHHHSEVNQEARPEVRPEVR	0	0	0	**2**	0	0	0	0	0

Changes compared to wt *SMT3*

N-terminus of 8H-Smt3-KallR-I96R

GG from previous modification

Modified N-terminus

B

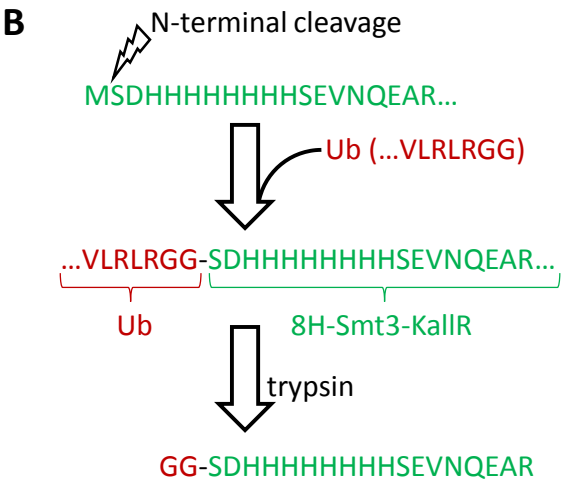

Figure 2.17: Detection of processed and modified N-terminus of 8H-Smt3-KallR-I96R

A) Summary of peptides from 8H-smt3-KallR-I96R, which were detected in the dataset generated as described in chapter 2.4.2. Depicted are results for the three strains *smt3-KallR* (which serves as a control in respect to the N-terminus), wild-type *8H-smt3-KallR-I96R* and *ulp2Δ 8H-smt3-KallR-I96R* as described in 2.4.2. B1, B2 and B3 are fractions of the SDS-PAGE which resolved the samples according to the molecular weight of the 8H-smt3-KallR-I96R-bound peptide (see ***Figure 2.14***). The molecular weight increases from B1 to B3. The numbers in the table indicate in how many runs the respective peptide was detected. n = 2 for each fraction. Up to two missed cleavages were allowed so that some peptides appear in longer variants, as well. Blue characters indicate changes in 8H-Smt3-KallR-I96R compared to Smt3. The green frame indicates detected N-terminal peptides of 8H-Smt3-KallR-I96R. Apparently, the leading methionine was cleaved. The GG marked in red is a modification of the N-terminus

of 8H-Smt3-KallR-I96R, which probably originates from previous ubiquitylation or modification by another modifier. The red frame highlights these modified N-terminal peptides. The data analysis was performed in collaboration with Kay Hofmann. **B)** Illustration of the processing and modification of the N-terminus of 8H-Smt3-KallR-I96R leading to the detection of the peptides shown in the red frame in A). Ubiquitin was chosen as example although modification by other protein modifiers is possible as explained in the main text.

residues than only -GG on the modified peptide. Additionally, these linear chains would be expected in fractions with higher molecular weight than B1 due to their resistance towards cleavage by LysC. Therefore, it can be concluded that another protein modifier has been conjugated to the N-terminus of 8H-Smt3-KallR-I96R. The most obvious candidate for such a modification is ubiquitin, which has a C-terminus ending with -RGG so that after tryptic cleavage -GG remains on the substrate peptide, as it is illustrated in ***Figure 2.17*** B. Another possible candidate for such a modification is Rub1 (the ortholog of human NEDD8) which would leave -GG on the target, as well. It appears that such an N-terminal modification of Smt3 has not been reported so far and it might be of importance for future experiments when Smt3-KallR or a derivative variant is applied. As explained before, previously it was unclear if Smt3-KallR is able to accept ubiquitylation at its N-terminus, for example when a substrate protein is targeted by a ULS. Now it seems likely that at least under certain conditions the N-terminus of Smt3 becomes ubiquitylated. However, at this point, it should be noted that the N-terminus of Smt3-KallR might be targeted as an alternative to the usually available lysine-residues in the N-terminal region. Therefore, still an open question is, if the N-terminus of Smt3 is still targeted when the lysine residues in close proximity are available. Moreover, with the size selection of peptides after the LysC treatment applied in the current experimental setup, it was very unlikely to detect putative sumoylation of the N-terminus, which would indicate that the formation of linear Smt3 chains is possible. The reason is that polypeptides encompassing a linear fusion of two LysC-resistant 8H-Smt3-KallR-I96R units have a significantly lower electrophoretic mobility than the ones extracted from the gel (see ***Figure 2.14*** B). This means, that although the respective peptides were not found in this experiment, the occurrence of linear Smt3 chains cannot be excluded, especially due to the fact that now it was observed that in principle the N-terminus of Smt3 can serve as a target for protein modifiers.

2.5 Growth phenotypes and respiratory competence of yeast strains lacking ULS or Ulp2

2.5.1 Strains lacking ULS or Ulp2 are generally respiratory competent

In the previous chapters, a putative connection between sumoylation and mitochondrial dynamics in yeast was investigated on the levels of proteins and their posttranslational modifications. The experiments conducted in this study did not point towards sumoylation of Dnm1. Still, as described before, the fact that yeast strains with defects in the control of sumoylated proteins exhibit fragmented mitochondria, suggested that, on a physiological level, possibly indirectly, there is an impact of sumoylation on the morphology of mitochondria. It is known that in *fzo1*Δ mutants, devoid of the key enzyme for mitochondrial fusion, mitochondria are fragmented, lose mtDNA (mitochondrial DNA) and yeast cells become respiratory deficient (Hermann et al., 1998; Rapaport et al., 1998). Therefore, an obvious question was if a lack of the control of sumoylated proteins causes an impairment of respiration as well. Mdm30 is an F-box protein within the ubiquitin ligase SCF^{Mdm30} mediating ubiquitylation of Fzo1 which in turn facilitates mitochondrial fusion (Cohen et al., 2011; Escobar-Henriques et al., 2006). At 37°C, *mdm30*Δ cells lose mitochondrial DNA and become respiratory deficient (Fritz et al., 2003). This observation was confirmed by a spot assay of *mdm30*Δ on YPGly at 37°C in the course of this study (data not shown). Encouraged by these reports, it was asked if an elevated temperature influences respiratory competence of ULS mutants and *ulp2*Δ. Therefore, and in order to get an impression of the general growth phenotypes, different mutant strains were grown on fermentable (glucose) and nonfermentable (glycerol) carbon sources at optimal growth temperature (30°C), as well as under heat stress (37°C) (***Figure 2.18***).

As expected, already under optimal growth conditions, on YPD at 30°C, some of the mutant strains displayed a growth defect (***Figure 2.18*** A, left panel). While *uls1*Δ grew very similar to the wild-type and *slx5*Δ had a comparably mild growth defect, the double mutant *uls1*Δ *slx5*Δ grew very slowly. This is in line with previous results (***Figure 2.7***) and suggests that Uls1 und Slx5-Slx8 have partly overlapping functions. The desumoylation defective strain *ulp2*Δ exhibited a growth defect which is even stronger than that of *uls1*Δ *slx5*Δ. The strain *dnm1*Δ, impaired in mitochondrial fission, did not show a growth defect under normal growth conditions. Furthermore, also *atg7*Δ did not show a prominent growth defect under the mentioned conditions. Atg7 is an E1 enzyme that mediates conjugation of the ubiquitin-like protein Atg12 to Atg5 and the conjugation of the ubiquitin-like protein Atg8 to PE (phosphatidylethanolamine) (Reggiori and Klionsky, 2013). Thereby Atg7 is essential for autophagy (Tanida et al., 1999) and *atg7*Δ loses mtDNA upon starvation (Medeiros et al., 2018). A *petite* isolate of *atg7*Δ which is not able to grow with only glycerol as carbon source (YPGly), was used as a control.

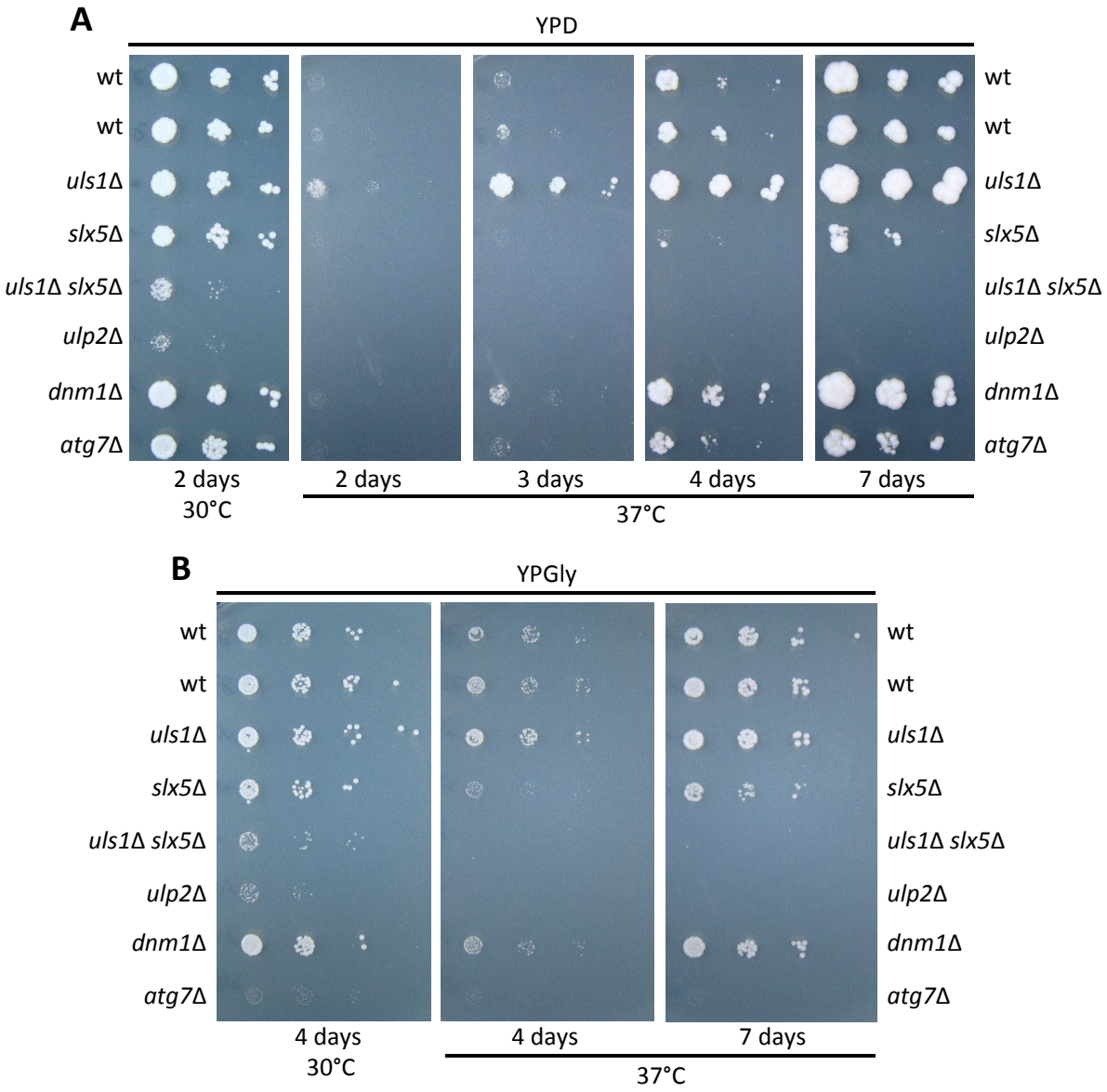

Figure 2.18: Comparison of the growth and respiratory competence of *ULS* mutants, *ulp2*Δ, *dnm1*Δ and a *petite atg7*Δ isolate
A) Spot assay of serial dilutions of the indicated yeast strains on YPD. On the plate shown in the left panel, the yeast grew at the optimal growth temperature 30°C for two days. The other panels show growth of the same strains on YPD at 37°C in the course of several days, as indicated. The strains are *uls1*Δ (YKU149), *slx5*Δ (YKU87), *uls1*Δ *slx5*Δ (YKU121), *ulp2*Δ (YKU1), *dnm1*Δ (MM6), *atg7*Δ (MS89, a *petite* isolate) and the congenic wild-type JD47-13C. **B)** Same as in A) but cells grew on YPGly with the nonfermentable carbon source glycerol. Spot assays were performed in technical duplicates.

When the same strains grew at 37°C, some differences to the above-mentioned phenotypes could be observed (***Figure 2.18*** A). First of all, strikingly and unexpectedly, at this higher temperature, *uls1*Δ grew much faster than the congenic wild-type. The spot assays for 30°C and 37°C were prepared from the exact same suspensions, therefore cells from the same *uls1*Δ suspension grew like wild-type at 30°C but much better than wild-type at 37°C. Spot assays prepared as technical duplicates confirmed these observations (data not shown). The underlying reason for this behavior cannot be determined at this point, however, in

a large-scale approach, it was found that mutations in genes encoding for subunits of the chromatin remodeling SWI/SNF complex provide high-temperature tolerance (Huang et al., 2018). Uls1 was also described as a member of the Snf2 family (Flaus and Owen-Hughes, 2011; Shah et al., 2010), so there might be a connection between both observations. It is conceivable that in *uls1*Δ there are general changes in the gene expression by induction or repression of genes which might be beneficial in a stress situation like heat stress. Furthermore, it was described that yeast cells which are exposed to mild stress, induce expression of ESR (environmental stress response) genes and are more resistant to severe stress afterwards (Berry and Gasch, 2008). Therefore, it can be imagined that also *uls1*Δ suffers from constant mild stress which in turn prepares this strain for growth at 37°C. In contrast, *slx5*Δ grew particularly slow at 37°C and showed, as previously described (Mullen et al., 2001), heterogeneous colony sizes. *uls1*Δ *slx5*Δ, as well as *ulp2*Δ did not display any growth at 37°C. This indicates that generally the control of sumoylated proteins is particularly important at higher temperatures. *Dnm1*Δ and *atg7*Δ did not show a prominent growth defect at 37°C.

As shown in ***Figure 2.18*** B, in principle all of the applied strains are able to grow on the nonfermentable carbon source glycerol with the exception of *atg7*Δ, which served as a control for the *petite* phenotype. *uls1*Δ *slx5*Δ and *ulp2*Δ grew much worse than wild-type yeast, however, this effect is in the same magnitude as on YPD. Therefore, it can be concluded that at least the majority of cells in both of these mutant strains are respiratory competent. At 37°C on YPGly, the results correspond to what was expected from the other spot assays. Again, *uls1*Δ grew better than wild-type at 37°C, however, the colony sizes in general were smaller on YPGly, so that this effect is not visible to the same degree as on YPD. *Slx5*Δ had, as usual, a growth defect but was able to grow on YPGly at 37°C, and is therefore also respiratory competent at elevated temperatures. As expected, *uls1*Δ *slx5*Δ and *ulp2*Δ were not able to grow at 37°C, however, here the carbon source is not the underlying reason.

Taken together, the here tested mutant strains *uls1*Δ, *slx5*Δ, *uls1*Δ *slx5*Δ, *ulp2*Δ and *dnm1*Δ are, correlating with their overall growth phenotypes, able to grow with glycerol as a sole carbon source, indicating that the majority of the cells of the respective strains are respiratory competent.

2.5.2 Synthetic sickness of *fzo1*Δ *slx5*Δ

Due to the lack of the key enzyme for mitochondrial fusion, Fzo1, the mitochondria in *fzo1*Δ are very fragmented and the strain is respiratory deficient (Rapaport et al., 1998). In our laboratory, it was observed that also *slx5*Δ has a tendency to give rise to cells with fragmented mitochondria (data no shown). Therefore, a question was if the additional deletion of *SLX5* in *fzo1*Δ worsens the phenotype, hypothetically due to a hyperactive fission machinery. For example, this could mean that mitochondria are even more fragmented than in *fzo1*Δ, which in turn might cause growth defects that exceed the known *petite* phenotype of *fzo1*Δ. In order to test this hypothesis, in wild-type yeast and in *fzo1*Δ, *SLX5* was deleted and the growth phenotypes of independently generated transformants were tested. *Fzo1*Δ by itself is already *petite*, so here the growth tests were performed on YPD (***Figure 2.19***).

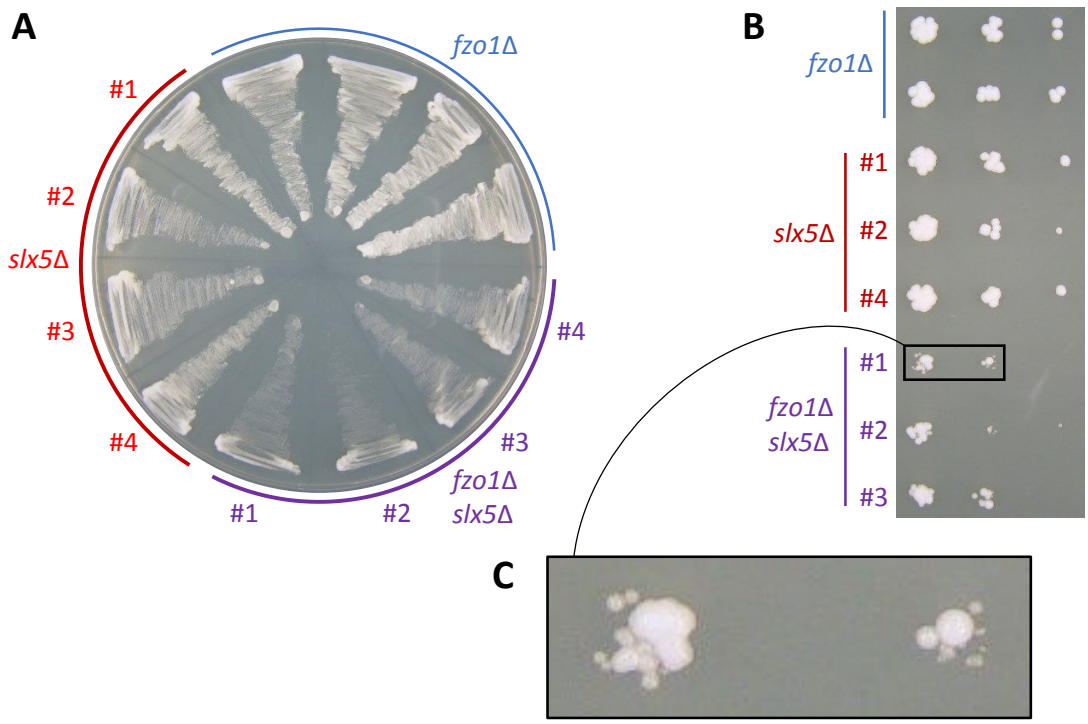

Figure 2.19: Slow growth and heterogeneous colony sizes of *fzo1*Δ *slx5*Δ suggest synthetic sickness

A) Streak outs of the indicated strains on YPD for comparison of the growth phenotypes. This photo was taken after growth for one day at 30°C. The strains are *fzo1*Δ (Sc. 4160, based on BY4741), *slx5*Δ (YSP52-1-4, based on BY4742) and *fzo1*Δ *slx5*Δ (YSP53-1-4, based on Sc. 4160). For the strain generation, *fzo1*Δ or the *MATα* congenic wild-type BY4742 were transformed with *slx5*Δ*::HIS3*. *Fzo1*Δ streak outs are technical replicates whereas streak outs of newly generated *slx5*Δ and *fzo1*Δ *slx5*Δ were prepared with four independent transformants each. **B)** Spot assay of serial dilutions of the indicated yeast strains and transformant numbers on YPD. This photo was taken after growth for one day at 30°C and growth for three days at room temperature. **C)** Magnified photo of *fzo1*Δ *slx5*Δ colonies to highlight the heterogeneous colony sizes.

First of all, the streak outs show that, after one day of incubation at 30°C, *fzo1*Δ had grown slightly better than *slx5*Δ (***Figure 2.19*** A). Interestingly, this changed after prolonged incubation since at later growth stages of the streak outs, *slx5*Δ continued to grow, whereas *fzo1*Δ slowed down growth at an earlier point

in time (data not shown). This suggests that, initially, *fzo1*Δ had a relatively normal growth rate, however, presumably due to failure in respiration, when the streak out becomes thicker and the nourishment with glucose is reduced, *fzo1*Δ cells do not generate a sufficient amount of energy for continued growth after a diauxic shift. Moreover, the streak outs indicate that the *fzo1*Δ *slx5*Δ streak outs had grown considerably less than *fzo1*Δ in the course of the one day prior to taking the photo (***Figure 2.19*** A). Also, after continued incubation, *fzo1*Δ *slx5*Δ had grown less than *fzo1*Δ (data not shown), which was confirmed by a spot assay (***Figure 2.19*** B). Furthermore, it is noticeable that the sizes of individual colonies of *fzo1*Δ *slx5*Δ were extremely heterogeneous (***Figure 2.19*** C). This could mean that, after mitosis and cytokinesis, a fraction of the daughter cells is physiologically impaired, possibly due to an adverse equipment with cell organelles. One possible explanation for this behavior would be that *fzo1*Δ *slx5*Δ fails to ensure correct distribution of mitochondria between mother and daughter cell. Even if these mitochondria are not respiratory competent, due to their roles in metabolism, a correctly organized inheritance might still be important. In order to investigate a putative effect of the *SLX5* deletion on the mitochondria morphology in *fzo1*Δ, fluorescence microscopy with mitochondria-targeted GFP was conducted. As expected, *fzo1*Δ showed very fragmented mitochondria but it was very difficult to evaluate if an already extreme fragmentation phenotype becomes even stronger upon deletion of *SLX5*, especially due to the fact that *slx5*Δ cells are much bigger in average than *fzo1*Δ (data not shown). Therefore, it can be summarized, that deletion of *SLX5* in *fzo1*Δ leads to an additional growth impairment, however, at this point it is not clear if this is caused by a stronger fragmentation of mitochondria.

2.5.3 Loss of ULS enzymes in *dnm1*Δ *fzo1*Δ leads to an increased *petite*-rate

At this point, one open question was if a loss of ULS enzymes, which leads to fragmentation of mitochondria, also causes a higher *petite* rate, be it in general or under specific conditions. Such an observation would suggest that, at least indirectly, the control of sumoylated proteins has an impact on mitochondrial function.

In a publication from Osman and colleagues, it was reported that *dnm1*Δ *fzo1*Δ, impaired in mitochondrial fission and fusion, distributed and inherited mtDNA normally. On the contrary, *dnm1*Δ *fzo1*Δ gave rise to an increased number of cells with nonfunctional mitochondrial genomes. These often exhibited structural rearrangements, which in turn caused inability of respiratory growth. As a consequence, after growth in synthetic glucose medium, a large fraction (23 %) of *dnm1*Δ *fzo1*Δ colonies was ρ^- (mtDNA present but not functional) but not ρ^0 (which would denote absence of mtDNA) (Osman et al., 2015).

In order to test if fragmentation of mitochondria in *uls1*Δ *slx5*Δ leads to an increased formation of ρ^- or ρ^0, as well, several methods were applied. One of these approaches made use of a deletion of *ADE2*. Usually, these *ade2*Δ colonies appear red due to an accumulation of a red pigment (Bharathi et al., 2016; Shadel, 1999; Sharma et al., 2003). However, *petite* colonies (ρ^- or ρ^0) of *ade2*Δ appear white and their color can be used in order to determine respiratory competence of colonies (Bharathi et al., 2016; Lai-Zhang et al., 1999; Shadel, 1999). Therefore, for the study presented here, diploids heterozygous for *ade2*Δ *dnm1*Δ *fzo1*Δ *uls1*Δ *slx5*Δ or *ade2*Δ *dnm1*Δ *fzo1*Δ P_{GAL1}-*ULS1* P_{GAL1}-*SLX5* were generated and, after sporulation and tetrad dissection, the color and respiratory competence of the obtained spores with the different genotypes were assessed.

However, it turned out that it was difficult to reliably determine the rates of *petite* formation with the *ade2*Δ mutants. Even though, in general it was observed that white colonies are indeed *petite,* a drawback of the method was that, in addition to white and red colonies, intermediate colors were found and that strains formed better growing white colonies, which are most likely *ade2* suppressors that avoid accumulation of the toxic red pigment. Specifically, for the *ade2*Δ *dnm1*Δ *fzo1*Δ triple mutant, it was found that the streak outs on YPD gave rise to red colonies and paler ("orange") colonies which were still more reddish than strains with a functional *ADE2* gene. From a number of these colonies, streak outs were made and it was noticed that the streak outs of orange colonies gave rise to only orange colonies. In contrast, after streak outs of red colonies, a mixture of red and orange colonies formed (***Figure 2.20*** A,B). The same streak outs on YPGly showed that the isolates only containing orange colonies were not respiratory competent whereas the red isolates containing a mixture of orange and red colonies were able to grow on YPGly (***Figure 2.20*** C). Therefore, the orange colonies of *ade2*Δ *dnm1*Δ *fzo1*Δ can be regarded as *petites*. Here, it should be noted that it is usual that on YPGly *ade2*Δ does not develop the red color. Furthermore, after a long incubation of *ade2*Δ *dnm1*Δ *fzo1*Δ on YPD, initially red colonies became orange in their periphery (***Figure 2.20*** D). For the experimental work with *ade2*Δ *dnm1*Δ *fzo1*Δ this was an obstacle since this finding, together with other general observations not shown here, suggests that red colonies, which are able to respire do not have a major growth advantage compared to *petite ade2*Δ *dnm1*Δ *fzo1*Δ. A possible explanation for this would be that, both the accumulation of the pigment in red colonies and respiratory incompetence of orange colonies, cause a growth defect. This in turn would mean that accumulation of the red pigment in *ade2*Δ already exerts a selection pressure, as also suggested by the fact that completely white *ade2*Δ suppressor colonies grow much better than their red predecessors (data not shown).

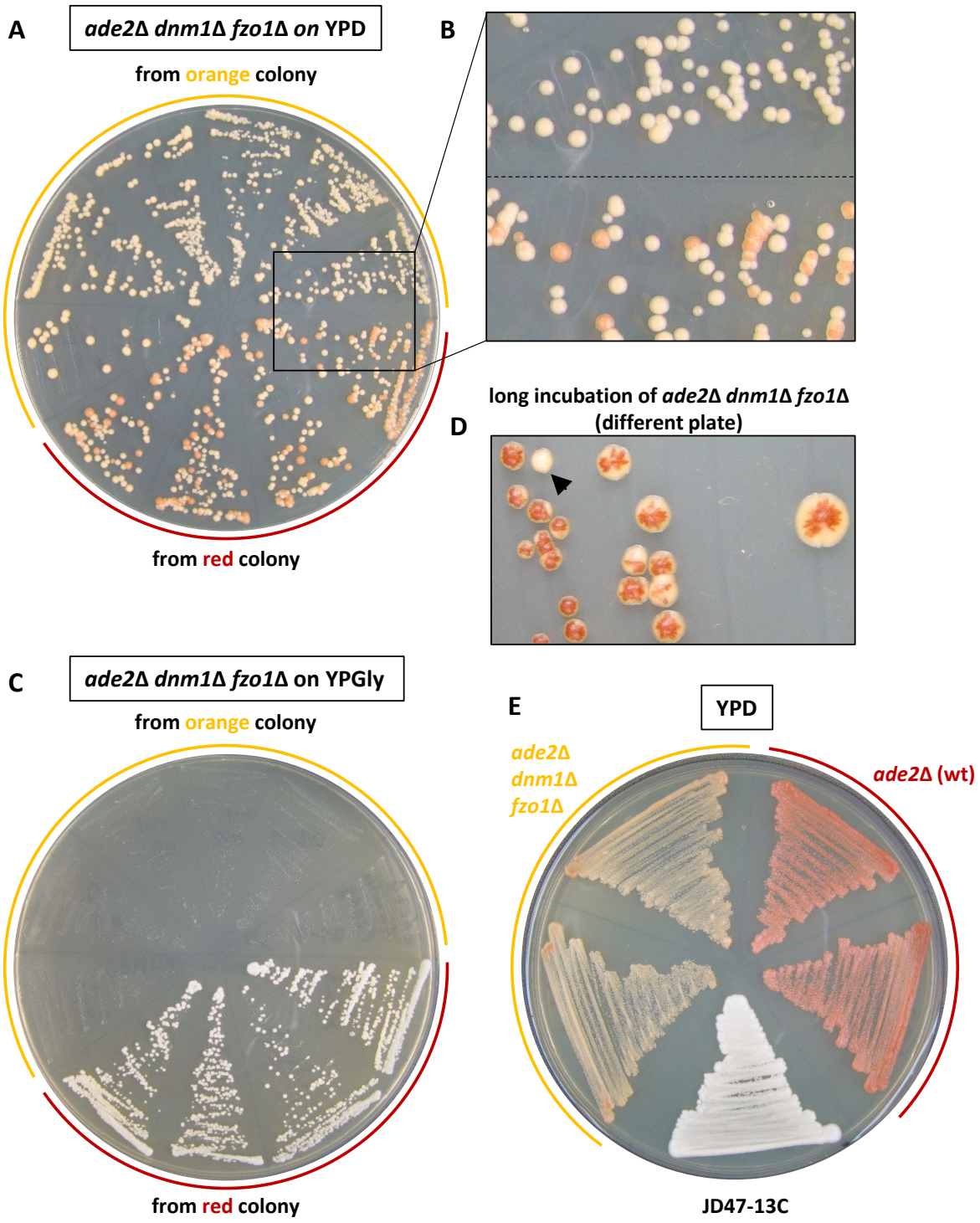

Figure 2.20: Formation of respiratory incompetent colonies of *ade2Δ dnm1Δ fzo1Δ*

A) Streak outs of previously identified single orange or red colonies of *ade2Δ dnm1Δ fzo1Δ* (YSP79-1) on YPD, incubated at 30°C. **B)** Magnification of an area of the plate shown in A). **C)** Streak outs of the same isolates as in A) but on YPGly at 30°C. **D)** Example of the growth phenotype of *ade2Δ dnm1Δ fzo1Δ*, freshly obtained by tetrad dissection, on YPD, 30°C, after prolonged incubation. The arrowhead points to a colony which is completely orange and therefore probably *petite*. **E)** Streak outs of *ade2Δ dnm1Δ fzo1Δ*, *ade2Δ* (YSP76-1) and the congenic wild-type JD47-13C on YPD and incubation at 30°C for two days.

The previously described effects can explain why, in general, a streak out of *ade2*Δ *dnm1*Δ *fzo1*Δ appears paler than that of *ade2*Δ (***Figure 2.20*** E). These observations are to some extend different from what was expected according to the aforementioned study wherein *ade2*Δ *dnm1*Δ *fzo1*Δ formed either deep red or much slower growing white, *petite* colonies (Osman et al., 2015). Therefore, it was decided that for the study presented here, the scoring of *petite* formation rate was not performed by color screening of *ade2*Δ but instead, single colonies of strains with functional *ADE2* were replica plated from YPD to YPGly, and the numbers of *petite* colonies were counted.

For this purpose, wild-type (one *trp1*Δ*63* and one *TRP1*), two isolates of *dnm1*Δ *fzo1*Δ, two isolates of *uls1*Δ *slx5*Δ and *dnm1*Δ *fzo1*Δ *uls1*Δ *slx5*Δ were cultivated on YPGly plates and afterwards in YPGly liquid medium in order to select for respiratory competent cells. From liquid YPGly, cells were plated on YPD and after a following incubation, replica plating on YPGly and YPD plates was performed, the latter one in order to confirm that the colonies were properly replica plated. If particularly small colonies were visible on YPD, these were individually streaked out on YPD and YPGly before replica plating. From the number of *petite* colonies on YPD, lacking growth on YPGly, the *petite* formation rates were determined. For illustration purposes, representative YPGly plates of wild-type, *dnm1*Δ *fzo1*Δ and *dnm1*Δ *fzo1*Δ *uls1*Δ *slx5*Δ are shown in ***Figure 2.21*** C-E.

For the wild-type, in the roughly 600 scored colonies, no *petite* colony was found (***Figure 2.21*** A, B), indicating that under the conditions applied here, with selective pressure immediately before plating on YPD, *petite* formation is a rare event in wild-type. The strain devoid of ULS enzymes, *uls1*Δ *slx5*Δ also showed a very low frequency of *petite* formation with 0.6 % on average across both isolates. In contrast, on average 8.2 % of *dnm1*Δ *fzo1*Δ colonies were *petite*. This number might appear small compared to the 23 % *petite* formation rate described in Osman et al., 2015. However, Osman and colleagues kept the yeast cultures in log-phase in synthetic glucose medium for 24 hours before plating the cells (Osman et al., 2015), thus for an extended period there was no selective pressure for respiration before cells were spread on YPD for scoring. In the method applied here, selective pressure for respiration was kept until the cells were plated on YPD. Under these conditions, in YPGly, *petite* cells can arise but these are probably not able to effectively propagate and their life span might be short. Therefore, it can be assumed that if a yeast culture grows with only glycerol as carbon source, a stable ratio between respiratory competent and *petite* cells is established that reflects the rate of *de novo* loss of mitochondrial DNA function. Taking into account these considerations, the fact that 8.2 % of *dnm1*Δ *fzo1*Δ colonies on YPD were *petite*, confirms a high *petite* formation rate of this strain.

A

Strain	Colonies in total	*petite* [%]
wild type (n=2)	594	0.0
dnm1Δ fzo1Δ (n=2)	606	8.2
uls1Δ slx5Δ (n=2)	448	0.6
uls1Δ slx5Δ dnm1Δ fzo1Δ (n=1)	188	17.0

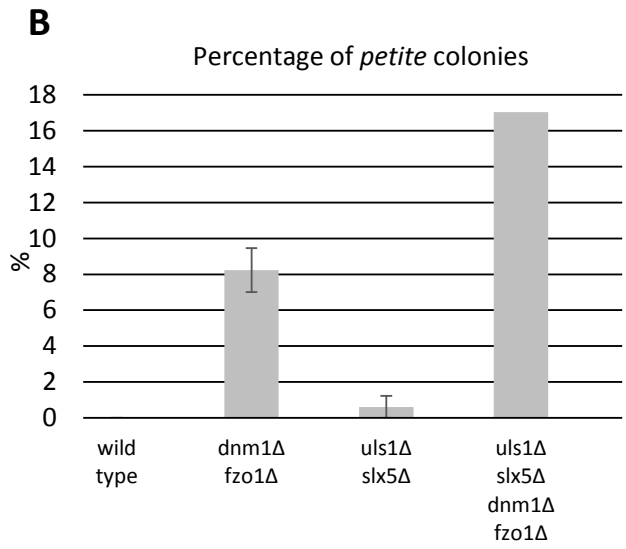

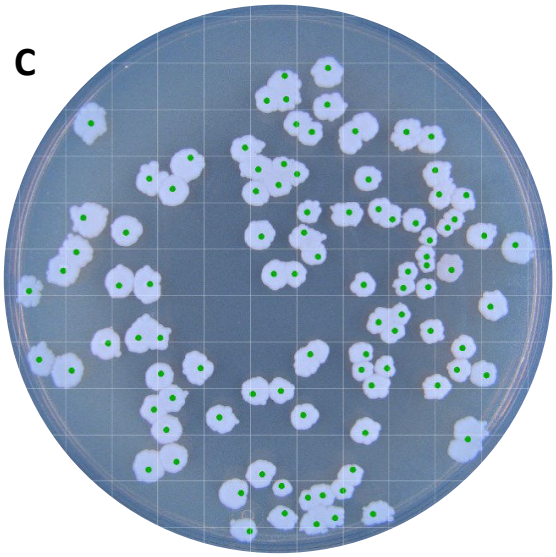

wild type on YPGly

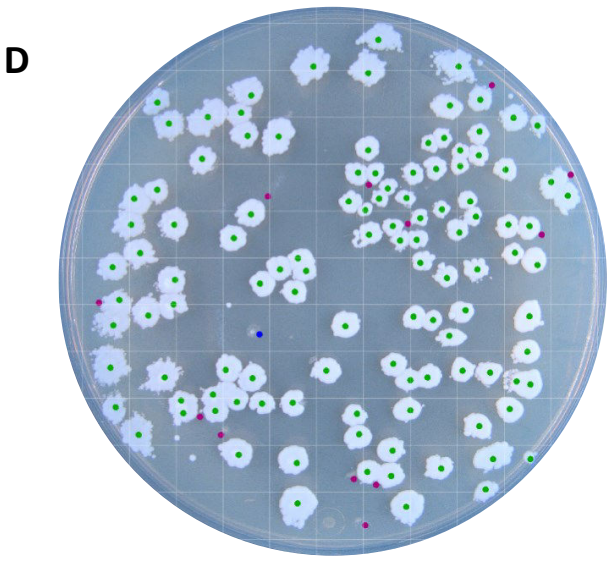

dnm1Δ fzo1Δ on YPGly

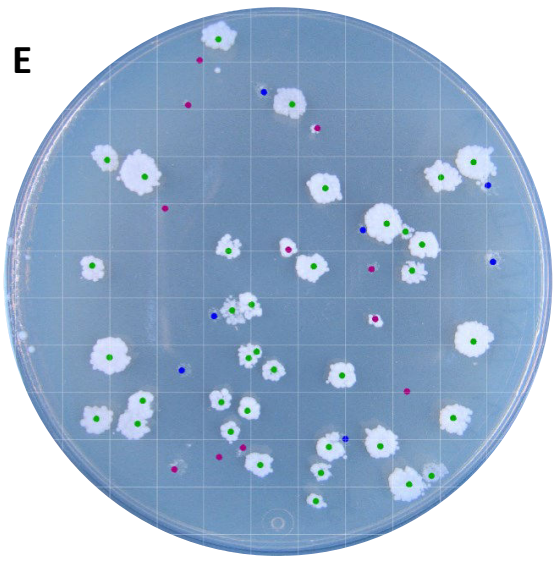

dnm1Δ fzo1Δ uls1Δ slx5Δ on YPGly

- replica plating indicates respiratory competence
- replica plating indicates *petite*
- colony was streaked out individually before replica plating

Figure 2.21: Loss of ULS enzymes causes a further increased petite formation rate in *dnm1Δ fzo1Δ*

A) Summary of results from this colony formation assay. The yeast strains were grown on YPGly plates and, from these streak

outs, liquid YPGly medium was inoculated. After one doubling in YPGly, a fraction of the culture was diluted with YPGly and the volumes were adjusted so that approximately 150 cells were plated on a YPD plate. *Uls1*Δ *slx5*Δ and *dnm1*Δ *fzo1*Δ *uls1*Δ *slx5*Δ generally had less colony forming cells per OD and, in order to compensate for this, a larger number of plates was prepared. Since *uls1*Δ *slx5*Δ and *dnm1*Δ *fzo1*Δ *uls1*Δ *slx5*Δ grew very slowly, a portion of plates was prepared after 24 hours incubation in YPGly, however as expected, this did not greatly change the *petite* rate, so the prepared plates were counted together for the displayed analysis. n = 2 means that plates of two different isolates were performed and the indicated percentage of *petite* colonies is the average of both isolates. The strains are wild-type (JD47-13C and MB2), *dnm1*Δ *fzo1*Δ (YSP109 and YSP110), *uls1*Δ *slx5*Δ (YKU102a and YKU121), and *dnm1*Δ *fzo1*Δ *uls1*Δ *slx5*Δ (YSP98-1). **B)** Bar chart of the result from A). **C) – E)** Representative YPGly plates generated by replica plating from YPD with wild-type (C, JD47-13C), *dnm1*Δ *fzo1*Δ (D, YSP109) and *dnm1*Δ *fzo1*Δ *uls1*Δ *slx5*Δ (YSP98-1). Green dots indicate respiratory competent colonies, blue dots indicate positions of not growing *petite* colonies, and purple dots indicate positions of colonies that have been individually tested before the replica plating. The phenotypes of colonies marked with a purple dot were assessed by streak outs on YPGly and YPD.

Additionally, by application of a mitochondrial marker in fluorescence microscopy, it was observed that mitochondria in *dnm1*Δ *fzo1*Δ exhibit an abnormal morphology, mostly with highly fused regions, similar to the mitochondrial morphology in *dnm1*Δ although this effect is milder in *dnm1*Δ *fzo1*Δ (data not shown). This observation indicates that also on a morphological level, mitochondria in *dnm1*Δ *fzo1*Δ behave abnormal.

Intriguingly, additional deletion of *ULS1* and *SLX5* in *dnm1*Δ *fzo1*Δ caused a doubling of the already high *petite* formation rate of *dnm1*Δ *fzo1*Δ. As a consequence, 17 % of the plated colonies of *dnm1*Δ *fzo1*Δ *uls1*Δ *slx5*Δ were *petite* despite the previously mentioned selective pressure immediately before plating. Summarized, these findings suggest that, in cells with functional fission and fusion, a lack of ULS enzymes does not result in an increased *petite* formation rate, however, in a situation where mitochondrial dynamics and therefore their quality control is impaired, the negative control of sumoylated proteins seems to be more critical for maintaining respiratory competence. One possible explanation would be that, in *uls1*Δ *slx5*Δ, nonfunctional mitochondria arise at a higher frequency, which would require quality control by fission and fusion.

2.6 Microscopic analysis of Dnm1 localization and mitochondrial morphology

2.6.1 Dnm1 is localized on mitochondria and at bud necks at physiological expression levels

In previous chapters, a direct connection between Dnm1 and sumoylation could not be demonstrated on a molecular level (chapters 2.1 – 2.4). However, the results of the growth assay for determination of the *petite* rates suggested that ULS enzymes contribute to maintaining respiratory competence which becomes visible in the absence of the fission and fusion machinery (chapter 2.5). Thus, it is still possible that sumoylation and mitochondrial function are connected more indirectly in *S. cerevisiae*. Therefore, in this chapter, the localization of Dnm1 and the mitochondrial morphology in different mutant strains are subjected to a closer examination.

In a first approach, *DNM1-mCherry* was expressed from a *CEN*-plasmid under control of P_{GALS}. At the same time, *OM45-GFP* was expressed from a *CEN*-plasmid for staining of mitochondria. Om45 is anchored to the outer mitochondrial membrane facing the IMS (intermembrane space) (Song et al., 2014). First of all, fluorescence microscopy revealed that Dnm1-mCherry spots of different sizes are detected upon expression from P_{GALS}. Often, very large spots were found, highlighted by red arrows, which are presumably aggregates containing Dnm1-mCherry (***Figure 2.22*** A). This confirms previous results from our laboratory (Christian Pichlo, Bachelor Thesis, 2011). As indicated by mitochondria staining with Om45-GFP, these spots do not seem to specifically localize to mitochondria in most cases. Furthermore, it is noticeable that solely overexpression of *DNM1-mCherry* in wild-type yeast does not cause an observable fragmentation phenotype and that many bud necks showed the presence of Dnm1, as highlighted by blue arrows. These results are in line with the previously mentioned study where additionally it was demonstrated that expression of *DNM1-mCherry* in *dnm1*Δ could partially rescue the hyperfusion phenotype of *dnm1*Δ (Christian Pichlo, Bachelor Thesis, 2011). Moreover, presumably due to the fact that both fluorophores were expressed from *CEN*-plasmids, the respective signal intensities varied among cells, as it can be seen in the examples (***Figure 2.22*** A). Like in wild-type, Dnm1-mCherry formed spots with different sizes and it was often localized to the bud neck also in *uls1*Δ *slx5*Δ. Thus, no major differences between wild-type and *uls1*Δ *slx5*Δ were found regarding Dnm1-mCherry localization (***Figure 2.22*** A).

In order to circumvent the problem of heterogeneous expression levels among cells and to microscopically analyze Dnm1 under more physiological expression levels, a new combination of constructs was applied. For this purpose, yeast strains from the laboratory collection were used which express *DNM1-GFP* from the authentic locus. Additionally, these strains were transformed with *OM45-mCherry* that integrates downstream of *LEU2.*

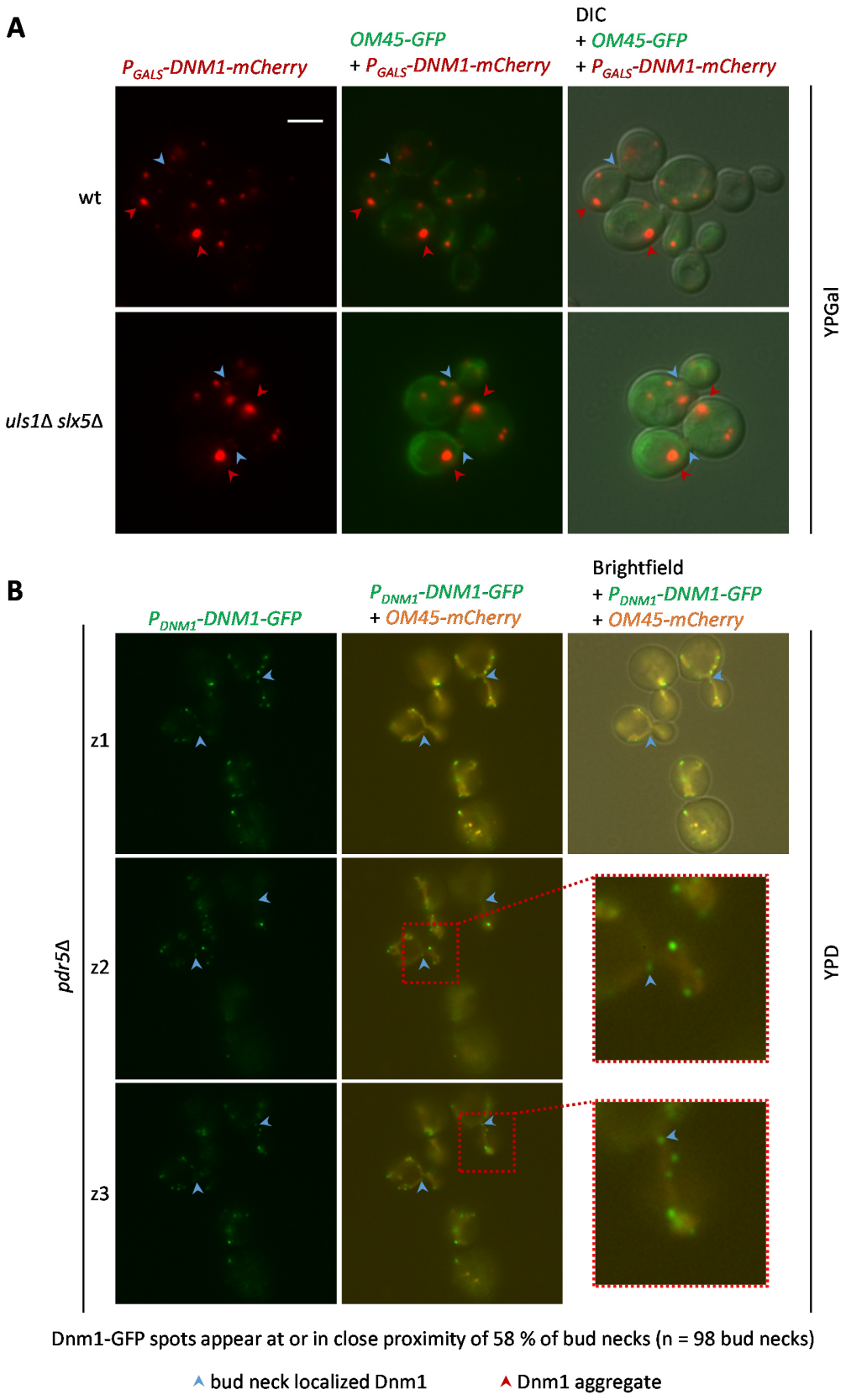

Figure 2.22: Expression of *DNM1-GFP* from the endogenous locus indicates localization on mitochondria and at bud necks
A) Fluorescence microscopy of wild-type (JD53) and *uls1Δ slx5Δ* (YKU121) harboring pCP1 (P_{GALS}-*DNM1-mCherry*) and OM45-GFP

(from the Graef group). Yeast strains grew in YPGal for one doubling prior to microscopy. Cultures were centrifuged and cell pellets resuspended in SGal complete for microscopy. The images were taken with the objective Zeiss Plan-Neofluar 100 x / 1.30 oil. Exposure times were 300 ms for brightfield with DIC (differential interference contrast), 1500 ms for GFP and 80 – 300 ms for mCherry. The scale bar indicates 5 µm. Blue arrows indicate bud neck localization of Dnm1 and red arrows indicate large spots of Dnm1-mCherry, presumably aggregates **B)** Fluorescence microscopy of *pdr5*Δ DNM1-GFP (MM16) with P_{ADH1}-*OM45-mCherry* as specified in the main text. Yeast strains grew in YPD for one doubling prior to microscopy. Cultures were centrifuged and cell pellets resuspended in SD complete for microscopy on poly-L-lysine coated glass slides (Sigma-Aldrich). The images were taken with the objective Zeiss Apochromat 100 x / 1.4 oil Iris. Exposure times were 35 ms for brightfield without DIC, 730 ms for GFP and 1500 ms for mCherry. For mCherry detection, this time another filter was used, therefore, the mitochondria are displayed in orange. Z-stacks with seven images in distances of 0.7 µm were prepared and three of these images are presented here. The scale bar from A) is also applicable for the images displayed here except for the highlighted magnified areas.

The transformed construct repairs *leu2-3,112* so that the transformants have a functional *LEU2* locus with P_{ADH1}-*OM45-mCherry* inserted downstream in the 3' non-coding region of the *LEU2* gene. With these strains expressing *DNM1-GFP* and *OM45-mCherry* from the genome, more homogenous signal intensities could be obtained.

Strikingly, in contrast to the previously shown results (***Figure 2.22*** A), Dnm1-GFP, upon expression from the genomic promoter, forms much smaller spots which are clearly localized to the mitochondria (***Figure 2.22*** B). Here, Dnm1-GFP appears in green spots on mitochondria which are displayed in orange. It was reported that Dnm1 forms helical oligomers (Mears et al., 2011). Therefore, the green spots probably indicate the position of these helices on mitochondria (***Figure 2.22*** B).

The finding of large aggregates upon expression of P_{GALS}-*DNM1-mCherry* and their absence in wild-type yeast expressing *DNM1-GFP* from its endogenous locus, suggests that aggregate formation is caused by the overexpression of *DNM1*. In chapter 2.1.1 it was already considered that Dnm1 is prone to aggregation at high temperatures, as also found in a large scale study (Wallace et al., 2015). Therefore, it seems plausible that Dnm1 also forms aggregates when expression levels are high, like it is apparently the case for P_{GALS}. This illustrates the importance of physiological expression levels when working with Dnm1. Furthermore, the staining of mitochondria indicates that the morphology appears wild-type-like, thus Dnm1-GFP is functional. Counting of bud neck localized Dnm1-GFP indicated that 58 % of the bud necks identified in brightfield showed presence of Dnm1-GFP which is exemplified in the magnified images in ***Figure 2.22*** B. This confirms results obtained with P_{GALS}-*DNM1-mCherry* (Christian Pichlo, Bachelor Thesis, 2011) (***Figure 2.22*** A). From a physiological point of view, localization of Dnm1 at the bud neck is plausible since the mitochondrial network has to be distributed between mother and daughter cell and, at one point, fission of the mitochondrial network is required for cell division.

2.6.2 Effects of mutations in the SUMO system on localization of Dnm1-GFP

Septins, for example Cdc11, which was investigated in previous chapters, are the most prominent SUMO substrates in *S. cerevisiae,* and the septins Cdc3, Cdc11 and Shs1 constitute a large fraction of cellular substrates (Johnson and Blobel, 1999). It was shown that these proteins are sumoylated at the mother cell side of the bud neck. Sumoylation of these septins, however, is apparently not essential for cell cycle progression. Still, it was hypothesized that sumoylated septins might serve to recruit other proteins which play a role in cytokinesis (Johnson and Blobel, 1999).

Fluorescence microscopy revealed that Dnm1 is frequently localized to the bud neck (Christian Pichlo, Bachelor Thesis, 2011) (chapter 2.6.1). In the same Bachelor Thesis, it was described that N-terminal translational fusion of 4xSmt3 to Dnm1-mCherry, expressed from P_{GALS}, enhanced bud neck localization (Christian Pichlo, Bachelor Thesis, 2011). Therefore, an open question was if sumoylation plays a role in targeting of Dnm1 to the bud neck. Since so far sumoylation of Dnm1 could not be found, *a priori* one consideration would be that Dnm1 is targeted to the bud neck by interaction with sumoylated proteins, be it directly or indirectly. In order to test this possibility, fluorescence microscopy with Dnm1-GFP and OM45-mCherry was conducted in *uba2-ts* mutant cells. These cells are strongly impaired in SUMO conjugation, even at growth-permissive temperatures (30°C), due to a hypomorphic allele of the *UBA2* gene encoding a subunit of SUMO-activating enzyme (Uba2-Aos1) causing temperature sensitivity for growth (Schwienhorst et al., 2000).

As shown in ***Figure 2.23***, Dnm1 was still localized to mitochondria and to the bud neck in the sumoylation impaired *uba2-ts* strain. This confirms results obtained by the application of P_{GALS}*-DNM1-mCherry* (Christian Pichlo, Bachelor Thesis, 2011). Therefore, probably sumoylation of septins or other factors at the bud neck is not essential for recruitment of Dnm1 and also, in general, targeting of Dnm1 to mitochondria does not seem to depend on sumoylation. Still, it has to be mentioned that residual sumoylation occurs even in *uba2-ts*. However, altogether at this point a major contribution of sumoylation to the regulation of Dnm1 localization appears to be unlikely. Overall *uba2-ts* showed the typical morphology for a strain impaired in sumoylation. This means that for example cells are generally very big, and the daughter cells grow very large while still being connected to the mother cell, which points towards defects in cell cycle progression. The fact that these cells appear very large has to be taken into account when the morphology of the mitochondrial network is analyzed, since larger cells tend to have a more extended mitochondrial network. Thus, a direct comparison of the degrees of interconnection in wild-type and *uba2-ts*, as well as the SUMO E3 ligase mutant *siz1*Δ *siz2*Δ, was very challenging and not further pursued.

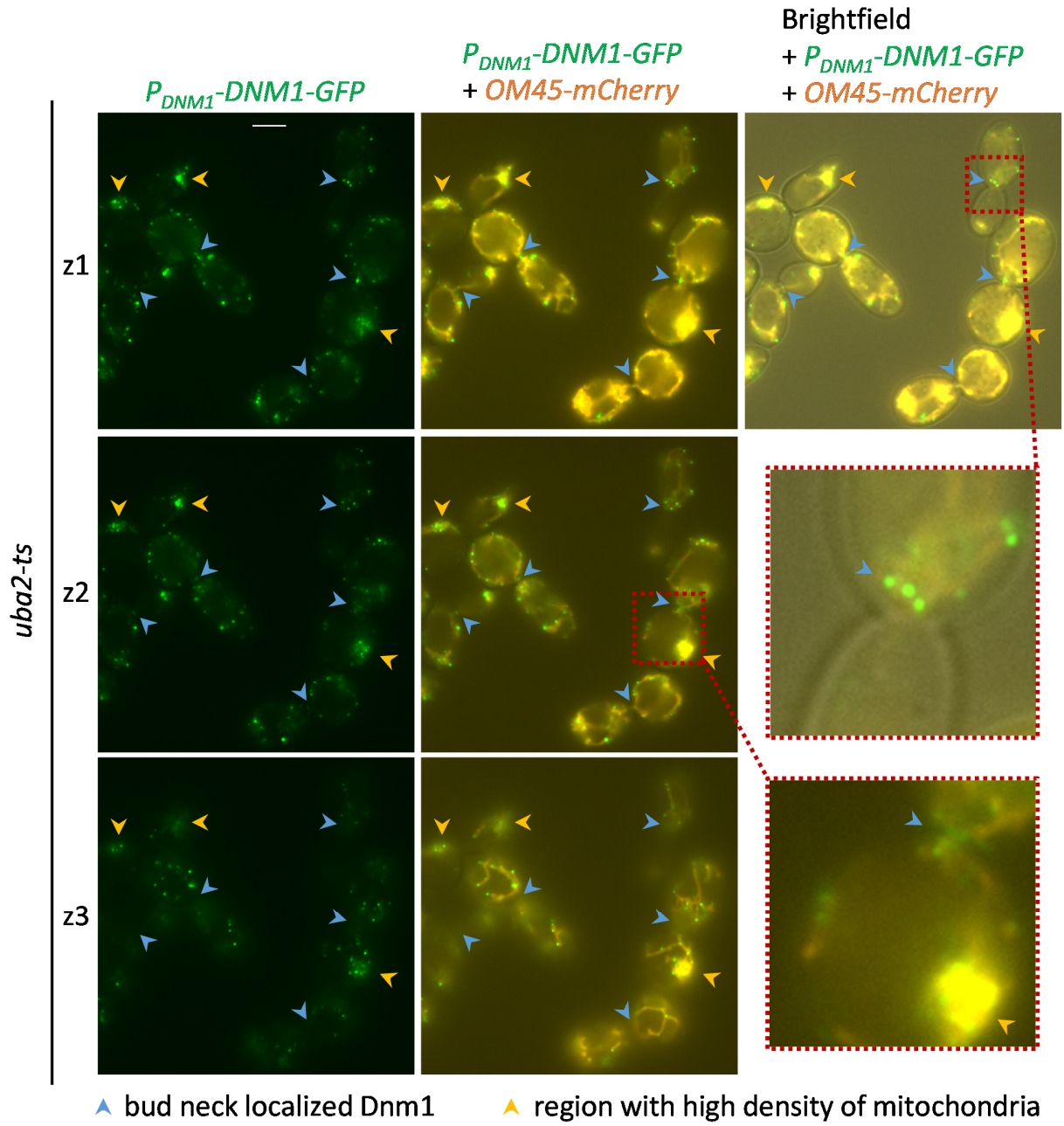

Figure 2.23: Dnm1 is localized to the bud neck in *uba2-ts*
Fluorescence microscopy of *uba2-ts2 DNM1-GFP* (MM22) with P_{ADH1}-*OM45-mCherry*. Yeast strains grew in YPD at 30°C for one doubling prior to microscopy. Cultures were centrifuged and cell pellets resuspended in SD complete for microscopy on poly-L-lysine coated glass slides (Sigma-Aldrich). The images were taken with the objective Zeiss Apochromat 100 x / 1.4 oil Iris. Exposure times were 35 ms for brightfield without DIC, 730 ms for GFP and 1500 ms for mCherry. The scale bar indicates 5 µm. Z-stacks with seven images in distances of 0.7 µm were prepared and three of these images are presented here. Blue arrows indicate bud neck localization of Dnm1 and orange arrows indicate regions with a high density of mitochondria.

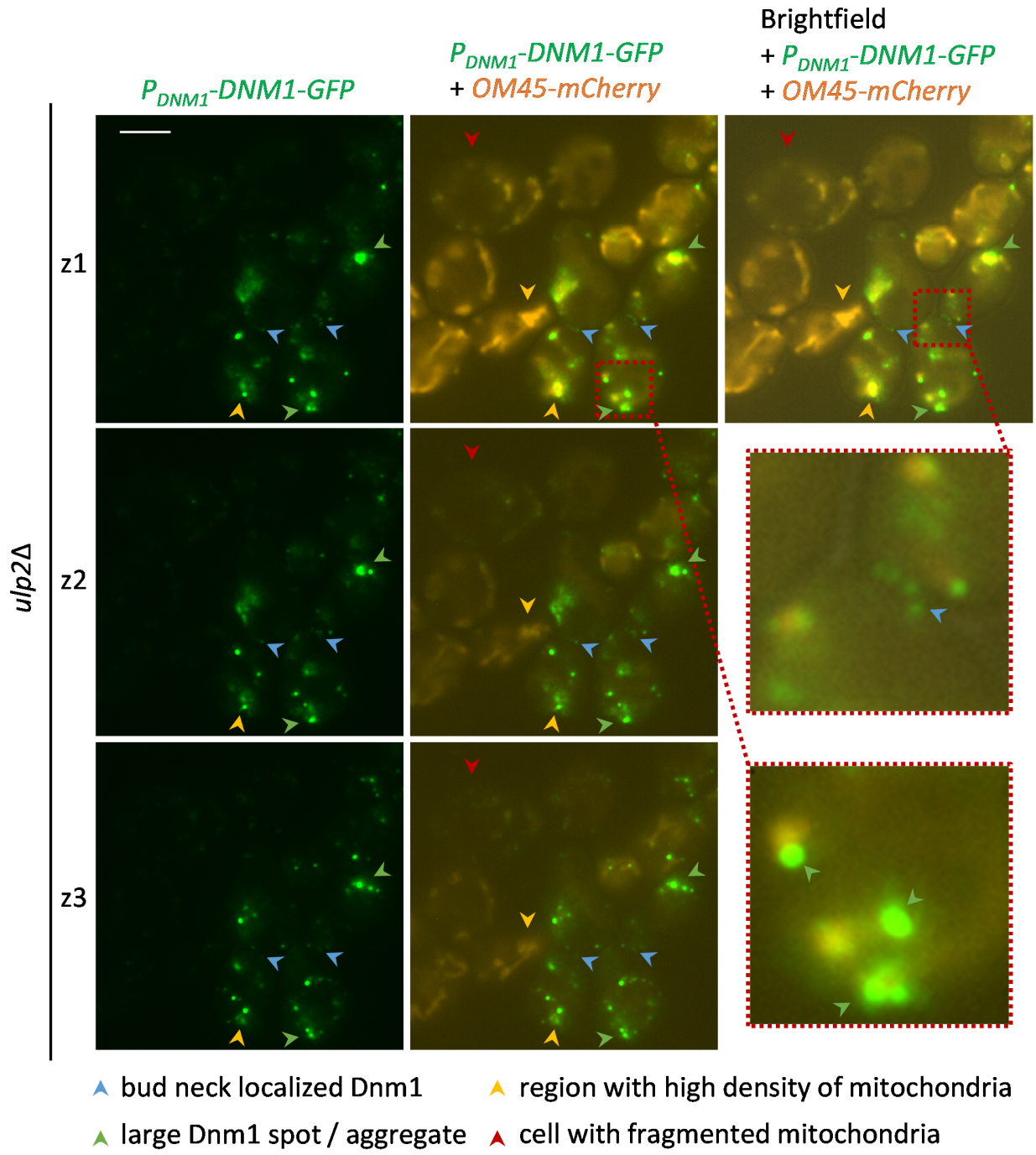

Figure 2.24: Dnm1 forms aggregates in *ulp2Δ*
Fluorescence microscopy of *ulp2Δ DNM1-GFP* (MM17) with P_{ADH1}-*OM45-mCherry*. Treatment of cultures and microscopy were performed as described for ***Figure 2.23***. The scale bar indicates 5 µm. Blue arrows indicate bud neck localization of Dnm1, orange arrows indicate regions with a high density of mitochondria, green arrows indicate putative Dnm1 aggregates, and red arrows indicate a cell with fragmented mitochondria.

Nevertheless, one observation was that in *uba2-ts*, a fraction of cells displayed regions with a very high density of mitochondria, as highlighted by orange arrows (***Figure 2.23***). Often, strong signals of Dnm1-GFP were found in the same spots, which suggests that the appearance of these regions with a high density of mitochondria is not caused by an absence of Dnm1. Recruitment of Dnm1 to these regions is possibly enhanced passively by the fact that the large mitochondria surface attracts Dnm1. At this point, it is unclear why these regions with a high density of mitochondria appear in *uba2-ts* and if this is directly caused by impaired sumoylation or rather a secondary effect in the overall abnormal *uba2-ts* cells.

Known from previous experiments (Christian Pichlo, Bachelor Thesis, 2011), and later confirmed by the application of an ltd (low temperature degron) variant of Ulp2 (chapter 2.6.3), is that mitochondria in cells devoid of Ulp2 often appear fragmented. Therefore, here it was analyzed if Dnm1-GFP shows distinct characteristics in *ulp2*Δ (***Figure 2.24***). First of all, apparently one peculiarity of *ulp2*Δ is that the protein levels of both fluorophores, Dnm1-GFP and OM45-mCherry, are very heterogeneous across cells in the same culture although both are expressed from genomic loci. In the example image, it can be observed that some cells exhibit a very strong signal for Dnm1-GFP while in other cells, it is almost not visible. Similar observations can be made when examining the signal intensities of OM45-mCherry (***Figure 2.24***). This suggests that generally, protein levels differ strongly between cells in *ulp2*Δ, probably due to misregulated gene expression and/or protein homeostasis.

Considering Dnm1-GFP, apparently localization at the bud neck (see example, ***Figure 2.24***) and on mitochondria (verified by additional images, data not shown) is not impaired in *ulp2*Δ. Together with the findings in *uba2-ts*, this suggests that in general terms, neither sumoylation nor desumoylation are critical for the regulation of Dnm1 localization. However, one striking observation was made in *ulp2*Δ. In this strain very large spots of Dnm1-GFP can be found, highlighted by green arrows. These spots are much larger than Dnm1-GFP spots observable in wild-type (***Figure 2.22*** B) and *uba2-ts* (***Figure 2.23***). Possibly, these large Dnm1-spots are aggregates which emerge specifically in *ulp2*Δ. One possible explanation would be that in these cells, the expression levels of Dnm1 are exceptionally high and this overexpression might lead to aggregation of Dnm1, similar to what was observed upon expression from P_{GALS} (***Figure 2.22*** A). In contrast, a Western Blot indicates average levels of Dnm1 across the culture. Therefore, the overall levels of Dnm1 in *ulp2*Δ appeared to be similar to the ones in wild-type (***Figure 2***). Another conceivable explanation for the formation of aggregates in *ulp2*Δ is based on the hypothesis that the large amount of polysumoylated proteins in *ulp2*Δ (***Figure 2***), and subsequent ubiquitylation of these conjugates, causes an overload of the proteasome system. This in turn might inhibit degradation of other proteins, like for example Dnm1.

Importantly, also this effect, if present, is probably heterogeneous across different cells. Altogether, these results strengthen the hypothesis that Dnm1 is prone to aggregation under certain conditions.

The morphology of mitochondria in *ulp2*Δ is analyzed in more detail with another mitochondrial marker (chapter 2.6.3) but already at this point, by the application of OM45-mCherry, it is visible that cells with fragmented mitochondria (red arrow) and cells containing a region with a high density of mitochondria (orange arrows) can be found, once again highlighting the physiological heterogeneity of *ulp2*Δ cells (***Figure 2.24***). For the sake of completeness, it should be mentioned that also in *uls1*Δ *slx5*Δ fluorescence microscopy with Dnm1-GFP and OM45-mCherry was performed. However, at this point no differences in the localization of Dnm1-GFP could be observed. In contrast to *ulp2*Δ, Dnm1-GFP did not form aggregates in *uls1*Δ *slx5*Δ, and, although the cells are also larger than wild-type cells, the protein levels of Dnm1-GFP and OM45-mCherry seemed to be more homogenous than in *ulp2*Δ (data not shown).

2.6.3 Temporary depletion of Ulp2 causes mitochondrial fragmentation

As mentioned earlier, in a previous study, it was already described that mitochondria in *uls1*Δ *slx5*Δ and *ulp2*Δ tend to be fragmented (Christian Pichlo, Bachelor Thesis, 2011). In order to confirm these observations in Ulp2-deficient cells and in order to exclude that long-term effects in *ulp2*Δ are responsible for this phenotype, the morphology of mitochondria was analyzed in *ulp2*Δ and the conditional *ltd-ULP2* mutant, which is explained later in this chapter. For mitochondria staining, a new construct was established. P_{TPI1}-*Su9(1-69)-GFP* was amplified from pYX142-mtGFP (Westermann and Neupert, 2000) by PCR and introduced into a plasmid which in turn can be used for homologous recombination of P_{TPI1}-*Su9(1-69)-GFP-*T_{CYC1} downstream of *LEU2*, as explained in chapter 2.6.1. *Su9(1-69)* encodes the first 69 amino acids of the F_0 ATPase subunit 9 of the mold *Neurospora crassa* and serves as a sequence for targeting to the mitochondrial matrix, where Su9(1-69) is cleaved from GFP by the activity of MPP (mitochondrial matrix processing protease) (Westermann and Neupert, 2000). An important advancement for the experiments outlined below was the expression of this mitochondria matrix marker from a genomic locus instead of a *CEN* or *2µ* plasmid, as described in the publication from Westermann and Neupert. Preliminary experiments with plasmid-based *Su9(1-69)-GFP* (in the following Su9(1-69)-GFP is termed mtGFP) showed that often the signal intensities are different across cells of the same sample (data not shown). This is a potential obstacle for systematic evaluation and comparison of phenotypes. In contrast, *mtGFP* expressed from a genomic locus resulted in uniform staining of mitochondria.

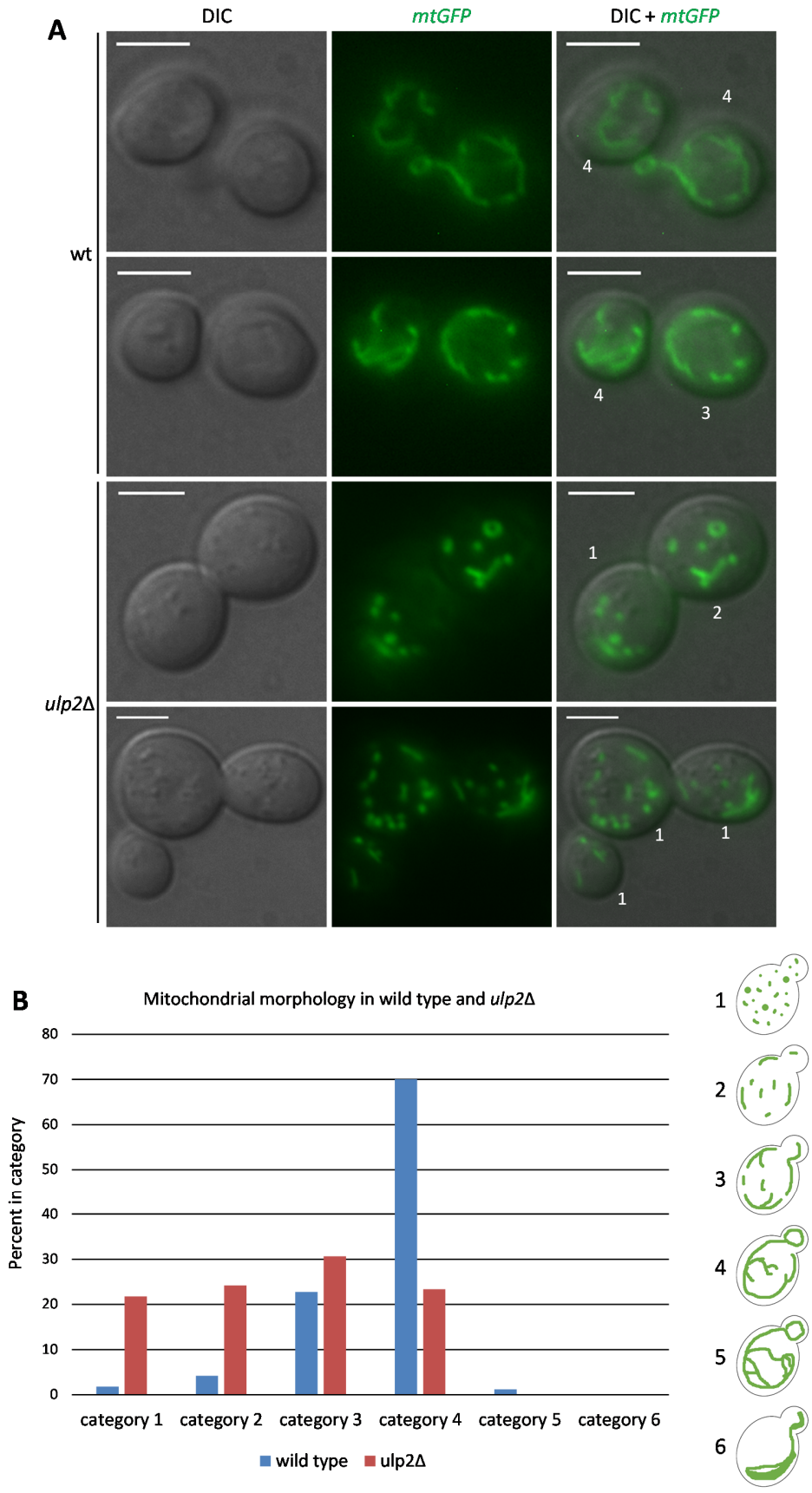

Figure 2.25: Fragmentation of mitochondria in *ulp2Δ*

A) Fluorescence microscopy of wild-type (JD47-13C) and *ulp2*Δ (YKU1), both expressing *mtGFP* after homologous recombination by the application of plasmid pSP57. Yeast strains grew on YPD-agar for one night prior to microscopy. Cells were resuspended in PBS for microscopy. The images were taken with the objective Zeiss Plan-Neofluar 100 x / 1.30 oil with additional 1.25 x magnification. Exposure times were 15 ms for DIC and 2000 ms for GFP. The scale bar indicates 4 µm. Z-stacks with nine images in distances of 0.8 µm were prepared. One of the images from the Z-stack was chosen and digitally merged with the displayed DIC-image. Typically an image with the focus 0.8 µm or 1.6 µm above or below the center of the cell was chosen for GFP detection. The numbers in white font indicate the classification of the representative cells. **B)** Classification of yeast cells into six categories according to their mitochondrial morphology as depicted on the right. Wild-type: n = 167, *ulp2*Δ: n = 124. See main text for further details on the approach for classification.

The fact that in principle all cells in a sample expressed *mtGFP* at similar rates, allowed choosing suitable cells in brightfield prior to taking a photo of stained mitochondria, so that the choice of cells for assessment of the mitochondrial phenotype could be made in an unbiased manner. Furthermore, this approach does not require prolonged selection for the auxotrophic marker once the transformants are generated. Results of such an analysis for *ulp2*Δ compared to the isogenic wild-type are presented in ***Figure 2.25***.

Representative images of mitochondria in wild-type and *ulp2*Δ show striking differences between both strains. Whereas mitochondria in wild-type yeast usually form a network which stretches throughout the cell including newly formed buds, mitochondria in *ulp2*Δ appear as individual spots or very short tubular structures (***Figure 2.25*** A). In order to obtain a more quantitative overview of the mitochondrial phenotypes in both strains, as described above, cells were chosen in brightfield, and then photos with DIC and for GFP were taken. The cells present in the images were then categorized into six categories describing mitochondrial phenotypes, according to the classification established by Christian Pichlo (Christian Pichlo, Bachelor Thesis, 2011) where they are described in detail. In brief, for this study, cells with mainly or only spots as mitochondria and without long tubules were classified as category 1, as it is the case for *fzo1*Δ. Cells with mostly short tubules but without a visible mitochondrial network were classified as category 2. Category 3 consists of cells where most of the mitochondrial staining belongs to a mitochondrial network but where separated mitochondria can be seen. In category 4, virtually only one, large, mitochondrial network is present in the cell without separated mitochondria. Cells with a single mitochondrial network with additional interconnections or extensions are classified as category 5. In category 6, the mitochondrial network is highly interconnected, in some cases net-like, and mostly concentrated in one region of the cell, like it is typically the case in *dnm1*Δ. Most wild-type cells belong to categories 3 or 4, as it was confirmed by the analysis presented here (***Figure 2.25*** B). In contrast, approximately 45 % of *ulp2*Δ cells belong to the two categories with the most fragmented mitochondria, namely 1 and 2, while only 6 % of the wild-type cells belong to either of these categories. When looking at category 1, describing very strong fragmentation, the difference between both strains is even larger. 22 % of *ulp2*Δ cells were counted as category 1 but only 2 % of wild-type (***Figure 2.25*** B). Altogether, this experiment with the newly established construct for mitochondria staining, confirmed that in *ulp2*Δ the

number of cells with fragmented mitochondria is strikingly increased, as previously described (Christian Pichlo, Bachelor Thesis, 2011).

As known from previous reports, *ulp2*Δ undergoes long-term adaptations, such as a specific aneuploidy, namely a doubling of the copy number of chromosomes I and XII (Ryu et al., 2016). Consistently, it was noticed that apparently *DNM1*, located on chromosome XII, is present in two copies in our haploid laboratory *ulp2*Δ strain YLD38-1 (chapter 2.1.2). In order to exclude that long-term adaptations are responsible for the fragmentation of mitochondria in *ulp2*Δ, strains expressing an ltd-variant of *ULP2* were generated. More specifically, *ltd-ULP2* is *Ub-N-term.degron-DHFR(K2)-ULP2*, expressed from the *ULP2* genomic locus, thereby replacing wild-type *ULP2*. From the resulting fusion protein, ubiquitin is cotranslationally cleaved by DUBs, so that an N-terminal phenylalanine is exposed, which is a destabilizing residue according to the N-end rule (Varshavsky, 1997). Additionally, murine DHFR (dihydrofolate reductase) (K2) is N-terminally fused to Ulp2. This variant is a thermo-labile version of DHFR with the mutations T39A and E173D which promotes protein degradation at elevated temperatures. It is used in order to achieve lower restrictive temperatures compared to degron constructs with wild-type DHFR. Therefore, in the following the applied construct is referred to as *ltd-ULP2* (*low-temperature degron ULP2*). The ltd described here was previously established and used in *Arabidopsis thaliana*, *Nicotiana benthamiana*, *Drosophila melanogaster*, *Drosophila* cell culture and *Saccharomyces cerevisiae* (Faden et al., 2016). In order to assess the effectivity of the ltd for Ulp2 degradation and to evaluate the growth phenotypes of the transformants, the growth of *ltd-ULP2* isolates was compared to wild-type and *ulp2*Δ at 25°C (data not shown), 30°C (data not shown), 33°C and 37°C. The growth assays revealed that up to 33°C, the *ltd-ULP2* transformants did not grow noticeably worse than the wild-type (***Figure 2.26*** A) but at 37°C, the *ltd-ULP2* transformants did not show any growth (***Figure 2.26*** B) except for single spontaneous suppressor colonies (***Figure 2.26*** C). As expected, growth of *ulp2*Δ was severely impaired at 33°C (***Figure 2.26*** A) and this strain was not viable at 37°C (***Figure 2.26*** B).

These results suggest that the function of ltd-Ulp2 at 33°C and lower temperatures is sufficient for cells to avoid growth impairment as it is the case for *ulp2*Δ. First of all, this means that the fusion protein as such is functional. This does not necessarily mean that ltd-Ulp2 is as stable as the wild-type variant at 33°C because it is well possible that even a reduced amount of Ulp2 is sufficient to maintain its functions. In another scenario, the levels of ltd-Ulp2 at 33°C are sufficiently low for causing accumulation of sumoylated proteins but this effect might be below a threshold where a growth defect becomes visible. In contrast, at 37°C no growth of *ltd-ULP2* transformants could be observed, like it is the case for *ulp2*Δ.

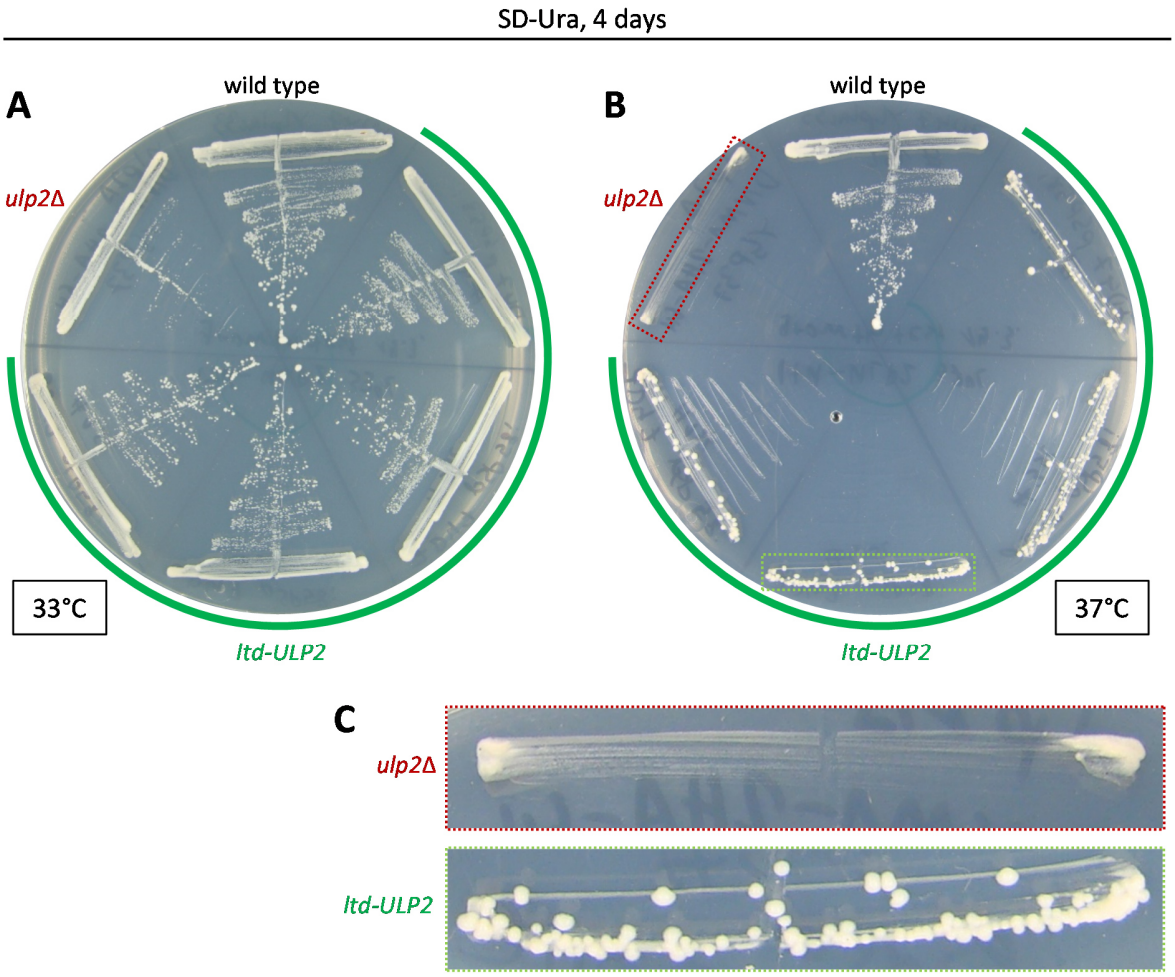

Figure 2.26: Low-temperature degron can be applied for depletion of Ulp2 at 37°C

A) Streak outs of the indicated strains on SD-Ura for comparison of the growth phenotypes at 33°C. The photo was taken after growth for four days. The strains are *ulp2*Δ *DNM1-2HA-6H::URA3* (YSP37; *DNM1-2HA-6H* can be ignored for this experiment), *ltd-ULP2* (four isolates of a transformation of JD47-13C with pSP58) and JD47-13C YCplac33. **B)** Same as A) but plate was incubated at 37°C for four days. **C)** Magnifications of the indicated areas for the documentation of suppressor formation in *ltd-ULP2*.

This indicates that ltd-Ulp2 is destabilized to an extent where it does no longer support cell viability at 37°C. Instead, at this temperature, the formation of single suppressor colonies can be observed of *ltd-ULP2* (***Figure 2.26*** C).

The fact that these suppressors did not appear in *ulp2*Δ, suggests that the degradation of Ulp2 was prevented by a secondary mutation in these cases. For their degradation the ltd fusion proteins require recognition by the E3 ubiquitin ligase Ubr1 (Faden et al., 2016). Therefore, *UBR1* is a likely target for suppressor mutations. Independently from these considerations, *ltd-ULP2* can be used in order to shut off Ulp2 function for the analysis of short term effects. However, the emergence of suppressors indicates that long incubation times at restrictive temperatures should be circumvented when working with *ltd*-mutants.

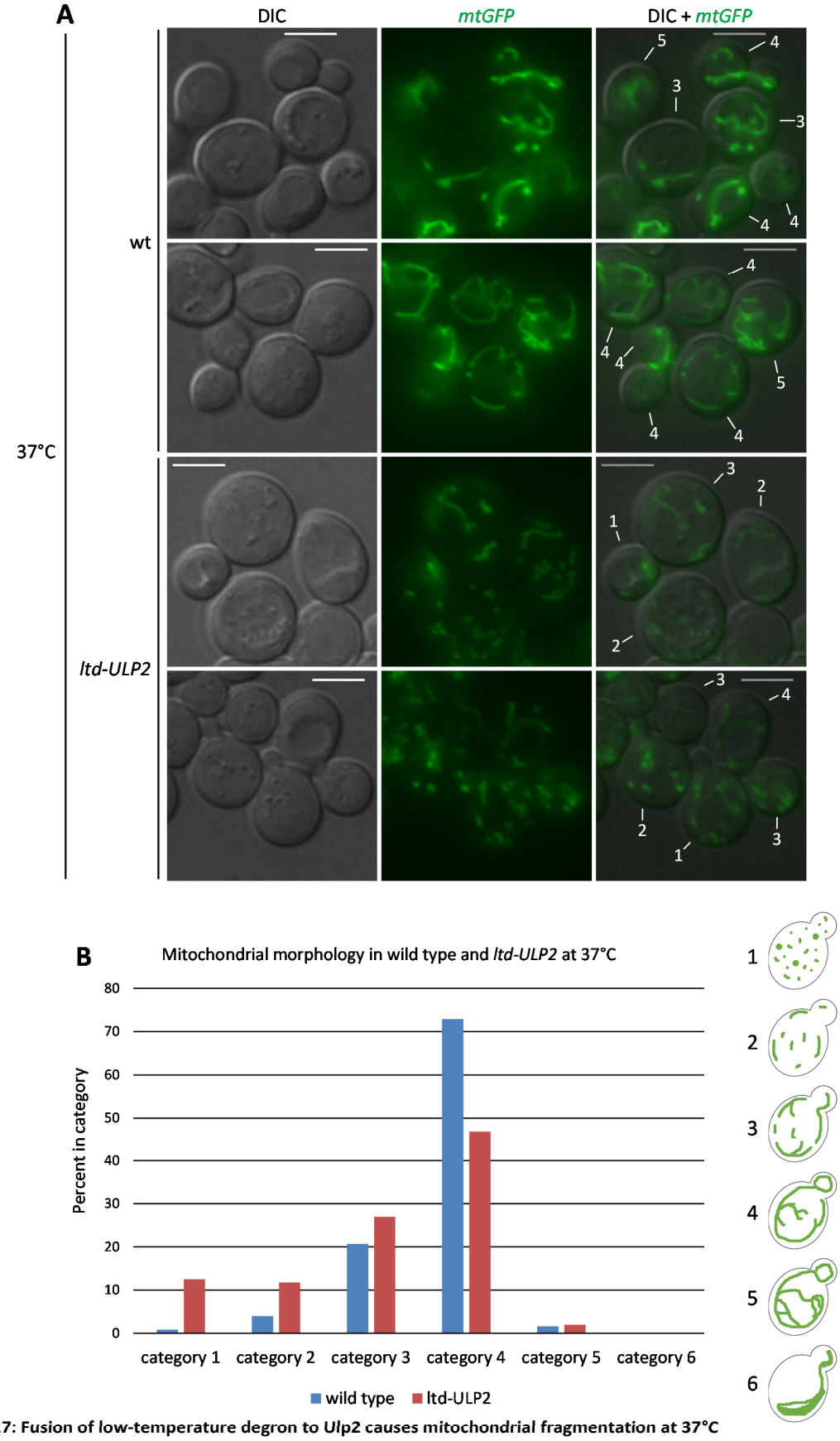

Figure 2.27: Fusion of low-temperature degron to *Ulp2* causes mitochondrial fragmentation at 37°C

A) Fluorescence microscopy of wild-type (JD47-13C) and *ltd-ULP2* (JD47-13C pSP58), both expressing *mtGFP* after homologous recombination by the application of pSP57. For both strains, a yeast culture was started in liquid SD-Ura at 25°C. After one doubling, the culture was split into three cultures and these were incubated at 25°C, 33°C or 37°C, respectively. After one day of incubation, the cultures were diluted to an OD_{600} and after five more hours, the fluorescence microscopy was performed. Shown here is the microscopy after incubation at 37°C. For microscopy, cells were resuspended in SD complete for microscopy. The images were taken with the objective Plan-Neofluar 100 x / 1.30 oil. Exposure times were ~ 230 ms for GFP. The scale bar indicates 5 µm. Z-stacks with nine images in distances of 0.7 µm were prepared. One of the images from the Z-stack was chosen and digitally merged with the displayed DIC-image. The numbers in white font indicate the classification of the representative cells. **B)** Classification of yeast cells into six categories according to their mitochondrial morphology as depicted on the right. Wild-type: n = 251, *ltd-ULP2*: n = 256. See main text for further details on the approach for classification.

As outlined above, and after verification of temperature sensitivity of *ltd-ULP2* transformants (***Figure 2.26*** B), the next step was to analyze the mitochondrial morphology of *ltd-ULP2*. Like *ulp2*Δ (***Figure 2.25***), an *ltd-ULP2* transformant with verified temperature sensitivity was transformed with *mtGFP*.

An experimental series was carried out with this newly generated strain and the congenic wild-type expressing *mtGFP*. For this experiment, both strains were incubated at 25°C, at 33°C and at 37°C and the mitochondrial morphology was analyzed microscopically. After three hours of incubation, no relevant increase in the fragmentation of mitochondria could be observed (data not shown). Therefore, the cultures were kept at the respective temperature overnight. On the following day, the cultures were diluted and, after one doubling, fluorescence microscopy was performed. The fact that *ltd-ULP2* still grew after one day at 37°C indicates that the lethality of this strain at the restrictive temperature only develops after prolonged incubation. This in turn allowed fluorescence microscopy after incubation for one day at 37°C. While at 33°C no prominent fragmentation phenotype was observed (data not shown), after one day at 37°C, *ltd-ULP2* exhibited a severe increase in mitochondrial fragmentation, as exemplified (***Figure 2.27*** A) and detailed by categorization of the mitochondria morphologies (***Figure 2.27*** B). In contrast, the congenic wild-type did not show mitochondrial fragmentation at 37°C (compare ***Figure 2.25*** B and ***Figure 2.27*** B). At this point, it should be noted that cells apparently tend to form clumps at 37°C, which is true for both wild-type and *ltd-ULP2*, however, this observation was independent from the mitochondrial morphology.

Mitochondrial fragmentation in *ltd-ULP2* required the application of the restrictive temperature 37°C, which suggests that the observed phenotype is indeed a consequence of the Ulp2 depletion in this transformant. Furthermore, the fact that the phenotype became visible in the course of one day makes it unlikely that it is a long-term adaptation by an aneuploidy even though the exact timing of aneuploidy formation in *ulp2*Δ has not been resolved (Ryu et al., 2016). On the other hand, the fact that incubation for three hours at 37°C was not sufficient to establish the phenotype in *ltd-ULP2* suggests that mitochondrial fragmentation is not an immediate consequence of Ulp2 loss. Probably, phenotype development requires Ulp2 depletion, accumulation of HMW SUMO conjugates and further downstream effects until an effect on mitochondrial morphology becomes apparent. Altogether, the experiment

presented here confirms that loss of Ulp2 leads to mitochondrial fragmentation and, at the same time, it appears likely that this effect involves intermediate steps like the accumulation of SUMO conjugates.

3 Discussion

As described in the introduction, different methods were established, refined, and applied in this study in order to investigate a putative link between the SUMO system and mitochondrial dynamics in budding yeast (chapter 1.5). Therefore, it was decided to structure the results section along the different methods that have been used. Correspondingly, the outcomes of the experiments have been interpreted and discussed to a large extend already in the respective sections. For this reason, in the following, a few specific aspects of this work are chosen for a more detailed discussion with a focus on the roles of respective methods.

3.1 Establishing methods for the detection of sumoylated proteins

Initially, a motivation for establishing methods to analyze SUMO conjugates was the question whether Dnm1 is sumoylated. Therefore, the findings in respect to PTMs of Dnm1 are summarized here. With different approaches, it could be shown that Dnm1 is apparently ubiquitylated and degraded by the proteasome, hence Dnm1 is a target of the UPS. The most direct evidence for ubiquitylation of Dnm1 could be obtained by application of a refined purification method for sumoylated or ubiquitylated proteins and subsequent detection of 6HA-tagged Dnm1 (***Figure 2.11***). In the course of this study many approaches were tested and obstacles had to be overcome in order to obtain a sufficiently clean and intense signal so that the modification of Dnm1 could be determined with certainty.

3.1.1 Determination of ideal conditions for denaturing purification of SUMO conjugates

The denaturing purification of SUMO conjugates in 8 M urea has several advantages over a native purification strategy. Most importantly, these are the prevention of SUMO cleavage by Ulp1 and Ulp2 and ensuring solubility of proteins in the sample. Initially, one major obstacle was that the purifications of 8H-Smt3 conjugates were not sufficiently clean and barely enriched in comparison to an untagged control when a purifiifcation with Ni^{2+}-NTA was performed (***Figure 2.10***). The critical improvement was the application of TALON beads, which use cobalt for the binding to polyhistidine-tagged substrates instead of nickel. By using cobalt-coated beads, the specificity of 8H-Smt3 purification could be enhanced to a degree where the corresponding control is almost free of detectable SUMO conjugates. The increased specificity of cobalt for polyhistidine-tagged proteins, compared to Ni^{2+}-NTA, was also described previously (Young et al., 2012). However, as also stated by the manufacturer of the here applied cobalt-coated beads, this

comes at the cost of reduced yield (information obtained from cube-biotech.com). These statements go in line with the observations made in this study. Furthermore, an elution with pH 4.5 was not sufficient for elution of 8H-Smt3 conjugates from Ni^{2+}-NTA, but instead apparently nonspecifically binding proteins were removed from the untagged controls ***(Figure 2.10*** B). An explanation for the strong binding of 8H-Smt3 conjugates to Ni^{2+}-NTA might be the fact that in a SUMO chain, each moiety bears an 8H-tag so that overall the binding affinity to the beads is probably higher than it is the case for other substrates. Altogether, since for the unambiguous determination of a PTM on a substrate, the purity of an elution is of higher importance than the yield, the establishment of a purification method with cobalt-coated beads was a crucial step.

Still, it has been described that the sumoylated fraction of a substrate is typically very small (Johnson, 2004). This remark was confirmed by the detection of sumoylated Cdc11 after purification by a commercially available polyclonal antibody (***Figure 2.11*** D). In this case, the band of sumoylated Cdc11 was not visible in the input, and unbound fractions and became visible only after enrichment in the process of purification. This in turn shows that it was very important to refine the method for Western blotting and detection, particularly due to the fact that SUMO conjugates often have a high molecular weight and are therefore difficult to transfer on a membrane. For this purpose, various parameters have been tested and combined. These are for example semi-dry transfer vs. wet transfer, nitrocellulose membrane vs. PVDF membrane, and self-made ECL solution vs. Femto ECL substrate.

The preferred method was determined and applied in the experiment shown in ***Figure 2.11***. The Western blot was performed with a wet transfer at 100 V and 400 mA for one hour with boric acid transfer buffer. The Western blotting device was kept cool during this procedure. With this method, optimal conditions for the transfer of sumoylated proteins were found. Possibly, even more important was the choice of a detection method. Since the detection with fluorescent antibodies and also ECL in combination with a camera based detection were not sufficiently sensitive, for the detection of SUMO substrates an ECL reaction was detected by X-ray film. The maximal sensitivity could be obtained with the Femto ECL substrate in combination with a long exposure time. However, here a potential problem was the formation of a general background produced by the membrane or nonspecifically binding antibodies. In this case, a crucial improvement was the change from a PVDF membrane to nitrocellulose, which allowed very long exposure times with a clean background.

Altogether, the fine-tuning of these methods was essential for the ability to detect modified forms of Dnm1. As a consequence, it could be demonstrated that Dnm1 is ubiquitylated. However, although the

method in principle works, as demonstrated by Cdc11, sumoylated forms of Dnm1 could not be detected. Therefore, it appears unlikely that a relevant fraction of Dnm1 is sumoylated under the tested conditions.

As a side note, it should be mentioned here that in parallel to the method development for yeast, an analogous approach was performed with human cells expressing 8H-SUMO1 for the subsequent detection of endogenous substrates which are simultaneously modified by SUMO2/3 and 8H-SUMO1. To this end, stably transfected cells expressing 8H-SUMO1 in a linear cleavable fusion with Arkadia to ensure similar expression levels were established in collaboration with Niels Gehring and analyzed by Western blotting. For control purposes, the same construct with a mutation in either the RING domain or the SOB (SUMO one binding) motif of Arkadia was applied (data not shown). With this setup, our previous laboratory member Annie Sriramachandran was able, using nickel beads, to provide data for the targeting of mixed SUMO1-SUMO2/3 chains by the ULS Arkadia in mammalian cell culture (Sriramachandran et al., 2019). Of course, it would be interesting to apply the latest methodology described in the current study in order to test if the purification of 8H-SUMO1-SUMO2/3 hybrid conjugates can be further improved to identify physiologically relevant substrates of the identified Arkadia-mediated targeting. However, since the focus of this study was the yeast system, the purifications of SUMO from mammalian cell culture were not continued further in the present thesis study.

3.1.2 Application of cleavage-resistant Smt3 variants for improved detection of SUMO conjugates

As an alternative to the abovementioned denaturing purification method, an approach was established that made use of a previously developed SUMO variant which is resistant towards cleavage by desumoylating enzymes (Petreska, 2013), most importantly by the highly active Ulp1. An advantage of this tool is that it allows the native purification of SUMO conjugates with antibody-coupled beads, which would not be possible in 8 M urea. In general, purifications with antibodies are expected to be more specific than IMAC. In the course of this study, the effect of this and other Smt3 variants were analyzed by Western blotting and from a physiological point of view.

First of all, by analysis of boiled yeast extracts, it was observed that already *in vivo* the levels of sumoylated proteins were much higher when *2HA-smt3-Q95P* was expressed (***Figure 2.5***). For optimal specificity, this detection was made was an anti-HA antibody, which of course did not detect wild-type Smt3 moieties that were still present in these cells. In order to differentiate between the effect of the mutation and the overexpression, untagged *SMT3* and *smt3-Q95P* were overexpressed, and detection with an anti-Smt3 antibody revealed that solely overexpression of *SMT3* does not have a large impact on overall sumoylation

although this variant does not require maturation (***Figure 2.8***). From a biological perspective, this indicates that in wild-type yeast under normal conditions, the availability of free Smt3 and its maturation are not the limiting factor for sumoylation, assuming that the rate of desumoylation remains constant. In contrast, the prevention of desumoylation by the Q95P mutation led to six-fold increased levels of SUMO conjugates in both, wild-type and *uls1*Δ *slx5*Δ (***Figure 2.5***). Together, these results suggest that for the adjustment of steady state levels of SUMO conjugates, desumoylation is a crucial process, possibly even the most decisive one. For the work with SUMO conjugates, this means that when an increase of SUMO conjugates is desired for experimental purposes, the strategy should focus on the prevention of desumoylation rather than increasing expression levels.

The Smt3 variants applied here also led to other interesting findings. *Uls1*Δ *slx5*Δ, as expected from previous reports (Uzunova et al., 2007), accumulated HMW SUMO conjugates that did not migrate out of the stacking gel. By the expression of *smt3-K11,15,19R-Q95P* the formation of these conjugates could be prevented. The reason is most likely that this Smt3 variant interrupted forming SUMO chains analogous to the chain termination of SUMO2/3 chains by SUMO1 in human cells. This finding confirms the previous expectation that the HMW SUMO conjugates detected in *uls1*Δ *slx5*Δ indeed bear SUMO chains.

Unexpectedly, the expression of cleavage-resistant Smt3-Q95P did not cause a growth defect in wild type or *uls1*Δ. This is to some extend surprising since *ulp2*Δ which is also impaired in the negative regulation of SUMO chains, has a very prominent growth defect (***Figure 2.18***). This discrepancy suggests that the accumulation of SUMO chains *per se* is not the only reason for a growth defect of *ulp2*Δ. However, when expression of cleavage-resistant Smt3 was induced in *uls1*Δ *slx5*Δ, this strain did not grow on an agar plate. Importantly, the Western blot results were obtained after three hours of expression, which is tolerated by these transformants. The growth tests suggest that, in a scenario where SUMO chains are not controlled by either desumoylation or ULS, these conjugates constitute a problem for the cell. Intriguingly, this effect was milder in *slx5*Δ, which still has functional Uls1. Considering that in comparison to Uls2, Uls1 is much less efficient in targeting SUMO chains for degradation, as demonstrated with linear chains (Lennard-Maximilian Döring, Master Thesis, 2017), this results was not expected and suggests that to some extent, Uls1 can compensate for Slx5 in counteracting SUMO chains. One hypothesis that might explain these observations would be that Uls1 and Slx8 cooperate in targeting of SUMO chains. Since both proteins have a RING-domain, such an interaction seems conceivable. In accordance with results from the abovementioned Western blot, expression of *smt3-K11,15,19R-Q95P* was slightly less toxic for *uls1*Δ *slx5*Δ. On the one hand, this makes sense since the accumulation of HMW conjugates is expected to be toxic and requires chain formation, on the other hand even this Smt3 variant caused a severe growth phenotype in

*uls1*Δ *slx5*Δ, which in turn suggests that also the accumulation of SUMO conjugates below HMW is harmful in *uls1*Δ *slx5*Δ (***Figure 2.7***).

When looking at a specific substrate, like Cdc11 (***Figure 2.6***), or at specific single bands in a band pattern (***Figure 2.5***), it became clear that not every specific SUMO conjugate is more abundant upon expression of *smt3-Q95P* in *uls1*Δ *slx5*Δ. One specific SUMO conjugate of Cdc11 could be identified in the boiled extract due to a band-shift that was induced by the N-terminal 2HA-tag. Upon overexpression of wild-type *2HA-SMT3*, this band shift was visible but the band was relatively faint. When the cleavage-resistant variant was expressed, this band was apparently stabilized, and the band-shift was well visible. This example demonstrates that stabilization of SUMO conjugates in combination with an induced band shift by the 2HA-tag can facilitate the identification of specific SUMO conjugates. Still, as noted above, it should be mentioned, that bands representing SUMO conjugates sometimes behave opposite of what was expected. The SUMO system is highly dynamic and the outcomes of changes in one of the parameters can be difficult to predict, in part due to the fact that so far it is not well understood how ULS enzymes select their targets. One previous and somewhat unexpected observation was that the overexpression of Siz1 led to a decrease in septin sumoylation (Takahashi and Kikuchi, 2008). Furthermore, *SIZ1* is a multi-copy suppressor of *ulp2*Δ (Strunnikov et al., 2001; Takahashi and Kikuchi, 2008), which appears paradoxical since in this case, a defect in desumoylation is relieved by increased expression of an E3 SUMO ligase. Altogether, these examples, together with the observations described in this thesis, show that the genetic interactions between components of the SUMO system are complex and can often not be explained satisfactorily with the current knowledge.

For investigating the putative sumoylation of Dnm1, Smt3-Q95P was applied in a native pulldown of Dnm1-2HA-6H with HA-antibody coated beads. As expected, also after native immunoprecipitation, samples with Smt3-Q95P had more conjugates than a purification without expression of this variant. Apparently modified forms of Dnm1 were detected in all of its immunopurifications. Detection with an anti-Smt3 antibody, however, could not unambiguously confirm specific sumoylated forms of Dnm1. Nevertheless, in the course of the study, the effects of *smt3-Q95P* expression were examined on protein level and from a physiological point of view. As demonstrated with Cdc11 as an example, this Smt3 variant is a useful tool for the identification of SUMO conjugates, and it can be used to enhance sumoylation *in vivo* without the need for an inhibition of SUMO proteases.

3.2 Posttranslational modification of Dnm1 and degradation by the UPS

In the following, a conclusive summary of the obtained results concerning the posttranslational modifications of Dnm1 is outlined. First of all, several independent approaches have pointed towards a ubiquitylation of Dnm1. Most importantly, as described above, a denaturing purification of ubiquitin with subsequent detection of Dnm1 provided direct evidence for ubiquitylation of Dnm1 (***Figure 2.11***). More indirectly, but still very importantly, it could be shown that Dnm1 is stabilized in a ubiquitylation-deficient strain (***Figure 2.1***). Together, this suggests that Dnm1 is ubiquitylated and that ubiquitylation promotes its degradation. Consequently, inhibition of the proteasome by MG132 led to a stabilization of Dnm1 to a similar degree (***Figure 2.2***), supporting the hypothesis that Dnm1 is degraded in a ubiquitin- and proteasome-dependent mechanism.

In addition, with ethanol treatment, a condition was found under which the steady state levels of Dnm1 are decreased (***Figure 2.3***). This effect correlates with increasing ethanol concentrations and is established already after 30 minutes, so it seems plausible that enhanced degradation of Dnm1 is responsible for this reduction and probably not changes in expression levels, considering that Dnm1 was shown to be a proteasome substrate, as described above. Interestingly, previously it was found that ethanol causes mitochondrial fragmentation, and that this requires Fis1 but not Dnm1. In the same study, it was reported that Fis1 mediates ethanol-induced apoptosis as well as mitochondrial fragmentation. However, apparently apoptosis and mitochondrial fragmentation did not correlate (Kitagaki et al., 2007). These results are difficult to explain with the view that Fis1 serves as a mitochondrial anchor that, together with the adaptors Mdv1 or Caf4 and Dnm1 drives mitochondrial fission. Therefore, possibly ethanol-induced mitochondrial fragmentation is a condition where mitochondria can divide by a mechanism that is independent from Dnm1. One hypothesis to explain Dnm1 degradation upon ethanol treatment would simply be that mitochondrial fragmentation goes along with the degradation of proteins that are associated with mitochondria, so this effect might be seen for other mitochondrial proteins, as well.

The identification of ubiquitylated forms of Dnm1 by IMAC and the generation of *6HA-DNM1* expressing strains, which allow detection of modified forms in boiled extracts, were the motivation to have a closer look at these modifications under different conditions. For the sake of completeness, it has to be mentioned that not all of the modifications detected after purification from boiled extracts are necessarily the ubiquitylated forms of Dnm1. However, it is very likely that at least the majority of the detected modified forms of Dnm1 are the ubiquitylated species described above. Still, it should be pointed out that the ubiquitylated forms of Dnm1 observed in the current study are not necessarily the same conjugates that lead to the degradation of Dnm1. For example, the mitochondrial fusion protein Fzo1 becomes

ubiquitylated in two different manners, one which promotes its function and one which leads to its degradation (Anton et al., 2013; Simões et al., 2018). In the study presented here, it was found that an increase of Dnm1 steady state levels does not cause an increase in the amount of ubiquitylated forms of Dnm1 (***Figure 2.2*** C). This might be taken as evidence that a mechanism exists, which keeps the amount of ubiquitylated Dnm1 constant, a modification that might have regulatory function. Deubiquitylating enzymes, which also act on Fzo1 (Anton et al., 2013; Simões et al., 2018), are suitable candidates for such a function. Furthermore, upon ethanol treatment, ubiquitylated forms of Dnm1 became reduced to an even stronger degree than unmodified Dnm1 (***Figure 2.3*** C). This would be in accordance with the thought that at least some of the ubiquitylated forms of Dnm1 could be involved in a dynamic regulation of Dnm1 acivity.

In contrast, despite of various and intense efforts, a sumoylation of Dnm1 could not be identified in this study. Contrary to Dnm1's ubiquitylated forms and sumoylated Cdc11, after purification of 8H-Smt3 with cobalt-coated beads, virtually no Dnm1 signals (other than the main band present in all purifications) were detected. Furthermore, Dnm1 levels were not significantly changed in mutants of the SUMO system, like *uba2-ts* (***Figures 2.1*** and ***2.2***), *siz1*Δ *siz2*Δ (***Figure 2.2***), *ulp2*Δ (***Figure 2.2***), or in *ULS* mutants (data not shown). Also overexpression of ULS enzymes did not change Dnm1 levels (data not shown). Taken together, under the tested conditions, Dnm1 is most likely not sumoylated to a relevant degree. Of course, it cannot be excluded that Dnm1 is sumoylated under specific conditions, such as cell cycle stages or in response to stress conditions. Furthermore, still it is a possibility that even with the improved methodology applied here, sumoylation levels are too low for detection. Therefore, at this point, direct involvement of sumoylation in the regulation of the activity of Dnm1, like it was shown for mammalian Drp1, could not be demonstrated. Instead, ubiquitylation of Dnm1 emerged as a potentially interesting PTM in respect to mitochondrial dynamics. Since the relevance of the ubiquitylation of Dnm1 only became clear in the course of this study, this specific modification was not analyzed in further detail, so far. In particular, since the complex regulation of Fzo1 ubiquitylation has been revealed in the last years, it would be very interesting to ask if a similar type of regulation plays a role for Dnm1. Logically, the next steps would be to ask what the relevant ubiquitin ligase is, whether DUBs are involved in regulation of ubiquitylated Dnm1, and if ubiquitylated forms serve other purposes than primarily degradation. Another layer of complexity might be provided by the report that Dnm1 can be degraded in a ubiquitin-independent manner by Blm10-associated proteasomes (Tar et al., 2014).

One aspect that might be independent from the previously discussed topics is that apparently Dnm1 tends to form aggregates. Previously, it was reported that Dnm1 aggregates upon heat-shock (Wallace et al.,

2015) and, also in the current study, conditions were found which apparently cause aggregation of Dnm1. Here, two conditions analyzed by fluorescence microscopy can be named. First, by comparison of Dnm1 after overexpression with endogenous Dnm1 levels, a drastic difference in localization became visible. While Dnm1 at normal expression levels is primarily found in spots along mitochondria, upon overexpression, a large fraction of Dnm1 was apparently aggregated in large spots (***Figure 2.22***). Furthermore, in *ulp2*Δ, Dnm1 apparently formed aggregates. One hypothesis is that *ulp2*Δ has a general proteolysis defect due to the overloading of the proteasome with HMW SUMO conjugates (Maria Miteva, PhD thesis, 2007). Consequently, a defect in proteostasis might arise, which would explain why Dnm1 tends to form aggregates in *ulp2*Δ. A constant turnover of Dnm1 might also be a mechanism to counteract such an aggregation. In addition, these findings highlighted the importance of working with endogenous Dnm1 levels.

3.3 Evaluation of results obtained by mass spectrometry

As described in detail in chapter 2.4, by the mass spectrometry approaches applied in this study, a number of new SUMO substrates and new sumoylation sites could be identified. However, it also has to be acknowledged that between different mass spectrometry runs and to the literature, there are differences in the identified SUMO substrates. The finding of well-known SUMO substrates in mass spectrometry experiments presented here, such as Cdc3, Ubc9 or Pol30, indicates that in principle the approach worked. Still, a question is why some prominent SUMO substrates were not identified among the top candidates, such as Cdc11.

One explanation could refer to the mechanism of the mass spectrometry run. A purification of 8H-Smt3 conjugates with subsequent digestion by LysC and trypsin inevitably contains a major fraction of peptides originating from SUMO itself. First of all, this most likely produces a strong background signal which might cover other detections. Secondly, with each injection, only a limited number of candidates can be identified. This in turn means that an oversaturation of the mass spectrometry detection is a potential problem for the identification of low-abundant proteins. This is a peculiarity of a purification via a PTM since in other applications, usually the protein which should be analyzed is enriched in the sample. In principle, one way to circumvent these problems is the prevention of accumulation of Smt3 peptides in the eluate. For example, for ubiquitin or the here applied 8H-Smt3-KallR-I96R, both leaving a –GG remnant after tryptic cleavage, it is possible to purifiy –GG remnant peptides by specific antibodies. Nevertheless, in another study, large fluctuations between mass spectrometry runs were described, as well, and the

extension of injection time was useful to achieve improved detection (Lamoliatte et al., 2017). For the sake of completeness, it shall be mentioned that the approaches from ***Figure 2.12*** and ***Figure 2.13*** are similar but some adjustments were made after the first round of mass spectrometry. This is discussed in more detail in the results section and detailed in the methods section.

Eventually, it was decided that the site-specific identification of sumoylation is suitable in order to enhance the reliability of identified substrates. Therefore, motivated by a report from Esteras and colleagues (Esteras et al., 2017), 8H-Smt3-KallR-I96R was generated and applied for mass spectrometry (see chapter 2.4.2 for introduction of the method). Substrate peptides identified by an attached –GG remnant can only occur by sumoylation with this Smt3 variant or potentially by ubiquitylation. Therefore, the previously performed purification with specific detection of –GG modified peptides, makes the identification of false positive candiadates much less likely. Furthermore, the practical use of these identifications is increased since the identified lysine residue can immediately by analyzed further by biochemical and genetic methods. The here discussed approach led to the identification of a set of sumoylation sites, which in part covers previously described sumoylation sites but also completely new targets were identified, as in the case of Vnx1. Moreover, additional sumoylation sites on previously described SUMO-substrates were detected, as discussed in detail for Net1 (chapter 2.4.2).

Intriguingly, a novel type of linkage on the N-terminus of Smt3 could be identified. N-terminal Smt3 peptides bearing a double-glycine modification suggested that SUMO can be ubiquitylated at its N-terminus after methionine has been removed (***Figure 2.17***). A direct implication of this finding is that a modification of Smt3-KallR at its N-terminus cannot be excluded with certainty in any experiment where this variant is involved. Open questions are still whether wild-type Smt3 is modified at its N-terminus, as well, and if Smt3 forms linear chains. Since the here discussed result was obtained immediately before submission of this thesis, this question could not be addressed further so far. However, one approach to test occurrence of linear SUMO chains *in vivo* would make use of the LysC-resistance of 8H-Smt3-KallR-I96R. A linear chain of this SUMO variant would be completely resistant to cleavage by LysC. This in turn means that when a yeast protein extract is digested by LysC, virtually all other proteins should be degraded into smaller peptides and a ladder-like pattern upon 8H-Smt3-KallR-I96R would most likely indicate the presence of linear SUMO chains. An occurrence of these chains was not described so far, so the proposed experiment might be worthwhile. Notably, 8H-Smt3-KallR-I96R seems to be toxic in yeast strains devoid of at least one ULS. For example *uls1*Δ transformants were obtained but grew relatively slow whereas in wild type, this SUMO variant did not cause a relevant growth defect (data not shown). Through other experiments from our laboratory, it is known that Smt3-KallR is not tolerated by mutants lacking ULS2, so

this effect is probably the underlying reason. The examination of this apparent toxicity is part of another project in our laboratory and not discussed in further detail at this point.

Recently, in our laboratory, steps towards a strategy for specific detection of sumoylated mitochondrial proteins were made (Joan Schröer, Master Thesis, 2021). Motivated by a previous study (Liao et al., 2018), the aim was to purify mitochondria via a FLAG-tag on Tom70. With a subsequent purification of 8H-Smt3, specifically mitochondrial SUMO substrates should be identified. Preliminary steps for such a purification of mitochondria were made, however, apparently the mechanic vulnerability of mitochondria during the incubation with beads is an obstacle, so that adjustments to the method are required.

3.4 Physiological connection between the SUMO system and mitochondrial dynamics

Three major observations were presented in this study, which suggest an interplay between the SUMO system and mitochondrial dynamics in *S. cerevisiae*. Firstly, in a *dnm1*Δ *fzo1*Δ, the presence of ULS enzymes is apparently required to maintain respiratory competence (***Figure 2.21***). This finding suggests an interaction which is independent from the core fission and fusion machinery. Therefore, a rather indirect effect might explain this phenotype, hypothetically, defects in the inheritance of mitochondria or a synthetic effect between the SUMO system and accumulation of mtDNA damage in *dnm1*Δ *fzo1*Δ (Osman et al., 2015). Second, it was found that in the course of one day at resticitve temperature, the loss of a Ulp2 variant with N-terminal low-temperature degron caused mitochondrial fragmentation (***Figure 2.27***). It was concluded that this effect is probably not caused by an acquired aneuploidy in *ulp2*Δ. This would suggest that accumulation of sumoylated proteins at least indirectly causes mitochondrial fragmentation. Third, in line with finding Dnm1 as a substrate for the UPS, an aggregation of this protein in *ulp2*Δ was observed (***Figure 2.24***). Whether this has a connection to the fragmentation phenotype is not yet clear, however, this experiment showed that the localization of a mitochondrial fission component is altered in *ulp2*Δ.

Altogether, these findings suggest an interaction between the SUMO system and mitochondrial dynamics on a physiological level. Still, it remains unclear if directly sumoylation of a factor of the mitochondrial dynamics regulating proteins is responsible for these observations. In this study, several tools have been established and refined, which can be applied for the identification of sumoylated proteins, which might be helpful for answering these questions. Moreover, with the ubiquitylation of Dnm1, a modification was identified which is certainly interesting for future work on mitochondrial fission. It will be interesting to find out which ubiquitin ligase is responsible and if DUBs play a regulatory role in this process.

4 Materials and Methods

4.1 Materials

4.1.1 *Saccharomyces cerevisiae* strains

Derived from background JD47-13C or JD53			
Strain name (Sc. number)	**Relevant genotype**	**Source**	**Derived from**
JD47-13C (Sc. 188)	*leu2-3,112 lys2-801 his3Δ200 trp1Δ63 ura3-52, MAT*a	Dohmen et al., 1995	served as wild type
JD53 (Sc. 378)	*leu2-3,112 lys2-801 his3Δ200 trp1Δ63 ura3-52, MAT*α	laboratory collection, Jürgen Dohmen	served as wild type
MB2 (Sc. 4275)	*leu2-3,112 lys2-801 his3Δ200 TRP1 ura3-52, MAT*a	laboratory collection Jürgen Dohmen	served as wild type
YSP28 1-3 (Sc. 4080, 4083, 4084)	*DNM1-2HA-6His-*T_{CYC1}*::URA3, MAT*a	this study	JD47-13C + integration of pSP42 (PacI digestion)
YSP29 1-3 (Sc. 4081, 4085, 4086)	*DNM1-2HA-6His-*T_{CYC1}*::URA3 uba1Δ::HIS3 uba1-ts26-CEN/TRP1, MAT*a	this study	JD77-1-1-pRS ts26 (*uba1-ts26*) + integration of pSP42 (PacI digestion)
YSP30 1-3 (Sc. 4082, 4087, 4088)	*DNM1-2HA-6His-*T_{CYC1}*::URA3 uba2Δ::HIS3 uba2-ts9-CEN/LEU2, MAT*a	this study	YSP11 (*uba2-ts9*) + integration of pSP42 (PacI digestion)
YSP38 (Sc. 4137)	*DNM1-2HA-6His-*T_{CYC1}*::URA3 uba2Δ::HIS3 uba2-ts15-CEN/LEU2, MAT*α	this study	JD90-1A-1ts15 (*uba2-ts15*) + integration of pSP42 (PacI digestion)
YSP31 (Sc. 4089)	*DNM1-FLAG-6His-*T_{CYC1}*::URA3, MAT*a	this study	JD47-13C + integration of pSP43 (PacI digestion)
YTL6 (Sc. 4445)	*DNM1-6HA::HIS3 TRP1, MAT*a	laboratory collection Timo Lange	MB2 + hom. rec. of PCR for *DNM1-6HA*
YGA34 *DNM1-6HA*	*DNM1-6HA::HIS3 pdr5Δ::hph, MAT*a	this study	YGA34 + hom. rec. of PCR for *DNM1-6HA*
YKU25-2a *DNM1-6HA*	*DNM1-6HA::HIS3 uba2-ts, MAT*a	this study	YKU25-2a (*uba2-ts*) + hom. rec. of PCR for *DNM1-6HA*
EJY326 *DNM1-6HA*	*DNM1-6HA::HIS3 siz1Δ::LEU2 siz2Δ::TRP1, MAT*a	this study	EJY326 (*siz1Δ siz2*Δ) + hom. rec. of PCR for *DNM1-6HA*
YLD38-1 *DNM1-6HA*	*DNM1-6HA::HIS3 ulp2Δ::NAT, MAT*α	this study	YLD38-1 (*ulp2*Δ) + hom. rec. of PCR for *DNM1-6HA*

YGA34 (Sc. 3106)	*pdr5Δ::hph, MAT*a	laboratory collection Ganapathy Kandasamy	JD47-13C
YKU121 (Sc. 2199)	*slx5Δ::HIS3 uls1Δ::kanMX , MAT*α	laboratory collection Kristina Uzunova	YKU16 (*uls1*Δ)
YKU149 (Sc. 2171)	*uls1Δ::kanMX, MAT*a	laboratory collection Kristina Uzunova	JD47-13C
YKU87 (Sc. 2169)	*slx5Δ::TRP1, MAT*a	laboratory collection Kristina Uzunova	JD47-13C
8H-SMT3 (Sc. 1879)	*8H-SMT3::TRP1, MAT*α	Wohlschlegel et al., 2004	JD53
Sc. 1879 *DNM1-6HA*	*8H-SMT3::TRP1 DNM1-6HA::HIS3, MAT*α	this study	Sc. 1879 + hom. rec. of PCR for *DNM1-6HA*
yAS18 (Sc. 2745)	*8H-SMT3::TRP1* P_{GAL1}*-ULS1::HIS3, MAT*α	laboratory collection Annie Sriramachandran	Sc. 1879
MM4-1 (Sc. 2363)	*8H-SMT3::TRP1 slx8Δ::kanMX, MAT*a	laboratory collection Maria Miteva	
YSP104-1 (Sc. 4628)	*8H-smt3-KallR-I96R::kanMX, MAT*a	this study	JD47-13C + hom. rec. of insert from pSP61 (SacI + NheI)
YSP106-1 (Sc. 4633)	*8H-smt3-KallR-I96R::kanMX ulp2Δ::NAT, MAT*α	this study	YLD38-1 (*ulp2*Δ) + hom. rec. of insert from pSP61 (SacI + NheI)
YSP103-1 (Sc. 4627)	*smt3-KallR::kanMX, MAT*a	this study	JD47-13C + hom. rec. of insert from pSP60 (SacI + NheI)
YKU1 (Sc. 2063)	*ulp2Δ::HIS3, MAT*a	laboratory collection Kristina Uzunova	JD47-13C
MM6 (Sc. 2477)	*dnm1Δ::kanMX, MAT*a	laboratory collection Maria Miteva	JD47-13C
MS89 (Sc. 3165)	*atg7Δ::kanMX, MAT*α *(petite)*	laboratory collection Marion Schnellhardt	JD53
YSP79-1 (Sc. 4364)	*dnm1Δ::HIS3 fzo1Δ::kanMX ade2Δ::LEU2, MAT*α	this study	MM10 (*slx5*Δ *uls1*Δ *dnm1*Δ) x YSP66 (*ade2*Δ) + hom. rec. of PCR for *fzo1*Δ + tetrad diss.
YSP109 (Sc. 4652)	*dnm1Δ::HIS3 fzo1Δ::kanMX*	this study	YLD29-1 (P_{GAL1}*-SLX5* P_{GAL1}*-SLX8*) x YSP79-1 + tetrad diss. isolate 7A
YSP110 (Sc. 4653)	*dnm1Δ::HIS3 fzo1Δ::kanMX*	this study	YLD29-1 x YSP79-1 + tetrad diss. isolate 9A
YKU102a (Sc. 2174)	*slx5Δ::TRP1 uls1Δ::kanMX, MAT*a	laboratory collection Kristina Uzunova	YKU16 (*uls1*Δ) x YKU87
YSP98-1 (Sc. 4383)	*slx5Δ::TRP1 uls1Δ::NAT dnm1Δ::HIS3 fzo1Δ::kanMX4*	this study	MM10 (*slx5*Δ *uls1*Δ *dnm1*Δ) x YSP66 (*ade2*Δ) + hom. rec. of PCR for *fzo1*Δ + tetrad diss.

MM16 pSP62	*DNM1-GFP::URA3* P_{ADH1}-*OM45-mCherry-*T_{CYC1}*::LEU2 pdr5Δ::kanMX, MAT*a	this study	MM16 (*DNM1-GFP pdr5Δ*) + hom. rec. of insert from pSP62 (NotI digestion)
MM22 pSP62	*DNM1-GFP::URA3* P_{ADH1}-*OM45-mCherry-*T_{CYC1}*::LEU2 uba2Δ::HIS3 uba2-ts2-CEN/LEU2, MAT*a	this study	MM22 (*DNM1-GFP uba2-ts2*) + hom. rec. of insert from pSP62 (NotI digestion)
MM17 pSP62	*DNM1-GFP::URA3* P_{ADH1}-*OM45-mCherry-*T_{CYC1}*::LEU2 ulp2Δ::HIS3, MAT*a	this study	MM17 (*DNM1-GFP ulp2Δ*) + hom. rec. of insert from pSP62 (NotI digestion)
JD47-13C pSP57	*mtGFP::LEU2, MAT*a	this study	JD47-13C + hom. rec. of insert from pSP57 (NotI digestion)
YKU1 pSP57	*mtGFP::LEU2 ulp2Δ::HIS3, MAT*a	this study	YKU1 + hom. rec. of insert from pSP57 (NotI digestion)
YSP37 (Sc. 4136)	*DNM1-2HA-6His-*T_{CYC1}*::URA3 ulp2Δ::HIS3, MAT*a	this study	YKU1 + integration of pSP42 (PacI digestion)
JD47-13C pSP58	*Ub-N-term.degron-DHFR(K2)-ULP2::URA3 (ltd-ULP2), MAT*a	this study	JD47-13C + integration of pSP58 (BamHI digestion)

Table 4.1: *Saccharomyces cerevisiae* strains used in this study which are derived from JD47-13C or JD53
For the strains generated in this study, the method and resource for generation is noted. Only strains with permanent changes to their genomic DNA are listed. Strains are sorted by their appearance in this thesis. hom. rec. = homologous recombination, diss. = dissection

Derived from background BY4741 or BY4742			
Strain name (Sc. number)	**Relevant genotype**	**Source**	**Derived from**
BY4741 (Sc. 4049)	*his3Δ1 leu2Δ0 met15Δ0 ura3Δ0, MAT*a	Brachmann et al., 1998, Euroscarf wild type	Served as wild type
BY4742 (Sc. 4019)	*his3Δ1 leu2Δ0 lys2Δ0 ura3Δ0, MAT*α	Brachmann et al., 1998, Euroscarf wild type	Served as wild type
fzo1Δ (Sc. 4160)	*fzo1Δ::kanMX, MAT*a *(petite)*	Euroscarf collection	BY4741
YSP52 1-4 (Sc. 4206 - 4209)	*slx5Δ::HIS3, MAT*α	this study	BY4742 + hom. rec. of PCR for *slx5Δ*
YSP53 1-4 (Sc. 4210-4213)	*slx5Δ::HIS3 fzo1Δ::kanMX, MAT*a	this study	Sc. 4160 + hom. rec. of PCR for *slx5Δ*

Table 4.2: *Saccharomyces cerevisiae* strains used in this study which are derived from BY4741 or BY4742
For the strains generated in this study, the method and resource for generation is noted. Only strains with permanent changes to their genomic DNA are listed. hom. rec. = homologous recombination

4.1.2 Plasmids

Plasmid name (Ec. number)	Details (plasmid type)	Source	Base plasmid
OM45-GFP (Ec. 4611)	*P_{TEF2}-OM45-yeGFP-T_{ADH1} hphMX6* (*CEN*/*LEU2*/*hphMX6*)	Martin Graef laboratory group	pRS315
pCP1 (Ec. 4628)	*P_{GALS}-DNM1-mCherry-T_{CYC1}* (*CEN*/*URA3*)	laboratory collection, Christian Pichlo	YCplac33
pJD658 (Ec. 3689)	*P_{GALS}-smt3-KallR-Q95P-stop-HA-T_{CYC1}* (*CEN*/*TRP1*)	laboratory collection, Jürgen Dohmen	YCplac22
pKU103 (Ec. 1847)	*P_{GAL1}-6His-Ub-T_{CYC1}* (*CEN*/*URA3*)	laboratory collection, Kristina Uzunova	
pMM43 (Ec. 1592)	*P_{GAL1}-2xHA-SMT3* (*CEN*/*LEU2*)	laboratory collection, Maria Miteva	YCplac111
pNP3 (Ec. 3402)	*P_{GAL1}-2xHA-smt3-Q95P* (*CEN*/*LEU2*)	laboratory collection, Natasha Petreska	YCplac111
pNP4 (Ec. 3403)	*P_{GAL1}-2xHA-smt3-K11,15,19R-Q95P* (*CEN*/*LEU2*)	laboratory collection, Natasha Petreska	YCplac111
pSP41 (Ec. 4108)	*P_{GAL1}-mCherry-smt3-Q95P* (*CEN*/*LEU2*)	this study	YCplac111
pSP42 (Ec. 4109)	*5'Δ-DNM1-2xHA-6His-T_{CYC1}* (integrative/*URA3*)	this study	YIplac211
pSP43 (Ec. 4110)	*5'Δ-DNM1-FLAG-6His-T_{CYC1}* (integrative/*URA3*)	this study	YIplac211
pSP45 (Ec. 4112)	*P_{GAL1}-SMT3* (*CEN*/*LEU2*)	this study	YCplac111
pSP46 (Ec. 4113)	*P_{GAL1}-smt3-Q95P* (*CEN*/*LEU2*)	this study	YCplac111
pSP57 (Ec. 4609)	*5'Δ-LEU2-P_{TPI1}-mtGFP-T_{LEU2}* (for homologous recombination into *LEU2*)	this study	pUC21
pSP58 (Ec. 4610)	*P_{ULP2}-Ub-N-term.degron-DHFR(K2)-ULP2-3'Δ* (integrative/*URA3*)	this study	YCplac111
pSP60 (Ec. 4635)	*P_{SMT3}-smt3-KallR-T_{SMT3}*(part1)-*T_{ADH1}-kanMX-T_{SMT3}*(part2) (for homologous recombination into *SMT3*/*kanMX*)	this study	pUC19
pSP61 (Ec. 4636)	*P_{SMT3}-8H-smt3-KallR-I96R-T_{SMT3}*(part1)-*T_{ADH1}-kanMX-T_{SMT3}*(part2) (for homologous recombination into *SMT3*/*kanMX*)	this study	pUC19
pSP62	*5'Δ-LEU2-P_{ADH1}-OM45-mCherry-T_{CYC1}-T_{LEU2}* (for homologous recombination into *LEU2*)	this study	pUC21

pUC19 (Ec. 1386)	base plasmid without marker for yeast	Yanisch-Perron et al., 1985	-
pUC21 (Ec. 383)	base plasmid without marker for yeast	Vieira and Messing, 1991	-
pRS315 (Ec. 255)	base plasmid *CEN*/*LEU2*	Sikorski and Hieter, 1989	-
YCplac111 (Ec. 202)	base plasmid *CEN*/*LEU2*	Gietz and Sugino, 1988	-
YCplac22 (Ec. 200)	base plasmid *CEN*/*TRP1*	Gietz and Sugino, 1988	-
YCplac33 (Ec. 201)	base plasmid *CEN*/*URA3*	Gietz and Sugino, 1988	-

Table 4.3: Plasmids used in this study and relevant base plasmids
Plasmids pUC19 and pUC21 were solely used for amplification of the indicated insert. All plasmids encode an ampicillin resistance gene for selection in *E. coli*. mtGFP = *Su9(1-69)-GFP*, *SU9* encodes the F_0 ATPase subunit 9 of *Neurospora crassa*

4.1.3 Oligonucleotides

Name	Sequence	Function
MM3324	CGCGCTGCAGATGGCTAGTTTAGAAGA TCTTATTCCTACTGTCAACAAGCTTCA GGATGTTATG	5'-DNM1 (mutated PstI-site), forward, verification of pSP42 insertion
MM3054	CCCGGATCCCTAGTGATGATGAATGGT GATGGACTGCATAGTCAGGTACGTC	BamHI-6His-2HA, reverse, verification of pSP42 insertion
JE4659	TTTTTAAGCTTTCACTTGTCATCGTCG	HindIII-FLAG, reverse, verification of pSP42 insertion
MM3425	CGCTGAACCTCCACTGACCG	*DNM1* internal at 1971 bp, forward, amplification of *DNM-6HA* from YTL6, testing for presence of *kanMX* (see notes below table)
MM2869	GGAAATGATCGTACCTATGGAC	*DNM1* downstr. at +316 bp, reverse, amplification of *DNM-6HA* from YTL6, testing for presence of *kanMX* (see notes below table)
MM3424	GCGAACTACTTAGAGAAAGG	*DNM1* internal at 1502 bp, forward, verification of *DNM-6HA*
DG2762	CGGCGGGGACGAGGCAAG	P_{TEF}, reverse, verification of *DNM1-6HA*
SP5046	AAAGGAGTTTGTGTCGTTTT	*FZO1* upstr. at -500 bp, forward, amplification of *fzo1Δ::kanMX* from Sc. 4160
SP5047	TTGTTGTCTTTTAAATGGAG	*FZO1* downstr. at +500 bp, reverse, amplification of *fzo1Δ::kanMX* from Sc. 4160
SP5294	CCAGCTCTTGAAACTCTTTT	*FZO1* upstr. at -610 bp, forward, verification of *fzo1Δ::kanMX*
JD903	CCTCAGTGGCAAATCCTAAC	*kanMX* internal, reverse, verification of *fzo1Δ::kanMX*

SP5295	GTTTGTGGTACTATTGTGGC	*FZO1* internal at bp 76, reverse, verification of *FZO1* in diploids
KU1834	GCGCAAGCTTCCGTACGGCGGGGCACTT	*HindIII-SMT3* downstream -500 bp, forward, verification of *smt3-KallR* and *8H-smt3-KallR-I96R*
MS1975	CCTGAGAAAGCAACCTGACC	P_{ADH1} at 129 bp, reverse, verification and sequencing of *smt3-KallR* and *8H-smt3-KallR-I96R*
MB5191	ACCAGGCCACCTCAGACTCTTTGTG	DHFR at 384 bp, forward, verification of pSP58 insertion
JD5264	GAAGAGTTATTCACGTCTAGTATCATC	ULP2 at 681 bp, reverse, verification of pSP58 insertion
AS3043	TTCCCCCATTCAGTTTCAC	*SLX5* upstr. at -639 bp, forward, amplification of *slx5Δ::HIS3* from YSP39
KU1802	CGAGCCCTTGTATTTTCATTACATC	*SLX5* downstr. at -530 bp, reverse, amplification of *slx5Δ::HIS3* from YSP39
JD902	GCGGCTACTAGTCTTACTGG	*s.p. HIS5* ("*HIS3*") at 598 bp, reverse, verification of *slx5Δ::HIS3*
SP4958	ACACATCTCATGTCAGCTCA	*SLX5* downstr. +600 bp, reverse, verification of *slx5Δ::HIS3*
JD2337	CGTCATTTGATACTACGCC	*SLX5* at 1367 bp, forward, verification of absence *of SLX5*
MM3133	GGGGAATTCAGTTGTCTCAACAGGAGAATGG	*EcoRI-DNM1* at 1673 bp, forward, cloning of pSP42 and pSP43, template pMM84
MM3053	CCCGGTACCCCAGAATATTACTAATAAGGGTTGC	*KpnI-DNM1*(w/o stop), reverse, construction of pSP42 and pSP43, template pMM84
PCR1	CGGGCCTCTTCGCTATT	YCplac backbone, sequencing of pSP42 and pSP43
SP4851	GCGCCTGCAGATGTCGGACTCAGAAGTC	*PstI-SMT3*, forward, cloning of pSP45 and pSP46, templates pSP44 and pSP41
JD297	CGCGCTGCAGGTACCCTAACCACCAATCTGTTCTCTGT	*PstI-KpnI-SMT3*(with stop), reverse, cloning of pSP45, template pSP44
PM1295	CGGGCCTCTTCGCTATTACGCC	YCplac backbone, sequencing of pSP45
NP4384	GCGGGTACCCTAACCACCAATCGGTTCTCTGTGAGCCTCAATAATATC	*KpnI-smt3-Q95P*(with stop), reverse, cloning of pSP46, template pSP41
PCR2	TTAGCTCACTCATTAGG	YCplac backbone, sequencing of pSP46
JD5209	CGCGAGCTCTACCCAAATGGACTGATTGTGAGGG	*SacI-*P_{TPI1}, forward, cloning of pSP57, template pYX142-mtGFP
JD5210	CGCGATATCAAGCTTTTATTTGTATAGTTCATCC	*EcoRV-HindIII-GFP*, reverse, cloning of pSP57, template pYX142-mtGFP
DG3344	AACTGCAGGATAAATGTATGTAGATTGC	T_{LEU2}, reverse, sequencing of pSP57

JD5156	GATGCTGTCGCCGAAGAAGTTAAG	*LEU2*, forward, sequencing of pSP57
IS996	CTCGAGCTCGTATGCGTGAAATGCGTG TAATGG	*XhoI-SacI-ULP2* downstream -910 bp, forward, cloning of pSP58, template yeast DNA
SP5275	GCGGAATTCGATATGTGGGGTTTGATG TGCAATAAAC	*EcoRI-G-*$P_{ULP2,}$ reverse, cloning of pSP58, template yeast DNA
MS359	GCGATTAAGTTGGGTAACGCC	YCplac backbone, sequencing of pSP58
JD1690	GGGATGTGCTGCAAGGCG	pUC19 backbone, sequencing of pSP60 and pSP61
JD5548	CGAAACTATATAGGATCCATGCATGGG GTGTACAATATGGACTTCCTCT	T_{LEU2}*-BamHI-NsiI-*P_{ADH1}, forward, cloning of pSP62, template *PMG6-pRS315-*P_{ADH1}*-Om45-GFP-NatMX6* from Graef group
JD5549	CGCCCTTGCTCACCATTGGGTACCCAA TTAAACCAGCACCGTCACCGTCC	*mCherry-KpnI-linker-OM45*, reverse, cloning of pSP62, template *PMG6-pRS315-*P_{ADH1}*-Om45-GFP-NatMX6* from Graef group
JD5550	GACGGTGCTGGTTTAATTGGGTACCCA ATGGTGAGCAAGGGCGA	*linker-KpnI-mCherry*, forward, cloning of pSP62, template pCP1
JD5551	ATGTATGTAGATTGCGGTCGACAAGCC TTCGAGCGTCCCAAAACCTTCTC	T_{LEU2}*-SalI-*T_{CYC1}, reverse, cloning of pSP62, template pCP1
DG2571	CGGAATTCACTAGTTGTATATGAGATA GTTGATTG	*EcoRI-SpeI-*P_{ADH1}, reverse, sequencing of pSP62
JH451	CCTTCCTTCATTCACGCACAC	P_{ADH1}, forward, sequencing of pSP62
JD105	TCGTTTCTGTCTTTTTC	T_{CYC1}, reverse, sequencing of pSP62

Table 4.4: Oligonucleotides used in this study and their function
upstr. = upstream (5' of ORF), downstr. = downstream (3' of ORF). Note: The PCR performed with MM3425 and MM2869 for *DNM1-6HA::kanMX* was not site-specific for the insert, however, importantly, this PCR revealed that after transformation of *ulp2*Δ two different alleles of *DNM1 w*ere present, one wild type and one with *DNM1-6HA::kanMX*. The site-specific verification of *DNM1-6HA::kanMX* was carried out with the primers MM3424 and DG2762.

4.1.4 Antibodies

Antibody, type	Host, class	Dilution used	Supplier
anti-HA (3F10), primary	rat, monoclonal	1:2000 - 1:1000	Sigma-Aldrich
anti-Pgk1 (22C5D8), primary	mouse, monoclonal	1:10000 - 1:5000	Thermo Fisher
anti-Tpi1, primary	rabbit, polyclonal	1:40000	laboratory collection
anti-ubiquitin (P4D1), primary	mouse, monoclonal	1:5000	Santa Cruz Biotechnology
anti-Smt3, primary	rabbit, polyclonal	1:10000	laboratory collection

anti-Cdc11 (y-415), primary	rabbit, polyclonal	1:5000 - 1:1000	Santa Cruz Biotechnology
anti-rat Alexa Fluor 680, secondary	goat, polyclonal	1:5000	Thermo Fisher
anti-rat DyLight 800, secondary	goat, polyclonal	1:5000	Thermo Fisher
anti-rat POD, secondary	goat, polyclonal	1:5000	Abcam
anti-mouse Alexa Fluor 680, secondary	goat, polyclonal	1:5000	Thermo Fisher
anti-mouse Alexa Fluor Plus 680, secondary	goat, polyclonal	1:5000	Thermo Fisher
anti-mouse 800, secondary	polyclonal	1:5000	Rockland
anti-mouse POD, secondary	goat, polyclonal	1:5000	Sigma-Aldrich
anti-rabbit 800, secondary	polyclonal	1:5000	Biomol
anti-rabbit Alexa Fluor Plus 800, secondary	goat, polyclonal	1:5000	Thermo Fisher
anti-rabbit POD, secondary	donkey, polyclonal	1:5000	VWR

Table 4.5: Antibodies used in this study
POD = peroxidase

4.1.5 Enzymes

Enzyme	Supplier
FastAP Alkaline Phosphatase	Thermo Fisher
DreamTaq DNA Polymerase	Thermo Fisher
S7 Fusion DNA Polymerase	Mobidiag
Beta-glucuronidase	Sigma-Aldrich
Restriction endonucleases (FastDigest)	Thermo Fisher
T4 DNA Ligase	New England Biolabs
RNase A	Omega Bio-Tek
Trypsin	provided by Krüger group
LysC	provided by Krüger group
In-Fusion HD Cloning Kit	Takara

Table 4.6: Enzymes used in this study

4.1.6 Chemicals and consumables

Name	Supplier
1 kb Ladder	New England Biolabs
Acetonitrile	Provided by Krüger group
Acrylamide mix (30% acrylamide / 0.7% bisacrylamide)	Carl Roth
Adenine	Carl Roth
Agar	Formedium
Agarose	Sigma-Aldrich
Ammonia	Provided by Krüger group
Ammonium bicarbonate	Provided by Krüger group
Ammonium sulfate	Carl Roth
Ampicillin	AppliChem

APS (ammonium persulfate)	Sigma-Aldrich
Bacto peptone	Thermo Fisher
Boric acid	Carl Roth
Bromophenol blue	Serva
Calcium dichloride	Acros Organics
Clarity ECL Western Blotting Substrate	Bio-Rad
cOmplete, EDTA-free Protease Inhibitor Cocktail Tablets	Sigma-Aldrich
Coomassie CBB G-250	Sigma-Aldrich
D(+)Glucose monohydrate	Carl Roth
Developer	Agfa
Disodium hydrogen phosphate	VWR
dNTPs (deoxynucleotide triphosphates)	New England Biolabs
DTT (dithiothreitol)	AppliChem
EDTA (Ethylenediaminetetraacetic acid)	Carl Roth
Ethanol	VWR
EZview Red Anti-HA Affinity Gel	Sigma-Aldrich
Fixer	Agfa
Formic acid	Provided by Krüger group
G418	Carl Roth
Galactose	VWR
Glacial acetic acid	VWR
Glass beads (425 – 600 µm)	Sigma-Aldrich
Glycerol	VWR
Glycine	VWR
HEPES (4-(2-hydroxyethyl)-1-piperazineethanesulfonic acid)	Provided by Krüger group
Hydrochloric acid	VWR
Hydrogen peroxide (30%)	Sigma-Aldrich
Hygromycin B	Cayman Chemical
Imidazole	Sigma-Aldrich
Immersion oil	Merck
Iodoacetamide	Provided by Krüger group
Isopropanol	VWR
L-Arginine	Carl Roth
L-Histidine	Merck
Liquid nitrogen	Lab filling system
L-Isoleucine	Carl Roth
Lithium acetate	Sigma-Aldrich
L-Leucine	AppliChem
L-Lysine	Carl Roth
L-Methionine	Merck
L-Phenylalanine	Carl Roth
L-Threonine	AppliChem

L-Tryptophan	VWR
Luminol	Carl Roth
Methanol	VWR
MG132	Sigma-Aldrich
Milk, powdered	Carl Roth
Milli-Q water	Lab filling system
Ni-NTA Superflow	Qiagen
Nitrocellulose membrane (0.2 µm pore size)	VWR
Nourseothricin	Jena Bioscience
NucleoSpin Gel and PCR Clean-up	Macherey-Nagel
Omega Bio-Tek E.Z.N.A Plasmid DNA Mini Kit	Omega Bio-Tek
PageRuler Plus Prestained Protein Ladder	Thermo Fisher
p-coumaric acid	Carl Roth
PEG (polyethylene glycol), 3015-3685 g/mol	Sigma-Aldrich
Phosphoric acid	Carl Roth
Ponceau S	Sigma-Aldrich
Potassium acetate	Merck
Potassium chloride	AppliChem
Potassium dihydrogen phosphate	VWR
PureCube Co-NTA MagBeads	Cube Biotech
PVDF (polyvinylidene difluoride) membrane (0.45 µm pore size)	VWR
Raffinose	Serva
REVERT Total Protein Stain	LI-COR
SDS (sodium dodecyl sulfate)	Serva
SDS-RPS (styroldivinylbenzol - reversed phase sulfonate)	Provided by Krüger group
Serva Stain Clear G	Serva
Sodium acetate	VWR
Sodium azide	Sigma
Sodium chloride	VWR
Sodium dihydrogen phosphate	Merck
Sodium hydroxide	Merck
Super RX-N X-ray film	Fujifilm
SuperSignal™ West Femto Maximum Sensitivity Substrate	Thermo Fisher
TALON® Metal Affinity Resin	Clontech/Takara
TCE (2,2,2-trichloroethanol)	Sigma-Aldrich
TEMED (tetramethylethylenediamine)	AppliChem
Thiourea	Provided by Krüger group
Trichloroacetic acid	Carl Roth
Tris (Tris-(hydroxymethyl)-aminomethane)	Carl Roth
Triton X-100	Sigma-Aldrich
Tryptone	Formedium
Uracil	Sigma-Aldrich

Urea	Carl Roth
Whatman paper	VWR
Yeast extract	Formedium
Yeast nitrogen base	Formedium
Zinc sulfate	Merck
β-mercaptoethanol	Sigma-Aldrich

Table 4.7: List of chemicals and consumables used in this study (buffers of enzymes and components of kits not listed)

4.1.7 Equipment

Name	Manufacturer
T3 Thermocycler	Biometra
Agarose gel electrophoresis chamber	Peqlab
Blue light table, dark reader	Clare Chemical Research
Camera for yeast plates	Sony
Centrifuge 5415 D	Eppendorf
Centrifuge 5424	Eppendorf
Centrifuge 5430 R	Eppendorf
Centrifuge 5810 R	Eppendorf
Centrifuge Allegra X-22R	Beckman-Coulter
Centrifuge Avanti J-20 XP	Beckman-Coulter
Developer for X-ray films Curix 60	Agfa
Electric stirrer	H + P
Fluorescence microscope Axioplan 2	Zeiss
Gel documentation system	Bio-Rad
Incubators innova 4230	New Brunswick Scientific
Macro pipette controller	Brand
Magnetic rack	Invitrogen
Micropipettes	Gilson
Microscope for tetrade dissection	Zeiss
Nanodrop	Eppendorf
Odyssey Imager	LI-COR
pH meter	Mettler Toledo
Power supplies	Biometra, Amersham Biosciences
Pump	KNF Lab
Rocking platform	Biometra
Rotating wheel (small, large)	University workshop, GLW
Scanner for X-ray films, 4870 photo	Epson
SDS-PAGE and wet Western blot system, large	Hoefer
SDS-PAGE and wet Western blot system, small	Bio-Rad
Semi-dry Western blot system	Bio-Rad
Spectrophotometer	Pharmacia Biotech

Thermomixer	Eppendorf
Vibrax shaker	Ika
Vortex	Ika

Table 4.8: List of Equipment

4.1.8 *Escherichia coli*

Strain name	Genotype	Source
XL1-Blue	*recA1 endA1 gyrA96 thi-1 hsdR17 supE44 relA1 lac* [*F´ proAB lacI^q ZΔM15 Tn10* (*Tetr*)]	laboratory collection

Table 4.9: *Escherichia coli* strain used in this study for cloning and amplification of plasmids

4.1.9 Media for *Saccharomyces cerevisiae*

***S. cerevisiae* medium**	**Composition**	**For treatments**
SD (synthetic defined / synthetic dextrose), omit uracil, leucine, tryptophan or histidine for selection	Yeast nitrogen base 6.7 g/l, glucose 20 g/l, leucine 60 mg/l, tryptophan 40 mg/l, histidine 10 mg/l, arginine 20 mg/l, isoleucine 60 mg/l, lysine 40 mg/l, methionine 10 mg/l, phenylalanine 60 mg/l, threonine 50 mg/l, adenine (in 0.1 M NaOH) 20 mg/l, uracil (in 0.1 M NaOH) 40 mg/l	
SRaff (synthetic raffinose)	Like SD but 20 g/l raffinose instead of glucose	Add galactose 20 g/l for induction of P_{GAL1}
SGal (synthetic galactose)	Like SD but 20 g/l galactose instead of glucose	
YPD (yeast extract peptone dextrose)	Bacto peptone 20 g/l, yeast extract 10 g/l, glucose 20 g/l	20 µM MG132, 2% - 10% ethanol (v/v), 1 mM H_2O_2
YPGal (yeast extract peptone galactose)	Like YPD but 20 g/l galactose instead of glucose	1 mM H_2O_2
YPGly (yeast extract peptone glycerol)	Like YPD but 3 % (v/v) glycerol instead of glucose; for growth of *ade2*Δ add adenine 20 mg/l	
GNA (presporulation plates)	5% Glucose, 1.7% bacto peptone, 1.3% NaCl, 1% yeast extract	
Supplement liquid sporulation medium	1% potassium acetate, 0.005% zinc sulfate, leucine 60 mg/l, tryptophan 40 mg/l, histidine 10 mg/l, arginine 20 mg/l, isoleucine 60 mg/l, lysine 40 mg/l, methionine 10 mg/l, phenylalanine 60 mg/l, threonine 50 mg/l, adenine (in 0.1 M NaOH) 20 mg/l, uracil (in 0.1 M NaOH) 40 mg/l	
	For antibiotic selection: hygromycin B 400 µg/ml, G418 250 µg/ml, nourseothricin 100 µg/ml	

	For plates: add agar 20 g/l	

Table 4.10: Media for *S. cerevisiae*
Listed are media for *S. cerevisiae* which have been applied for experiments presented in this study. For specific experiments, treatments were conducted as described in the results section and under 4.2.17.

4.1.10 Media for *Escherichia coli*

***E. coli* medium**	**Composition**
LB (+ ampicillin)	NaCl 10 g/l, tryptone 10 g/l, yeast extract 5 g/l (for selection: ampicillin 100 µg/ml) for plates: add agar 20 g/l

Table 4.11: Media for *E. coli*

4.2 Methods

4.2.1 Polymerase chain reaction

A typical application of the PCR (polymerase chain reaction) method is the amplification of DNA fragments for the construction of a plasmid, a process termed cloning. Usually, for cloning purposes, a high-fidelity DNA polymerase was applied. In contrast, in order to verify the genotype of a yeast strain, an analytic PCR without the need for high fidelity was carried out with the DreamTaq DNA polymerase. For this purpose, a very small amount of yeast cells freshly grown on a plate overnight was taken with a pipet tip and resuspended in 1 µl water in a PCR tube. The suspension was incubated in a microwave for one minute with the lid of the tube open. Recipes for both types of PCR are listed below (***Table 4.12***).

High-fidelity PCR		**PCR for verification**	
Component	**Volume**	**Component**	**Volume**
5 x HF buffer	20 µl	10 x DreamTaq buffer green	2 µl
dNTPs (10 mM each)	2 µl	dNTPs (10 mM each)	0.4 µl
S7 Fusion Polymerase	1 µl	DreamTaq Polymerase	0.1 µl
Primer 1 (100 µM)	0.5 µl	Primer 1 (100 µM)	0.1 µl
Primer 2 (100 µM)	0.5 µl	Primer 2 (100 µM)	0.1 µl
Template plasmid / genomic DNA	0.25 µl / 1 µl	Yeast suspension	1 µl
Milli-Q water	75.75 µl / 75 µl	Milli-Q water	16.3 µl
Total	100 µl	Total	20 µl

Table 4.12: Recipes for high-fidelity PCR and for PCR for the verification of yeast strains

Typical programs for both types of PCR reactions are detailed below (***Table 4.13***).

High-fidelity PCR			PCR for verification		
Step	**Temperature**	**Duration**	**Step**	**Temperature**	**Duration**
1 Denaturation	98°C	5 minutes	1 Denaturation	95°C	3 minutes
2 Denaturation	98°C	55 seconds	2 Denaturation	95°C	30 seconds
3 Annealing	Tm – 5°C	55 seconds	3 Annealing	Tm – 5°C	30 seconds
4 Extension	72°C	Depending on length, minimum 30 sec per kb	4 Extension	72°C	Depending on length, minimum 1 min per kb
Repeat steps 2 – 4 29 times			Repeat steps 2 – 4 34 times		
5 Final Extension	72°C	5 minutes	5 Final Extension	72°C	10 minutes
6 Short-term storage	4°C	Ongoing	6 Short-term storage	4°C	Ongoing

Table 4.13: PCR programs for high-fidelity PCR and for PCR for the verification of yeast strains

4.2.2 Agarose gel electrophoresis

For purification and analytical purposes, DNA samples, like PCR reactions or restriction digestions, were separated by size in an electric field in agarose gels. The gels were prepared by suspending 1% agarose in TAE-buffer (Tris-acetate-EDTA-buffer: 40 mM Tris (Tris-(hydroxymethyl)-aminomethane), 20 mM sodium acetate, 1 mM EDTA (ethylenediaminetetraacetic acid) with subsequent heating in a microwave until the agarose is dissolved. The liquid (~ 30 – 50 ml) was poured into a tray for preparation of the gel. Immediately after pouring, 3 µl Serva Stain Clear G (Serva) was added to the warm liquid, it was distributed and a comb for wells was placed in the gel. After solidification, the agarose gel was taken out of the tray and placed in an electrophoresis chamber filled with TAE-buffer. 10 X DreamTaq Buffer Green (Thermo Fisher) was added to a DNA sample to a working concentration of 1 x. An appropriate amount (usually the complete PCR volume) of so prepared DNA was loaded into a well of the agarose gel. Additionally, 5 µl of a DNA ladder, for example 1 kb Ladder (NEB), was loaded into a well. The gel electrophoresis was typically carried out for 20 minutes with 110 V. For preparative purposes, the desired band was cut out of the gel on a blue light table and weighed. For analytical purposes, the agarose gel was imaged in a UV light gel documentation system.

4.2.3 DNA purification

DNA recovered from agarose gel electrophoresis, a crude PCR reaction, or a restriction digestion were purified by application of the kit “NucleoSpin Gel and PCR Clean-up” (Macherey-Nagel) according to the

manufacturer's protocol. Usually, the elution was performed in 30 µl except for very low concentrated samples where this volume was reduced to 15 µl.

4.2.4 Restriction digestion of DNA

Restriction digestion of DNA was performed for two major purposes. These are the preparation of cloning or the verification of clones of a newly constructed plasmid. Below, representative recipes for restriction digestions are listed (***Table 4.14***).

	Volume		
Component	**Digestion of plasmid for cloning**	**Digestion of purified PCR for cloning**	**Digestion of plasmid for verification**
10 x FD Buffer (green)	2 µl	2 µl	1 µl
Milli-Q water	10 µl	1 µl	5 µl
DNA	6 µl plasmid miniprep	15 µl purified PCR	3 µl plasmid miniprep
Restriction endonuclease 1	1 µl	1 µl	0.5 µl
Restriction endonuclease 2	1 µl	1 µl	0.5 µl
Total	20 µl	20 µl	10 µl

Table 4.14: Recipes for different purposes of restriction digestions

If desired, additionally 1 µl FastAP alkaline phosphatase was added to the vector digestion. The restriction digestion reaction was incubated for 1 hour at 37°C, and heat inactivation was performed according to the required temperature and time for the applied endonucleases.

4.2.5 DNA Ligation

Usually immediately before ligation, an agarose gel electrophoresis with a fraction of the digested and purified fragments was performed in order to verify the purity and to compare the DNA concentrations of the respective bands. According to this analysis, the ligation reaction was set up in a way that five times more insert molecules are added than vector molecules. For a three-part ligation, both inserts were added in five times the amount of the vector. Depending on the length of the DNA fragments and their estimated concentrations, the ligation mix was prepared as follows (***Table 4.15***).

In order to evaluate ligation efficiency, the same mix was prepared with water instead of insert. The ligation mix was incubated at room temperature for one hour and for demanding ligations additionally overnight at 4°C.

Component	Volume
10 x ligation buffer	2 µl
Vector (plasmid backbone)	0.5 µg
Insert	5 x molecule amount of vector
T4 DNA ligase (Thermo Fisher)	1 µl
Milli-Q water	Fill up to 20 µl
Total	20 µl

Table 4.15: Recipe for ligation

4.2.6 In-Fusion cloning

As an alternative to the conventional cloning method at sites of restriction digestions, if desired the In-Fusion cloning method was applied. In brief, by this technique, one or more inserts can be assembled into the linearized vector by homologous ends. An example recipe for an In-Fusion reaction is given below, following the manufacturer's manual (Takara) (***Table 4.16***).

Component	Amount / Volume
Purified PCR fragment	100 ng (insert : vector ratio 2:1 molecules)
Linearized vector	100 ng (insert : vector ratio 2:1 molecules)
5 x In-Fusion HD Enzyme Premix	2 µl
Milli-Q water	Fill up to 10 µl
Total	10 µl

Table 4.16: Recipe for In-Fusion cloning reaction

For control purposes, the same mixture was prepared with water instead of insert. The mixtures were incubated at 50°C for 45 minutes.

4.2.7 Transformation of *Escherichia coli*

The following protocol is a shortened version of the conventional protocol for *E. coli* transformation that was applied successfully during this thesis. For each transformation, a 100 µl aliquot of chemically competent *E. coli* XL1-Blue, previously stored at -80°C, was thawed on ice. 10 µl ligation mix, 5 µl In-Fusion mix, or 1 µl pure plasmid were added and the sample was incubated for 5 minutes on ice. After a heat-shock at 42°C for 45 seconds, 1 ml LB-medium was added to the cells and the sample was incubated at 37°C for 15 minutes with shaking at 300 rpm in a thermomixer. Afterwards, the suspension was spun at 16100 rcf in a microcentrifuge for one minute. The supernatant was discarded and the pellet was

resuspended in 100 µl LB-medium. The suspension was plated on an LB + ampicillin plate. The plate was incubated overnight at 37°C and the colonies were picked for plasmid isolation.

4.2.8 Preparation of chemically competent *E. coli*

In order to obtain transformation competent cells, 5 ml LB-medium was inoculated with a small amount of *E. coli* XL1-Blue from the -80°C stock. Cells grew overnight at 37°C while shaking and on the following day, 100 ml LB-medium was inoculated with an OD_{600} of 0.2 and incubated at 37°C with shaking. The culture grew to an OD_{600} of 0.6 and was transferred to a precooled 50 ml tube. It was centrifuged at 1800 rcf and 4°C for 10 minutes. The supernatant was removed and the pellet resuspended in 25 ml ice-cold $CaCl_2$ (0.1 M). After incubation on ice for 20 minutes, the suspension was centrifuged again at 1800 rcf and 4°C for 10 minutes. The supernatant was discarded and the pellet resuspended in 3 ml pre-cooled 0.1 M $CaCl_2$ with 15% glycerol. This suspension was incubated on ice for one hour and aliquots of 100 µl were prepared and stored at -80°C.

4.2.9 Plasmid isolation from *E. coli*

Typically, after an *E. coli* transformation and growth of colonies on LB + ampicillin, colonies were picked with a pipet tip and 3 ml LB + ampicillin medium was inoculated. The cultures were incubated at 37°C overnight and on the following day the plasmid isolation was performed. The plasmid isolation (also termed miniprep) was carried out with the "Omega Bio-Tek E.Z.N.A Plasmid DNA Mini Kit" (Omega Bio-Tek) according to the manufacturer's manual. The elution was usually carried out with 50 µl elution buffer. The concentration was usually 300 ng/µl – 500 ng/µl, as measured by Nanodrop.

4.2.10 DNA sequencing

For DNA sequencing, 9 µl of a purified analytical PCR or 4 µl plasmid miniprep and 5 µl water were sent. 1 µl of an oligonucleotide (100 µM) was added to the DNA into the same tube. For the reaction, the "Lightrun NXP (night express)" service from Eurofins was used. Analysis of DNA sequences and *in silico* plasmid construction were made with the software Benchling.

4.2.11 Preparation of glycerol stocks

For *E. coli* glycerol stocks, a culture was grown in LB + ampicillin at 37°C overnight and 200 µl of the overnight culture were added to 200 µl 75% glycerol so that the final concentration of glycerol was 15%. For *S. cerevisiae*, yeast freshly grown on agar plates was resuspended in 15% glycerol. In both cases, the suspension was directly frozen at -80°C.

4.2.12 Cultivation of *Saccharomyces cerevisiae*

In brief, streak outs of *S. cerevisiae* on agar plates were carried out by using a toothpick, and plates were usually incubated for 2 – 3 day at 30°C. For liquid culture, usually a preculture was started by resuspension of cells from a plate in 2 ml medium. This preculture was incubated at 30°C overnight and on the following day, the OD_{600} was measured in a dilution of 1:50. A larger culture volume, according to the experiment, was inoculated with an OD_{600} of 0.25. Generally, liquid cultures were shaking at 160 rpm. For harvesting, the cultures typically grew for 1 – 2 doublings and the desired volume was filled into a 15 ml tube or a 50 ml tube. The cells were centrifuged at 3200 rcf for 5 minutes, the supernatant was removed, and the pellet was frozen in liquid nitrogen and stored at -80°C. This description applies to the standard growth conditions, however, for specific experiments, cells were treated differently. For the experiments presented in this thesis, this is described individually in the respective figure legends. If not indicated differently, yeast grew at 30°C.

4.2.13 Transformation of *S. cerevisiae*

Transformation of *S. cerevisiae* was carried out by application of the lithium acetate/single-stranded carrier DNA/polyethylene glycol method. The protocol described below is a modified version of the technique described by Gietz and Woods (Gietz and Woods, 2002). For the transformation of yeast, an overnight culture was diluted to an OD_{600} of 0.25 as described above. The culture grew to at least OD_{600} of 0.6 and 5 ml were filled into a 15 ml tube. The culture was spun at 3200 rcf for 5 minutes and the supernatant was discarded. The pellet was resuspended in 1 ml sterile water and transferred into a microcentrifuge tube. This was spun shortly for 8 seconds (centrifuge Eppendorf 5415 D), and the supernatant was removed. Once again, the pellet was resuspended in 1 ml sterile water, the suspension was spun shortly for 8 seconds, and the supernatant was removed. Then, the pellet was resuspended in 100 µl sterile water, and the suspension was added to the transformation mix (***Table 4.17***).

Component	Volume
50% PEG (Polyethylene glycol)	240 µl
1 M lithium acetate	35 µl
E. coli carrier DNA	2.5 µl
DNA	*CEN*-plasmid: 1.5 µl Restriction digestion of plasmid: 10 µl Purified PCR: depends on concentration, for *DNM1-6HA* 5 µl of purified colony PCR
Total	279 µl – 285 µl

Table 4.17: Recipe for transformation mix

After addition of the cell suspension, the transformation mix was vortexed for 2 seconds. Subsequently, the mix was incubated at 30°C for 25 minutes followed by a heat-shock at 42°C for 20 minutes. Afterwards, the mix was centrifuged shortly for 8 seconds, and the supernatant was removed. The pellet was resuspended in 50 µl sterile water and plated on an appropriate agar plate for selection. Up to two transformations could be plated on one plate. Usually, the plate was incubated at 30°C, and after 2 – 3 days, the colonies of transformants could be picked.

For transformation of yeast with a *kanMX* based construct, instead of directly plating on a plate, the cell suspension was added to 1.5 ml of YPD. For the development of a resistance, the culture was kept at room temperature overnight while rotating on a wheel. The lid of the tube was locked with a cap to avoid opening of the tube due to gas formation. After incubation overnight, 500 µl of the culture were transferred into a new microcentrifuge tube. The culture was spun shortly for 8 seconds, the supernatant was removed and the pellet was taken up in 200 µl sterile water. From this, one or two platings were performed with 100 µl each. In both cases, only one transformation was plated on a plate. Usually, the plate was incubated at 30°C and after 2 – 3 days, the colonies of transformants could be picked.

4.2.14 Crossing, sporulation and tetrad dissection of *S. cerevisiae*

In order to cross two haploid yeast strains, one strain with *MAT*a and one strain with *MAT*α were streaked out on YPD in a way that both strains are mixed and diluted across the plate so that haploid cells mate. After growth for one day, the cells were replica-plated with a velvet cloth to a plate selecting for one marker per strain so that only diploids could grow. After growth for 2 – 3 days, diploids were picked, streaked out, and grown on the same medium for additional selection. For sporulation, cells were streaked out and grown on YPD for one day. Subsequently, cells were grown on GNA for one day, followed by a second streak out on GNA. From this GNA plate, a small amount of cells was added to liquid sporulation medium. This culture was incubated at 25°C for 5 days and at 30°C for 3 days, both with shaking.

After this incubation, the formation of tetrads was verified by light microscopy and the asci were enzymatically digested. For this purpose, 100 µl of the culture were transferred into a microcentrifuge tube and a short spin for 8 seconds was conducted. The supernatant was removed and the pellet was resuspended in 150 µl sterile water. 10 µl of β-glucuronidase were added to the suspension and it was incubated at 37°C for 45 minutes. Importantly, the required amount of β-glucuronidase and the incubation conditions depended on the quality of the enzyme, so adjustments were necessary. 50 µl of the digested sample were plated on YPD and, after drying of the liquid, the tetrads were dissected by the use of a light microscope with micromanipulator.

4.2.15 *S. cerevisiae* spot assay

For the comparison of growth phenotypes, spot assays were performed. On the day before the spot assay, yeast strains were freshly streaked out on YPD. Immediately before spot assay, a 96-well plate was sterilized with UV-light with 2000 joule. Yeast cells grown overnight were resuspended in 200 µl sterile water in a microcentrifuge tube. The OD_{600} of suspensions was measured at a dilution of 1:100 and accordingly the yeast suspension was diluted to an OD_{600} of 0.1. These dilutions were transferred to wells in the 96-well plate in one row. For the following dilution series, in three rows 90 µl sterile water was added to wells. The dilutions were performed by serial transfer of 10 µl suspension from one row to the next one containing 90 µl water. In total, four rows were prepared with OD_{600} of 0.1, 0.01, 0.001 and 0.0001, respectively. With a metal replica-plater, a small amount of the suspensions was transferred to the desired plates.

4.2.16 *S. cerevisiae* colony formation assay

With the colony formation assay, the frequency of *petite* formation in different yeast strains was assessed. Prior to the actual experiment, the strains were streaked out on YPGly plates in order to select for respiratory competent cells. From such a plate, 2 ml liquid YPGly was inoculated, which selects for respiratory competent cells, as well. The cultures were incubated over night and 5 ml YPGly was inoculated with an OD_{600} of 0.25. After one doubling, the colony formation assay was carried out. For this purpose, 1 ml of a culture with an OD_{600} of 0.5 was transferred to a sterile microcentrifuge tube. For cultures with different OD_{600}, the volume was adjusted to have the same number of cells in each tube. After a short spin of 8 seconds, the supernatant was removed and 1 ml YPGly was added so that all suspensions have an OD_{600} of 0.5 in 1 ml. As described for typical haploid *Saccharomyces cerevisiae* strains

(https://research.fhcrc.org/content/dam/stripe/hahn/methods/yeast_genetics/yeast_OD_cells.pdf), it was calculated that 100 µl of a suspension with an OD_{600} of 0.0001 corresponds to 150 cells. Therefore, in consecutive dilution steps with YPGly, this desired dilution was prepared. 100 µl of the final dilution, corresponding to ideally 150 cells, were plated on a YPD plate and spread with a Drigalski spatula. Of each culture grown in YPGly, three independent dilutions were prepared and plated on three plates. For the strains *uls1*Δ *slx5*Δ (Sc. 2199) and *uls1*Δ *slx5*Δ *dnm1*Δ *fzo1*Δ, additionally the liquid cultures were further incubated overnight and, on the next day, an appropriate volume of the culture was taken and used for the colony formation assay with three plates of both strains. As explained in the results section, this extended growth in YPGly is not expected to and did not have a relevant effect on the results.

When yeast colonies were sufficiently grown, photos of the plates were taken and particularly small colonies were streaked out on YPGly and YPD for individual determination of the phenotype. This was done in order to prevent fusion of smaller colonies with bigger ones during replica-plating. Afterwards, with each plate, three replica-platings were performed. The same cloth was stamped onto two YPGly plates and YPD in that order. The last plating on YPD ensured that a sufficient amount of cells had been taken up by the cloth and stamped on YPGly before. The plates were incubated, and when sufficiently grown, photos of the plates were taken.

The replica-plating on YPD was used to determine the number of stamped colonies and, together with the photo taken before replica-plating, as an indicator for the expected positions of colonies on YPGly. On YPGly plates, the colonies were grouped into three classes and counted. These classes were 1) Growing on YPGly, 2) not growing on YPGly, and 3) individually streaked out before replica-plating. For assistance with manual counting of the colonies, the program DotDotGoose (version 1.5.1) from the American Museum of Natural History, Center for Biodiversity and Conservation was used (https://biodiversityinformatics.amnh.org/open_source/dotdotgoose/). This program is useful for manual counting of different categories and management of the results.

4.2.17 Treatments of *S. cerevisiae* for experimental purposes

In brief, different treatments of yeast cultures are described for the results presented in this thesis. For proteasome inhibition, the yeast strain *pdr5*Δ was applied. After one doubling, MG132 was added to a working concentration of 20 µM. The cultures grew for additional 2 hours before harvesting.

For the treatment with ethanol, cultures grew from an OD_{600} of 0.25 to 0.7. Then the desired volume of ethanol was added to the culture. For this study, concentrations between 2% and 10% ethanol were

applied. If less than 10% ethanol was added, water was used to adjust the culture volumes. After 30 minutes of incubation, the cultures were harvested.

Usually, for the expression of genes under control of P_{GAL1}, the overnight culture grew with 2% raffinose as carbon source. Also the main culture grew with 2% raffinose for one doubling. Then, galactose was added to a working concentration of 2% in order to induce gene expression. Glucose had to be omitted in order to allow induction by galactose (Johnston et al., 1994). For the expression of SUMO variants, yeast cells were incubated for 3 more hours before harvesting. For fluorescence microscopy, yeast harboring the plasmid pCP1 grew in YPGal for one doubling prior to microscopy.

For induction of oxidative stress, after 1 – 2 doublings, H_2O_2 was added to YPD in a working concentration of 1 mM. After 10 minutes of treatment, the culture was harvested.

Temperature-sensitive strains were generally kept at 25°C until the actual experiment was performed. For the experiment presented in chapter 2.1.1, the strains *uba1-ts26*, *uba2-ts9* and *uba2-ts15* grow either in 30°C until harvesting, which can be regarded as permissive temperature, or the cultures were shifted to 37°C after one doubling. At this restrictive temperature, cultures were incubated for 3.5 additional hours prior to harvesting. For the experiment presented in chapter 2.1.2 and for fluorescence microscopy, *uba2-ts* grew at 30°C. Here, it should be noted that even at non-restrictive temperature, *uba1-ts* and *uba2-ts* are strongly impaired in ubiquitin and SUMO activation, respectively, but only to an extent that still allows growth. The strain *ltd-ULP2* was initially grown at 25°C and, after one doubling, the culture was split into three cultures and these were incubated at 25°C, 33°C or 37°C. After one day of incubation, the cultures were diluted and after five more hours, the fluorescence microscopy was performed.

4.2.18 Fluorescence microscopy

Usually, yeast cells were grown in liquid medium for 1 – 2 doublings prior to fluorescence microscopy except where indicated otherwise. When the desired OD_{600} was reached, 1 ml of culture was centrifuged at 1000 rcf for 1 minute and the supernatant was removed. The pellet was resuspended in SD medium, SGal medium or PBS (phosphate-buffered saline: 137 mM NaCl, 2.7 mM KCl, 8.1 mM Na_2HPO_4, 1.5 mM KH_2PO_4, pH 7.4) and 1 µl of this suspension was placed on a microscope slide and covered with a cover slip. In the course of this study, several techniques for immobilizing yeast cells were tested. In conclusion, the application of poly-L-lysine coated glass slides (Sigma-Aldrich) was chosen as the best option and from this point in time, the respective microscope slides were used.

Fluorescence microscopy was carried out with the fluorescence microscope Zeiss Axioplan 2 and with the software AxioVision Rel 4.7 (Zeiss). For microscopy, a magnification of 100 x was used, provided by one of the two objectives Zeiss Plan-Neofluar 100 x / 1.30 oil or Zeiss Apochromat 100 x / 1.4 oil, both of which required oil immersion. As indicated in the figure legend, for the microscopy of *ulp2*Δ, an additional magnification of 1.25 x was applied. When the objective Zeiss Plan-Neofluar was used, a slider for DIC (differential interference contrast) was inserted for brightfield microscopy. The used filters are listed in ***Table 4.18***. The exposure times of the respective channels differed between the experiments and are noted in the figure legends. For Z-stacks, usually the distance between two images was 0.7 – 0.8 µm, depending on the cell size. After fluorescence microscopy, the software AxioVision was used for viewing the images and for analysis of phenotypes. For image adjustments and assembly of figures for this thesis, the programs IrfanView and GIMP were used. Specifically, where desired, GIMP allowed to digitally merge brightfield and GFP-signals, which applies for the fluorescence microscopy shown in chapter 2.6.3. This was done since, usually, the mitochondrial morphology is difficult to judge when they are viewed in the periphery of cells. Therefore, for the representative figures in chapter 2.6.3, the GFP channel of an image with a focus slightly above or below the cell periphery was merged with a brightfield photo.

Since the exact parameters for fluorescence microscopy differed between experiments, the relevant information is provided in the respective figure legends.

Fluorophore	Filter
mCherry	F41-007 HQ-Cy3 HQ545/30 (excitation) Q570LP HQ610/75 (emission)
mCherry	F41-035 HQ-DsRed HQ565/30 (excitation) Q585LP HQ620/60 (emission)
GFP	F41-054 HQ-Cy2 HQ480/40 (excitation) Q505LP HQ527/30 (emission)

Table 4.18: Filters used for fluorescence microscopy
Listed are the filters used in this study. For mCherry, both of the listed filters were applicable. Filter "HQ-Cy3" gives a more orange color whereas filter "HQ-DsRed" gives a deeper red color. The filters are part of the filter set 1046-281.

4.2.19 Boiling of yeast cells for protein extraction

In order to extract proteins from yeast cells for subsequent analysis by SDS-PAGE, yeast cells were boiled. For this purpose, stored cell pellets were taken from the -80°C freezer and placed on ice. To each pellet,

LLB (Laemmli loading buffer: 0.0625 M Tris–HCl, pH 6.8, 2% SDS, 10% glycerol, 2% β-mercaptoethanol, 0.005% bromophenol blue) was added at a ratio of 33.3 µl per 1 OD * ml pellet size. In this thesis OD * ml defines the pellet size which is the product (*) of the multiplication of the measured OD_{600} and the harvested volume in ml. The pellets were resuspended by vortexing, and the suspension was transferred into a microcentrifuge tube. Subsequently, the suspension was boiled at 99°C for 5 minutes. Afterwards, the sample was kept at room temperature for 5 minutes. Then, the sample was spun shortly for 8 seconds in order to separate cell debris from the solution, and the supernatant was transferred into a fresh microcentrifuge tube. This lysate could be stored at -20°C and at any time be loaded for SDS-PAGE.

4.2.20 Glass bead lysis of yeast cells under denaturing conditions

For the purpose of subsequent protein purification, proteins were extracted from yeast by glass bead lysis. In the following, the procedure is described as it was performed for purification of 8H-Smt3 and 6H-ubiquitin (see chapter 2.3.2). In this case, the glass bead lysis was performed for cell pellets with a size of 200 OD * ml. Firstly, cell pellets were taken from the -80°C freezer and placed on ice. Lysis buffer (8 M urea, 100 mM NaH_2PO_4, 10 mM Tris, pH 8.0) was added to cell pellets at a ratio of 25 µl buffer per 1 OD * ml pellet size (5 ml in this case). The suspension was filled into a 15 ml tube together with 2 ml glass beads (425 – 600 µm). Due to the denaturing properties of the buffer and reduced solubility of urea at lower temperatures, the following steps were performed at room temperature. The suspension with glass beads was vortexed 4 times for 1 minute with pauses of at least 1 minute in between. For better mixing of the components, two of these vortexing rounds were performed with the tube placed horizontally on the vortex. Afterwards, the whole suspension was poured into a specific centrifuge tube for Beckman-Coulter Avanti J-20 XP and spun at 30,000 rcf for 20 minutes.

After centrifugation, 100 µl of the supernatant were taken as input fraction and, on the following day, at the end of the purification procedure (see below), 25 µl 5 x LLB were added to the input sample. This sample was boiled at 99°C for 5 minutes and stored at -20°C.

The remaining supernatant, due to a loss of liquid between glass beads only ~ 3.5 ml, was applied in the subsequent purification.

4.2.21 Purification of 8H-SUMO and 6H-ubiquitin conjugates under denaturing conditions

With the lysate prepared by glass bead lysis as described above, a purification of 8H-SUMO and 6H-ubiquitin conjugates was performed with the IMAC (immobilized metal ion affinity chromatography) method. For this purpose, magnetic cobalt-coated beads were applied (PureCube Co-NTA MagBeads, Cube Biotech). All steps were performed at room temperature. For one purification, 100 µl slurry was pipetted into a 5 ml tube (Eppendorf) and, for equilibration, 5 ml lysis buffer (see above) were added to the slurry. A magnetic rack was used to concentrate the magnetic beads at the site of the tube and the supernatant was removed with a pipet tip attached to a pump. This equilibration step was repeated once. The glass bead lysate (~ 3.5 ml) was added to the magnetic beads, and this mixture rotated on a wheel at room temperature over night. On the following day, a magnetic rack was applied to the tube and first of all 100 µl sample were collected as unbound fraction and boiled in LLB, as described before. All of the remaining supernatant was removed, and 5 ml wash buffer (same as lysis buffer but pH 6.5, see section 4.2.20) were added. The sample rotated on a wheel for 5 minutes, and the magnetic rack was applied until the beads were collected on one side of the tube. The same washing step was repeated once and, subsequently, as a third washing step, only 1.5 ml wash buffer were added and the suspension was transferred to a 1.5 ml lo-bind tube (Eppendorf) by pouring. Again, the sample rotated for 5 minutes, was applied to the magnetic rack, and the supernatant was removed. After removal of the wash buffer, 110 µl elution buffer (8 M urea, 100 mM NaH_2PO_4, 10 mM Tris, 500 mM imidazole, pH 7) were added to the beads, and the sample rotated for 1 hour 45 minutes. Afterwards, the sample was centrifuged at 20000 rcf for 1 minute. The magnetic rack was applied and the eluate (120 µl including some remaining wash buffer) was added to 30 µl 5 x LLB. The sample was boiled as described previously. If more than 120 µl supernatant was in the tube (usually maximal 10 µl), the excess was discarded. To the liquid-free beads, 150 µl 1.5 x LLB were added, and the beads were boiled as described for the other samples. Samples were stored at -20°C. After this procedure, the purified 8H-tagged SUMO conjugates or 6H-tagged ubiquitin conjugates, as well as the respective free forms, were present in the eluate and in the boiled beads fractions, which were subsequently analyzed by SDS-PAGE and Western blotting. For evaluation of input levels and purification efficiency, often the previously taken fractions of input and unbound material were analyzed as well.

In the course of the study, the purification procedure was developed further, and the abovementioned protocol is the latest and preferred method for purification of His-tagged proteins under denaturing conditions. However, the results presented in chapter 2.3.1 were obtained with non-magnetic agarose beads and therefore a slightly different protocol. This experiment revealed that cobalt-coated beads

(TALON Metal Affinity Resin, Clontech/Takara) are much more suitable for purification of 8H-Smt3 than nickel-coated beads (Ni-NTA Superflow, Qiagen). The developed protocol can be applied if magnetic beads are not available. Due to the similarity to the protocol specified before, the method for denaturing purification with non-magnetic cobalt-beads is not described here separately but can be found in detail in the publication Pabst et al., 2019.

4.2.22 Purification of HA-tagged Dnm1 under native conditions

As an alternative to the previously described denaturing purification, for the detection of possibly modified Dnm1, Ulp-resistant SUMO variants were expressed as described above and Dnm1-2HA-6H was purified by agarose beads coated with HA (hemagglutinin) antibody (EZview Red Anti-HA Affinity Gel, Sigma-Aldrich). For the experiment presented in this study, a pellet size of 18 OD * ml was used. During the following procedure, the beads and protein lysate were kept cool, either in 4°C or on ice. For the pipetting of beads, a cut pipet tip was used. For one purification, 30 µl HA-beads slurry was pipetted into a lo-bind microcentrifuge tube (Eppendorf). For equilibration, 500 µl ice-cold native lysis buffer (50 mM Tris-Cl pH 7.4, 150 mM NaCl, 1 mM EDTA, 1% Triton, 1 x protease inhibitor (cOmplete, EDTA-free Protease Inhibitor Cocktail Tablets) were added to the beads and gently mixed. This mix was centrifuged at 100 rcf at 4°C for 1 minute. The supernatant was removed and the equilibration step repeated twice.

For the native glass bead lysis, a yeast pellet was taken from -80°C, placed on ice and immediately 600 µl ice-cold lysis buffer were added. The cells were resuspended and the suspension transferred to a 1.5 ml lo-bind tube. To this tube, 150 µl glass beads (425 – 600 µm) were added. The sample was vortexed in the cold room (4°C) 4 times for 1 minute with 1 minute pauses on ice in between. Afterwards, the sample was spun at 30000 rcf at 4°C for 20 minutes. From the supernatant, 20 µl were taken as input fraction, added to 5 µl 5 x LLB and boiled at 99°C for 5 minutes. After binding and the first wash, fractions were taken accordingly, therefore this is not mentioned separately.

The supernatant (~ 500 µl could be recovered), was added to 30 µl equilibrated HA-beads and the binding was allowed by rotating on a wheel at 4°C for 4 hours. After binding, the sample was spun with 100 rcf at 4°C for 1 minute. The sample was placed on ice for 4 minutes in order to allow all beads to settle. After removal of the supernatant, 1 ml ice-cold native wash buffer (50 mM Tris-Cl pH 7.4, 150 mM NaCl) was added. Instead of rotating, beads were equally distributed in the liquid by gently inverting the tube. The sample was spun with 100 rcf at 4°C for 1 minute and the supernatant was removed. The washing step was repeated twice and, between the second and the third wash step, the beads were carefully transferred

to a fresh lo-bind tube. After the third wash, in order to obtain maximal yield, no elution by peptide was performed but directly 60 µl 2 x LLB were added to the liquid-free beads. The sample was boiled at 99°C for 5 minutes and stored at -20°C.

4.2.23 SDS-PAGE

For the separation of protein samples according to the protein masses, an SDS-PAGE (sodium dodecyl sulfate polyacrylamide gel electrophoresis) was performed. Originally, this methods was developed by U. K. Laemmli (Laemmli, 1970). The recipes for resolving gel and stacking gel used for this study are listed below (***Table 4.19***). It has to be noted that the percentage of acrylamide was adjusted individually to the requirements for the respective experiment, which is specified in the figure legends. In general, gels with acrylamide concentrations ranging from 6% to 12% were used.

Resolving gel (exemplary for 8% acrylamide) (~ 15 ml, sufficient for two minigels)	
Component	**Volume**
1.5 M Tris, pH 8.8	3.75 ml
Acrylamide mix (30% acrylamide / 0.7% bisacrylamide)	4 ml
Water	6.85 ml
10% SDS (sodium dodecyl sulfate)	150 µl
TCE (2,2,2-trichloroethanol)	75 µl
10% APS (ammonium persulfate)	150 µl
TEMED (tetramethylethylenediamine)	30 µl
Stacking gel (10 ml, sufficient for two minigels)	
Component	**Volume**
1 M Tris, pH 6.8	1.25 ml
Acrylamide mix (30% acrylamide / 0.7% bisacrylamide)	1.3 ml
Water	7.23 ml
10% SDS	100 µl
10% APS	100 µl
TEMED (immediately before pouring)	20 µl

Table 4.19: Recipes for resolving and stacking gels

The components for the resolving gel were mixed and quickly pipetted between two glass plates with a space of usually 1 mm or 1.5 mm. Isopropanol was immediately added on top of the poured resolving gel in order to smooth the surface. After 15 minutes, the isopropanol was removed and the stacking gel was added. A comb with the desired number of wells was inserted and, after approximately 45 minutes, the gel was ready for use.

For minigels, the gel electrophoresis was carried out with the Mini-Protean 3 Cell system from Bio-Rad. The gel was placed in the running chamber and LRB (Laemmli running buffer: 25 mM Tris (pH 8.3), 192 mM glycine, 0.1% SDS) was filled into the inner chamber. The outer chamber was filled with LRB + 0.1 M sodium acetate. The samples and 2 -3 µl of a molecular weight marker (PageRuler Plus Prestained Protein Ladder, Thermo Fisher) were loaded into wells. If samples were previously frozen, they were boiled at 99°C for 5 minutes before loading. Typically, the electrophoresis was conducted at 120 V and 150 mA. The running time was chosen specifically for each experiment.

If a very fine separation of bands was desired, large gels (~ 14 cm x 14 cm) were cast and run with the Hoefer SE 600 series system. In this case, the electrophoresis was carried out with 300 V maximum (should not be reached) and 50 mA (should be constant).

After SDS-PAGE, the protein bands could be visualized due to the previously added TCE (Ladner et al., 2004). For this purpose, the protein gel was imaged in a gel documentation system with UV-light.

4.2.24 Western blot

With the Western blot method, proteins were transferred from the polyacrylamide gel to a membrane. For most of the experiments, proteins were transferred to a nitrocellulose membrane (0.2 µm pore size). For a minority of experiments, PVDF (polyvinylidene difluoride) membranes (0.45 µm pore size) were used. In the case of PVDF, the membrane was incubated in methanol for 5 minutes before use. Furthermore, two different methods for the Western blot were carried out. In the figure legends of the individual experiments, the specific method is noted.

One method applied for Western blotting was the semi-dry transfer with the Trans-Blot® SD Semi-Dry Transfer Cell (Bio-Rad). For this method, the gel, the nitrocellulose membrane and Whatman paper were soaked in standard transfer buffer (25 mM Tris, 192 mM glycine, 20% methanol) for 10 minutes. For each gel, two thick or four thin layers of Whatman paper were required. The sizes of the membrane and Whatman paper were chosen according to the gel size and depending on the decision if the stacking gel is blotted along with the resolving gel. The “transfer sandwich” was assembled as follows, from anode to cathode: one thick (or two thin) Whatman paper, membrane, polyacrylamide gel, one thick (or two thin) Whatman paper. The transfer was conducted at 25 V with variable electric current and duration. These parameters are noted in the figure legends.

An alternative method for the Western blot was the wet transfer. This could be carried out with the Mini-Protean 3 system from Bio-Rad for small gels or with the Hoefer SE 600 for large gels. In both cases, boric acid transfer buffer (50 mM boric acid, 10% methanol, pH 8.5) was used. The "transfer sandwich" was assembled as described above but with three Whatman papers per side and flanked by one sponge on each side. The setup was prepared in buffer, so that all components were wet. The cartridge with the "transfer sandwich" was closed and placed in the Western blot tank filled with boric acid transfer buffer. The settings for the transfer are noted in the figure legends. Usually, the transfer was run in the cold room.

4.2.24.1 Detection of proteins by fluorescent antibodies

Fluorophore-bearing antibodies were only applied in combination with a nitrocellulose membrane. The following steps were performed in a tray shaking on a rocking platform. After the transfer of proteins, the membrane was blocked with 4% milk in PBS for at least 20 minutes in order to prevent unspecific binding of antibodies. The blocking solution was removed and the primary antibody solution (4% milk in PBS with 0.03% NaN_3 + desired primary antibodies) was added. The membrane was incubated in the cold room overnight and the primary antibody solution was saved for reuse. The membrane was washed 4 times in PBS for 5 minutes each. Then, the secondary antibody solution (4% milk in PBS with NaN_3 + desired secondary antibodies with fluorophores) was added to the membrane, and the membrane was incubated for 1 hour protected from light. The secondary antibody solution was saved for reuse. Protected from light, the membrane was washed 4 times in PBS for 5 minutes each. After removal of the last washing solution, the membrane was analyzed by using a LI-COR Odyssey Imager. The detections were made at 700 nm (shown in red) and 800 nm (shown in green).

4.2.24.2 Detection of proteins by ECL

For detection of proteins by ECL (enhanced chemiluminescence), secondary antibodies coupled to POD (peroxidase) were applied. This was done for nitrocellulose as well as PVDF membranes and in principle works with both types. However, during optimization of Western blot conditions, it was noticed that this detection method, especially if a very sensitive ECL substrate was used, produces a strong background on PVDF membranes. Therefore, the experiments performed at later stages of this study were performed with nitrocellulose. After the transfer of proteins, the membrane was blocked with 4% milk in PBS for at least 20 minutes. The blocking solution was removed and the primary antibody solution (4% milk in PBS with NaN_3 + desired primary antibody) was added. The membrane was incubated in the cold room

overnight, and the primary antibody solution was saved for reuse. The membrane was washed 4 times in PBS for 5 minutes each. Then the secondary antibody solution (4% milk in PBS + desired secondary antibody coupled to POD) was added to the membrane and the membrane was incubated for 1 hour. The secondary antibody solution was removed, and the membrane was washed 4 times in PBS for 5 minutes each. After the last washing step, both solutions of the ECL substrate were mixed and spread on the membrane so that it had contact to all areas of the membrane. ECL substrates used were SuperSignal™ West Femto Maximum Sensitivity Substrate (Thermo Fisher), Clarity ECL Western Blotting Substrate (Bio-Rad) or self-made ECL substrate (solution I: 986 µl Tris-Cl (100 mM, pH 8.5), *p*-coumaric acid (90 mM), 10 µl luminol; solution II: 1 ml Tris-Cl, 0.6 µl H_2O_2), as indicated in the figure legends. Subsequently, the membrane was placed in a cassette and covered with an X-ray film (Fujifilm, Super RX-N). After the desired exposure time (ranging from a few seconds to overnight), the film was placed in a developing machine and, by virtue of developer and fixer, the bands became visible.

4.2.25 Coomassie Staining

The Coomassie staining for visualization of proteins in a polyacrylamide gel was performed by following a protocol optimized for staining before mass spectrometry, described under the name “Candiano Recipe” (Dyballa and Metzger, 2012). After SDS-PAGE, the gel was rinsed with milli-Q water and the gel was incubated in 12% TCA (trichloroacetic acid) at room temperature for 1 hour while shaking.

1 liter of the Coomassie solution (0.12% (w/v) CBB G-250 in 10% (w/v) ammonium sulfate, 10% (v/v) phosphoric acid, 20% (v/v) methanol) was prepared as follows. 200 ml sterile Milli-Q water were mixed with 118 ml 85% phosphoric acid. To this, 100 g ammonium sulfate were added and, after dissolving, 1.2 g CBB (Coomassie brilliant blue) G-250 were added. After stirring for 30 minutes, water was added until 800 ml were reached. Then 200 ml methanol were added and the Coomassie solution was ready to use.

The polyacrylamide gel was incubated in Coomassie solution at room temperature overnight while shaking. On the following day, the gel was transferred to a fresh tray and destaining was performed with 25% methanol for 2 hours with 7 exchanges of the methanol. The stained gel was photographed on a white light table.

4.2.26 Staining methods for membranes

For the general staining of proteins on a membrane, it was incubated in Ponceau S and destained with water.

An alternative staining method, which can be quantified with the LI-COR Odyssey Imager, was the REVERT Total Protein Stain from LI-COR. For this staining immediately after transfer and before blocking, the membrane was incubated in REVERT Total Protein Stain solution until the bands were visible in blue color. Then, the membrane was washed with wash solution (6.7% (v/v) glacial acetic acid, 30% (v/v) methanol in water) until excess staining was removed. The Total Protein Stain was imaged with the LI-COR Odyssey Imager in the 700 nm channel. After imaging, the staining was removed by incubation in removal solution (0.1% sodium hydroxide, 30% (v/v) methanol, in water) for 10 minutes.

4.2.27 Mass spectrometric analysis of SUMO substrates

In the following, the method for protein purification and mass spectrometric analysis of 8H-SUMO conjugates as presented in ***Figure 2.13*** is described. A pellet with a size of 2500 OD*ml was taken out of - 80°C, kept on ice and 10 ml lysis buffer (8 M urea, 100 mM NaH_2PO_4, 10 mM Tris, pH 8.0) were added. The pellet suspension was split into two samples in 50 ml tubes (~ 7.5 ml per sample including cells). Each of these samples contained 1250 OD*ml yeast in total. For both strains, *8H-SMT3::TRP1* and the congenic wildtype MB2, 2 pellets and therefore 4 individual pulldowns were prepared. To each sample, 3.5 ml glass beads were added, and the samples were vortexed 4 times for 1 minute at room temperature. The suspension was poured into centrifuge tubes for Beckman-Coulter Avanti J-20 XP. The sample was centrifuged at 30,000 rcf for 20 minutes.

In between, 150 µl magnetic cobalt-coated beads (PureCube Co-NTA MagBeads, Cube Biotech) were equilibrated by washing twice with 10 ml lysis buffer (for details of handling beads, see section 4.2.21). A fraction of the supernatant was collected and boiled for analytic purposes, and approximately 5 ml supernatant was added to the equilibrated beads. Additional 5 ml lysis buffer were added and the sample was rotated on a wheel overnight.

On the following day, the magnetic rack was applied to beads and first of all, an unbound fraction was collected and the remaining supernatant was removed with a pump. 5 ml wash buffer (8 M urea, 100 mM NaH_2PO_4, 10 mM Tris, pH 6.5) were added, and the beads were transferred to a 5 ml tube (Eppendorf). The beads were rotated on a wheel for 5 minutes, the magnetic rack was applied, and the supernatant was removed. The washing was repeated twice and, after the third washing step, beads were taken up in

200 µl digest buffer (6 M urea, 2 M thiourea, 10 mM HEPES, 5 mM DTT (added freshly), pH 8.0), and transferred to 1.5 ml lo-bind tubes. These were rotated on a wheel for 5 minutes, the magnetic rack was applied, and the supernatant was put aside.

150 µl digest buffer were added to the beads and the samples rotated for 1 hour at room temperature. Then, 11.8 µl 550 mM iodoacetamide was added to the sample, it was vortexed, and rotated on a wheel in the dark for 30 minutes. 1.62 µl LysC (0.5 µg/µl) were added to the sample, and rotation was conducted for 2 hours. Afterwards, the sample was diluted with 486 µl 50 mM ABC (ammonium bicarbonate) so that the (thio)urea concentration was 2 M. 1.62 µl trypsin (0.5 µg/µl) were added to the sample, which then rotated on a wheel overnight at room temperature.

On the following day, the sample was applied to the magnetic rack, and 550 µl sample were saved, corresponding to the actual digestion sample analyzed by mass spectrometry. 6 µl formic acid were added to the sample and it was spun at 380 rcf for 5 minutes to remove precipitated protein.

Stage tips containing 2 layers of SDS-RPS (styroldivinylbenzol - reversed phase sulfonate) were prepared and equilibrated as follows (taken from the protocol provided by the Krüger group, the centrifugation was carried out in Eppendorf 5810R and a rotor for spinning stage tips in boxes of pipet tips):

Buffer A: 0.1% formic acid in Milli-Q water
Buffer B: 80% acetonitrile, 0.1% formic acid

- 20 µL methanol were added to the stage tip and centrifuged at 2,600 rpm for 2 minutes
- 20 µL buffer B were added to the stage tip and centrifuged at 2,600 rpm for 2 minutes
- 20 µL buffer A were added to the stage tip and centrifugation at 2,600 rpm for 2 minutes
- 20 µL buffer A were added to the stage tip and centrifugation at 2,600 rpm for 30 seconds
- approximately 1-2 mm of buffer A should remain on top of the SDB-RPS material
- where required, 5 µl additional buffer A were added on top of SDB-RPS

Afterwards, 200 µl of sample was loaded onto the stage tips and centrifuged at 2600 rcf for 5 minutes. This step was repeated twice in order to load the complete digestion. Then, the stage tips were spun as follows (taken from the protocol provided by the Krüger group):

- stage tips were washed with 100 µl buffer A and centrifuged at 2,600 rpm for 3 minutes
- stage tips were washed with 100 µl buffer B and centrifuged at 2,600 rpm for 3 minutes
- stage tips were washed with 100 µl buffer B and centrifuged at 2,600 rpm for 3 minutes
- the stage tip was dried by blowing out liquid with a syringe
- the stage tips loaded with protein were stored at 4°C until immediately before the mass spectrometry run

The procedure for the previous mass spectrometry run (***Figure 2.12***) was similar to the one detailed above, but adjustments were made, so the main differences are summarized below (***Table 4.20***).

Figure 2.12	***Figure 2.13***
1 M NH_4HCO_3 in lysis buffer	no NH_4HCO_3 added in lysis buffer
non-magnetic cobalt beads (Takara/Clontech) (for handling of non-magnetic beads, see section 4.2.22)	magnetic cobalt beads (Cube Biotech)
2 ml slurry of beads	150 µl slurry of beads
separation of beads by centrifugation	separation of beads by magnet
digestion after elution with pH 4.3	digestion on beads

Table 4.20: Main differences of procedures between mass spectrometry shown in *Figures 2.12* and *2.13*

4.2.28 Identification of sumoylation sites by mass spectrometry

Denaturing protein purification:

For the purification of SUMO conjugates and subsequent identification of sumoylation sites, the SUMO variant 8H-Smt3-KallR-I96R was applied. Smt3-KallR served as a control. For the following procedure, pellet sizes of 2000 OD*ml were applied. Lysis buffer and wash buffer were the same as described in section 4.2.27. The pellet was taken out from the -80°C freezer, kept on ice, and 10 ml lysis buffer were added. The suspension (~15 ml) was distributed into 10 2-ml tubes. To each suspension of 1.5 ml, 500 µl glass beads (425 – 600 µm) were added. The samples were shaken with a Vibrax shaker at 2000 rpm and room temperature, 6 times for 1 minute, with 1 minute breaks in between. The samples were spun at 30,000 rcf for 20 minutes, and the supernatant of one experiment was collected in a single 15 ml tube. 125 µl slurry of magnetic cobalt beads (Cube Biotech) were pipetted into a 15 ml tube, and equilibrated as previously described. 10 ml of protein sample were added to equilibrated beads and rotated on a wheel at room temperature over night.

On the following day, samples were applied to the magnetic rack, and the supernatant was removed with a pump. 5 ml wash buffer were added and the beads were transferred into 5 ml tubes (Eppendorf). The samples were rotated on a wheel for 5 minutes. Samples were applied to the magnetic rack, and the supernatant was removed. The washing step was repeated 3 times. After the 4^{th} wash, 100 µl elution buffer (8 M urea, 100 mM Na_2HPO_4, 10 mM Tris, 500 mM imidazole, pH 8.0) were added and vortexed. The sample was spun at 3250 rcf for 5 minutes in order to collect the beads, and the complete sample at the bottom of the tube before this sample was transferred to a PCR tube. There, it was rotated on a wheel for 30 minutes and then applied to the magnetic rack. The supernatant (110 - 120 µl) was kept as “eluate”.

LysC digestion, SDS-PAGE and Coomassie staining:

To the sample, 0.6 µl 1 M DTT were added, and the sample rotated on a wheel for 1 hour. Then, 9.4 µl 550 mM iodoacetamide were added, the sample was vortexed, and rotated for 30 minutes in the dark. 1.25 µl LysC (0.5 µg/µl) were added, and the sample rotated on a wheel overnight. To 112.5 µl LysC-digestion, 28.1 µl 5 x LLB were added, and the samples were loaded on a large polyacrylamide gel. In the following, the Coomassie staining was carried out as described above.

In-gel tryptic digestion:

After staining over night, the staining solution was discarded, and destaining was performed as previously described. At this point, bands containing the LysC-resistant 8H-smt3-KallR-I96R variant were visible in the gel. This band and two regions with slightly larger molecular weight were cut out with a scalpel and saved in microcentrifuge tubes so that, per purification, three samples were obtained. As expected, for Smt3-KallR, no band was visible, therefore gel pieces at the corresponding positions were cut out. For a detailed description of the fractions, see results section 2.4.2. The gel pieces were stored in Milli-Q water at 4°C overnight. On the next day, it was proceeded with an in-gel digestion. For this purpose, each gel piece was cut into several smaller pieces and these pieces were collected in a 96 deepwell plate. Milli-Q water was added to cover the gel pieces. When this was carried out for all samples, the water was discarded, and 100 µl (200 µl for b3, see results) 50% acetonitrile were added. The deepwell plate was shaken for 15 minutes, and the solution was discarded. This washing step was repeated. 100 µl (200 µl for b3) acetonitrile were added, and the plate was shaken for 15 minutes. The solution was discarded afterwards.

For better destaining of the gel pieces, 100 µl 50 mM ammonium bicarbonate were added, and incubated for 5 minutes while shaking. The solution was discarded and 50% acetonitrile was added. Again, the samples were incubated for 5 minutes while shaking, and the solution was discarded. Afterwards, the same was done with 100% acetonitrile. This procedure (ammonium bicarbonate, 50% acetonitrile, 100% acetonitrile) was repeated twice. The gel pieces were dried in a speed vac concentrator for 5 minutes. Then, 100 µl trypsin solution (10 ng/µl in 50 mM ammonium bicarbonate) were added, and the gel pieces were allowed to take up the liquid for 30 minutes at 4°C. 50 mM ammonium bicarbonate was added to cover the gel pieces, and the samples were digested at 37°C overnight.

Extraction of peptides:

On the following day, the supernatant was transferred into a new 96 deepwell plate. The gel pieces were incubated in 100 µl 30% acetonitrile/3% trifluoroacetic acid for 20 minutes. The supernatant was added

to the previously transferred supernatant. Then, the gel pieces were incubated in 100 µl 100% trifluoroacetic acid for 20 minutes and, again, the supernatant was combined with the previously taken one. The so collected supernatant fractions contained the peptides for analysis. These samples were treated in a speed vac concentrator for 3 hours to remove organic solvents. Afterwards, the remaining sample volume was 100 µl – 200 µl, and 2 µl formic acid was added.

Sample purification and elution:

For sample collection and purification, the stage tip purification protocol was applied, essentially as previously described. The samples were stored in the stage tip membrane at 4°C until use. The elution of samples was performed by members of the Krüger group. For this purpose, peptides were eluted with 30 µl 1% ammonia in 60% acetonitrile. The samples were incubated in this solution for 15 minutes and eluted into a 96 well plate. Then, the samples were dried by a speed vac concentrator, resuspended in buffer for mass spectrometry ("buffer R from Krüger group") and transferred to a 96 well plate.

Analysis of peptides by mass spectrometry (this text was provided from the Krüger group):

Proteome samples were analyzed using a liquid chromatography tandem mass spectrometry on a Q-Exactive™ Plus Hybrid Quadrupole-Orbitrap™ (Thermo Fisher). Chromatographic peptide separation was achieved on PoroShell 120 packed 50 cm analytical columns coupled to an EASY-nLC 1000 HPLC system and a binary buffer system consisting of buffer A (0.1% FA (formic acid)) and buffer B (80% ACN (acetonitrile)/0.1% FA (formic acid)). Samples derived from the in-gel digestion were measured over a 60 minutes gradient, raising the content of buffer B from 13 to 48% over 35 minutes and from 48 to 75% over 5 minutes, and from 75% to 95% over 5 minutes. The column was washed with 95% buffer B for 5 minutes, then buffer B was reduced to 7% over 5 minutes and the column was re-equilibrated with 7% buffer B for 5 minutes. Full MS spectra (300–1,750 m/z) were recorded at a resolution (R) of 70,000, maximum injection time (max. IT) of 20 ms and AGC target of 3e6. The ten most abundant ion peptides in each full MS scan were selected for HCD fragmentation at nominal collisional energy (NCE) of 28. MS2 spectra were recorded at R = 35,000, a maximum IT of 120 ms and an AGC target of 5e5.

4.2.29 Accessibility of data and materials

The data presented in this study is stored on the Dohmen group internal server (\\sofs2.unikoeln.de\AG_Dohmen\Stefan Pabst Data storage). Detailed information on plasmids and yeast strains can be obtained from the group internal Filemaker database and for the most relevant plasmids from the group internal workspace on Benchling.

References

Albuquerque, C.P., Yeung, E., Ma, S., Fu, T., Corbett, K.D., and Zhou, H. (2015). A Chemical and Enzymatic Approach to Study Site-Specific Sumoylation. PLOS ONE *10*, e0143810.

Albuquerque, C.P. de, Liang, J., Gaut, N.J., and Zhou, H. (2016). Molecular Circuitry of the SUMO (Small Ubiquitin-like Modifier) Pathway in Controlling Sumoylation Homeostasis and Suppressing Genome Rearrangements. Journal of Biological Chemistry *291*, 8825–8835.

Albuquerque, C.P. de, Suhandynata, R.T., Carlson, C.R., Yuan, W.-T., and Zhou, H. (2018). Binding to small ubiquitin-like modifier and the nucleolar protein Csm1 regulates substrate specificity of the Ulp2 protease. Journal of Biological Chemistry *293*, 12105–12119.

Amerik, A.Y., and Hochstrasser, M. (2004). Mechanism and function of deubiquitinating enzymes. Biochimica et Biophysica Acta (BBA) - Molecular Cell Research *1695*, 189–207.

Amm, I., Sommer, T., and Wolf, D.H. (2014). Protein quality control and elimination of protein waste: The role of the ubiquitin–proteasome system. Biochimica et Biophysica Acta (BBA) - Molecular Cell Research *1843*, 182–196.

Anton, F., Dittmar, G., Langer, T., and Escobar-Henriques, M. (2013). Two deubiquitylases act on mitofusin and regulate mitochondrial fusion along independent pathways. Mol Cell *49*, 487–498.

Arbel, M., Bronstein, A., Sau, S., Liefshitz, B., and Kupiec, M. (2020). Access to PCNA by Srs2 and Elg1 Controls the Choice between Alternative Repair Pathways in Saccharomyces cerevisiae. MBio *11*.

Aufderheide, A., Beck, F., Stengel, F., Hartwig, M., Schweitzer, A., Pfeifer, G., Goldberg, A.L., Sakata, E., Baumeister, W., and Förster, F. (2015). Structural characterization of the interaction of Ubp6 with the 26S proteasome. PNAS *112*, 8626–8631.

Baczyk, D., Audette, M.C., Drewlo, S., Levytska, K., and Kingdom, J.C. (2017). SUMO-4: A novel functional candidate in the human placental protein SUMOylation machinery. PLOS ONE *12*, e0178056.

Bai, C., Sen, P., Hofmann, K., Ma, L., Goebl, M., Harper, J.W., and Elledge, S.J. (1996). SKP1 Connects Cell Cycle Regulators to the Ubiquitin Proteolysis Machinery through a Novel Motif, the F-Box. Cell *86*, 263–274.

Basaiawmoit, R.V., and Rattan, S.I.S. (2010). Cellular Stress and Protein Misfolding During Aging. In Protein Misfolding and Cellular Stress in Disease and Aging: Concepts and Protocols, P. Bross, and N. Gregersen, eds. (Totowa, NJ: Humana Press), pp. 107–117.

Bauer, S.L., Chen, J., and Åström, S.U. (2019). Helicase/SUMO-targeted ubiquitin ligase Uls1 interacts with the Holliday junction resolvase Yen1. PLOS ONE *14*, e0214102.

Bayer, P., Arndt, A., Metzger, S., Mahajan, R., Melchior, F., Jaenicke, R., and Becker, J. (1998). Structure determination of the small ubiquitin-related modifier SUMO-1. Journal of Molecular Biology *280*, 275–286.

Békés, M., Prudden, J., Srikumar, T., Raught, B., Boddy, M.N., and Salvesen, G.S. (2011). The dynamics and mechanism of SUMO chain deconjugation by SUMO-specific proteases. J Biol Chem *286*, 10238–10247.

Bencsath, K.P., Podgorski, M.S., Pagala, V.R., Slaughter, C.A., and Schulman, B.A. (2002). Identification of a Multifunctional Binding Site on Ubc9p Required for Smt3p Conjugation. Journal of Biological Chemistry *277*, 47938–47945.

Ben-Zvi, A., Miller, E.A., and Morimoto, R.I. (2009). Collapse of proteostasis represents an early molecular event in Caenorhabditis elegans aging. PNAS *106*, 14914–14919.

Bernhardt, D., Müller, M., Reichert, A.S., and Osiewacz, H.D. (2015). Simultaneous impairment of mitochondrial fission and fusion reduces mitophagy and shortens replicative lifespan. Sci Rep *5*, 7885.

Bernier-Villamor, V., Sampson, D.A., Matunis, M.J., and Lima, C.D. (2002). Structural Basis for E2-Mediated SUMO Conjugation Revealed by a Complex between Ubiquitin-Conjugating Enzyme Ubc9 and RanGAP1. Cell *108*, 345–356.

Berry, D.B., and Gasch, A.P. (2008). Stress-activated Genomic Expression Changes Serve a Preparative Role for Impending Stress in Yeast. Mol Biol Cell *19*, 4580–4587.

Bharathi, V., Girdhar, A., Prasad, A., Verma, M., Taneja, V., and Patel, B.K. (2016). Use of ade1 and ade2 mutations for development of a versatile red/white colour assay of amyloid-induced oxidative stress in saccharomyces cerevisiae. Yeast *33*, 607–620.

Bleazard, W., McCaffery, J.M., King, E.J., Bale, S., Mozdy, A., Tieu, Q., Nunnari, J., and Shaw, J.M. (1999). The dynamin-related GTPase Dnm1 regulates mitochondrial fission in yeast. Nat Cell Biol *1*, 298–304.

Bohren, K.M., Nadkarni, V., Song, J.H., Gabbay, K.H., and Owerbach, D. (2004). A M55V Polymorphism in a Novel SUMO Gene (SUMO-4) Differentially Activates Heat Shock Transcription Factors and Is Associated with Susceptibility to Type I Diabetes Mellitus. Journal of Biological Chemistry *279*, 27233–27238.

Brachmann, C.B., Davies, A., Cost, G.J., Caputo, E., Li, J., Hieter, P., and Boeke, J.D. (1998). Designer deletion strains derived from Saccharomyces cerevisiae S288C: A useful set of strains and plasmids for PCR-mediated gene disruption and other applications. Yeast *14*, 115–132.

Braschi, E., Zunino, R., and McBride, H.M. (2009). MAPL is a new mitochondrial SUMO E3 ligase that regulates mitochondrial fission. EMBO Rep *10*, 748–754.

Braun, R.J., and Westermann, B. (2011). Mitochondrial dynamics in yeast cell death and aging. Biochemical Society Transactions *39*, 1520–1526.

Britton, M., Lucas, M.M., Downey, S.L., Screen, M., Pletnev, A.A., Verdoes, M., Tokhunts, R.A., Amir, O., Goddard, A.L., Pelphrey, P.M., et al. (2009). Selective Inhibitor of Proteasome's Caspase-like Sites Sensitizes Cells to Specific Inhibition of Chymotrypsin-like Sites. Chemistry & Biology *16*, 1278–1289.

Bylebyl, G.R., Belichenko, I., and Johnson, E.S. (2003). The SUMO Isopeptidase Ulp2 Prevents Accumulation of SUMO Chains in Yeast. J. Biol. Chem. *278*, 44113–44120.

Cagnac, O., Leterrier, M., Yeager, M., and Blumwald, E. (2007). Identification and Characterization of Vnx1p, a Novel Type of Vacuolar Monovalent Cation/H+ Antiporter of Saccharomyces cerevisiae. Journal of Biological Chemistry *282*, 24284–24293.

Cagnac, O., Baghour, M., Jaime-Pérez, N., Aranda-Sicilia, M.N., Sánchez-Romero, M.E., Rodríguez-Rosales, M.P., and Venema, K. (2020). Deletion of the N-terminal domain of the yeast vacuolar (Na+,K+)/H+ antiporter Vnx1p improves salt tolerance in yeast and transgenic Arabidopsis. Yeast *37*, 173–185.

Chen, X.L., Reindle, A., and Johnson, E.S. (2005). Misregulation of 2µm Circle Copy Number in a SUMO Pathway Mutant. Molecular and Cellular Biology *25*, 4311–4320.

Cheng, C.-H., Lo, Y.-H., Liang, S.-S., Ti, S.-C., Lin, F.-M., Yeh, C.-H., Huang, H.-Y., and Wang, T.-F. (2006). SUMO modifications control assembly of synaptonemal complex and polycomplex in meiosis of Saccharomyces cerevisiae. Genes Dev. *20*, 2067–2081.

Cheng, J., Kang, X., Zhang, S., and Yeh, E.T.H. (2007). SUMO-Specific Protease 1 Is Essential for Stabilization of HIF1α during Hypoxia. Cell *131*, 584–595.

Cogliati, S., Frezza, C., Soriano, M.E., Varanita, T., Quintana-Cabrera, R., Corrado, M., Cipolat, S., Costa, V., Casarin, A., Gomes, L.C., et al. (2013). Mitochondrial Cristae Shape Determines Respiratory Chain Supercomplexes Assembly and Respiratory Efficiency. Cell *155*, 160–171.

Cohen, M.M., Amiott, E.A., Day, A.R., Leboucher, G.P., Pryce, E.N., Glickman, M.H., McCaffery, J.M., Shaw, J.M., and Weissman, A.M. (2011). Sequential requirements for the GTPase domain of the mitofusin Fzo1 and the ubiquitin ligase SCFMdm30 in mitochondrial outer membrane fusion. Journal of Cell Science *124*, 1403–1410.

Collins, G.A., Gomez, T.A., Deshaies, R.J., and Tansey, W.P. (2010). Combined chemical and genetic approach to inhibit proteolysis by the proteasome. Yeast *27*, 965–974.

Contamine, V., and Picard, M. (2000). Maintenance and Integrity of the Mitochondrial Genome: a Plethora of Nuclear Genes in the Budding Yeast. Microbiol Mol Biol Rev *64*, 281–315.

Cox, E., Hwang, W., Uzoma, I., Hu, J., Guzzo, C.M., Jeong, J., Matunis, M.J., Qian, J., Zhu, H., and Blackshaw, S. (2017). Global Analysis of SUMO-Binding Proteins Identifies SUMOylation as a Key Regulator of the INO80 Chromatin Remodeling Complex. Molecular & Cellular Proteomics *16*, 812–823.

Denison, C., Rudner, A.D., Gerber, S.A., Bakalarski, C.E., Moazed, D., and Gygi, S.P. (2005). A Proteomic Strategy for Gaining Insights into Protein Sumoylation in Yeast. Molecular & Cellular Proteomics *4*, 246–254.

Desai, N., Brown, A., Amunts, A., and Ramakrishnan, V. (2017). The structure of the yeast mitochondrial ribosome. Science *355*, 528–531.

Desterro, J.M.P., Rodriguez, M.S., and Hay, R.T. (1998). SUMO-1 Modification of IκBα Inhibits NF-κB Activation. Molecular Cell *2*, 233–239.

Dhingra, N., and Zhao, X. (2017). A guide for targeted SUMO removal. Genes Dev *31*, 719–720.

Dieckhoff, P., Bolte, M., Sancak, Y., Braus, G.H., and Irniger, S. (2004). Smt3/SUMO and Ubc9 are required for efficient APC/C-mediated proteolysis in budding yeast. Molecular Microbiology *51*, 1375–1387.

Dohmen, R.J., Stappen, R., McGrath, J.P., Forrová, H., Kolarov, J., Goffeau, A., and Varshavsky, A. (1995). An Essential Yeast Gene Encoding a Homolog of Ubiquitin-activating Enzyme. Journal of Biological Chemistry *270*, 18099–18109.

Dolezal, P., Likic, V., Tachezy, J., and Lithgow, T. (2006). Evolution of the Molecular Machines for Protein Import into Mitochondria. Science *313*, 314–318.

Döring, Lennard-Maximilian (2017). Insights into substrate recognition by SUMO-targeted ubiquitin ligases in *S. cerevisiae*. Master Thesis, University of Cologne.

Dunn, C.D., Lee, M.S., Spencer, F.A., and Jensen, R.E. (2006). A Genomewide Screen for Petite-negative Yeast Strains Yields a New Subunit of the i-AAA Protease Complex. MBoC *17*, 213–226.

Dyballa, N., and Metzger, S. (2012). Fast and Sensitive Coomassie Staining in Quantitative Proteomics. In Quantitative Methods in Proteomics, K. Marcus, ed. (Totowa, NJ: Humana Press), pp. 47–59.

Eckhoff, J., and Dohmen, R.J. (2015). In Vitro Studies Reveal a Sequential Mode of Chain Processing by the Yeast SUMO (Small Ubiquitin-related Modifier)-specific Protease Ulp2. J Biol Chem *290*, 12268–12281.

Eddins, M.J., Varadan, R., Fushman, D., Pickart, C.M., and Wolberger, C. (2007). Crystal Structure and Solution NMR Studies of Lys48-linked Tetraubiquitin at Neutral pH. Journal of Molecular Biology *367*, 204–211.

Eifler, K., and Vertegaal, A.C.O. (2015). SUMOylation-mediated regulation of cell cycle progression and cancer. Trends Biochem Sci *40*, 779–793.

Elmore, Z.C., Donaher, M., Matson, B.C., Murphy, H., Westerbeck, J.W., and Kerscher, O. (2011). Sumo-dependent substrate targeting of the SUMO protease Ulp1. BMC Biology *9*, 74.

Endo, T., and Yamano, K. (2009). Multiple pathways for mitochondrial protein traffic. *390*, 723–730.

Escobar-Henriques, M., Westermann, B., and Langer, T. (2006). Regulation of mitochondrial fusion by the F-box protein Mdm30 involves proteasome-independent turnover of Fzo1. Journal of Cell Biology *173*, 645–650.

Esteras, M., Liu, I.-C., Snijders, A.P., Jarmuz, A., and Aragon, L. (2017). Identification of SUMO conjugation sites in the budding yeast proteome. Microbial Cell *4*, 331–341.

Faden, F., Ramezani, T., Mielke, S., Almudi, I., Nairz, K., Froehlich, M.S., Höckendorff, J., Brandt, W., Hoehenwarter, W., Dohmen, R.J., et al. (2016). Phenotypes on demand via switchable target protein degradation in multicellular organisms. Nat Commun *7*, 12202.

Fang, N.N., Ng, A.H.M., Measday, V., and Mayor, T. (2011). Hul5 HECT ubiquitin ligase plays a major role in the ubiquitylation and turnover of cytosolic misfolded proteins. Nature Cell Biology *13*, 1344–1352.

Fannjiang, Y., Cheng, W.-C., Lee, S.J., Qi, B., Pevsner, J., McCaffery, J.M., Hill, R.B., Basañez, G., and Hardwick, J.M. (2004). Mitochondrial fission proteins regulate programmed cell death in yeast. Genes Dev *18*, 2785–2797.

Ficarro, S.B., McCleland, M.L., Stukenberg, P.T., Burke, D.J., Ross, M.M., Shabanowitz, J., Hunt, D.F., and White, F.M. (2002). Phosphoproteome analysis by mass spectrometry and its application to Saccharomyces cerevisiae. Nature Biotechnology *20*, 301–305.

Finley, D., Özkaynak, E., and Varshavsky, A. (1987). The yeast polyubiquitin gene is essential for resistance to high temperatures, starvation, and other stresses. Cell *48*, 1035–1046.

Finley, D., Bartel, B., and Varshavsky, A. (1989). The tails of ubiquitin precursors are ribosomal proteins whose fusion to ubiquitin facilitates ribosome biogenesis. Nature *338*, 394–401.

Finley, D., Ulrich, H.D., Sommer, T., and Kaiser, P. (2012). The Ubiquitin–Proteasome System of Saccharomyces cerevisiae. Genetics *192*, 319–360.

Fisk, H.A., and Yaffe, M.P. (1999). A Role for Ubiquitination in Mitochondrial Inheritance in Saccharomyces cerevisiae. Journal of Cell Biology *145*, 1199–1208.

Flaus, A., and Owen-Hughes, T. (2011). Mechanisms for ATP-dependent chromatin remodelling: the means to the end. The FEBS Journal *278*, 3579–3595.

Fleming, J.A., Lightcap, E.S., Sadis, S., Thoroddsen, V., Bulawa, C.E., and Blackman, R.K. (2002). Complementary whole-genome technologies reveal the cellular response to proteasome inhibition by PS-341. Proc Natl Acad Sci U S A *99*, 1461–1466.

Foury, F. (1989). Cloning and Sequencing of the Nuclear Gene MIP1 Encoding the Catalytic Subunit of the Yeast Mitochondrial DNA Polymerase. Journal of Biological Chemistry *264*, 20552–20560.

Fritz, S., Weinbach, N., and Westermann, B. (2003). Mdm30 Is an F-Box Protein Required for Maintenance of Fusion-competent Mitochondria in Yeast. MBoC *14*, 2303–2313.

Furukawa, K., Mizushima, N., Noda, T., and Ohsumi, Y. (2000). A Protein Conjugation System in Yeast with Homology to Biosynthetic Enzyme Reaction of Prokaryotes. Journal of Biological Chemistry *275*, 7462–7465.

Garcia-Dominguez, M., and Reyes, J.C. (2009). SUMO association with repressor complexes, emerging routes for transcriptional control. Biochimica et Biophysica Acta (BBA) - Gene Regulatory Mechanisms *1789*, 451–459.

Gareau, J.R., and Lima, C.D. (2010). The SUMO pathway: emerging mechanisms that shape specificity, conjugation and recognition. Nat Rev Mol Cell Biol *11*, 861–871.

Gietz, R.D., and Sugino, A. (1988). New yeast-Escherichia coli shuttle vectors constructed with in vitro mutagenized yeast genes lacking six-base pair restriction sites. Gene *74*, 527–534.

Gietz, R.D., and Woods, R.A. (2002). Transformation of yeast by lithium acetate/single-stranded carrier DNA/polyethylene glycol method. In Methods in Enzymology, C. Guthrie, and G.R. Fink, eds. (Academic Press), pp. 87–96.

Gillies, J., Hickey, C.M., Su, D., Wu, Z., Peng, J., and Hochstrasser, M. (2016). SUMO Pathway Modulation of Regulatory Protein Binding at the Ribosomal DNA Locus in Saccharomyces cerevisiae. Genetics *202*, 1377–1394.

Girardini, M., Maniaci, C., Hughes, S.J., Testa, A., and Ciulli, A. (2019). Cereblon versus VHL: Hijacking E3 ligases against each other using PROTACs. Bioorganic & Medicinal Chemistry *27*, 2466–2479.

Glotzer, M., Murray, A.W., and Kirschner, M.W. (1991). Cyclin is degraded by the ubiquitin pathway. Nature *349*, 132–138.

Gray, M.W., Burger, G., and Lang, B.F. (1999). Mitochondrial Evolution. Science *283*, 1476–1481.

Groll, M., Heinemeyer, W., Jäger, S., Ullrich, T., Bochtler, M., Wolf, D.H., and Huber, R. (1999). The catalytic sites of 20S proteasomes and their role in subunit maturation: A mutational and crystallographic study. PNAS *96*, 10976–10983.

Grou, C.P., Pinto, M.P., Mendes, A.V., Domingues, P., and Azevedo, J.E. (2015). The de novo synthesis of ubiquitin: identification of deubiquitinases acting on ubiquitin precursors. Sci Rep *5*, 12836.

Gundogdu, M., and Walden, H. (2019). Structural basis of generic versus specific E2–RING E3 interactions in protein ubiquitination. Protein Science *28*, 1758–1770.

Guo, C., Hildick, K.L., Luo, J., Dearden, L., Wilkinson, K.A., and Henley, J.M. (2013). SENP3-mediated deSUMOylation of dynamin-related protein 1 promotes cell death following ischaemia. The EMBO Journal *32*, 1514–1528.

Guterman, A., and Glickman, M.H. (2004). Complementary Roles for Rpn11 and Ubp6 in Deubiquitination and Proteolysis by the Proteasome. Journal of Biological Chemistry *279*, 1729–1738.

Haglund, K., Sigismund, S., Polo, S., Szymkiewicz, I., Di Fiore, P.P., and Dikic, I. (2003). Multiple monoubiquitination of RTKs is sufficient for their endocytosis and degradation. Nat Cell Biol *5*, 461–466.

Hammermeister, M., Schödel, K., and Westermann, B. (2010). Mdm36 Is a Mitochondrial Fission-promoting Protein in Saccharomyces cerevisiae. MBoC *21*, 2443–2452.

Hannich, J.T., Lewis, A., Kroetz, M.B., Li, S.-J., Heide, H., Emili, A., and Hochstrasser, M. (2005). Defining the SUMO-modified Proteome by Multiple Approaches in Saccharomyces cerevisiae. Journal of Biological Chemistry *280*, 4102–4110.

Harder, Z., Zunino, R., and McBride, H. (2004). Sumo1 conjugates mitochondrial substrates and participates in mitochondrial fission. Curr Biol *14*, 340–345.

Heinemeyer, W., Fischer, M., Krimmer, T., Stachon, U., and Wolf, D.H. (1997). The Active Sites of the Eukaryotic 20 S Proteasome and Their Involvement in Subunit Precursor Processing. Journal of Biological Chemistry *272*, 25200–25209.

Hermann, G.J., Thatcher, J.W., Mills, J.P., Hales, K.G., Fuller, M.T., Nunnari, J., and Shaw, J.M. (1998). Mitochondrial Fusion in Yeast Requires the Transmembrane GTPase Fzo1p. J Cell Biol *143*, 359–373.

Hickey, C.M., Wilson, N.R., and Hochstrasser, M. (2012). Function and regulation of SUMO proteases. Nat Rev Mol Cell Biol *13*, 755–766.

Ho, C.-W., Chen, H.-T., and Hwang, J. (2011). UBC9 Autosumoylation Negatively Regulates Sumoylation of Septins in Saccharomyces cerevisiae. J Biol Chem *286*, 21826–21834.

Hochstrasser, M. (1996). Ubiquitin-Dependent Protein Degradation. Annual Review of Genetics *30*, 405–439.

Hoege, C., Pfander, B., Moldovan, G.-L., Pyrowolakis, G., and Jentsch, S. (2002). RAD6-dependent DNA repair is linked to modification of PCNA by ubiquitin and SUMO. Nature *419*, 135–141.

Höpfler, M., Kern, M.J., Straub, T., Prytuliak, R., Habermann, B.H., Pfander, B., and Jentsch, S. (2019). Slx5/Slx8-dependent ubiquitin hotspots on chromatin contribute to stress tolerance. EMBO J *38*, e100368.

Horigome, C., Bustard, D.E., Marcomini, I., Delgoshaie, N., Tsai-Pflugfelder, M., Cobb, J.A., and Gasser, S.M. (2016). PolySUMOylation by Siz2 and Mms21 triggers relocation of DNA breaks to nuclear pores through the Slx5/Slx8 STUbL. Genes Dev. *30*, 931–945.

Huang, C.-J., Lu, M.-Y., Chang, Y.-W., and Li, W.-H. (2018). Experimental Evolution of Yeast for High-Temperature Tolerance. Molecular Biology and Evolution *35*, 1823–1839.

Huang, J., Brito, I.L., Villén, J., Gygi, S.P., Amon, A., and Moazed, D. (2006). Inhibition of homologous recombination by a cohesin-associated clamp complex recruited to the rDNA recombination enhancer. Genes Dev. *20*, 2887–2901.

Huibregtse, J.M., Scheffner, M., Beaudenon, S., and Howley, P.M. (1995). A family of proteins structurally and functionally related to the E6-AP ubiquitin-protein ligase. PNAS *92*, 2563–2567.

Ichimura, Y., Kirisako, T., Takao, T., Satomi, Y., Shimonishi, Y., Ishihara, N., Mizushima, N., Tanida, I., Kominami, E., Ohsumi, M., et al. (2000). A ubiquitin-like system mediates protein lipidation. Nature *408*, 488–492.

Ii, T., Mullen, J.R., Slagle, C.E., and Brill, S.J. (2007). Stimulation of in vitro sumoylation by Slx5–Slx8: Evidence for a functional interaction with the SUMO pathway. DNA Repair *6*, 1679–1691.

Jalal, D., Chalissery, J., and Hassan, A.H. (2017). Genome maintenance in Saccharomyces cerevisiae: the role of SUMO and SUMO-targeted ubiquitin ligases. Nucleic Acids Research *45*, 2242–2261.

Janke, C., Magiera, M.M., Rathfelder, N., Taxis, C., Reber, S., Maekawa, H., Moreno-Borchart, A., Doenges, G., Schwob, E., Schiebel, E., et al. (2004). A versatile toolbox for PCR-based tagging of yeast genes: new fluorescent proteins, more markers and promoter substitution cassettes. Yeast *21*, 947–962.

Jia, Y., Claessens, L.A., Vertegaal, A.C.O., and Ovaa, H. (2019). Chemical Tools and Biochemical Assays for SUMO Specific Proteases (SENPs). ACS Chem. Biol. *14*, 2389–2395.

Joazeiro, C.A.P., and Weissman, A.M. (2000). RING Finger Proteins: Mediators of Ubiquitin Ligase Activity. Cell *102*, 549–552.

Johnson, E.S. (2004). Protein Modification by SUMO. Annu. Rev. Biochem. *73*, 355–382.

Johnson, E.S., and Blobel, G. (1997). Ubc9p Is the Conjugating Enzyme for the Ubiquitin-like Protein Smt3p. Journal of Biological Chemistry *272*, 26799–26802.

Johnson, E.S., and Blobel, G. (1999). Cell cycle-regulated attachment of the ubiquitin-related protein SUMO to the yeast septins. J Cell Biol *147*, 981–994.

Johnson, E.S., and Gupta, A.A. (2001). An E3-like Factor that Promotes SUMO Conjugation to the Yeast Septins. Cell *106*, 735–744.

Johnson, E.S., Schwienhorst, I., Dohmen, R.J., and Blobel, G. (1997). The ubiquitin-like protein Smt3p is activated for conjugation to other proteins by an Aos1p/Uba2p heterodimer. EMBO J *16*, 5509–5519.

Johnston, M., Flick, J.S., and Pexton, T. (1994). Multiple mechanisms provide rapid and stringent glucose repression of GAL gene expression in Saccharomyces cerevisiae. Mol Cell Biol *14*, 3834–3841.

Jürgen Dohmen, R. (2004). SUMO protein modification. Biochimica et Biophysica Acta (BBA) - Molecular Cell Research *1695*, 113–131.

Kaeberlein, M., and Guarente, L. (2002). Saccharomyces cerevisiae MPT5 and SSD1 function in parallel pathways to promote cell wall integrity. Genetics *160*, 83–95.

Keiten-Schmitz, J., Schunck, K., and Müller, S. (2020). SUMO Chains Rule on Chromatin Occupancy. Front. Cell Dev. Biol. *0*.

Kennedy, B.K., Gotta, M., Sinclair, D.A., Mills, K., McNabb, D.S., Murthy, M., Pak, S.M., Laroche, T., Gasser, S.M., and Guarente, L. (1997). Redistribution of Silencing Proteins from Telomeres to the Nucleolus Is Associated with Extension of Life Span in S. cerevisiae. Cell *89*, 381–391.

Kirisako, T., Kamei, K., Murata, S., Kato, M., Fukumoto, H., Kanie, M., Sano, S., Tokunaga, F., Tanaka, K., and Iwai, K. (2006). A ubiquitin ligase complex assembles linear polyubiquitin chains. The EMBO Journal *25*, 4877–4887.

Kispal, G., Sipos, K., Lange, H., Fekete, Z., Bedekovics, T., Janáky, T., Bassler, J., Aguilar Netz, D.J., Balk, J., Rotte, C., et al. (2005). Biogenesis of cytosolic ribosomes requires the essential iron–sulphur protein Rli1p and mitochondria. EMBO J *24*, 589–598.

Kisselev, A.F., van der Linden, W.A., and Overkleeft, H.S. (2012). Proteasome Inhibitors: An Expanding Army Attacking a Unique Target. Chemistry & Biology *19*, 99–115.

Kitagaki, H., Araki, Y., Funato, K., and Shimoi, H. (2007). Ethanol-induced death in yeast exhibits features of apoptosis mediated by mitochondrial fission pathway. FEBS Letters *581*, 2935–2942.

Klecker, T., Wemmer, M., Haag, M., Weig, A., Böckler, S., Langer, T., Nunnari, J., and Westermann, B. (2015). Interaction of MDM33 with mitochondrial inner membrane homeostasis pathways in yeast. Sci Rep *5*, 18344.

Klug, H., Xaver, M., Chaugule, V.K., Koidl, S., Mittler, G., Klein, F., and Pichler, A. (2013). Ubc9 Sumoylation Controls SUMO Chain Formation and Meiotic Synapsis in Saccharomyces cerevisiae. Molecular Cell *50*, 625–636.

Knipscheer, P., van Dijk, W.J., Olsen, J.V., Mann, M., and Sixma, T.K. (2007). Noncovalent interaction between Ubc9 and SUMO promotes SUMO chain formation. EMBO J *26*, 2797–2807.

Kocaturk, N.M., and Gozuacik, D. (2018). Crosstalk Between Mammalian Autophagy and the Ubiquitin-Proteasome System. Front. Cell Dev. Biol. *0*.

Komander, D., and Rape, M. (2012). The Ubiquitin Code. Annu. Rev. Biochem. *81*, 203–229.

Koyuncu, S., Loureiro, R., Lee, H.J., Wagle, P., Krueger, M., and Vilchez, D. (2021). Rewiring of the ubiquitinated proteome determines ageing in C. elegans. Nature *596*, 285–290.

Kroetz, M.B., Su, D., and Hochstrasser, M. (2009). Essential Role of Nuclear Localization for Yeast Ulp2 SUMO Protease Function. MBoC *20*, 2196–2206.

Krumova, P., Meulmeester, E., Garrido, M., Tirard, M., Hsiao, H.-H., Bossis, G., Urlaub, H., Zweckstetter, M., Kügler, S., Melchior, F., et al. (2011). Sumoylation inhibits α-synuclein aggregation and toxicity. J Cell Biol *194*, 49–60.

Labbadia, J., and Morimoto, R.I. (2013). Huntington's disease: underlying molecular mechanisms and emerging concepts. Trends in Biochemical Sciences *38*, 378–385.

Ladner, C.L., Yang, J., Turner, R.J., and Edwards, R.A. (2004). Visible fluorescent detection of proteins in polyacrylamide gels without staining. Analytical Biochemistry *326*, 13–20.

Laemmli, U.K. (1970). Cleavage of Structural Proteins during the Assembly of the Head of Bacteriophage T4. Nature *227*, 680–685.

Lai-Zhang, J., Xiao, Y., and Mueller, D.M. (1999). Epistatic interactions of deletion mutants in the genes encoding the F1-ATPase in yeast Saccharomyces cerevisiae. The EMBO Journal *18*, 58–64.

Lallemand-Breitenbach, V., Jeanne, M., Benhenda, S., Nasr, R., Lei, M., Peres, L., Zhou, J., Zhu, J., Raught, B., and de Thé, H. (2008). Arsenic degrades PML or PML–RARα through a SUMO-triggered RNF4/ubiquitin-mediated pathway. Nat Cell Biol *10*, 547–555.

Lammer, D., Mathias, N., Laplaza, J.M., Jiang, W., Liu, Y., Callis, J., Goebl, M., and Estelle, M. (1998). Modification of yeast Cdc53p by the ubiquitin-related protein Rub1p affects function of the SCFCdc4 complex. Genes Dev. *12*, 914–926.

Lamoliatte, F., McManus, F.P., Maarifi, G., Chelbi-Alix, M.K., and Thibault, P. (2017). Uncovering the SUMOylation and ubiquitylation crosstalk in human cells using sequential peptide immunopurification. Nature Communications *8*, 14109.

Laporte, D., Salin, B., Daignan-Fornier, B., and Sagot, I. (2008). Reversible cytoplasmic localization of the proteasome in quiescent yeast cells. J Cell Biol *181*, 737–745.

Lecker, S.H., Goldberg, A.L., and Mitch, W.E. (2006). Protein Degradation by the Ubiquitin–Proteasome Pathway in Normal and Disease States. JASN *17*, 1807–1819.

Lee, D.H., and Goldberg, A.L. (1996). Selective Inhibitors of the Proteasome-dependent and Vacuolar Pathways of Protein Degradation in Saccharomyces cerevisiae. J. Biol. Chem. *271*, 27280–27284.

Lee, D.H., and Goldberg, A.L. (1998). Proteasome inhibitors: valuable new tools for cell biologists. Trends in Cell Biology *8*, 397–403.

Lee, M.W., Lee, E.Y., Lai, G.H., Kennedy, N.W., Posey, A.E., Xian, W., Ferguson, A.L., Hill, R.B., and Wong, G.C.L. (2017). Molecular Motor Dnm1 Synergistically Induces Membrane Curvature To Facilitate Mitochondrial Fission. ACS Cent Sci *3*, 1156–1167.

Lehtonen, Š., Sonninen, T.-M., Wojciechowski, S., Goldsteins, G., and Koistinaho, J. (2019). Dysfunction of Cellular Proteostasis in Parkinson's Disease. Front Neurosci *13*, 457.

Li, S.-J., and Hochstrasser, M. (1999). A new protease required for cell-cycle progression in yeast. Nature *398*, 246–251.

Liang, J., Singh, N., Carlson, C.R., Albuquerque, C.P., Corbett, K.D., and Zhou, H. (2017). Recruitment of a SUMO isopeptidase to rDNA stabilizes silencing complexes by opposing SUMO targeted ubiquitin ligase activity. Genes Dev *31*, 802–815.

Liang, Y.-C., Lee, C.-C., Yao, Y.-L., Lai, C.-C., Schmitz, M.L., and Yang, W.-M. (2016). SUMO5, a Novel Poly-SUMO Isoform, Regulates PML Nuclear Bodies. Sci Rep *6*, 26509.

Liao, P.-C., Boldogh, I.R., Siegmund, S.E., Freyberg, Z., and Pon, L.A. (2018). Isolation of mitochondria from Saccharomyces cerevisiae using magnetic bead affinity purification. PLOS ONE *13*, e0196632.

Liew, C.W., Sun, H., Hunter, T., and Day, C.L. (2010). RING DOMAIN DIMERIZATION IS ESSENTIAL FOR RNF4 FUNCTION. Biochem J *431*, 23–29.

Lin, D., Tatham, M.H., Yu, B., Kim, S., Hay, R.T., and Chen, Y. (2002). Identification of a Substrate Recognition Site on Ubc9. Journal of Biological Chemistry *277*, 21740–21748.

Liu, X., Yin, Y., Wu, J., and Liu, Z. (2014). Structure and mechanism of an intramembrane liponucleotide synthetase central for phospholipid biosynthesis. Nature Communications *5*, 4244.

Lohr, D., Venkov, P., and Zlatanova, J. (1995). Transcriptional regulation in the yeast GAL gene family: a complex genetic network. The FASEB Journal *9*, 777–787.

London, M.K., Keck, B.I., Ramos, P.C., and Dohmen, R.J. (2004). Regulatory mechanisms controlling biogenesis of ubiquitin and the proteasome. FEBS Letters *567*, 259–264.

MacGilvray, M.E., Shishkova, E., Place, M., Wagner, E.R., Coon, J.J., and Gasch, A.P. (2020). The phosphoproteome response to dithiothreitol reveals unique versus shared features of Saccharomyces cerevisiae stress responses. J Proteome Res *19*, 3405–3417.

Mahajan, R., Delphin, C., Guan, T., Gerace, L., and Melchior, F. (1997). A Small Ubiquitin-Related Polypeptide Involved in Targeting RanGAP1 to Nuclear Pore Complex Protein RanBP2. Cell *88*, 97–107.

Makhnevych, T., Ptak, C., Lusk, C.P., Aitchison, J.D., and Wozniak, R.W. (2007). The role of karyopherins in the regulated sumoylation of septins. J Cell Biol *177*, 39–49.

Maleszka, R., Skelly, P.J., and Clark-Walker, G.D. (1991). Rolling circle replication of DNA in yeast mitochondria. EMBO J *10*, 3923–3929.

Malina, C., Larsson, C., and Nielsen, J. (2018). Yeast mitochondria: an overview of mitochondrial biology and the potential of mitochondrial systems biology. FEMS Yeast Research *18*.

Marques, A.J., Palanimurugan, R., Matias, A.C., Ramos, P.C., and Dohmen, R.J. (2009). Catalytic Mechanism and Assembly of the Proteasome. Chem. Rev. *109*, 1509–1536.

Matic, I., van Hagen, M., Schimmel, J., Macek, B., Ogg, S.C., Tatham, M.H., Hay, R.T., Lamond, A.I., Mann, M., and Vertegaal, A.C.O. (2008). In Vivo Identification of Human Small Ubiquitin-like Modifier Polymerization Sites by High Accuracy Mass Spectrometry and an in Vitro to in Vivo Strategy. Molecular & Cellular Proteomics *7*, 132–144.

Matunis, M.J., Coutavas, E., and Blobel, G. (1996). A novel ubiquitin-like modification modulates the partitioning of the Ran-GTPase-activating protein RanGAP1 between the cytosol and the nuclear pore complex. Journal of Cell Biology *135*, 1457–1470.

McDowell, G.S., and Philpott, A. (2013). Non-canonical ubiquitylation: Mechanisms and consequences. The International Journal of Biochemistry & Cell Biology *45*, 1833–1842.

McGrath, J.P., Jentsch, S., and Varshavsky, A. (1991). UBA 1: an essential yeast gene encoding ubiquitin-activating enzyme. EMBO J *10*, 227–236.

Mears, J.A., Lackner, L.L., Fang, S., Ingerman, E., Nunnari, J., and Hinshaw, J.E. (2011). Conformational changes in Dnm1 support a contractile mechanism for mitochondrial fission. Nat Struct Mol Biol *18*, 20–26.

Medeiros, T.C., Thomas, R.L., Ghillebert, R., and Graef, M. (2018). Autophagy balances mtDNA synthesis and degradation by DNA polymerase POLG during starvation. Journal of Cell Biology *217*, 1601–1611.

Mendl, N., Occhipinti, A., Müller, M., Wild, P., Dikic, I., and Reichert, A.S. (2011). Mitophagy in yeast is independent of mitochondrial fission and requires the stress response gene WHI2. Journal of Cell Science *124*, 1339–1350.

Metzger, M.B., Pruneda, J.N., Klevit, R.E., and Weissman, A.M. (2014). RING-type E3 ligases: Master manipulators of E2 ubiquitin-conjugating enzymes and ubiquitination. Biochimica et Biophysica Acta (BBA) - Molecular Cell Research *1843*, 47–60.

Meyer, H.-J., and Rape, M. (2014). Enhanced Protein Degradation by Branched Ubiquitin Chains. Cell *157*, 910–921.

Miteva, Maria (2007). Proteolytic Mechanisms Controlling SUMO Protein Modification. PhD Thesis, University of Cologne.

Miteva, M., Keusekotten, K., Hofmann, K., Praefcke, G.J.K., and Dohmen, R.J. (2010). Sumoylation as a Signal for Polyubiquitylation and Proteasomal Degradation. In Conjugation and Deconjugation of Ubiquitin Family Modifiers: Subcellular Biochemistry, M. Groettrup, ed. (New York, NY: Springer), pp. 195–214.

Mizushima, N., Noda, T., Yoshimori, T., Tanaka, Y., Ishii, T., George, M.D., Klionsky, D.J., Ohsumi, M., and Ohsumi, Y. (1998). A protein conjugation system essential for autophagy. Nature *395*, 395–398.

Morawe, T., Hiebel, C., Kern, A., and Behl, C. (2012). Protein Homeostasis, Aging and Alzheimer's Disease. Mol Neurobiol *46*, 41–54.

Mostowy, S., and Cossart, P. (2012). Septins: the fourth component of the cytoskeleton. Nat Rev Mol Cell Biol *13*, 183–194.

Mozdy, A.D., McCaffery, J.M., and Shaw, J.M. (2000). Dnm1p Gtpase-Mediated Mitochondrial Fission Is a Multi-Step Process Requiring the Novel Integral Membrane Component Fis1p. J Cell Biol *151*, 367–380.

Mullen, J.R., and Brill, S.J. (2008). Activation of the Slx5–Slx8 Ubiquitin Ligase by Poly-small Ubiquitin-like Modifier Conjugates. Journal of Biological Chemistry *283*, 19912–19921.

Mullen, J.R., Kaliraman, V., Ibrahim, S.S., and Brill, S.J. (2001). Requirement for Three Novel Protein Complexes in the Absence of the Sgs1 DNA Helicase in Saccharomyces cerevisiae. Genetics *157*, 103–118.

Mullen, J.R., Chen, C.-F., and Brill, S.J. (2010). Wss1 Is a SUMO-Dependent Isopeptidase That Interacts Genetically with the Slx5-Slx8 SUMO-Targeted Ubiquitin Ligase. Molecular and Cellular Biology *30*, 3737–3748.

Mumberg, D., Müller, R., and Funk, M. (1994). Regulatable promoters of Saccharomyces cerevisiae: comparison of transcriptional activity and their use for heterologous expression. Nucleic Acids Research *22*, 5767.

Murakami, Y., Matsufuji, S., Kameji, T., Hayashi, S., Igarashi, K., Tamura, T., Tanaka, K., and Ichihara, A. (1992). Ornithine decarboxylase is degraded by the 26S proteasome without ubiquitination. Nature *360*, 597–599.

Murata, S., Yashiroda, H., and Tanaka, K. (2009). Molecular mechanisms of proteasome assembly. Nat Rev Mol Cell Biol *10*, 104–115.

Murray, A.W., Solomon, M.J., and Kirschner, M.W. (1989). The role of cyclin synthesis and degradation in the control of maturation promoting factor activity. Nature *339*, 280–286.

Newman, H.A., Meluh, P.B., Lu, J., Vidal, J., Carson, C., Lagesse, E., Gray, J.J., Boeke, J.D., and Matunis, M.J. (2017). A high throughput mutagenic analysis of yeast sumo structure and function. PLOS Genetics *13*, e1006612.

Nillegoda, N.B., Theodoraki, M.A., Mandal, A.K., Mayo, K.J., Ren, H.Y., Sultana, R., Wu, K., Johnson, J., Cyr, D.M., and Caplan, A.J. (2010). Ubr1 and Ubr2 Function in a Quality Control Pathway for Degradation of Unfolded Cytosolic Proteins. Mol Biol Cell *21*, 2102–2116.

Osman, C., Noriega, T.R., Okreglak, V., Fung, J.C., and Walter, P. (2015). Integrity of the yeast mitochondrial genome, but not its distribution and inheritance, relies on mitochondrial fission and fusion. PNAS *112*, E947–E956.

Otsuga, D., Keegan, B.R., Brisch, E., Thatcher, J.W., Hermann, G.J., Bleazard, W., and Shaw, J.M. (1998). The Dynamin-related GTPase, Dnm1p, Controls Mitochondrial Morphology in Yeast. Journal of Cell Biology *143*, 333–349.

Ozkaynak, E., Finley, D., Solomon, M.J., and Varshavsky, A. (1987). The yeast ubiquitin genes: a family of natural gene fusions. EMBO J *6*, 1429–1439.

Paasch, F., den Brave, F., Psakhye, I., Pfander, B., and Jentsch, S. (2018). Failed mitochondrial import and impaired proteostasis trigger SUMOylation of mitochondrial proteins. J Biol Chem *293*, 599–609.

Pabst, Stefan (2015). SUMO-dependent degradation of Nis1, Dnm1 and Cdc11 in *Saccharomyces cerevisiae*. Master Thesis, University of Cologne.

Pabst, S., Döring, L.-M., Petreska, N., and Dohmen, R.J. (2019). Chapter Nine - Methods to study SUMO dynamics in yeast. In Methods in Enzymology, M. Hochstrasser, ed. (Academic Press), pp. 187–210.

Panse, V.G., Küster, B., Gerstberger, T., and Hurt, E. (2003). Unconventional tethering of Ulp1 to the transport channel of the nuclear pore complex by karyopherins. Nat Cell Biol *5*, 21–27.

Panse, V.G., Hardeland, U., Werner, T., Kuster, B., and Hurt, E. (2004). A Proteome-wide Approach Identifies Sumoylated Substrate Proteins in Yeast. Journal of Biological Chemistry *279*, 41346–41351.

Parker, J.L., and Ulrich, H.D. (2012). A SUMO-interacting motif activates budding yeast ubiquitin ligase Rad18 towards SUMO-modified PCNA. Nucleic Acids Res *40*, 11380–11388.

Parker, J.L., Bucceri, A., Davies, A.A., Heidrich, K., Windecker, H., and Ulrich, H.D. (2008). SUMO modification of PCNA is controlled by DNA. The EMBO Journal *27*, 2422–2431.

van de Pasch, L.A.L., Miles, A.J., Nijenhuis, W., Brabers, N.A.C.H., Leenen, D. van, Lijnzaad, P., Brown, M.K., Ouellet, J., Barral, Y., Kops, G.J.P.L., et al. (2013). Centromere Binding and a Conserved Role in Chromosome Stability for SUMO-Dependent Ubiquitin Ligases. PLOS ONE *8*, e65628.

Patton, E.E., Willems, A.R., Sa, D., Kuras, L., Thomas, D., Craig, K.L., and Tyers, M. (1998). Cdc53 is a scaffold protein for multiple Cdc34/Skp1/F-box protein complexes that regulate cell division and methionine biosynthesis in yeast. Genes Dev. *12*, 692–705.

Pedrajas, J.R., Miranda-Vizuete, A., Javanmardy, N., Gustafsson, J.-Å., and Spyrou, G. (2000). Mitochondria of Saccharomyces cerevisiae Contain One-conserved Cysteine Type Peroxiredoxin with Thioredoxin Peroxidase Activity. Journal of Biological Chemistry *275*, 16296–16301.

Peng, B., Williams, T.C., Henry, M., Nielsen, L.K., and Vickers, C.E. (2015). Controlling heterologous gene expression inyeast cell factories on different carbon substrates and across the diauxic shift: acomparison of yeast promoter activities. Microbial Cell Factories *14*, 91.

Petreska, Natasha (2013). Stabilisierung von SUMO-Konjugaten in *S. cerevisiae*. Bachelor Thesis, University of Cologne.

Pichlo, Christian (2011). Einfluss der SUMO-Proteinmodifikation auf die Lokalisation der Dynamin-ähnlichen GTPase Dnm1. Bachelor Thesis, University of Cologne.

Pickart, C.M. (2001). Mechanisms Underlying Ubiquitination. Annu. Rev. Biochem. *70*, 503–533.

Pickart, C.M., and Cohen, R.E. (2004). Proteasomes and their kin: proteases in the machine age. Nat Rev Mol Cell Biol *5*, 177–187.

Powers, E.T., Morimoto, R.I., Dillin, A., Kelly, J.W., and Balch, W.E. (2009). Biological and Chemical Approaches to Diseases of Proteostasis Deficiency. Annu. Rev. Biochem. *78*, 959–991.

Praefcke, G.J.K., Hofmann, K., and Dohmen, R.J. (2012). SUMO playing tag with ubiquitin. Trends in Biochemical Sciences *37*, 23–31.

Prudden, J., Pebernard, S., Raffa, G., Slavin, D.A., Perry, J.J.P., Tainer, J.A., McGowan, C.H., and Boddy, M.N. (2007). SUMO-targeted ubiquitin ligases in genome stability. EMBO J *26*, 4089–4101.

Prudent, J., Zunino, R., Sugiura, A., Mattie, S., Shore, G.C., and McBride, H.M. (2015). MAPL SUMOylation of Drp1 Stabilizes an ER/Mitochondrial Platform Required for Cell Death. Mol Cell *59*, 941–955.

Rapaport, D., Brunner, M., Neupert, W., and Westermann, B. (1998). Fzo1p Is a Mitochondrial Outer Membrane Protein Essential for the Biogenesis of Functional Mitochondria in Saccharomyces cerevisiae. Journal of Biological Chemistry *273*, 20150–20155.

Reggiori, F., and Klionsky, D.J. (2013). Autophagic Processes in Yeast: Mechanism, Machinery and Regulation. Genetics *194*, 341–361.

Reindle, A., Belichenko, I., Bylebyl, G.R., Chen, X.L., Gandhi, N., and Johnson, E.S. (2006). Multiple domains in Siz SUMO ligases contribute to substrate selectivity. Journal of Cell Science *119*, 4749–4757.

Robberecht, W., and Philips, T. (2013). The changing scene of amyotrophic lateral sclerosis. Nat Rev Neurosci *14*, 248–264.

Ross, C.A., and Poirier, M.A. (2004). Protein aggregation and neurodegenerative disease. Nat Med *10*, S10–S17.

Rothenbusch, U., Sawatzki, M., Chang, Y., Caesar, S., and Schlenstedt, G. (2012). Sumoylation regulates Kap114-mediated nuclear transport. EMBO J *31*, 2461–2472.

Ryu, H.-Y., Wilson, N.R., Mehta, S., Hwang, S.S., and Hochstrasser, M. (2016). Loss of the SUMO protease Ulp2 triggers a specific multichromosome aneuploidy. Genes Dev *30*, 1881–1894.

Ryu, H.-Y., López-Giráldez, F., Knight, J., Hwang, S.S., Renner, C., Kreft, S.G., and Hochstrasser, M. (2018). Distinct adaptive mechanisms drive recovery from aneuploidy caused by loss of the Ulp2 SUMO protease. Nat Commun *9*, 5417.

Saeki, Y. (2017). Ubiquitin recognition by the proteasome. The Journal of Biochemistry *161*, 113–124.

Sala, A.J., Bott, L.C., and Morimoto, R.I. (2017). Shaping proteostasis at the cellular, tissue, and organismal level. Journal of Cell Biology *216*, 1231–1241.

Sarangi, P., and Zhao, X. (2015). SUMO-mediated regulation of DNA damage repair and responses. Trends Biochem Sci *40*, 233–242.

Sato, A., Nakada, K., and Hayashi, J.-I. (2006). Mitochondrial dynamics and aging: Mitochondrial interaction preventing individuals from expression of respiratory deficiency caused by mutant mtDNA. Biochimica et Biophysica Acta (BBA) - Molecular Cell Research *1763*, 473–481.

Scagliola, A., Mainini, F., and Cardaci, S. (2020). The Tricarboxylic Acid Cycle at the Crossroad Between Cancer and Immunity. Antioxidants & Redox Signaling *32*, 834–852.

Scaglione, K.M., Basrur, V., Ashraf, N.S., Konen, J.R., Elenitoba-Johnson, K.S.J., Todi, S.V., and Paulson, H.L. (2013). The Ubiquitin-conjugating Enzyme (E2) Ube2w Ubiquitinates the N Terminus of Substrates. Journal of Biological Chemistry *288*, 18784–18788.

Schmidt, M., Haas, W., Crosas, B., Santamaria, P.G., Gygi, S.P., Walz, T., and Finley, D. (2005). The HEAT repeat protein Blm10 regulates the yeast proteasome by capping the core particle. Nat Struct Mol Biol *12*, 294–303.

Schröer, Joan (2021). Development of a pulldown method for the purification of Saccharomyces cerevisiae mitochondria. Master Thesis, University of Cologne.

Schulz, S., Chachami, G., Kozaczkiewicz, L., Winter, U., Stankovic-Valentin, N., Haas, P., Hofmann, K., Urlaub, H., Ovaa, H., Wittbrodt, J., et al. (2012). Ubiquitin-specific protease-like 1 (USPL1) is a SUMO isopeptidase with essential, non-catalytic functions. EMBO Rep *13*, 930–938.

Schweitzer, A., Aufderheide, A., Rudack, T., Beck, F., Pfeifer, G., Plitzko, J.M., Sakata, E., Schulten, K., Förster, F., and Baumeister, W. (2016). Structure of the human 26S proteasome at a resolution of 3.9 Å. Proc Natl Acad Sci U S A *113*, 7816–7821.

Schwienhorst, I., Johnson, E.S., and Dohmen, R.J. (2000). SUMO conjugation and deconjugation. Mol Gen Genet *263*, 771–786.

Seol, J.H., Feldman, R.M.R., Zachariae, W., Shevchenko, A., Correll, C.C., Lyapina, S., Chi, Y., Galova, M., Claypool, J., Sandmeyer, S., et al. (1999). Cdc53/cullin and the essential Hrt1 RING–H2 subunit of SCF define a ubiquitin ligase module that activates the E2 enzyme Cdc34. Genes Dev. *13*, 1614–1626.

Sesaki, H., and Jensen, R.E. (1999). Division versus Fusion: Dnm1p and Fzo1p Antagonistically Regulate Mitochondrial Shape. Journal of Cell Biology *147*, 699–706.

Seufert, W., Futcher, B., and Jentsch, S. (1995). Role of a ubiquitin-conjugating enzyme in degradation of S- and M-phase cyclins. Nature *373*, 78–81.

Shadel, G.S. (1999). Yeast as a Model for Human mtDNA Replication. Am J Hum Genet *65*, 1230–1237.

Shah, P.P., Zheng, X., Epshtein, A., Carey, J.N., Bishop, D.K., and Klein, H.L. (2010). Swi2/Snf2-Related Translocases Prevent Accumulation of Toxic Rad51 Complexes during Mitotic Growth. Molecular Cell *39*, 862–872.

Shaner, N.C., Campbell, R.E., Steinbach, P.A., Giepmans, B.N.G., Palmer, A.E., and Tsien, R.Y. (2004). Improved monomeric red, orange and yellow fluorescent proteins derived from Discosoma sp. red fluorescent protein. Nature Biotechnology *22*, 1567–1572.

Sharma, K.G., Kaur, R., and Bachhawat, A.K. (2003). The glutathione-mediated detoxification pathway in yeast: an analysis using the red pigment that accumulates in certain adenine biosynthetic mutants of yeasts reveals the involvement of novel genes. Arch Microbiol *180*, 108–117.

Shen, H., Heacock, P.N., Clancey, C.J., and Dowhan, W. (1996). The CDS1 Gene Encoding CDP-diacylglycerol Synthase In Saccharomyces cerevisiae Is Essential for Cell Growth (∗). Journal of Biological Chemistry *271*, 789–795.

Shin, E.J., Shin, H.M., Nam, E., Kim, W.S., Kim, J.-H., Oh, B.-H., and Yun, Y. (2012). DeSUMOylating isopeptidase: a second class of SUMO protease. EMBO Rep *13*, 339–346.

Shirai, C., and Mizuta, K. (2008). SUMO Mediates Interaction of Ebp2p, the Yeast Homolog of Epstein-Barr Virus Nuclear Antigen 1-Binding Protein 2, with a RING Finger Protein Ris1p. Bioscience, Biotechnology, and Biochemistry *72*, 1881–1886.

Shou, W., Seol, J.H., Shevchenko, A., Baskerville, C., Moazed, D., Chen, Z.W.S., Jang, J., Shevchenko, A., Charbonneau, H., and Deshaies, R.J. (1999). Exit from Mitosis Is Triggered by Tem1-Dependent Release of the Protein Phosphatase Cdc14 from Nucleolar RENT Complex. Cell *97*, 233–244.

Shou, W., Sakamoto, K.M., Keener, J., Morimoto, K.W., Traverso, E.E., Azzam, R., Hoppe, G.J., Feldman, R.M.R., DeModena, J., Moazed, D., et al. (2001). Net1 Stimulates RNA Polymerase I Transcription and Regulates Nucleolar Structure Independently of Controlling Mitotic Exit. Molecular Cell *8*, 45–55.

Sikorski, R.S., and Hieter, P. (1989). A system of shuttle vectors and yeast host strains designed for efficient manipulation of DNA in Saccharomyces cerevisiae. Genetics *122*, 19–27.

Simões, T., Schuster, R., den Brave, F., and Escobar-Henriques, M. (2018). Cdc48 regulates a deubiquitylase cascade critical for mitochondrial fusion. ELife *7*, e30015.

Song, J., Tamura, Y., Yoshihisa, T., and Endo, T. (2014). A novel import route for an N-anchor mitochondrial outer membrane protein aided by the TIM23 complex. EMBO Rep *15*, 670–677.

Srikumar, T., Lewicki, M.C., Costanzo, M., Tkach, J.M., van Bakel, H., Tsui, K., Johnson, E.S., Brown, G.W., Andrews, B.J., Boone, C., et al. (2013). Global analysis of SUMO chain function reveals multiple roles in chromatin regulation. J Cell Biol *201*, 145–163.

Sriramachandran, A.M., and Dohmen, R.J. (2014). SUMO-targeted ubiquitin ligases. Biochimica et Biophysica Acta (BBA) - Molecular Cell Research *1843*, 75–85.

Sriramachandran, A.M., Meyer-Teschendorf, K., Pabst, S., Ulrich, H.D., Gehring, N.H., Hofmann, K., Praefcke, G.J.K., and Dohmen, R.J. (2019). Arkadia/RNF111 is a SUMO-targeted ubiquitin ligase with preference for substrates marked with SUMO1-capped SUMO2/3 chain. Nat Commun *10*, 3678.

Stingele, J., Schwarz, M.S., Bloemeke, N., Wolf, P.G., and Jentsch, S. (2014). A DNA-Dependent Protease Involved in DNA-Protein Crosslink Repair. Cell *158*, 327–338.

Strunnikov, A.V., Aravind, L., and Koonin, E.V. (2001). Saccharomyces cerevisiae SMT4 Encodes an Evolutionarily Conserved Protease With a Role in Chromosome Condensation Regulation. Genetics *158*, 95–107.

Suhandynata, R.T., Quan, Y., Yang, Y., Yuan, W.-T., Albuquerque, C.P., and Zhou, H. (2019). Recruitment of the Ulp2 protease to the inner kinetochore prevents its hyper-sumoylation to ensure accurate chromosome segregation. PLOS Genetics *15*, e1008477.

Sun, H., Leverson, J.D., and Hunter, T. (2007). Conserved function of RNF4 family proteins in eukaryotes: targeting a ubiquitin ligase to SUMOylated proteins. EMBO J *26*, 4102–4112.

Sun, S., Zhou, J.-Y., Yang, W., and Zhang, H. (2014). Inhibition of protein carbamylation in urea solution using ammonium-containing buffers. Analytical Biochemistry *446*, 76–81.

Suresh, H.G., Pascoe, N., and Andrews, B. (2020). The structure and function of deubiquitinases: lessons from budding yeast. Open Biol. *10*, 200279.

Swaney, D.L., Beltrao, P., Starita, L., Guo, A., Rush, J., Fields, S., Krogan, N.J., and Villén, J. (2013). Global analysis of phosphorylation and ubiquitylation crosstalk in protein degradation. Nat Methods *10*.

Swatek, K.N., and Komander, D. (2016). Ubiquitin modifications. Cell Res *26*, 399–422.

Tadauchi, T., Matsumoto, K., Herskowitz, I., and Irie, K. (2001). Post-transcriptional regulation through the HO 3'-UTR by Mpt5, a yeast homolog of Pumilio and FBF. The EMBO Journal *20*, 552–561.

Takahashi, Y., and Kikuchi, Y. (2008). Cytoplasmic sumoylation by PIAS-type Siz1-SUMO ligase. Cell Cycle *7*, 1738–1744.

Takahashi, Y., Toh-e, A., and Kikuchi, Y. (2001). A novel factor required for the SUMO1/Smt3 conjugation of yeast septins. Gene *275*, 223–231.

Tamura, Y., Harada, Y., Nishikawa, S., Yamano, K., Kamiya, M., Shiota, T., Kuroda, T., Kuge, O., Sesaki, H., Imai, K., et al. (2013). Tam41 Is a CDP-Diacylglycerol Synthase Required for Cardiolipin Biosynthesis in Mitochondria. Cell Metabolism *17*, 709–718.

Tan, W., Wang, Z., and Prelich, G. (2013). Physical and Genetic Interactions Between Uls1 and the Slx5–Slx8 SUMO-Targeted Ubiquitin Ligase. G3 Genes|Genomes|Genetics *3*, 771–780.

Tanaka, K., Nishide, J., Okazaki, K., Kato, H., Niwa, O., Nakagawa, T., Matsuda, H., Kawamukai, M., and Murakami, Y. (1999). Characterization of a Fission Yeast SUMO-1 Homologue, Pmt3p, Required for Multiple Nuclear Events, Including the Control of Telomere Length and Chromosome Segregation. Molecular and Cellular Biology *19*, 8660–8672.

Tang, G.-Q., Deshpande, A.P., and Patel, S.S. (2011). Transcription Factor-dependent DNA Bending Governs Promoter Recognition by the Mitochondrial RNA Polymerase. Journal of Biological Chemistry *286*, 38805–38813.

Tanida, I., Mizushima, N., Kiyooka, M., Ohsumi, M., Ueno, T., Ohsumi, Y., and Kominami, E. (1999). Apg7p/Cvt2p: A Novel Protein-activating Enzyme Essential for Autophagy. MBoC *10*, 1367–1379.

Tar, K., Dange, T., Yang, C., Yao, Y., Bulteau, A.-L., Salcedo, E.F., Braigen, S., Bouillaud, F., Finley, D., and Schmidt, M. (2014). Proteasomes Associated with the Blm10 Activator Protein Antagonize Mitochondrial Fission through Degradation of the Fission Protein Dnm1. J Biol Chem *289*, 12145–12156.

Tatham, M.H., Jaffray, E., Vaughan, O.A., Desterro, J.M.P., Botting, C.H., Naismith, J.H., and Hay, R.T. (2001). Polymeric Chains of SUMO-2 and SUMO-3 Are Conjugated to Protein Substrates by SAE1/SAE2 and Ubc9. Journal of Biological Chemistry *276*, 35368–35374.

Tatham, M.H., Geoffroy, M.-C., Shen, L., Plechanovova, A., Hattersley, N., Jaffray, E.G., Palvimo, J.J., and Hay, R.T. (2008). RNF4 is a poly-SUMO-specific E3 ubiquitin ligase required for arsenic-induced PML degradation. Nat Cell Biol *10*, 538–546.

Tenno, T., Fujiwara, K., Tochio, H., Iwai, K., Morita, E.H., Hayashi, H., Murata, S., Hiroaki, H., Sato, M., Tanaka, K., et al. (2004). Structural basis for distinct roles of Lys63- and Lys48-linked polyubiquitin chains. Genes to Cells *9*, 865–875.

Theodoraki, M.A., Nillegoda, N.B., Saini, J., and Caplan, A.J. (2012). A Network of Ubiquitin Ligases Is Important for the Dynamics of Misfolded Protein Aggregates in Yeast. J Biol Chem *287*, 23911–23922.

Thrower, J.S., Hoffman, L., Rechsteiner, M., and Pickart, C.M. (2000). Recognition of the polyubiquitin proteolytic signal. EMBO J *19*, 94–102.

Tilokani, L., Nagashima, S., Paupe, V., and Prudent, J. (2018). Mitochondrial dynamics: overview of molecular mechanisms. Essays in Biochemistry *62*, 341–360.

Ulrich, H.D. (2008). The Fast-Growing Business of SUMO Chains. Molecular Cell *32*, 301–305.

Uzunova, K., Göttsche, K., Miteva, M., Weisshaar, S.R., Glanemann, C., Schnellhardt, M., Niessen, M., Scheel, H., Hofmann, K., Johnson, E.S., et al. (2007). Ubiquitin-dependent proteolytic control of SUMO conjugates. J Biol Chem *282*, 34167–34175.

Varshavsky, A. (1997). The N-end rule pathway of protein degradation. Genes to Cells *2*, 13–28.

Vieira, J., and Messing, J. (1991). New pUC-derived cloning vectors with different selectable markers and DNA replication origins. Gene *100*, 189–194.

Vogt, B., and Hofmann, K. (2012). Bioinformatical Detection of Recognition Factors for Ubiquitin and SUMO. In Ubiquitin Family Modifiers and the Proteasome: Reviews and Protocols, R.J. Dohmen, and M. Scheffner, eds. (Totowa, NJ: Humana Press), pp. 249–261.

Vögtle, F.-N., Prinz, C., Kellermann, J., Lottspeich, F., Pfanner, N., and Meisinger, C. (2011). Mitochondrial protein turnover: role of the precursor intermediate peptidase Oct1 in protein stabilization. MBoC *22*, 2135–2143.

Vögtle, F.-N., Burkhart, J.M., Gonczarowska-Jorge, H., Kücükköse, C., Taskin, A.A., Kopczynski, D., Ahrends, R., Mossmann, D., Sickmann, A., Zahedi, R.P., et al. (2017). Landscape of submitochondrial protein distribution. Nat Commun *8*, 290.

Walden, H., and Rittinger, K. (2018). RBR ligase-mediated ubiquitin transfer: a tale with many twists and turns. Nat Struct Mol Biol *25*, 440–445.

Wallace, E.W.J., Kear-Scott, J.L., Pilipenko, E.V., Schwartz, M.H., Laskowski, P.R., Rojek, A.E., Katanski, C.D., Riback, J.A., Dion, M.F., Franks, A.M., et al. (2015). Reversible, Specific, Active Aggregates of Endogenous Proteins Assemble upon Heat Stress. Cell *162*, 1286–1298.

Wang, J., and Maldonado, M.A. (2006). The ubiquitin-proteasome system and its role in inflammatory and autoimmune diseases. Cell Mol Immunol *3*, 255–261.

Wang, Z., and Prelich, G. (2009). Quality Control of a Transcriptional Regulator by SUMO-Targeted Degradation. Molecular and Cellular Biology *29*, 1694–1706.

Wang, T., Cao, Y., Zheng, Q., Tu, J., Zhou, W., He, J., Zhong, J., Chen, Y., Wang, J., Cai, R., et al. (2019). SENP1-Sirt3 Signaling Controls Mitochondrial Protein Acetylation and Metabolism. Mol Cell *75*, 823-834.e5.

Wang, Z., Wu, C., Aslanian, A., Yates, J.R., III, and Hunter, T. (2018). Defective RNA polymerase III is negatively regulated by the SUMO-Ubiquitin-Cdc48 pathway. ELife *7*, e35447.

Waples, W.G., Chahwan, C., Ciechonska, M., and Lavoie, B.D. (2008). Putting the Brake on FEAR: Tof2 Promotes the Biphasic Release of Cdc14 Phosphatase during Mitotic Exit. MBoC *20*, 245–255.

Wasiak, S., Zunino, R., and McBride, H.M. (2007). Bax/Bak promote sumoylation of DRP1 and its stable association with mitochondria during apoptotic cell death. J Cell Biol *177*, 439–450.

Wei, Y., Diao, L.-X., Lu, S., Wang, H.-T., Suo, F., Dong, M.-Q., and Du, L.-L. (2017). SUMO-Targeted DNA Translocase Rrp2 Protects the Genome from Top2-Induced DNA Damage. Molecular Cell *66*, 581-596.e6.

Weisshaar, S.R., Keusekotten, K., Krause, A., Horst, C., Springer, H.M., Göttsche, K., Dohmen, R.J., and Praefcke, G.J.K. (2008). Arsenic trioxide stimulates SUMO-2/3 modification leading to RNF4-dependent proteolytic targeting of PML. FEBS Letters *582*, 3174–3178.

Wen, D., Wu, J., Wang, L., and Fu, Z. (2017). SUMOylation Promotes Nuclear Import and Stabilization of Polo-like Kinase 1 to Support Its Mitotic Function. Cell Reports *21*, 2147–2159.

Wendler, P., and Enenkel, C. (2019). Nuclear Transport of Yeast Proteasomes. Front Mol Biosci *6*, 34.

Westermann, B. (2008). Molecular Machinery of Mitochondrial Fusion and Fission. Journal of Biological Chemistry *283*, 13501–13505.

Westermann, B. (2014). Mitochondrial inheritance in yeast. Biochimica et Biophysica Acta (BBA) - Bioenergetics *1837*, 1039–1046.

Westermann, B., and Neupert, W. (2000). Mitochondria-targeted green fluorescent proteins: convenient tools for the study of organelle biogenesis in Saccharomyces cerevisiae. Yeast *16*, 1421–1427.

Wilinski, D., Qiu, C., Lapointe, C.P., Nevil, M., Campbell, Z.T., Tanaka Hall, T.M., and Wickens, M. (2015). RNA regulatory networks diversified through curvature of the PUF protein scaffold. Nature Communications *6*, 8213.

Wingfield, P. (2017). N-Terminal Methionine Processing. Curr Protoc Protein Sci *88*, 6.14.1-6.14.3.

Wohlschlegel, J.A., Johnson, E.S., Reed, S.I., and Yates, J.R. (2004). Global Analysis of Protein Sumoylation in Saccharomyces cerevisiae. Journal of Biological Chemistry *279*, 45662–45668.

Xie, Y., and Varshavsky, A. (2001). RPN4 is a ligand, substrate, and transcriptional regulator of the 26S proteasome: A negative feedback circuit. PNAS *98*, 3056–3061.

Xie, Y., Kerscher, O., Kroetz, M.B., McConchie, H.F., Sung, P., and Hochstrasser, M. (2007). The Yeast Hex3·Slx8 Heterodimer Is a Ubiquitin Ligase Stimulated by Substrate Sumoylation. Journal of Biological Chemistry *282*, 34176–34184.

Xu, G., and Jaffrey, S.R. (2013). Proteomic identification of protein ubiquitination events. Biotechnology and Genetic Engineering Reviews *29*, 73–109.

Yanisch-Perron, C., Vieira, J., and Messing, J. (1985). Improved M13 phage cloning vectors and host strains: nucleotide sequences of the M13mpl8 and pUC19 vectors. Gene *33*, 103–119.

Young, C.L., Britton, Z.T., and Robinson, A.S. (2012). Recombinant protein expression and purification: A comprehensive review of affinity tags and microbial applications. Biotechnology Journal *7*, 620–634.

Zhang, Y., and Chan, D.C. (2007). Structural basis for recruitment of mitochondrial fission complexes by Fis1. PNAS *104*, 18526–18530.

Zhang, C., Roberts, T.M., Yang, J., Desai, R., and Brown, G.W. (2006). Suppression of genomic instability by SLX5 and SLX8 in Saccharomyces cerevisiae. DNA Repair (Amst) *5*, 336–346.

Zhao, X., and Blobel, G. (2005). A SUMO ligase is part of a nuclear multiprotein complex that affects DNA repair and chromosomal organization. PNAS *102*, 4777–4782.

Zhao, Q., Xie, Y., Zheng, Y., Jiang, S., Liu, W., Mu, W., Liu, Z., Zhao, Y., Xue, Y., and Ren, J. (2014). GPS-SUMO: a tool for the prediction of sumoylation sites and SUMO-interaction motifs. Nucleic Acids Research *42*, W325–W330.

Zhou, W., Ryan, J.J., and Zhou, H. (2004). Global Analyses of Sumoylated Proteins in Saccharomyces cerevisiae: Induction of protein sumoylation by cellular stresses. Journal of Biological Chemistry *279*, 32262–32268.

Zuin, A., Isasa, M., and Crosas, B. (2014). Ubiquitin Signaling: Extreme Conservation as a Source of Diversity. Cells *3*, 690–701.

Zunino, R., Schauss, A., Rippstein, P., Andrade-Navarro, M., and McBride, H.M. (2007). The SUMO protease SENP5 is required to maintain mitochondrial morphology and function. Journal of Cell Science *120*, 1178–1188.

Acknowledgements

First and foremost, I want to thank Prof. Dr. Jürgen Dohmen for being such an encouraging, motivating and considerate supervisor for me during my time in his group. In every discussion, I could sense the enormous passion that you have for science and I really, really enjoyed our profound conversations. The certainty that you deeply care for all of the members of the group was a very important aspect for my decision to spend such a long time in your laboratory. I appreciate it very much that you invested so much effort and time in supporting my work and that you always have an open ear and take time for everybody who asks for an advice or support in any way. Thank you very, very much! A very special thanks also goes to all of the current and former members of the Dohmen lab. Especially, I want to address Lenny for being such a perfect lab partner. We did not only share the lab for the largest part of my time as a PhD student but also we had so many funny and intense conversations. Right now I am thinking back to all the great matches that we played together, be it padel, football or table football as "SUMO fighters R 2.47". In the same breath I would like to thank the current PhD students Jessica and Friederike for all the enjoyable moments that we spent together, particularly during lunch but of course also in our free time. I am sure that without you as my co-students, my time in the lab would have been less fun. In the same line, a huge thank goes to all current and former lab members with whom I have shared my time. In particular I want to mention Paula who has also accompanied me on my way from the very first day in the lab and is always there for a piece of good advice that helps staying on the right track. In addition, Kerstin, Tanja and Sigrid have to be mentioned who have always been a great support for my daily work and surely contributed to a nice working environment. Not to forget the previous lab members who have accompanied me for a part of my time in the Dohmen group. I am especially grateful for the supervision I received from Annie and in the earlier days from Palani, one of the kindest persons I have ever met, may he rest in peace. Furthermore, I am so thankful to have met many great persons in the lab like Julia (my former warmhearted and energetic lab mate), Vishal (thank you for all the advice and all the nice time!), Steffi, Maria and Roshini. Last but not least, thank you to all students, whom I was allowed to supervise and to share a lab with, for the pleasant atmosphere. For general support in every aspect concerning the PhD program, I want to thank the mito-RTG and the GSfBS, in particular Katerina and Isabell. Regarding the work for my thesis, I am very grateful for the collaboration with the Krüger group, especially Theresa and Clara, in the mass spectrometry analysis, Prof. Dr. Kay Hofmann for helping in the analysis of MS data and general discussions on the topic, and Prof. Dr. Niels Gehring for the nice collaboration in the Arkadia project. Along the same lines, I thank Prof. Dr. Kay Hofmann, Prof. Dr. Jan Riemer and Dr. Karsten Klopffleisch for agreeing to be my thesis committee. At this point, it is exceptionally important to me to thank my parents and my sister

Jasmin for always being there when I need support and with being so patient, especially when, once in a while, things are not going as planned. At any time you were so understanding, helpful and overall a great backing. Thank you for everything that you have done for me and your support in any imaginable way! Of course, just as important is the immense moral support and loyalty that I receive from all of my friends. Without you, all that I am doing would surely be much harder, so you can be assured that you also have a large impact on the possibility to reach my goals. At this point, especially I want to say thank you to Alex, Dorian and Naïra who have motivated me in particular when times were difficult. You cannot imagine what your support means to me and I thank you from the bottom of my heart!

Erklärung zur Dissertation
gemäß der Promotionsordnung vom 12. März 2020

Diese Erklärung muss in der Dissertation enthalten sein.
(This version must be included in the doctoral thesis)

„Hiermit versichere ich an Eides statt, dass ich die vorliegende Dissertation selbstständig und ohne die Benutzung anderer als der angegebenen Hilfsmittel und Literatur angefertigt habe. Alle Stellen, die wörtlich oder sinngemäß aus veröffentlichten und nicht veröffentlichten Werken dem Wortlaut oder dem Sinn nach entnommen wurden, sind als solche kenntlich gemacht. Ich versichere an Eides statt, dass diese Dissertation noch keiner anderen Fakultät oder Universität zur Prüfung vorgelegen hat; dass sie - abgesehen von unten angegebenen Teilpublikationen und eingebundenen Artikeln und Manuskripten - noch nicht veröffentlicht worden ist sowie, dass ich eine Veröffentlichung der Dissertation vor Abschluss der Promotion nicht ohne Genehmigung des Promotionsausschusses vornehmen werde. Die Bestimmungen dieser Ordnung sind mir bekannt. Darüber hinaus erkläre ich hiermit, dass ich die Ordnung zur Sicherung guter wissenschaftlicher Praxis und zum Umgang mit wissenschaftlichem Fehlverhalten der Universität zu Köln gelesen und sie bei der Durchführung der Dissertation zugrundeliegenden Arbeiten und der schriftlich verfassten Dissertation beachtet habe und verpflichte mich hiermit, die dort genannten Vorgaben bei allen wissenschaftlichen Tätigkeiten zu beachten und umzusetzen. Ich versichere, dass die eingereichte elektronische Fassung der eingereichten Druckfassung vollständig entspricht."

Teilpublikationen:

Pabst, S., Döring, L.-M., Petreska, N., and Dohmen, R.J. (2019). Chapter Nine - Methods to study SUMO dynamics in yeast. In Methods in Enzymology, M. Hochstrasser, ed. (Academic Press), pp. 187–210.

08.08.2021, Stefan Pabst Stefan Pabst
Datum, Name und Unterschrift